

Centre Eau Terre Environnement

## **ÉVALUATION DES RESSOURCES GÉOTHERMIQUES ASSOCIÉES AU CONTEXTE EXTENSIF DU NORD DE MADAGASCAR**

Rajaobelison Miora Mirah

Thèse présentée pour l'obtention du grade de  
**Philosophiae Doctor (Ph.D.)**  
en sciences de la Terre

### **Jury d'évaluation**

Président du jury et  
examinateur interne

Geneviève Bordeleau  
INRS

Examinateur externe

Pooneh Maghoul  
Université Polytechnique Montréal

Examinateur externe

Patrick Baud  
Université de Strasbourg

Directeur de recherche

Jasmin Raymond  
INRS

Codirecteur de recherche

Michel Malo  
INRS



*"For there is nothing covered, that shall not be revealed;  
neither hid, that shall not be known."*

## **REMERCIEMENTS**

Avant toute chose, et au terme de la rédaction de ce mémoire, je rends grâce au Très Haut, Abba Père qui, par sa présence et la santé qu'il m'a accordée, m'a permis de réaliser ce travail.

À Jasmin Raymond, merci d'avoir accepté de diriger et d'orienter ce projet de recherche selon mes intérêts. Lorsque j'ai commencé ce doctorat, je ne connaissais pas grand-chose à l'énergie géothermique. J'ai appris non seulement sur les mécanismes de transfert de chaleur mais aussi votre pragmatisme dans le transfert de qualités humaines et professionnelles dont vous faites preuve pour la gestion et la motivation de votre équipe.

Au Professeur Michel Malo, merci d'avoir accepté de co-encadrer ce travail. Merci pour votre disponibilité et pour toutes les discussions, pour la rigueur et la précision de vos révisions.

À Geneviève Bordeleau, Pooneh Maghoul et Patrick Baud. Merci d'avoir accepté de porter un regard critique sur ce travail et d'avoir jugé cette thèse de manière constructive.

Je suis très reconnaissante à l'équipe de terrain qui m'a aidée et facilitée le travail de terrain : à Rochard Hambinintsoa et Mr Faly pour leur aide et leurs discussions sur le terrain à Ambilobe. À Parfait, qui s'est démené pour dégager un chemin pour atteindre les affleurements près des champs de cacao à Ambanja !

Au Programme international de géosciences de l'UNESCO (IGCP) pour avoir fourni un cadre permettant de renforcer la collaboration entre les membres du groupe IGCP-636 qui s'intéressent à la recherche géothermique.

À Juliet Newson pour sa générosité et qui m'a toujours poussé à persévérer dans ce domaine et d'y progresser.

À mon frère Élie R. et mon big brother Claude, merci pour toutes les discussions, le brainstorming, vos soutiens.

À Mimi et Lucio qui sont devenus comme une partie de ma famille ici au Canada et avec qui je partage tous les bons moments surtout chaque Sabbat.

À tous mes amis du 1309 avec qui j'ai partagé le quotidien des bureaux pendant ces quelques années à l'INRS Aurélie, Pier, Benjamin, Arnaud, William, Octavio : un grand merci.

À mes parents et à mes sœurs, pour qui ce mémoire a été écrit, pour leur soutien constant et leur patience dans mes études. Veuillez, trouvez dans ce modeste travail, ma plus grande reconnaissance.

## **Financement**

L'aide financière pour ce programme de doctorat a été fournie par la Bourse canadienne de la Francophonie et par le Conseil de recherches en sciences naturelles et en génie du Canada (CRSNG) par le biais d'une subvention à la découverte octroyée à Jasmin Raymond ainsi que l'aide financière de l'INRS via les crédits de bourse octroyés à Michel Malo et Jasmin Raymond.

## RÉSUMÉ

Les ressources géothermiques des grandes zones de failles à contexte tectonique extensif sont maintenant convoitées bien qu'elles ne représentent que 10 % de la ressource géothermique actuellement exploitée dans le monde. Pour arriver à développer ce type de ressources, il faut améliorer les méthodes d'exploration des systèmes géothermiques des zones de failles. La région Nord de Madagascar comprend de grandes zones de failles extensives avec des sources thermales qui indiquent la présence d'une source géothermique. L'exploitation de l'énergie géothermique dans cette région contribuerait à assurer une sécurité et un approvisionnement énergétique durable tout en garantissant une faible empreinte environnementale. L'objectif de cette thèse est de mieux comprendre les mécanismes de transfert thermique associés aux ressources géothermiques dans les grandes zones de failles à contexte tectonique extensif dans le Nord de Madagascar. L'idée est de bien délimiter les contextes favorables au développement géothermique de cette région, et par le fait même, améliorer les méthodes d'exploration.

Un catalogue des systèmes géothermiques à Madagascar a été établi à partir d'informations sur les contextes géologiques combinées à la température des réservoirs déduite des géothermomètres chimiques, permettant de caractériser les systèmes géothermiques pour l'ensemble de Madagascar. L'évaluation des propriétés pétrophysiques des roches de la région Nord a ensuite été réalisée sur le terrain et en laboratoire à partir des échantillons d'affleurements rocheux utilisés comme analogues des formations géologiques profondes. Les unités thermostratigraphiques définies selon le concept de thermofaciès montrent que les systèmes géothermiques sont qualifiés de pétrothermaux à transitoires dans lesquels le transfert de chaleur par conduction domine les roches à faible perméabilité alors que les failles et les roches fracturées impliquent une convection forcée donnant lieu aux sources chaudes. Les propriétés des failles favorisant la remontée de fluides géothermiques ont été déterminées à partir de simulations numériques avec des modèles bidimensionnels d'écoulement de fluide couplé au transfert de chaleur en régime permanent. Les failles avec un pendage en direction de l'écoulement des eaux souterraines ou situées dans une zone de décharge hydraulique, soit près d'une rivière, étaient les plus favorables à l'ascension des fluides.

Ces travaux contribuent à l'avancement des connaissances scientifiques concernant l'influence des failles sur la remontée des fluides par convection forcée. Les résultats ont permis de justifier et de définir les prochaines phases d'exploration, en ciblant les failles et les zones de failles pour

la région Nord de Madagascar afin d'envisager l'exploitation future de ses ressources géothermiques.

Mots-clés : énergie, géothermie, rift, faille, conductivité thermique, perméabilité, transfert de chaleur, convection forcée.

## ABSTRACT

The geothermal resources of large tectonically extensive fault zones are now coveted even though they represent only 10 % of the world's currently exploited geothermal resource. In order to develop this type of resource, it is necessary to improve exploration methods for geothermal systems in fault zones. The northern region of Madagascar has large extensive fault zones with thermal springs that indicate the presence of a geothermal source. The exploitation of geothermal energy in this region would help to ensure a secure and sustainable energy supply while guaranteeing a small environmental footprint. The objective of this thesis is to better understand the heat transfer mechanisms associated with geothermal resources in large fault zones with extensive tectonic context in northern Madagascar. The idea is to appropriately delineate the contexts favourable to geothermal development in this region, and thereby improve exploration methods.

A catalogue of geothermal systems in Madagascar has been established based on information on geological contexts combined with reservoir temperatures deduced from chemical geothermometers, allowing the characterisation of geothermal systems for the whole Madagascar. The evaluation of the petrophysical properties of the rocks of the northern region was then carried out in the field and in the laboratory using rock outcrop samples as analogues of the deep geological formations. The thermostratigraphic units defined according to the thermofacies concept show that the geothermal systems are qualified as transient petrothermal in which conductive heat transfer dominates the low permeability rocks while faults and fractured rocks involve forced convection giving rise to the hot springs. The properties of faults favouring upwelling of geothermal fluids were determined from numerical simulations with two-dimensional fluid flow models coupled with steady-state heat transfer. Faults dipping towards groundwater flow or located in a hydraulic discharge zone, near a river, were the most favourable for fluid ascent.

This work contributes to the advancement of scientific knowledge concerning the influence of faults on the ascent of fluids by forced convection. The results have made it possible to justify and define the next phases of exploration, targeting faults and fault zones for the northern region of Madagascar in order to consider the future exploitation of its geothermal resources.

Keywords: energy, geothermal, rift, fault, thermal conductivity, permeability, thermofacies, heat transfer, forced convection, numerical modelling.

# TABLE DES MATIÈRES

<b>REMERCIEMENTS .....</b>	<b>III</b>
FINANCEMENT.....	IV
<b>RÉSUMÉ .....</b>	<b>V</b>
<b>ABSTRACT .....</b>	<b>VII</b>
<b>TABLE DES MATIÈRES .....</b>	<b>VIII</b>
<b>LISTE DES FIGURES.....</b>	<b>XIII</b>
<b>LISTE DES TABLEAUX .....</b>	<b>XVII</b>
<b>LISTE DES ÉQUATIONS .....</b>	<b>XIX</b>
<b>NOMENCLATURE .....</b>	<b>XXI</b>
<b>1 INTRODUCTION.....</b>	<b>1</b>
1.1 MISE EN CONTEXTE .....	1
1.2 REVUE DE LITTÉRATURE.....	3
1.2.1 <i>Contexte tectonique et distribution des ressources géothermiques dans le monde .....</i>	3
1.2.2 <i>Système et réservoir géothermique .....</i>	6
1.2.3 <i>La ressource géothermique de l'Afrique .....</i>	7
1.2.4 <i>Contexte tectonique de Madagascar en relation avec son potentiel géothermique .....</i>	9
1.3 PROBLÉMATIQUE ET OBJECTIFS.....	12
1.4 MÉTHODOLOGIE .....	15
1.5 STRUCTURE DE LA THÈSE .....	16
<b>2 PREMIER ARTICLE: CLASSIFICATION OF GEOTHERMAL SYSTEMS IN MADAGASCAR.....</b>	<b>19</b>
2.1 INTRODUCTION .....	19
2.2 GEOGRAPHICAL AND GEOLOGICAL SETTINGS.....	21
2.3 DEVELOPMENT OF A GEOTHERMAL SYSTEM CLASSIFICATION .....	25
2.4 CLASSES OF GEOTHERMAL SYSTEMS .....	26
2.5 CONCEPTUAL MODELS AND GEOTHERMAL SYSTEM CLASSES .....	30
2.5.1 <i>North region .....</i>	31
2.5.2 <i>Central region.....</i>	37
2.5.3 <i>West region .....</i>	42
2.6 DISCUSSION.....	46
2.6.1 <i>Analogue geothermal systems.....</i>	46
2.6.2 <i>Heat source and heat transfer mechanism .....</i>	49
2.6.3 <i>Fluid origin and flow .....</i>	50
2.7 CONCLUDING REMARKS .....	51

### **3 DEUXIÈME ARTICLE: ASSESSMENT OF PETROPHYSICAL ROCK PROPERTIES IN NORTH MADAGASCAR: IMPLICATIONS FOR GEOTHERMAL RESOURCE EXPLORATION**

**53**

3.1	INTRODUCTION .....	55
3.2	GEOLOGIC SETTINGS .....	57
3.2.1	<i>Ambilobe</i> .....	57
3.2.2	<i>Ambanja</i> .....	60
3.3	MATERIALS AND LABORATORY ANALYSIS.....	62
3.3.1	<i>Sample preparation and measurement workflow</i> .....	62
3.3.2	<i>Hydraulic properties</i> .....	65
3.3.3	<i>Thermal properties</i> .....	66
3.3.4	<i>Heat-producing elements and radiogenic heat production</i> .....	67
3.4	RESULTS.....	68
3.4.1	<i>Lithology and petrography</i> .....	68
3.4.2	<i>Hydraulic properties</i> .....	71
3.4.3	<i>Thermal properties</i> .....	76
3.4.4	<i>Heat-producing elements and radiogenic heat production</i> .....	79
3.5	DISCUSSION.....	80
3.5.1	<i>Implications of mineral content on petrophysical properties and heat production</i> .....	80
3.5.2	<i>Hydraulic properties</i> .....	81
3.5.3	<i>Thermal properties</i> .....	88
3.5.4	<i>Heat Production</i> .....	88
3.5.5	<i>Heat transfer mechanism</i> .....	89
3.5.6	<i>Implications for geothermal exploration</i> .....	91
3.6	CONCLUSIONS.....	92

### **4 TROISIÈME ARTICLE: UNDERSTANDING HEAT TRANSFER ALONG EXTENSIONAL FAULTS: THE CASE OF AMBIOLOBE AND AMBANJA GEOTHERMAL SYSTEMS IN MADAGASCAR.....**

**93**

4.1	INTRODUCTION .....	95
4.2	GEOLOGICAL SETTING.....	97
4.2.1	<i>Tectonic framework and fault system</i> .....	97
4.2.2	<i>Favorable structural patterns</i> .....	99
4.2.3	<i>Lithosphere structure and geological formation</i> .....	101
4.3	NUMERICAL MODEL DEVELOPPEMENT .....	102
4.3.1	<i>Conceptual models</i> .....	102
4.3.2	<i>Physical mechanisms simulated</i> .....	103
4.4	GEOMETRY AND UNIT PROPERTIES .....	104
4.4.1	<i>Thermohydraulic properties</i> .....	106

4.4.2	<i>Internal heat generation</i> .....	106
4.4.3	<i>Faults properties</i> .....	106
4.5	MESHING .....	106
4.6	BOUNDARY CONDITIONS.....	108
4.6.1	<i>Groundwater flow</i> .....	108
4.6.2	<i>Heat transfer</i> .....	108
4.7	PARAMETERS SENSITIVITY .....	110
4.8	RESULTS.....	110
4.8.1	<i>2D subsurface temperature distribution</i> .....	110
4.8.2	<i>Parameters sensitivity</i> .....	114
4.9	DISCUSSION.....	116
4.9.1	<i>Implications of groundwater flow boundary conditions</i> .....	116
4.9.2	<i>Implications of faults on groundwater flow and heat transfer</i> .....	117
4.9.3	<i>Parameters sensitivity</i> .....	118
4.9.4	<i>Model limitation</i> .....	119
4.9.5	<i>Geothermal exploration</i> .....	120
4.10	CONCLUSIONS.....	121
<b>5</b>	<b>DISCUSSION GÉNÉRALE ET CONCLUSIONS.....</b>	<b>123</b>
5.1	LES PRINCIPAUX RESULTATS DE LA THESE ET SES CONTRIBUTIONS.....	123
5.2	IMPLICATIONS POUR L'EXPLORATION GEOTHERMIQUE DANS LES ZONES GEOTHERMIQUES D'AMBILOBE ET D'AMBANJA.....	125
5.2.1	<i>Ambilobe</i> .....	125
5.2.2	<i>Ambanja</i> .....	126
5.3	ÉTAPES FUTURES POUR UN DEVELOPPEMENT GEOTHERMIQUE DE LA REGION DU NORD DE MADAGASCAR .....	127
5.3.1	<i>Sondages géophysiques pour imager les structures profondes</i> .....	128
5.3.2	<i>Forage d'exploration carotté pour intercepter les failles profondes</i> .....	129
5.3.3	<i>Mesure de température dans les forages, réalisation de diagraphies et évaluation de la distribution spatiale des propriétés hydrauliques</i> .....	129
5.3.4	<i>Amélioration des modèles numériques basés sur les données géophysiques et de forages et définition de cibles pour les forages de production</i> .....	130
5.3.5	<i>Forage de production d'un plus gros diamètre et essais packer pour évaluer la perméabilité de façon <i>in situ</i> dans les zones de failles</i> .....	131
5.4	ÉVALUATION PRELIMINAIRE ECONOMIQUE .....	131
5.5	ÉVALUATION DE L'EMPREINTE CARBONE POUR L'APPLICATION DE L'ENERGIE GEOTHERMIQUE COMPAREE A CELLE DE LA BIOMASSE .....	132
<b>6</b>	<b>BIBLIOGRAPHIE.....</b>	<b>135</b>





## LISTE DES FIGURES

FIGURE 1.1	A) SOURCES D'ENERGIES CONSOMMEES A MADAGASCAR, ET B) SOURCES D'ENERGIES POUR LA PRODUCTION D'ELECTRICITE A MADAGASCAR (MINISTÈRE DE L'ENERGIE ET DES HYDROCARBURES, 2015; THE WORLD FACTBOOK, 2021). ....	2
FIGURE 1.2	RESEAU DE TRANSMISSION DE L'ELECTRICITE A MADAGASCAR (WORLD BANK, 2017).....	2
FIGURE 1.3	CHAMPS GEOTHERMIQUES DEVELOPPES DANS LE MONDE ET CONTEXTE TECTONIQUE (MODIFIE DE MOECK, 2014). MADAGASCAR SE SITUE DANS LA PLAQUE AFRICAINE ET EST DELIMITE EN ROUGE.....	6
FIGURE 1.4	SCHEMA STRUCTURAL DU RIFT EST-AFRICAIN (D'APRES CHOROWICZ, 1990) ET DE SON PROLONGEMENT SOUS-MARIN (MOUGENOT ET AL., 1986). MADAGASCAR AVEC SES PRINCIPALES STRUCTURES DE DEFORMATION SE SITUE DANS LA BRANCHE SUD-EST DU RIFT. ....	8
FIGURE 1.5	STRUCTURES NEOTECTONIQUES ACTUELLEMENT RECONNUES A MADAGASCAR (MODIFIEE D'APRES ARTHAUD ET AL., 1990; LARDEAUX ET AL., 1999; TUCKER ET AL., 2014) MONTRANT LA SEISMICITE ENREGISTREE DEPUIS 1973 (IRIS BASE DE DONNEES DE WWW.IRIS.EDU). LES MECANISMES DES TREMBLEMENTS DE TERRE DE MAGNITUDE $Mw \geq 5$ INDIQUENT UNE DOMINANCE DE FAILLES NORMALES (BERTIL ET AL., 1998).....	11
FIGURE 2.1	A) SIMPLIFIED GEOLOGICAL MAP OF MADAGASCAR (MODIFIED FROM ROIG ET AL., 2012; TUCKER ET AL., 2014), SHOWING THE LOCATION OF HOT SPRINGS AND THE GEOTHERMAL AREAS OF INTEREST (BESAIRIE, 1959; GUNNL AUGSSON ET AL., 1981). (B) AVERAGE CRUSTAL THICKNESS BENEATH SEDIMENTARY BASINS AND THE PRECAMBRIAN SHIELD IN THE GEOTHERMAL AREAS OF INTEREST (RINDRAHARISAONA ET AL., 2013; PRATT ET AL., 2017; ANDRIAMPENOMANANA ET AL., 2017).....	24
FIGURE 2.2	(A) LOCATION OF AMBILOBE GEOTHERMAL AREA, (B) DETAILED GEOLOGY SHOWING THE POSITION OF HOT SPRINGS, (MODIFIED FROM ROIG ET AL., 2012), AND (C) CONCEPTUAL MODEL OF AMBILOBE GEOTHERMAL SYSTEM IN THE ANDAVAKOERA FAULT ZONE. THE VERTICAL SCALE OF THE ELEVATION PROFILE, WHICH WAS CREATED USING ASTER IMAGERY, HAS BEEN EXAGGERATED COMPARED TO THE DEPTH SCALE, WHICH IS BASED ON THE STRUCTURE OF THE CRUST AND UPPERMOST MANTLE BENEATH MADAGASCAR (ANDRIAMPENOMANANA ET AL., 2017) .....	33
FIGURE 2.3	(A) LOCATION OF AMBANJA GEOTHERMAL AREA, (B) DETAILED GEOLOGY SHOWING POSITION OF THERMAL SPRINGS, (MODIFIED FROM ROIG ET AL., 2012), AND (C) CONCEPTUAL MODEL OF THE AMBANJA GEOTHERMAL SYSTEM IN THE SAMBIRANO GRABEN. THE VERTICAL SCALE OF THE ELEVATION PROFILE, WHICH WAS CREATED USING ASTER IMAGERY, HAS BEEN EXAGGERATED COMPARED TO THE DEPTH SCALE, WHICH IS BASED ON THE STRUCTURE OF THE CRUST AND UPPERMOST MANTLE BENEATH MADAGASCAR (ANDRIAMPENOMANANA ET AL., 2017) .....	36
FIGURE 2.4	(A) LOCATION OF THE ITASY GEOTHERMAL AREA, (B) DETAILED GEOLOGY SHOWING THE POSITION OF THERMAL SPRINGS (MODIFIED FROM ANDRIANAIVO ET AL., 2010B), AND (C) CONCEPTUAL MODEL OF THE ITASY PULL-APART BASIN GEOTHERMAL SYSTEM, (MODIFIED FROM ANDRIANAIVO ET AL., 2010A). THE VERTICAL SCALE OF THE ELEVATION PROFILE, WHICH WAS CREATED USING ASTER IMAGERY, HAS BEEN EXAGGERATED COMPARED TO THE DEPTH SCALE, WHICH IS BASED ON THE STRUCTURE OF THE CRUST AND UPPERMOST MANTLE BENEATH MADAGASCAR (ANDRIAMPENOMANANA ET AL., 2017).....	39
FIGURE 2.5	(A) LOCATION OF THE ANTSIRABE GEOTHERMAL AREA, (B) DETAILED GEOLOGY SHOWING THE POSITION OF THE HOT SPRINGS, (MODIFIED FROM RUFER 2009), AND (C) CONCEPTUAL MODEL OF THE ANTSIRABE BASIN GEOTHERMAL SYSTEM, (ADAPTED FROM RASOANIMANANA ET AL., 2012). THE VERTICAL SCALE OF THE ELEVATION PROFILE, WHICH WAS CREATED USING ASTER IMAGERY, HAS BEEN EXAGGERATED COMPARED TO THE DEPTH SCALE, WHICH IS BASED ON THE	

STRUCTURE OF THE CRUST AND UPPERMOST MANTLE BENEATH MADAGASCAR (ANDRIAMPENOMANANA ET AL., 2017).....	41
FIGURE 2.6 (A) LOCATION OF THE MIANDRIVAZO AND MORONDAVA GEOTHERMAL AREAS, (B) DETAILED GEOLOGY SHOWING THE POSITION OF THERMAL SPRINGS (MODIFIED FROM ROIG ET AL., 2012), AND (C) CONCEPTUAL MODEL OF THE MIANDRIVAZO-MORONDAVA GEOTHERMAL SYSTEMS. THE ELEVATION PROFILE WAS COMPILED USING ASTER IMAGERY, AND THE DEPTH SCALE IS BASED ON THE SEISMIC PROFILE (DU TOIT ET AL., 1997; PIQUÉ ET AL., 1999A). .....	45
FIGURE 3.1 (A) LOCATION OF THE AMBILLOBE AND AMBANJA GEOTHERMAL AREAS IN NORTH MADAGASCAR, AND (B AND C) GEOLOGICAL MAPS OF THE STUDY AREAS, (MODIFIED FROM ROIG ET AL., 2012), SHOWING TEMPERATURE DATA (GUNNL AUGSSON ET AL., 1981) AND THE NUMBERED LOCATIONS OF COLLECTED ROCK SAMPLES. ROSE DIAGRAMS ILLUSTRATE THE PRINCIPAL TREND OF FAULTS AND FRACTURES USING FIELD DATA COLLECTED IN 2018. .....	58
FIGURE 3.2 SYNTHESIZED STRATIGRAPHIC COLUMN OF THE AMBILLOBE AND AMBANJA GEOTHERMAL AREAS (ADAPTED FROM BESAIRIE, 1946). SAME LEGEND AS FIGURE 3.1. ....	59
FIGURE 3.3 PHOTOGRAPHS OF OUTCROP EXPOSURES IN THE AMBILLOBE AREA (NUMBERS IN PARENTHESES REFER TO THE SAMPLE LOCATIONS IN FIGURE 3.1): (A, 6) WEATHERED BASEMENT ROCKS FROM BETSIAKA GROUP; (B, 1) GREENISH-GREY TO BROWN PERMIAN SANDSTONES IN AN ABANDONED QUARRY NEAR THE VILLAGE OF ANKATOKO; (C, 2) TYPICAL PERMIAN SANDSTONE FORMATION FROM THE SAKAMENA GROUP, WITH CLOSE-UP OF ONE OF THE DARK REDDISH PURPLE LAYERS; (D, 5) EOTRIASSIC SHALE SHOWING FISSILE TEXTURE, WITH CLOSE-UP OF THE WEATHERED SURFACE AND SEALED FRACTURE NETWORK; AND (E, 9 AND 10) TRIASSIC SANDSTONES IN AN ARTISANAL ACTIVE QUARRY, WITH CLOSE-UP OF LAMINATIONS. ....	60
FIGURE 3.4 PHOTOGRAPHS OF OUTCROP EXPOSURES IN THE AMBANJA AREA (NUMBERS IN PARENTHESES REFER TO THE SAMPLE LOCATIONS IN FIGURE 3.1): (A, 13) AND (B, 11–12) PARAGNEISS FROM PROTEROZOIC BASEMENT ROCKS WITH A CLOSE-UP OF THE GNEISSIC TEXTURE; (C) CLIFF SECTION OF LATERITE-CAPPED BROWN TO RUSTY RED, WEATHERED TRIASSIC SANDSTONE IN CONTACT WITH THE WEATHERED BASEMENT; AND (D, 11) TRIASSIC SANDSTONE CUT BY A FRACTURE (BLACK DOTTED LINE), WITH CLOSE-UP OF FRESHLY BROKEN SANDSTONE WHERE A PORTABLE PERMEAMETER WAS USED TO TAKE PERMEABILITY MEASUREMENTS. ....	62
FIGURE 3.5 SUMMARY OF STEPS TO ASSESS HYDRAULIC AND THERMAL PROPERTIES IN OUTCROP EXPOSURES AND ROCK SAMPLES.....	64
FIGURE 3.6 THIN SECTION PHOTOMICROGRAPHS (PLANE-POLARIZED LIGHT) OF SANDSTONE AND SHALE FROM THE AMBILLOBE AND AMBANJA AREAS OF NORTH MADAGASCAR (NUMBERS IN PARENTHESES REFER TO SAMPLE LOCATIONS IN FIGURE 3.1): (A, 1 AND B, 4) PERMIAN SANDSTONE WITH MEDIUM-GRAINED, WELL-SORTED, ANGULAR TO SUBROUNDED QUARTZ (Qz) AND FELDSPAR GRAINS, MUSCOVITE (Ms) AND ORGANIC MATTER (Om); (C, 9 AND D, 17) MEDIUM-GRAINED TRIASSIC SANDSTONE WITH MODERATELY TO WELL-SORTED, ANGULAR TO SUBROUNDED QUARTZ AND FELDSPAR GRAINS WITH PREVALENT INTERGRANULAR MICROFISSEURES; (E, 1) FOSSIL-FREE EOTRIASSIC SHALE SHOWING COMPACTION CLEAVAGE (PC); (F, 1) EOTRIASSIC SHALE WITH MICROMETRIC VEINS OF QUARTZ AND ALTERATION; (G, 2) SCANNED IMAGE OF ENTIRE THIN SECTION OF BRECCIA; AND (H) CLASSIFICATION OF THE SANDSTONE SAMPLES USING A TERNARY QFL DIAGRAM. ....	69
FIGURE 3.7 THIN SECTION PHOTOMICROGRAPHS (PLANE-POLARIZED LIGHT) OF BASEMENT ROCKS FROM THE AMBILLOBE AND AMBANJA AREAS IN NORTH MADAGASCAR (NUMBERS IN PARENTHESES REFER TO SAMPLE LOCATIONS IN FIGURE 3.1): (A, 11) BIOTITE PARAGNEISS WITH LEPODOBLASTIC TEXTURE, (B, 11) PARAGNEISS WITH GARNET-RICH GRANOBLASTIC TEXTURE; (C, 3) ORTHOGNEISS; (D, 6) AMPHIBOLITE; (E, 7) MICA SCHIST; (F, 14) SYENITE; (G, 14) PORPHYRITIC BASALT; AND (H) TERNARY QFM DIAGRAM COMBINED WITH QP DIAGRAM SHOWING THE MAJOR MINERAL CONTENTS OF THE PARAGNEISS SAMPLES FROM THE AMBILLOBE AND AMBANJA AREAS AND THEIR MAIN COMPOSITIONAL RANGE. THE PLOTTED PARAGNEISS SAMPLES ARE FROM THOMAS ET AL. (2009). Qz=QUARTZ, Ms=MUSCOVITE, Bt=BIOTITE, Pl=PLAGIOLCLASE,	

MC=MICROCLINE, FSP=FELDSPAR, AMP=AMPHIBOLE, HBL=HORNBLENDE, NPH=NEPHELITE, AUG=AUGITE, AEG=AEGIRINE. ....	70
FIGURE 3.8 COMPARISON OF PERMEABILITY VALUES OBTAINED WITH A HAND-HELD PERMEAMETER AND A GAS PERMEAMETER-POROSIMETER. P STANDS FOR PERMIAN AND T FOR TRIAS.....	74
FIGURE 3.9 A) PERMEABILITY AND B) POROSITY VERSUS CONFINING PRESSURE FOR ANALYZED ROCK SAMPLES FROM THE AMBILOBE AND AMBANJA AREAS. A LOGARITHMIC REGRESSION CURVE IS SHOWN FOR EACH SAMPLE.....	76
FIGURE 3.10 CROSS-PLOT OF PERMEABILITY VERSUS POROSITY FOR ALL STUDIED LITHOTYPES. ....	76
FIGURE 3.11 WHISKER PLOTS OF THERMAL PROPERTIES CLASSIFIED BY GEOLOGICAL UNIT FOR BASEMENT AND SEDIMENTARY ROCKS FROM THE AMBILOBE AND AMBANJA AREAS.....	78
FIGURE 3.12 THERMAL PROPERTIES AS A FUNCTION OF POROSITY. THE LINES CORRESPOND TO THE TREND OF A) THERMAL CONDUCTIVITY CALCULATED FOR DRY SAMPLES USING THE MAXWELL EQUATION (HEAP ET AL., 2020), B) EFFECTIVE DIFFUSIVITY AND C) VOLUMETRIC HEAT CAPACITY. ....	79
FIGURE 3.13 EXPECTED HEAT TRANSFER MECHANISM ACCORDING TO THE THERMOFACIES CONCEPT OF SASS ET AL. (2012). DATA FROM OTHER GEOTHERMAL SYSTEMS ARE ALSO PRESENTED: HUNGARY BASIN (SASS ET AL., 2012), RHINE GRABEN (HAFFEN ET AL., 2013; HETTKAMP ET AL., 1999), AND KAROO BASIN (CAMPBELL ET AL., 2016A; CAMPBELL ET AL., 2016B) .....	90
FIGURE 3.14 POROSITY VERSUS PERMEABILITY DATA FROM THIS STUDY LINKED TO POTENTIAL GEOTHERMAL DEVELOPMENT, BASED ON THE DIAGRAM DEVELOPED BY (MOECK, 2014; MOECK ET AL., 2019). EGS= ENHANCED GEOTHERMAL SYSTEM.....	91
FIGURE 4.1 SIMPLIFIED GEOLOGICAL MAP WITH CLOSE-UP TO TECTONIC FRAMEWORK OF BEMARIVO DOMAIN IN NORTHERN MADAGASCAR (MODIFIED FROM THOMAS ET AL., 2009; ARMISTEAD ET AL., 2019) AND WHERE THE AREAS OF INTEREST: AMBILOBE AND AMBANJA ARE LOCATED. THE GEOLOGICAL MAP IN THE RIGHT SIDE SHOWS THE MAIN SIX GEODYNAMIC PRECAMBRIAN DOMAINS THAT FORM THE MADAGASCAR SHIELD (MODIFIED FROM DE WAELE ET AL., 2011; TUCKER ET AL., 2014). .	98
FIGURE 4.2 (A) LOCATION OF AMBILOBE AND AMBANJA GEOTHERMAL AREAS WITH (B) AND (C) BEING DETAILED GEOLOGY (MODIFIED FROM ROIG ET AL., 2012). THE ROSE DIAGRAMS ILLUSTRATE THE MAJOR DIRECTION OF FAULTS AND FRACTURES THAT WAS ESTABLISHED FROM FIELD DATA COLLECTED IN 2018. ....	100
FIGURE 4.3 CHEMICAL COMPOSITION OF WATER ON A TERNARY NA-K-MG DIAGRAM (GIGGENBACH, 1988) FOR HOT SPRINGS OF AMBILOBE (AMBL) AND AMBANJA (AMBJ). THE CONCENTRATION OF Na, K, Mg WAS REPORTED BY GUNNL AUGSSON ET AL., (1981). ....	101
FIGURE 4.4 GEOMETRY AND BOUNDARY CONDITIONS OF THE 2D NUMERICAL MODEL BASED ON THE GEOLOGICAL CROSS-SECTION (AA') AND (BB') IN FIGURE 4.2 REPRESENTING A) AMBILOBE IN THE ANDAVAKOERA NORMAL FAULT ZONE WITH BASEMENT–SEDIMENTS CONTACT, AND B) AMBANJA GRABEN. RIV STANDS FOR RIVER. ....	103
FIGURE 4.5 FINITE ELEMENT MESH OF THE 2D NUMERICAL MODELS FOR A) AMBILOBE IN THE ANDAVAKOERA NORMAL FAULT ZONE WITH BASEMENT–SEDIMENTS CONTACT, AND B) THE GRABEN OF AMBANJA. .....	107
FIGURE 4.6 A MESH CONVERGENCE STUDY A) FOR AMBILOBE AND B) FOR AMBANJA MODELS.....	108
FIGURE 4.7 SIMULATED TEMPERATURE DISTRIBUTION FOR AMBILOBE 2D MODEL CONSIDERING THE VARIATION OF THE FAULT DIP AND THE VARIATION OF THE HEAT FLUX AT THE 10 KM DEPTH. THE BLACK ARROWS SHOW THE VELOCITY FIELD AND FLOW DIRECTION, THE WHITE LINES ARE ISOTHERMS .....	111
FIGURE 4.8 TEMPERATURE PROFILES AS A FUNCTION OF DEPTH ALONG THE FAULT LINES FOR THE AMBILOBE 2D MODEL. THE TEMPERATURE PROFILES IN SCENARIO 0 ARE OBTAINED FROM AN AVERAGE CUTLINE DRAWN IN THE MODEL WITHOUT FAULTS.....	112

FIGURE 4.9	SIMULATED TEMPERATURE DISTRIBUTION FOR AMBANJA 2D MODEL CONSIDERING THE VARIATION OF THE FAULT DIP AND THE VARIATION OF THE HEAT FLUX AT THE 10 KM DEPTH. THE BLACK ARROWS SHOW THE VELOCITY FIELD AND FLOW DIRECTION, THE WHITE LINES ARE ISOTHERMS.....	113
FIGURE 4.10	TEMPERATURE PROFILES AS A FUNCTION OF DEPTH ALONG THE FAULT LINES FOR THE AMBANJA 2D MODEL. THE TEMPERATURE PROFILES IN SCENARIO 0 ARE OBTAINED FROM AN AVERAGE CUTLINE DRAWN IN THE MODEL WITHOUT FAULTS.....	114
FIGURE 4.11	DEPTH VARIATION OF RESERVOIR TEMPERATURE ALONG THE FAULT LINES FOR THE AMBLOBE 2D MODEL ACCORDING TO DIFFERENT SCENARIOS OF FAULT DIPS A) AS A FUNCTION OF HEAT FLOW AND FAULT APERTURE, AND B) AS A FUNCTION OF HEAT FLOW AND FAULT PERMEABILITY. THE DOTTED LINE INDICATES THE TREND OF DEPTH VARIATION.....	115
FIGURE 4.12	DEPTH VARIATION OF RESERVOIR TEMPERATURE ALONG THE FAULT LINES FOR THE AMBANJA 2D MODEL ACCORDING TO DIFFERENT SCENARIOS OF FAULT DIPS A) AS A FUNCTION OF HEAT FLOW AND FAULT APERTURE, AND B) AS A FUNCTION OF HEAT FLOW AND FAULT PERMEABILITY. THE DOTTED LINE INDICATES THE TREND OF DEPTH VARIATION.....	116
FIGURE 5.1	PROGRAMME D'EXPLORATION GEOTHERMIQUE POUR LES ZONES D'INTERET : AMBLOBE ET AMBANJA. LES DIFFERENTES PHASES COMPORTENT LES ACTIVITES A POURSUIVRE, LES ANALYSES ET LES OPTIONS DE DECISION QUI SONT BASEES SUR LES STRATEGIES POUR L'EXPLORATION DANS LES REGIONS A CONTEXTE EXTENSIF PROPOSEES PAR HERVEY ET AL., (2014); SERTAC ET AL., (2015).....	128

## LISTE DES TABLEAUX

TABLEAU 1.1	CLASSIFICATION DES SOURCES GEOTHERMIQUES SELON DIFFERENTS AUTEURS .....	4
TABLE 2.1	EXAMPLE OF THE GEOTHERMAL SYSTEM CLASSIFICATION FOR MADAGASCAR .....	26
TABLE 2.2	GEOLOGICAL AND TECTONIC CONTROLS FOR PROSPECTIVE AREAS IN MADAGASCAR.....	28
TABLE 2.3	GEOLOGICAL AND GEOTHERMAL CHARACTERISTICS FOR PROSPECTIVE AREAS IN MADAGASCAR .....	29
TABLE 2.4	GEOTHERMAL SYSTEM CLASSES FOR PROSPECTIVE AREAS IN MADAGASCAR.....	30
TABLE 2.5	SHARED FEATURES BETWEEN MADAGASCAR GEOTHERMAL AREAS AND GLOBAL ANALOGUES ..	49
TABLE 3.1	SUMMARY OF GEOLOGICAL MATERIAL SAMPLED AND USED IN THE PRESENT STUDY, INDICATING AGE AND GEOLOGICAL UNIT. OUTCROP LOCATIONS CORRESPOND TO FIGURE 3.1 .....	63
TABLE 3.2	HYDRAULIC PROPERTIES OF ROCKS FROM THE AMBILLOBE AND AMBANJA AREAS. ....	72
TABLE 3.3	HEAT-PRODUCING ELEMENTS, ROCK DENSITIES AND RADIOGENIC HEAT PRODUCTION OF THE MAIN GEOLOGICAL UNITS IN THE AMBILLOBE AND AMBANJA AREAS.....	80
TABLE 3.4	AVERAGE POROSITY AND PERMEABILITY OBTAINED FROM MEASUREMENTS ON CORE PLUGS: EXAMPLES FROM AROUND THE WORLD COMPARED TO ROCK UNITS IN THE AMBILLOBE AND AMBANJA GEOTHERMAL AREAS. THE MEAN PERMEABILITY FOR THE PRESENT STUDY CORRESPONDS TO THE AVERAGE OF VALUES OBTAINED FROM THE PORTABLE PERMEAMETER AND COMBINED GAS POROSIMETER-PERMEAMETER .....	84
TABLE 4.1	FAULT SCENARIOS.....	103
TABLE 4.2	MODEL INPUT PARAMETERS .....	105
TABLE 4.3	MESH STATISTICS OF AMBILLOBE AND AMBANJA 2D MODELS .....	107
TABLE 4.4	DATA FROM SELECTED METEOROLOGICAL STATIONS IN MADAGASCAR.....	109
TABLE 4.5	PARAMETERS FOR HEAT TRANSFER BOUNDARY CONDITION.....	109



## **LISTE DES ÉQUATIONS**

ÉQUATION 3.1 .....	65
ÉQUATION 3.2 .....	67
ÉQUATION 4.1 .....	67
ÉQUATION 4.2 .....	107
ÉQUATION 4.3 .....	109
ÉQUATION 4.4 .....	109



## NOMENCLATURE

	<b>Symbol</b>	<b>Unit</b>
A	Radiogenic heat production	$\mu\text{W m}^{-3}$
c	Specific heat	$\text{J kg}^{-1} \text{K}^{-1}$
Df	Aperture	m
Kf	Fracture permeability	$\text{m}^2$
T	Temperature	$^{\circ}\text{C}$
Q	Heat flow	$\text{mW m}^{-2}$
z	Altitude, depth	m, km
<b>Greek letters</b>		
$\alpha$	Thermal diffusivity	$\text{m}^2 \text{s}^{-1}$
$\Delta$	Variation	---
$\kappa$	Permeability	$\text{m}^2$
$\lambda$	Thermal conductivity	$\text{W m}^{-1} \text{K}^{-1}$
$\rho$	Density	$\text{kg m}^{-3}$
$\rho_c$	Volumetric heat capacity	$\text{J m}^{-3} \text{K}^{-1}$
$\emptyset, \varphi$	Porosity	%, fraction
<b>Subscript</b>		
LC	Lower crust	
max	Maximum	
min	Minimum	
UC	Upper crust	
<b>Abreviation</b>		
CPD	Curie depth point	
F1, F2	Fault1, Fault 2	
EGS	Enhanced/Engineered Geothermal Systems	
GRS	Gamma-ray spectrometry	
LCOE	Levelized Cost of Energy	
GES	Gaz à effet de serre	
NNE	North North East / Nord-Nord-Est	
NNW	North North West	
NNO	Nord-Nord-Ouest	
S	South / Sud	
SE	South East / Sud-Est	
SSE	South South East / Sud-Sud-Est	
SSW	South South West	
SSO	Sud-Sud-Ouest	
TCS	Thermal conductivity scanner	
UNCF	United Nations Framework Classification	
USD	US dollars	
USA	United States of America	

# **1 INTRODUCTION**

---

## **1.1 Mise en contexte**

Le modèle de croissance économique de Madagascar pose un problème environnemental majeur considérant la structure de sa consommation d'énergie (Voninirina et al., 2014). La principale source d'énergie à Madagascar dépend essentiellement des énergies fossiles et de la biomasse telle que le charbon de bois (Figure 1.1a). Selon les données de 2016 (The World Factbook, 2021), l'électricité est produite à partir des combustibles fossiles pour 74 % de la capacité totale installée, 24 % à partir des centrales hydroélectriques et 2 % provenant d'autres sources (Figure 1.1b). Le taux moyen d'électrification est de 39 % dont 23 % seulement dans le rural contre 64 % en milieu urbain et avec un réseau de transmission peu développé (Figure 1.2). L'insécurité énergétique à Madagascar reste un frein pour son développement social et économique et porte un enjeu majeur dans sa politique de protection de l'environnement malgré le fait, qu'il fasse partie des pays dont le taux d'émission de CO<sub>2</sub> est encore bas, soit 0.152/tonne/habitant (The World Factbook, 2021).

Toutefois, des nouvelles dispositions ont été inscrites dans la politique énergétique de Madagascar en tenant compte de son impact sur l'économie et sans omettre la prise en considération des impacts environnementaux. À cet effet, dans la nouvelle politique nationale énergétique (2015 - 2030), le gouvernement Malagasy prévoit une amélioration de la couverture nationale en électricité de 15 % à 70 % en accroissant la part des énergies renouvelables à 85 % dans le mix pour la transition énergétique, selon le Ministère de l'énergie et des hydrocarbures (2015). Ces énergies renouvelables peuvent offrir des retombées économiques considérables, tout en garantissant une faible empreinte environnementale. Parmi ces sources, la production d'électricité à partir des centrales géothermiques connaît une croissance significative. De par son contexte géologique, les projets similaires réussis dans les pays africains, notamment au Kenya et en Tanzanie, incitent Madagascar à définir son potentiel géothermique. Ces travaux sont réalisés à travers l'initiative «Mise en cartographie stratégique des ressources d'énergie renouvelable», en cours depuis 2013 avec l'appui financier de la Banque mondiale. Madagascar fait partie des pays qui participent à la phase initiale de ce programme et les travaux de ce doctorat aideront à bonifier sa réalisation. L'objectif est d'accroître le taux de desserte en électricité en milieu rural. Cependant, les ressources géothermiques n'ont été que sommairement explorées à ce jour et il manque encore une expertise locale pour appuyer avec des bases scientifiques ce secteur industriel.

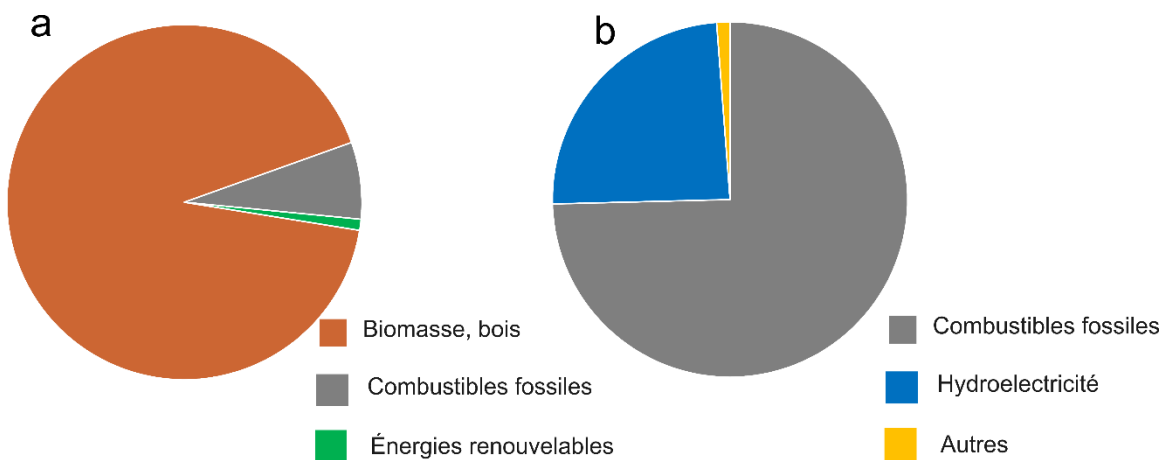


**Figure 1.1** a) Sources d'énergies consommées à Madagascar, et b) sources d'énergies pour la production d'électricité à Madagascar (Ministère de l'énergie et des hydrocarbures, 2015; The World Factbook, 2021).

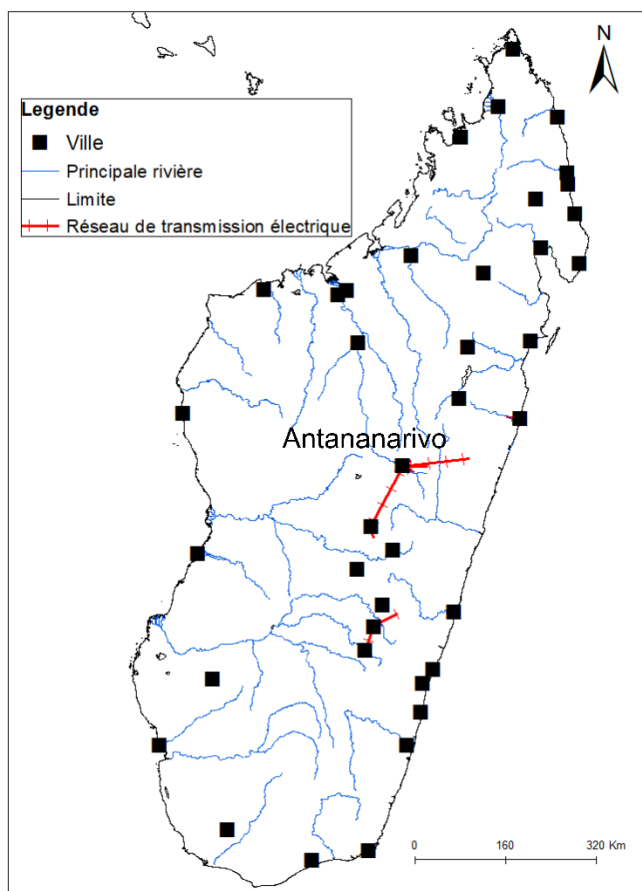


**Figure 1.2** Réseau de transmission de l'électricité à Madagascar (World Bank, 2017)

Le but de cette thèse est de mieux comprendre la formation des ressources géothermiques dans les grandes zones de failles à contexte tectonique extensif de la région Nord de Madagascar. L'idée est de développer des connaissances scientifiques pour mieux délimiter les contextes favorables au développement géothermique de cette région.

## 1.2 Revue de littérature

### 1.2.1 Contexte tectonique et distribution des ressources géothermiques dans le monde

Le contexte tectonique et les structures de déformation engendrées, ainsi que le contexte géologique associé, peuvent contrôler et expliquer la distribution et l'existence des champs géothermiques et permettent de caractériser le système et la ressource géothermique qui y sont reliés. La distribution des champs géothermiques développés dans le monde associée au contexte tectonique est présentée à la carte de la figure 1.3.

Un champ géothermique est une zone géographique, généralement une zone d'activité géothermique à la surface de la terre. Dans les cas où cette activité ne se manifeste pas en surface, ce terme peut être utilisé pour indiquer la superficie en surface correspondant au réservoir géothermique en profondeur (Dickson et al., 2003; Axelsson, 2008).

Un système géothermique se définit par l'existence d'une source de chaleur, d'un volume de roche suffisamment poreux ou fracturé et perméable (l'aquifère) appelé réservoir au niveau duquel circule le fluide ou source d'énergie géothermique<sup>1</sup> qui est majoritairement de l'eau, et d'une formation imperméable dite couverture ou cap rock (Dickson et al., 2003; Williams et al., 2011).

La source (ou ressource) d'énergie géothermique est catégorisée sur la base de la température, de l'enthalpie qui est proportionnelle à la température, de l'état physique et de l'exergie qui est la

---

<sup>1</sup> La source d'énergie géothermique - "énergie thermique contenue dans un corps de roche, de sédiments et/ou de sol, y compris tout fluide contenu, qui est disponible pour l'extraction et la conversion en produits énergétiques. (...) La source d'énergie géothermique résulte de tout flux entrant ou sortant ou de la production interne d'énergie au sein du système pendant une période déterminée" traduit de (UNCF, Falcone et al., 2016).

capacité de la source à effectuer un travail thermodynamique pour la conversion de chaleur en énergie électrique (Tableau 1.1):

**Tableau 1.1 Classification des sources géothermiques selon différents auteurs.**

Température (°C)	<150	150-200	>200	Axelsson (2008); Hochstein (1990); Muffler et al., (1978); Williams et al., (2011)
Enthalpie (kJ/kg)	Basse <800	Moyenne 800	Haute > 800	Axelsson (2008); Dickson et al. (2003)
Phase du fluide mobile dans le réservoir	Liquide	Liquide/vapeur	Vapeur	Sanyal (2005); White (1973b)
Exergie (SExi)	<0.05	0.05-0.5	>0.5	Lee (2001)

La source de chaleur a pour principale origine une intrusion magmatique toujours en fusion et situé dans la croûte supérieure à des profondeurs de 5 à 10 km, une intrusion magmatique récemment cristallisée qui est en cours de refroidissement au niveau de la croûte ou la désintégration des éléments radioactifs (U, Th, K) d'un corps magmatique ou d'une formation rocheuse qui en est principalement enrichi.

Au niveau de ces champs géothermiques, le gradient géothermique et le flux de chaleur qui en découle y sont généralement plus élevés. Un grand nombre de champs géothermiques explorés se trouvent ainsi le long des zones d'extension, de subduction et au niveau des bassins d'arrière-arc, où l'on peut retrouver des anomalies de fusion, c'est-à-dire là où il y a une activité tectonique et volcanique récente, principalement le long des limites de plaques tectoniques actives (Muffler et al., 1978) ; Figure 1.3.

a) Contexte magmatique :

Les ressources de haute enthalpie se retrouvent généralement dans divers contextes **magmatiques**, soit de points chauds ou de volcanisme de points chauds (par ex.: Hawaï), - d'arcs volcaniques de zone de subduction (par ex. : Java), d'extension océanique ou de ridges méridionaux (par ex. : Islande) et de plutonisme récent et d'extension (par ex.: Lardello-Italie).

Au niveau des marges actives de subduction, de grandes zones de la croûte atteignent une température supérieure à 300°C à une faible profondeur. Ces zones subissent des conditions de fusion à quelques kilomètres de profondeur. Le magmatisme calco-alcalin généré est à l'origine des intrusions, des suites granitiques observées à de faibles profondeurs ainsi qu'au volcanisme apparenté de composition intermédiaire à felsique. Ce phénomène convectif à l'échelle de la

lithosphère est également responsable de la concentration des radioéléments U, K et Th dans la croûte supérieure, ce qui contribue au potentiel géothermique sur les continents (Ledru et al., 2010).

b) Contexte non magmatique

Les systèmes géothermiques à haute enthalpie sont aussi fréquents dans les contextes d'extension et de transtension **non magmatiques**, comme plus précisément dans la province du Great Basin ou Basin and Range au sud-ouest des États-Unis ou encore dans l'ouest de la Turquie, où les failles normales sont les principaux contrôles de l'activité géothermique, et dans les bassins pull-apart ayant des systèmes de failles coulissantes (par ex : Salton Trough, Californie).

Des systèmes de basse enthalpie se trouvent également dans le contexte ci-dessus, ainsi que dans des environnements tectoniques relativement calmes, des bassins sédimentaires profonds comme dans le bassin de Paris et les bassins de l'Allemagne du Nord, ou au niveau des marges de plaques convergentes telles que les bassins molassiques d'avant-arc comme celui de la chaîne alpine (Moeck, 2014).

L'exploitation des ressources géothermiques dans les zones qui se situent dans des contextes tectoniques d'extension est encore généralement restreinte. Les domaines d'extension où la convection forcée ou naturelle a été identifiée comme le principal mécanisme de transfert thermique, comme pour la province du Basin and Range aux États-Unis et dans l'ouest de la Turquie, représentent moins de 10 % de la production géothermique mondiale.

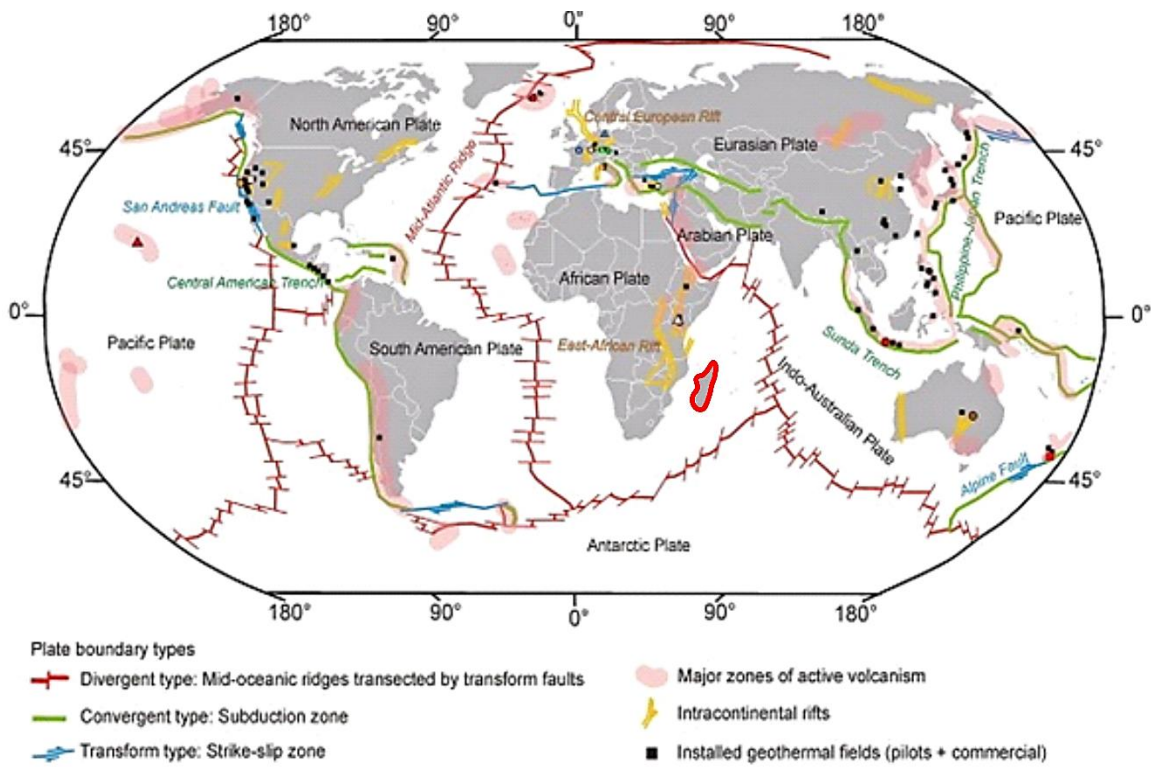


**Figure 1.3 Champs géothermiques développés dans le monde et contexte tectonique (modifié de Moeck, 2014).** Madagascar se situe dans la plaque africaine et est délimité en rouge.

### 1.2.2 Système et réservoir géothermique

Connaître les caractéristiques des réservoirs géothermiques permet d'aider à comprendre la nature de la ressource, d'évaluer son exploitabilité et de déterminer son potentiel de conversion de chaleur en énergie électrique. Le but est de prévoir la performance d'un réservoir géothermique et de définir les stratégies appliquées pour son exploitation. Cette étape est importante, particulièrement lors des travaux préliminaires d'exploration.

En ce sens, des travaux ont été publiés sur la classification des systèmes géothermiques basés sur la température du fluide et sa capacité à produire de l'énergie tels que présentés plus haut dans le Tableau 1.1 (Muffler, 1979; Hochstein et al., 1990; Nicholson, 1993; Axelsson, 2008; Sanyal, 2005; Williams et al., 2011; Moeck, 2014).

De récents travaux proposent un catalogue sur la classification des systèmes géothermiques, soulignant l'importance de l'environnement géologique (Moeck, 2014) auquel le réservoir est associé. Les contextes tectoniques, structuraux, lithostratigraphiques et hydrogéologiques, ainsi que les implications face au mode de transfert de la chaleur sont des critères de cette classification. Les récents progrès technologiques du domaine, permettent également de

distinguer les systèmes géothermiques ouvrages (EGS – enhanced geothermal systems) qui peuvent être aménagés dans des environnements peu perméables puisque leur développement repose sur la stimulation du réservoir (par ex: Gallup, 2009; Genter et al., 2010). Les travaux de Sass et al., (2012) ont également défini les systèmes géothermiques en proposant un concept de thermofaciès, soit une classification thermohydraulique basée sur la corrélation des propriétés pétrophysiques (perméabilité, conductivité thermique) des unités rocheuses avec leur faciès lithostratigraphique et le mécanisme de transfert de chaleur (convection naturelle et forcée versus conduction) qui domine le système.

Selon ces auteurs (Sass et al., 2012; Moeck, 2014), une région tectoniquement active avec un volcanisme ou plutonisme récent induisant un gradient géothermique élevé et dont le réservoir est constitué de roches ayant une perméabilité et une porosité appréciable implique un régime de transfert de chaleur convectif naturel. Un contexte extensif non magmatique dans lequel les failles et les fractures sont responsables d'une perméabilité et d'une porosité de valeur intermédiaire implique un transfert de chaleur par convection forcée. À l'opposé, de faible perméabilité et porosité impliquent un transfert de chaleur par conduction où les formations géologiques profondes sont chauffées par le flux de chaleur terrestre et/ou par la dégradation des éléments radioactifs dans des systèmes appelés pétrothermaux.

### **1.2.3 La ressource géothermique de l'Afrique**

Les ressources en énergie géothermique de l'Afrique, comme celles du reste du monde, sont réparties et développées de manière inégale sur le continent. Cette ressource se trouve dans 21 pays (Omenda, 2018), dont la majorité se situe dans le grand système du Rift est-africain (EARS; East African Rift System; Figure 1.4), l'une des principales structures tectoniques de la planète, qui s'étend sur environ 6 500 km du Moyen-Orient (mer Morte et vallée de la Jordanie) au nord, jusqu'au Mozambique et à Madagascar au sud (Chorowicz, 1990). Le reste des pays étant en Afrique du Nord et de l'Ouest. Ce système est constitué de trois bras principaux : le rift de la mer Rouge ; le rift du golfe d'Aden ; et l'EARS qui se développe à travers l'Érythrée, l'Éthiopie, le Kenya, la Tanzanie, la Zambie, le Malawi et le nord du Mozambique au-dessous duquel se trouve une croûte continentale amincie (Figure 1.4).

L'Afrique en matière de sources d'énergie géothermique renouvelable, en utilisant la technologie actuelle, a une puissance installée de plus de 20 000 MWe (Nyakabwa-Atwoki, 2020 et les références qui y sont citées), mais cette ressource reste inexploitée ce qui, à ce jour, place le

continent dans une pauvreté énergétique, c'est-à-dire que la demande énergétique n'est pas satisfaite par l'offre.

Ces pays d'Afrique et les autres du continent se sont engagés à tenir des promesses ambitieuses pour atteindre l'objectif "Énergie durable pour tous" (SE4ALL; Sustainable Energy for All) en 2030.

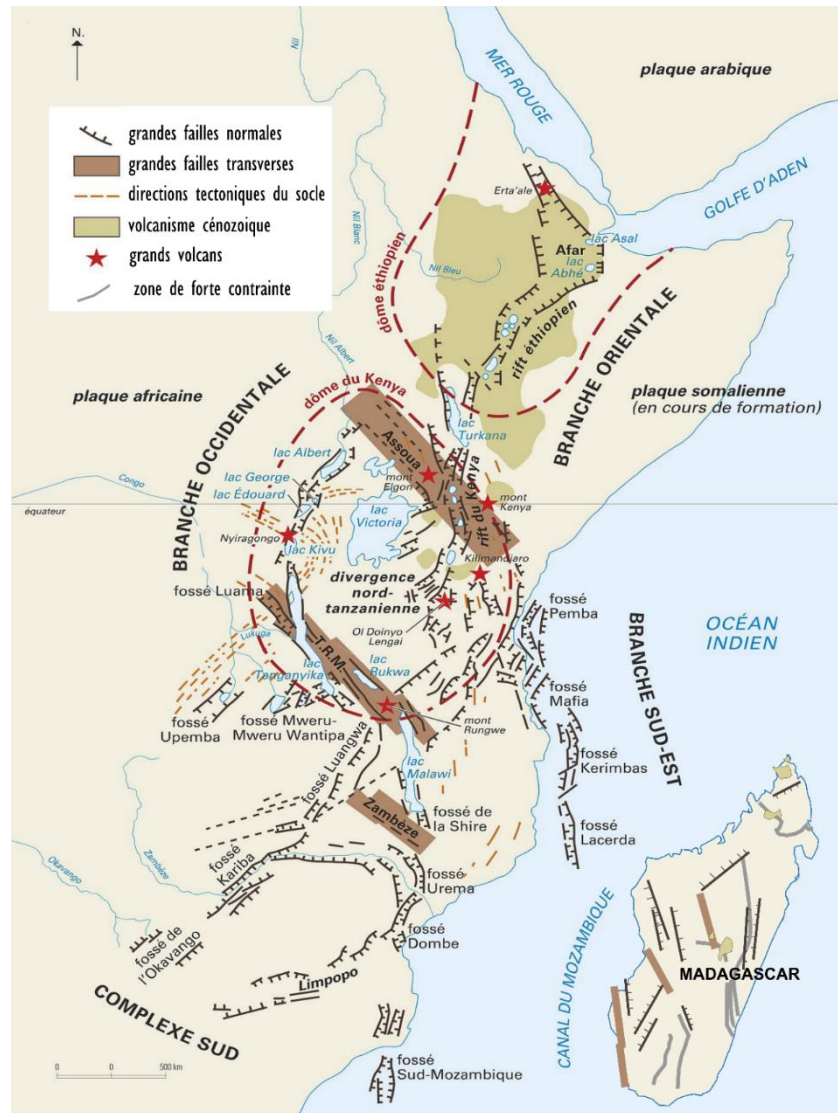


**Figure 1.4 Schéma structural du Rift est-africain (d'après Chorowicz, 1990) et de son prolongement sous-marin (Mougenot et al., 1986). Madagascar avec ses principales structures de déformation se situe dans la branche sud-est du rift.**

#### **1.2.4 Contexte tectonique de Madagascar en relation avec son potentiel géothermique**

Le contexte et l'histoire tectonique de Madagascar sont résumés ci-dessous afin de décrire la répartition et l'existence des champs géothermiques identifiés à Madagascar.

Les premières évaluations du potentiel géothermique à Madagascar ont d'ailleurs débuté par des travaux de reconnaissance et d'inventaire des sources d'eaux thermales et ont permis d'identifier huit sites potentiels parmi lesquels six ont été désignés prioritaires selon les températures des réservoirs estimées à plus de 150°C (Gunnlaugsson et al., 1981; Chovelon, 1984) :

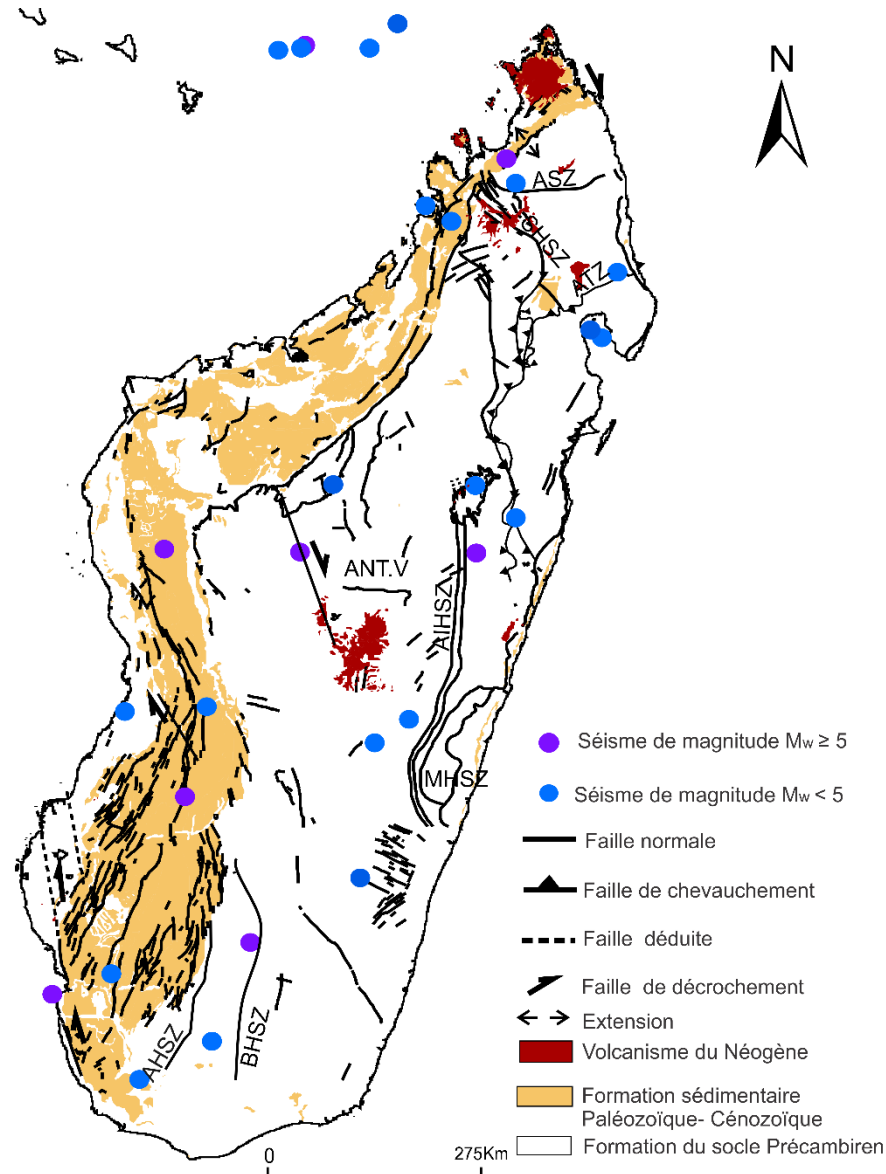
- Au Nord : Ambilobe et Ambanja;
- Dans le Centre Ouest et le Centre Sud : Itasy et Antsirabe;
- À l'Ouest : Miandrivazo et Monrondava.

Ces sites sont répartis dans les régions de contextes géologiques particuliers que sont d'une manière générale le socle volcanique, le socle tectono-métamorphique et les bassins sédimentaires Malagasy.

Le contexte tectonique général de Madagascar peut se résumer à un socle précambrien considérablement retravaillé par de multiples événements orogéniques tout au long du Protérozoïque, constituant ainsi les ceintures tectoniques du Néoprotérozoïque d'arc océanique, d'arc continental, et d'accrétion continentale (De Wit, 2003; Kusky et al., 2007; Phethean et al., 2016). Ce socle est découpé en six unités tectono-métamorphiques (De Wit, 2003; Collins, 2006; Tucker et al., 2014). On compte trois principaux bassins au nord, au nord-ouest et à l'ouest. Les dépôts qui les constituent sont datés du Carbonifère à l'Actuel et peuvent atteindre 8 km d'épaisseur. Ils sont déposés en discordance sur la partie ouest du socle, au-dessous de laquelle la croûte est inhabituellement mince d'une épaisseur de 12 km (Wysession et al., 2016 ; Rindraharisaona et al., 2017). Il s'agit de bassins marginaux mis en place pendant le rift Africain au Jurassique (rift de Karoo). Ce dernier s'est avorté au Crétacé inférieur et la côte ouest de Madagascar a évolué en une marge passive qui a connu un cycle de transgression-régression jusqu'à la fin du Crétacé (Razafimbelo, 1987; Rajaomazava, 1992; Rasamimanana et al., 1998b; De Wit, 2003).

Les zones d'accidents majeurs (failles et fractures d'extension) et les zones de cisaillement (Figure 1.5) se trouvent aussi bien dans le socle que dans les bassins sédimentaires (Arthaud et al., 1990; Collins, 2006; Kusky et al., 2007; Lardeaux et al., 1999; Martelat et al., 2000; Tucker et al., 2014). Le contact socle-bassin sédimentaire est d'ailleurs en certains endroits marqué par

des failles extensives. Certaines de ces failles et fractures majeures sont associées aux épisodes volcaniques du Néogène au Quaternaire dont les plus récents, se sont manifestés : 1- dans le Centre soit  $8.62 \pm 0.09$  Ma, (Cucciniello et al., 2016; Cucciniello et al., 2017) et ~3 Ma (Rufer, 2009; Bardintzeff et al., 2010), 2- dans le Nord ~17 Ma à 0.83 Ma (Estrade et al., 2014 et les références qui y sont citées), et 3- dans Sud-Ouest de Madagascar soit ~12 Ma (Melluso et al., 2018). De nombreuses intrusions alcalines du Cénozoïque seraient également associées à des fractures d'extension N65°E à N85°E du Plio-Quaternaire d'après Chorowicz et al., (1997).



ANT. V = Antananarivo high strain zone; AIHSZ = Angavo-Ifanadiana high strain zone; ATZ = Andaparaty thrust zone; BHSZ = Beraketa high strain zone; MHSZ = Maroala high strain zone; SHSZ -ASZ= Sandrakota-Antsaba high strain zone

**Figure 1.5 Structures néotectoniques actuellement reconnues à Madagascar (modifiée d'après Arthaud et al., 1990; Lardeaux et al., 1999; Tucker et al., 2014) montrant la séismicité enregistrée depuis 1973 (IRIS base de données de [www.iris.edu](http://www.iris.edu)). Les mécanismes des tremblements de terre de magnitude  $M_w \geq 5$  indiquent une dominance de failles normales (Bertil et al., 1998).**

Les structures cassantes ont trois directions principales : N0-N020; N140-N160 et N100-N110. Ces directions sont rattachées aux principales phases de rift :

- les failles NNE-SSO et NNO-SSE sont liées à l'extension du Trias au Jurassique (rift de Karoo);
- les directions N140-N160 (Jurassique-Crétacé supérieur) constituent des failles secondaires dextres d'un système de failles coulissantes cohérent avec le développement de la Ride Davie.

Dans d'autres endroits, ces failles NNO-SSE sont associées à une extension qui coïncide avec le volcanisme du Crétacé supérieur lié au rift indo-malagasy ou au volcanisme de point chaud Marion ;

- les failles N100-110 correspondent à la direction des dykes doléritiques d'affinité alcaline du Crétacé. Au cours du Tertiaire et du Quaternaire, ces failles ont été fortement réactivées. Les failles les plus anciennes ont été réactivées lors de l'extension crustale entre Madagascar et l'Afrique, qui a redémarré au Miocène et s'est poursuivie au Pliocène et au Quaternaire. Ces failles sont encore actives aujourd'hui avec une sismicité actuelle observée de magnitude  $Mw > 5$  (Rasamimanana, 1996 ; Bertil et al., 1998; Piqué et al., 1999b; données IRIS de [www.iris.edu](http://www.iris.edu) 2021). Quant aux structures ductiles liées à l'orogenèse pan-africaine du Néoprotérozoïque (zone de cisaillement), elles ont été réactivées pendant le rift du Crétacé.

Les travaux de Bertil et al., (1998); Piqué et al., (1999b) montrent que Madagascar serait soumis à un régime extensif de direction générale E-W, responsable de l'amincissement de sa lithosphère, et parallèle à celui qui affecte le Rift est-africain où la direction générale des grands bassins faillés est subméridienne (Figure 1.4).

Ce contexte tectonique général est à l'origine des ressources géothermiques de Madagascar où des régions géologiques favorables à l'activité géothermique ont été définies, lesquelles sont associées soit à un contexte magmatique (plutonisme du Protérozoïque et volcanisme du Cénozoïque) ou non magmatique, d'extension ou de transtension (extension du début Tertiaire et Plio-Quaternaire). Ce contexte tectonique extensif responsable de l'amincissement de la croûte ainsi que l'existence d'un délamination de la lithosphère malagasy et des panaches mantelliques à Madagascar (Wysession et al., 2016; Pratt et al., 2017; Tsekhmistrenko et al., 2021) permet à la source de chaleur provenant du manteau de se trouver plus près de la surface.

Toutefois, le développement d'un champ géothermique dépend fortement de la compréhension du cadre géologique à différentes échelles de l'espace. Cette compréhension permet d'élucider des problèmes critiques au-delà de la température, tels que la porosité, la perméabilité, l'étendue spatiale des réservoirs potentiels, le cadre structural, et les caractéristiques physiques au niveau du système et de la ressource géothermique.

### 1.3 Problématique et objectifs

L'existence d'un champ géothermique est conditionnée par des zones présentant à la fois un gradient géothermique et une transmissivité hydraulique élevée (Varet, 2012). Divers types

d'environnements géologiques permettent la superposition de ces deux conditions en prenant en compte les cadres tectonique et pétrographique ainsi que la nature du fluide hydrothermal contenu dans le réservoir.

En général, le processus d'évaluation des ressources géothermiques peut être subdivisé en deux phases, comme pour l'évaluation des systèmes d'hydrocarbures. Dans la phase initiale, on évalue les "chances de découverte" et on délimite les ressources géothermiques favorables. La deuxième phase, qui suit les premières activités de forage et d'essais en puits, examine les "chances de développement" et étudie si les ressources favorables de la phase initiale conviennent à la production d'énergie géothermique et comment ces réservoirs appropriés peuvent être développés (Moeck et al., 2014).

Évaluer le potentiel géothermique demande ainsi de caractériser les formations géologiques ayant un potentiel de réservoir, c'est-à-dire définir la distribution de la température du sous-sol influencée par le flux de chaleur et les propriétés thermiques de la roche, et le régime d'écoulement et les propriétés hydrauliques des roches en fonction de la profondeur. La perméabilité et la conductivité thermique figurent parmi les paramètres clés pour caractériser un système géothermique (Sass et al., 2012).

Or, l'un des défis majeurs dans l'évaluation des ressources géothermiques dans la phase précoce ou initiale d'exploration où les données de forages profonds demeurent absentes, est l'utilisation des données de surface pour conceptualiser de façon réaliste la ressource géothermique présente à quelques kilomètres de profondeur. Ce modèle conceptuel constitue le premier élément essentiel qui soutient le développement d'un projet ou d'un programme d'exploration géothermique.

Le contexte tectonique d'extension associé à Madagascar est favorable au développement des ressources géothermiques, par analogie à ceux de la province du Bassin and Range aux États-Unis et de la région ouest de la Turquie. Ces derniers se trouvent par contre dans des terrains plus jeunes et non dans des formations du Paléozoïque et du bouclier précambrien tels qu'à Madagascar où les propriétés hydrauliques de ces formations seraient probablement moins favorables à la formation d'évidents réservoirs géothermiques efficaces, mais dont les failles actives pourraient être hautement perméables. Dans un tel contexte, les zones de failles jouent un rôle majeur dans l'écoulement des fluides et la formation des sources thermales, étant le principal indice qui laisse croire à la présence de ressources géothermiques. Selon l'état de connaissances actuelles, l'évaluation du potentiel géothermique de Madagascar est sommaire à cause de l'absence de données et de forages profonds. La distribution des anomalies thermiques

et des manifestations thermales dans le Nord de Madagascar est peu documentée, or il est important d'en connaître leurs origines afin de les expliquer. Les régions géothermiques dans le Nord de Madagascar correspondent à des zones de faille extensive : la zone de faille d'Andavakoera et le graben de Sambirano, qui constituent les deux principaux secteurs d'étude. Ces derniers comprennent respectivement les principales villes d'Ambovomby et d'Ambilobe dont la demande en énergie transparaît par un besoin d'électrification et d'approvisionnement en chaleur de l'industrie de transformation agroalimentaire. Les questions clés suivantes ont donc été abordées dans cette étude ; elles permettent de définir les objectifs de cette thèse qui ont influencé le choix de la méthodologie et des travaux réalisés :

- Comment catégoriser les ressources des sites géothermiques identifiés à Madagascar selon le niveau d'information géologique disponible, sachant qu'aucun forage profond n'a été réalisé?
- Quels sont les mécanismes de transfert thermique qui affectent les formations géologiques pouvant contenir les ressources géothermiques et comment les propriétés hydrauliques et thermiques de ces formations affleurant en surface peuvent favoriser ou limiter l'exploration des ressources?
- Quel est l'impact des failles sur les conditions d'écoulement et de température en profondeur et quelles cibles peuvent être visées pour une exploration géothermique plus poussée?

Ainsi, l'objectif principal de cette thèse de doctorat est de mieux comprendre les mécanismes de transfert thermique qui affectent les systèmes géothermiques du Nord de Madagascar situés en contexte d'extension, dominé par des formations métamorphiques et cristallines du socle protérozoïque. De cet objectif découlent des sous-objectifs qui ont été définis selon les questions clés, soit :

- Identifier les contextes géologiques favorables au développement des sites géothermiques à Madagascar ;
- Proposer un modèle conceptuel des systèmes géothermiques selon la classification précédemment identifiée pour les trois grandes zones de développement prioritaire;
- Caractériser les systèmes géothermiques de deux zones d'intérêt au Nord, soit Ambilobe et Ambovomby, en identifiant les structures géologiques dominantes qui affectent les processus d'écoulement d'eau souterraine et de transfert de chaleur ayant un impact sur la distribution de la ressource géothermique ;
- Évaluer l'applicabilité des méthodes expérimentales basées sur des observations de

- surface afin de comprendre et d'anticiper les processus de transfert thermique en profondeur dans les milieux hétérogènes et fracturés ;
- Classifier les unités rocheuses des deux zones d'intérêt selon une échelle thermo-hydrostratigraphique en vue de prévoir leur extraction de chaleur;
  - Simuler les processus d'écoulement et de transfert thermique à l'échelle de la croûte en considérant les effets des failles qui affecteront la distribution des vecteurs d'écoulement et de la température en profondeur.

## 1.4 Méthodologie<sup>2</sup>

Afin de répondre aux questions clés définies dans cette étude, la méthodologie mise de l'avant dans le projet a été adaptée aux conditions géologiques que présentent les zones d'intérêt, tout en respectant les moyens financiers et techniques disponibles.

La démarche méthodologique s'est basée sur des techniques d'observation et de modélisation de surface, de l'échelle du terrain à celle du laboratoire en utilisant l'infrastructure et les équipements de laboratoire disponibles à l'INRS. Ces techniques visent à caractériser le champ géothermique à partir de l'identification des contextes géologiques combinés aux données bibliographiques disponibles, notamment la température des réservoirs géothermiques déduite des géothermomètres chimiques qui sont basés sur l'analyse des éléments des sources chaudes en surface. Un travail de terrain a été réalisé pour une reconnaissance du contexte géologique à l'échelle des zones géothermiques étudiées et pour échantillonner des roches sur les principaux affleurements, utilisés comme analogues des formations géologiques profondes. Sur le terrain, nous avons mesuré la perméabilité des roches en affleurement à l'aide d'un perméamètre portatif et évalué les concentrations d'éléments producteurs de chaleur, tels que l'uranium  $^{238}\text{U}$ , le thorium  $^{232}\text{Th}$  et le potassium  $^{40}\text{K}$ , à l'aide d'un spectromètre gamma portatif. Toutefois, la majorité des analyses des propriétés thermiques et hydrauliques pour les deux zones d'étude ont été réalisées en laboratoire à l'aide d'appareils pouvant mesurer les propriétés thermohydrauliques des roches échantillonnées et des carottes élaborées à partir de ces échantillons. Le porosimètre-perméamètre combiné a permis de mesurer sous différentes valeurs de pression la perméabilité et la porosité. La mesure de conductivité et de la diffusivité thermique des roches s'est faite au

---

<sup>2</sup> Les méthodes et appareils de mesure ainsi que les dispositifs expérimentaux et les différents protocoles de mesures sont décrits de façon plus approfondie dans les articles qui constituent le cœur de la thèse.

moyen d'un scanner optique infrarouge à température ambiante. La simulation des mécanismes d'écoulement et du transfert de chaleur associés à des failles crustales à l'échelle des zones étudiées a finalement été effectuée par modélisation numérique avec le logiciel d'éléments finis COMSOL Multiphysics.

## 1.5 Structure de la thèse

Cette thèse est basée sur trois articles scientifiques qui répondent aux trois principales questions clés soulevées dans cette étude. Deux de ces articles ont déjà été publiés dans une revue scientifique avec un comité de lecture (chapitre 2 et chapitre 3) et le troisième est prêt à être soumis à une revue scientifique (chapitre 4). Cette thèse est organisée selon les chapitres suivants :

- Chapitre 2 : Classification des systèmes géothermiques de Madagascar

Ce chapitre passe en revue l'état des connaissances sur les systèmes géothermiques des régions géothermiques identifiées par les précédents travaux d'exploration effectués à Madagascar. Un premier catalogue des systèmes géothermiques de chaque région d'intérêt a été proposé. Le catalogue introduit les types de *geothermal play*<sup>3</sup> proposés par Moeck (2014). Cela a permis de mieux décrire et définir les caractéristiques dominantes des classes de systèmes géothermiques et de développer un modèle conceptuel correspondant au système pour chaque région. La classification est principalement basée sur l'identification des contextes géologiques combinés aux données disponibles, notamment la température anticipée des réservoirs géothermiques déduite des géothermomètres chimiques. Il s'agit d'une première classification exhaustive des systèmes géothermiques à Madagascar basée sur le contexte tectonique du pays.

- Chapitre 3 : Évaluation des propriétés pétrophysiques des roches dans le nord de Madagascar : implications pour l'exploration des ressources géothermiques.

L'évaluation du potentiel géothermique a été approfondie pour deux zones au nord de Madagascar. La pétrographie, la minéralogie, la porosité, la perméabilité, les propriétés

---

<sup>3</sup> En géothermie, un *geothermal play type* représente un cadre géologique tectonique stratigraphique ou structural particulier, comprenant une source de chaleur, une voie de migration de la chaleur, une capacité de stockage de la chaleur/du liquide et le potentiel de récupération économique de la chaleur (Moeck, 2014).

thermiques et la production de chaleur radiogénique des unités métamorphiques et magmatiques du socle protérozoïque et des unités sédimentaires du Cénozoïque – étant les formations dominantes dans les régions d'Ambilobe et d'Ambaranja – ont été caractérisées dans le but de mieux comprendre les mécanismes de transfert thermique qui affectent les ressources. Les affleurements rocheux ont été échantillonnés et utilisés comme analogues des réservoirs profonds. À partir de ces propriétés thermo-hydrauliques, des unités thermostratigraphiques ont été définies selon le concept de thermofaciès proposé par Sass et al. (2012). Cela a permis d'identifier les mécanismes de transfert de chaleur associés aux ressources géothermiques dans les contextes tectoniques d'extension des zones d'Ambilobe et d'Ambaranja.

- Chapitre 4: Comprendre les transferts thermiques le long des failles d'extension : cas des systèmes géothermiques d'Ambilobe et d'Ambaranja à Madagascar.

Suite à une caractérisation des formations géologiques, le rôle que jouent les failles dans les mécanismes de transfert thermique qui affectent les ressources géothermiques a été approfondi pour les zones d'Ambilobe et d'Ambaranja. L'écoulement d'eau souterraine et les transferts thermiques ont été simulés pour évaluer la distribution de la température en profondeur à l'aide de modèles 2D représentant la zone de faille normale d'Ambilobe et le graben d'Ambaranja. Les modèles 2D sont basés sur les modèles conceptuels des systèmes géothermiques de la région du Nord, présentés dans le chapitre 2. Les propriétés thermohydrauliques évaluées dans le chapitre 3 sont utilisées comme intrants pour les développements des modèles du chapitre 4. Différents scénarios de pendage des failles ont été établis parce que les données de la carte géologique sur le pendage des failles présentent des incertitudes et que ce pendage peut affecter la remontée des fluides chauds. Nous avons cherché à reproduire la température des sources chaudes près de la surface, car c'est la seule information disponible dans la région pour vérifier la validité des modèles. Les simulations ont permis de mieux comprendre le rôle des failles sur le transfert thermique par convection forcée donnant lieu aux sources thermales observées dans le Nord de Madagascar.

- Chapitre 5: Conclusions et travaux futurs : Les principaux résultats de cette thèse y sont résumés et leurs contributions y sont discutées pour enfin présenter les perspectives pour des travaux futurs.

## **2 PREMIER ARTICLE: CLASSIFICATION OF GEOTHERMAL SYSTEMS IN MADAGASCAR**

---

### **Classification des systèmes géothermiques à Madagascar**

#### **Auteurs :**

<sup>1</sup>M. Rajaobelison, <sup>1</sup>J. Raymond, <sup>1</sup>M. Malo and <sup>2</sup>C. Dezayes

<sup>1</sup> Institut national de la recherche scientifique, 490 de la Couronne, Québec, QC G1K 9A9,  
Canada

<sup>2</sup> Bureau de recherches géologiques et minières, 3 Avenue Claude Guillemin, 45100 Orléans,  
France

#### **Titre de la revue ou du Journal:**

Geothermal Energy

28 juillet 2020

<https://doi.org/10.1186/s40517-020-00176-7>

#### **Contribution des auteurs :**

MR a travaillé sur la collecte des données et a rédigé le manuscrit. JR et MM ont dirigé le projet, en fournissant des idées et des objectifs ainsi qu'un soutien logistique ; CD a fourni des commentaires et des idées utiles pour améliorer les modèles conceptuels. Tous les auteurs ont relu le manuscrit et ont apporté leurs commentaires et leurs idées

## 2.1 Introduction

The first investigation into the geothermal potential of Madagascar was compiling an inventory of the hot springs (Besairie, 1959) which was followed two decades later by an assessment of the geochemical characteristics of geothermal energy sources using chemical and isotopic analysis and chemical geothermometers on samples of hot spring water (Gunnlaugsson et al., 1981). The results provided a general characterization of the geothermal regions of Madagascar (Andrianaivo, 2011). The prospective areas in this study have been subject to geological assessments, including structural geology (Andrianaivo et al., 2010a). Knowing that geothermal exploration in Madagascar is at an early stage and that there is currently no geothermal power production in the country, this study reviews the available results from previous work with the objective to better understand the factors affecting the geothermal energy source and to produce the first catalogue of geothermal systems in Madagascar. The aim of the classification is to highlight the dominant characteristics of each area.

A ‘geothermal system’ in the hydrothermal regime can be described schematically as “convecting water in the upper crust of the Earth, which, in a confined space, transfers heat from a heat source to a heat sink, usually the free surfaces” (Hochstein, 1990). According to this definition, the geothermal system comprises three main elements: a heat source, a permeable formation and a fluid, which is the heat carrier transferring thermal energy (Dickson et al., 2003). A geothermal system can also be defined as “all parts of the hydrological system involved, including the recharge zone, all subsurface parts and the outflow of the system” (Axelsson, 2008). Moreover, Williams et al. (2011) propose a broader definition that encompasses resources outside the hydrothermal regime: “any localized geologic setting where portions of the Earth’s thermal energy may be extracted from a circulating fluid and transported to a point of use”. Taking into account these definitions, it is important not to confuse the classification of geothermal systems with associated geothermal resources as the geothermal resources can be located in almost every geosystem but is not located everywhere in a geosystem. In addition, the definition of ‘resources’ has been considerably refined when referring to a ‘geothermal energy source’ in the terminology adopted by the United Nations Framework Classification for Resources (UNFC-Falcone et al., 2016), and can be classified according to the geothermal reservoir temperature (Muffler et al., 1978; Hochstein, 1990; Sanyal, 2005),

the dominant physical state of the fluids (White, 1973a ; Nicholson, 1993), and the enthalpy (Dickson et al., 2003) and exergy of the geothermal fluids (Lee, 2001). Moreover, the distribution of the geothermal energy source is controlled by geological and tectonic contexts (Armstead, 1973; Muffler, 1975). Erdlac et al. (2008) presented five key parameters that must be defined for a geothermal classification system to be considered appropriate: the geologic environment, the geological features or structural setting, the crustal “heat source”, the resource category (specifically, “the medium within which the heat is to be found and produced”), and the rock type hosting the geothermal energy source.

In light of the above, the classification of geothermal systems must consider all the aspects of the geothermal energy source in a consistent manner. According to Moeck (2014), the critical element in the characterization, assessment and development of geothermal systems is the type of geothermal energy source. The more explicit the classification, the better and more practical the overview of the geothermal energy source types for defining their utilization and anticipating the heat transfer mechanisms allowing production. Moreover, recent advances in the geothermal play concept in which the type is based on geologic criteria have allowed geothermal systems to be grouped and separated according to their geologic characteristics and heat transport mechanisms to establish a catalogue of geothermal play types at the global or regional scale (Moeck, 2014; Moeck et al., 2015; Moeck, 2018; Moeck et al., 2019; Schintgen et al., 2019). Thus, the limiting issue in geothermal system classification is not only the lack of available data but also the quality, which is dependent on the stage of geothermal exploration. Therefore, multiple authors have proposed classifications based on the following: (A) the reservoir equilibrium state, which can be dynamic or static based on the circulation of the reservoir fluid and whether the dominant mechanism of heat transfer is conduction or convection (Nicholson, 1993); (B) fluid temperature and enthalpy combined with the corresponding dominant physical state (Sanyal, 2005; Axelsson, 2008); (C) the thermofacies concept, which classifies systems as petrothermal or hydrothermal based on the thermohydraulic characterization of rock units and the correlation between the petrophysical properties of the bedrock (permeability, thermal conductivity), their lithostratigraphic facies and the mechanism of heat transfer (Sass et al., 2012); and (D) the anticipated technological means for developing the system, which distinguishes enhanced geothermal systems (EGS; Gallup, 2009).

For the initial geothermal assessment of a region, classifying the geothermal systems is one of the key elements to start the characterization, evaluation and development of geothermal energy sources (Williams et al., 2011). In this sense, the information should be organized to highlight and identify the value of particular data, especially geological settings and subsurface temperature. Geological settings are often critical in the assessment and exploration of geothermal energy sources as they can be used to anticipate the system's utilization and potential production mechanisms. Additionally, a detailed understanding of surface geological settings can help improve geothermal system classification for use in decision-making at the pre-drilling phase of exploration. This type of classification is, in fact, a low-cost tool, providing reliable cataloguing data applicable to site-specific field development.

This work is the first attempt to develop a catalogue of geothermal systems in Madagascar. The classification is primarily based on the identification of geological settings combined with the available data, including the temperature of geothermal reservoirs inferred from chemical geothermometers. Our work generally follows the alternative scheme proposed by Moeck (2014), which introduces geothermal play types, because we believe it better describes the characteristics of the geothermal system classes found in Madagascar. Our study conceives conceptual models for each class in selected prospective areas. The proposed classification and associated conceptual models represent one step in organizing the existing information in a manner that makes it useful as a guide in decision-making processes. The proposed classification should be seen as a starting point rather than an end product as it can be improved for each region once more subsurface data become available.

## 2.2 Geographical and Geological Settings

Madagascar is the largest island situated in the Indian Ocean, separated from Africa by the Mozambican Channel. The geology of Madagascar is characterized by a Precambrian shield composed of Archaean to Proterozoic magmatic and metamorphic rocks, which are exposed in the eastern two-thirds of the island (Figure 2.1a). This Precambrian basement was remarkably reworked by several intense tectonic and orogenic processes during the Neoproterozoic Pan-African orogeny between 600–800 Ma (Windley et al., 1994; De Wit, 2003). It is divided into six main tectono-metamorphic domains, namely Vohibory, Bemarivo, Ikalamavoina, Androy-Anosyan and Antananarivo

(De Wit, 2003; Collins, 2006; Tucker et al., 2014), and separated from each other by tectonic contacts comprising ductile high-strain or shear zones (Giese et al., 2011; Tucker et al., 2014).

The remaining third of the island, along its western side, is covered by extensive sedimentary basins (Figure 2.1a). From north to south, the three main basins are Ambilobe (Diego), Mahajanga and Morondava. There are also smaller basins along the eastern coast. These basins preserve a nearly complete record of deposits from Upper-Carboniferous to Mid-Jurassic, which are the equivalent of the Gondwana sequences in India and the Karoo sequences in Africa. In Madagascar, these deposits are divided into the Sakoa, Sakamena and Isalo groups (Besairie, 1952), overlain by Quaternary to Recent unconsolidated sediments.

The sedimentary basins and associated structures formed in response to aborted Permo-Triassic Karoo rifting and the subsequent separation from Eastern Africa in the Jurassic and from India in the Cretaceous (Razafimbelo, 1987; Piqué et al., 1999b). The latter initiated late Cretaceous volcanism (Rasamimanana et al., 1998a; Bardintzeff et al., 2010), predominantly along the western, southern and eastern margins of the island (Figure 2.1a). The Jurassic rifting of Madagascar from Eastern Africa is also responsible for the thinning of the crust beneath the basins, which averages  $30 \pm 5$  km thick, including 2 to 8 km of sedimentary rocks (Rindraharisaona et al., 2017; Andriampenomanana et al., 2017). However, the Neogene to Quaternary tectonic reactivation resulted in renewed Cenozoic volcanic activity in the central region (Rufer et al., 2006), as well as in the northern part where numerous alkaline intrusions are associated with extensional faults of Plio-Quaternary (Chorowicz et al., 1997; Cucciniello et al., 2016) and early Tertiary age (Rossi, 1980). The Moho is found at an average depth of 40 km and 33 km in the central and northern regions, respectively (Andriampenomanana et al., 2017). The lithosphere of Madagascar is encountered at an average depth of 50 km (Figure 2.1b). Serval authors (Wysession et al., 2016; Paul et al., 2017; Pratt et al., 2017; Andriampenomanana et al., 2017) have assumed that the lithosphere has been significantly modified beneath the northern, central and southwestern regions of the island where major Cenozoic volcanic provinces and uplift are present (Roberts et al., 2012).

Six different areas in various parts of Madagascar have been identified as interesting geothermal prospectives (Figure 2.1a): Ambilobe and Ambanja (North), Itasy and Antsirabe (Central), and Miandrivazo and Morondava (West). Studies from the 1980s used

geothermometer analysis to demonstrate that these areas have an expected geothermal reservoir temperature between 120°C and 240°C (Gunnlaugsson et al., 1981; Sarazin et al., 1986). The development of geothermal energy sources, primarily for electricity production and other direct uses (Andrianaivo, 2011), can benefit these regions where electricity is currently supplied by hydropower and imported fossil fuels, and where economy is based essentially on agriculture, trade and mining. In this study, we have focused on these six areas to better qualify and understand the geothermal energy source potential.

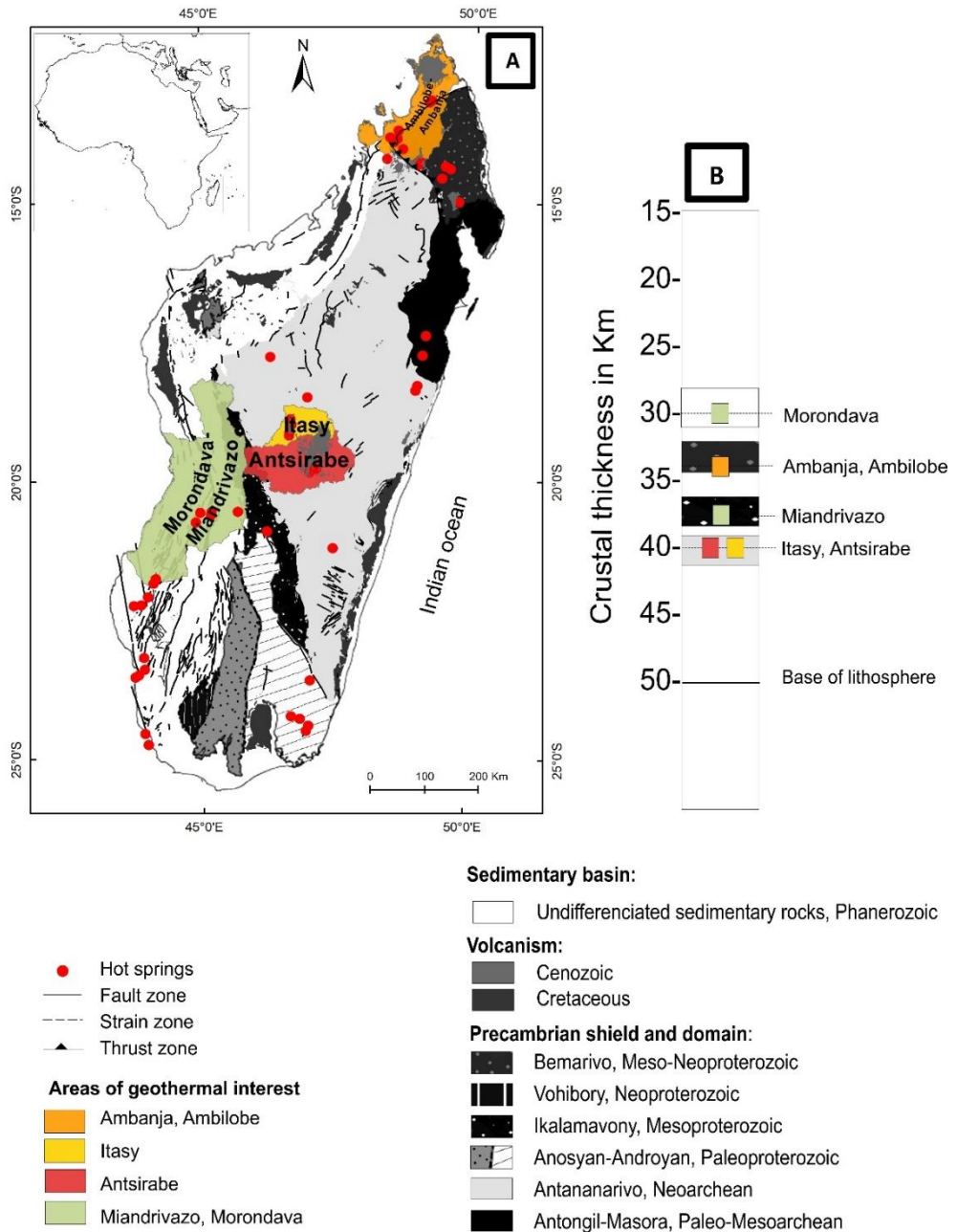


**Figure 2.1** a) Simplified geological map of Madagascar (modified from Roig et al., 2012; Tucker et al., 2014), showing the location of hot springs and the geothermal areas of interest (Besairie, 1959; Gunnlaugsson et al., 1981). (b) Average crustal thickness beneath sedimentary basins and the

Precambrian shield in the geothermal areas of interest (Rindraharisaona et al., 2013; Pratt et al., 2017; Andriampenomanana et al., 2017).

### 2.3 Development of a geothermal system classification

In this work, the geothermal systems in the six areas of interest are classified using a combination of different criteria, such as the geological setting, the potential geothermal reservoir temperature and the dominant physical state of the fluids. The data in published literature were reviewed, and the following steps were followed to establish the geothermal system classification.

1- The first step consisted of characterizing the geological environment by highlighting the tectonic and structural settings at the regional scale in each area. The analysis of tectonic data was based on up-to-date geological maps and the available literature for the tectono-metamorphic domains of Madagascar (Figure 2.1). This information was then used to infer the dominant geologic control on fluid flow or the heat migration pathway, geothermal play type and heat source. These elements were used to develop the catalogue of geothermal systems in Madagascar, similar to the manner proposed by Erdlac (2011) for classifying geothermal energy sources in a geothermal power classification system and by Moeck (2014); Moeck (2018) and Moeck et al., (2015) for cataloguing geothermal plays.

2- The second step was to study the geothermal characteristics of Madagascar's geothermal areas in relation to their geological setting. The predominant geological formations identified in the prospective areas include trap formations or cap rocks that limit the escape of heat, as well as host rocks from which geothermal energy source can potentially be extracted. The results of hot spring analyses and geothermometer studies were used to deduce the dominant mobile phase of fluids in the deep geothermal reservoir using the classification proposed by Sanyal (2005). This means all low-temperature systems are considered liquid-dominated, the moderate-temperature systems are almost exclusively liquid-dominated, and the high-temperature systems include both liquid- and vapour-dominated resources.

3- The third and last step was to identify the relevant geothermal systems and classify them by heat source type according to their geological environment, followed by the physical state of the mobile fluid phase based on the estimated geothermal reservoir temperature, as shown in Table 2.1 (Rezaie et al., 2013). Three qualifiers (low, moderate

or high) are used for the temperature range of the geothermal reservoir based on the work of Sanyal (2005), who set the range for low to moderate at 150-230°C, and for moderate to high at 190-300°C.

As a basis for discussion, prospect areas arising from this classification were compared to global analogue regions that have similar geothermal characteristics, but where a more advanced stage of geothermal development exists.

**Table 2.1 Example of the geothermal system classification for Madagascar**

	Geological setting/ heat source	Dominant physical state of the mobile fluid phase	Temperature of geothermal reservoir
	Graben border-fault/shallow Moho	Liquid-dominated	Moderate
Classification of geothermal system	Graben border-fault-liquid-dominated moderate-temperature		

## 2.4 Classes of geothermal systems

Before assigning a class to the studied geothermal systems, the prospective areas were first characterized in terms of tectono-metamorphic domain, geological system or plate tectonic setting, geothermal play type and heat source (Table 2.2). They were then characterized by geological formation and geothermal characteristics (Table 2.3). Finally, the prospective areas were assigned to three classes of geothermal system, as defined in Table 2.4.

As outlined in Table 2.2, the geological formations of the six prospective areas can be grouped by the tectono-metamorphic domain. The Ambilobe and Ambanja areas are part of the Bemarivo Domain. The Itasy and Antsirabe areas belong to the Antananarivo Domain. The Miandrivazo area is in the Ikalamavony Domain and the Morondava area is in the Morondava Basin. Each area is also characterized by its geologic system or plate tectonic setting, which are sedimentary-basement fault boundary, graben, pull-apart basin, and passive margin basin. The geothermal play – an extensional domain – is the same for all the prospective areas. Thus, faults and fractures control the fluid migration pathway. Most of the faults with N-S, NNE-SSW and NNW-SSE trends are related to Cenozoic volcanism in Madagascar (Rasamimanana, 1996; Melluso et al., 2000; Rufer et al., 2006). The more ancient faults were reactivated during the crustal extension between Madagascar and Africa, which restarted in Miocene times and continued during the

Pliocene and Quaternary. Those faults are still active today (Rasamimanana, 1996; Bertil et al., 1998; Piqué et al., 1999b).

Although these geothermal areas are situated in the volcanic provinces of the North (Ambohitra and Ambilobe) and Central regions (Itasy and Antsirabe), this volcanism is old and considered to be a fossil system. The latest volcanic activity is Miocene to Pleistocene in age, 17 to 1.8 Ma  $\pm$ 0.13 and 28 to 3 Ma, respectively (Bardintzeff et al., 2010; Estrade et al., 2014). The magmatism related to volcanism is considered to be extinct, up to 50,000 years old, according to McCoy-West et al., (2011). The isotopic and trace-element composition of the basalts from these volcanic provinces indicates that the deep source of the related magma was derived from the lower part of the lithospheric mantle (Bardintzeff et al., 2010). Therefore, even if fossil magma chambers exist, they cannot be considered the main source of heat. However, the extensional tectonics and the crustal thinning below these volcanic provinces, where the average thickness is 33-40 km (Andriampenomanana et al., 2017), correspond to regions of upwelling asthenosphere (Wysession et al., 2016; Pratt et al., 2017), the origin of the heat source. In the Miandrivazo area and the Morondava sedimentary basin, magmatism occurred during the Cretaceous and did not constitute the heat source.

Table 2.3 highlights the predominant geological formations of the geothermal areas, including the potential host rocks containing the geothermal energy source or hot fluids, the range of temperature for the hot springs, the range of temperature at depth, the dominant chemical composition of the fluids, and the main mobile phase. For all six areas, the Precambrian to Cambrian basement is dominated by paragneiss, orthogneiss and schists. In Ambilobe and Morondava, the Permian to Triassic sedimentary units that overlie the basement comprise sandstone, shale, clay, and limestone marls belonging to the Karoo Supergroup sequence. These rock units can be considered for geothermal exploration. According to the chemical geothermometer analysis conducted by Gunnlaugsson et al., (1981), the predicted geothermal reservoir temperature is in the range of 140-180°C for the Ambilobe area, 140-200°C for Ambohitra, 170-240°C for Itasy, 150-240°C for Antsirabe, 140-170°C for Miandrivazo, and below 150°C for Morondava. According to Sanyal (2005), these expected reservoir temperatures indicate that the dominant mobile phase is liquid for the fluids in all six areas. The water chemistry of Ambilobe and Ambohitra is characterized by moderate to high carbon dioxide concentration (200-1000 ppm CO<sub>2</sub>) with low chloride content (<300 ppm Cl). Water from Itasy and

Antsirabe has a high carbon dioxide concentration, ranging between 1000 and 4000 ppm CO<sub>2</sub>, with moderate to low salinity and a chloride content of 400 to 500 ppm Cl. Water from Miandrivazo and Morondava has low carbon dioxide concentration (< 200 ppm CO<sub>2</sub>) and moderate chloride (500-1200 ppm Cl) and basinal characteristics, such as saline NaCl-dominated brine.

Finally, as presented in Table 2.4, the three main geothermal systems defined for each area are:

- a. Graben border-fault liquid-dominated moderate-temperature systems for Ambilobe and Miandrivazo;
- b. Fossil magmatic liquid-dominated moderate-temperature systems for Ambanja, Itasy and Antsirabe;
- a. Sedimentary liquid-dominated low-temperature systems for Morondava.

**Table 2.2 Geological and tectonic controls for prospective areas in Madagascar**

Region	North		Central		West			
Area	Ambilobe	Bemarivo	Itasy	Antsirabe	Miandrivazo	Morondava		
Tectono-metamorphic domain			Antananarivo		Ikalamavony	Morondava basin		
Plate tectonic setting or geologic system	Sedimentary/basement normal fault boundary	Intracontinental rift			Sedimentary/basement normal fault boundary	Sedimentary passive margin basin with horst and graben structures		
		Graben	Pull-apart basin	Half-graben				
Geothermal play type	Extensional domain							
Dominant geologic control	Faults/fractures							
Heat source	Shallow Moho	Shallow Moho and fossil magma chamber			Shallow Moho			
Selected references	Rossi (1980) Lardeaux et al., (1999) Tucker et al., (2014) Estrade (2014) Cucciniello et al., (2016)	Reed (1983) Hochstein (1988) Rasoanimanana et al., (2012) Rufer (2009) Andrianaivo et al., (2010b)			Razafimbolo (1987) Rajaomazava (1992) Piqué et al., (1999a) Reeves (2014) Rindraharisaona et al., (2017)			

**Table 2.3 Geological and geothermal characteristics for prospective areas in Madagascar**

Region	North			Central		West		Source
Area	Ambilobe	Ambanja	Itasy	Antsirabe	Miandrivazo	Morondava		
Dominant geological formations	Sandstone and shale of the Isalo and Sakamena groups	Paragneiss and migmatite of the Sambirano Group	Migmatitic gneiss, paragneiss and schist of the Ambatolampy Group	Orthogneiss and tonalitic-granite of the Dabolava Suite	Sandstone, limestone, clay and marl of the Isalo, Sakamena groups	Interpreted from geological maps		
Temperature of hot springs (°C)	47-78	48-72	24-57	38-57	30-55	39-42	Besairie (1959) Gunnlaugsson et al., (1981) Hambinintsoa et al., (2017)	
Temperature of geothermometer (°C)	140-180	140-200	170-240	150-240	140-170	120-140	Gunnlaugsson et al., (1981)	
Dominant chemical composition of fluids	Moderate to high CO <sub>2</sub> (200-1000 ppm) and low Cl (< 300 ppm)		High CO <sub>2</sub> (1000-4000 ppm) and Cl (400-500 ppm)		Low CO <sub>2</sub> < 200 ppm and moderate Cl (500-1200 ppm) Saline brine, NaCl-dominated Basinal or infiltration fluids?		Gunnlaugsson et al., (1981) Hambinintsoa et al., (2017)	
Mobile fluid phase in the geothermal reservoir	Liquid-dominated						Interpreted according to temperature of geothermal reservoir	

**Table 2.4 Geothermal system classes for prospective areas in Madagascar**

Region	North		Central		West	
Area	Ambilobe	Ambohitra	Itasy	Antsirabe	Miandrivazo	Morondava
Geological environment and heat source	Graben border-fault Shallow Moho	Graben Shallow Moho and fossil magma chamber	Volcanic Shallow Moho and fossil magma chamber		Graben border-fault Shallow Moho	Sedimentary Shallow Moho
Physical state of the mobile fluid phase				Liquid-dominated		
Fluid enthalpy			Moderate			Low
Class	Graben border-fault liquid-dominated moderate-temperature	Fossil-magmatic liquid-dominated moderate-temperature		Graben border-fault liquid-dominated moderate-temperature		Sedimentary liquid-dominated low-temperature

## 2.5 Conceptual models and geothermal system classes

A conceptual model was prepared for the geothermal system identified for each prospective area on the basis of the data in Tables 2.2, 2.3 and 2.4. Models are presented as interpreted 2D cross-sections on which the physical features of the system are drawn, including geological structures and fluid flow that is ultimately controlled by the geological structures (Wallis et al., 2018; Hinz et al., 2016). The models were developed following the approach reviewed by Axelsson (2013). They are descriptive or qualitative models built to better understand the factors controlling the heat source, formation permeability and fluid migration.

In this paper, the term ‘host rock’ identifies the dominant geological formations of the potential geothermal reservoir based on the information in Table 2.3. It should be noted that porosity and permeability data are often insufficient to properly define the geothermal reservoir potential of the host rocks. Given the early stage of geothermal exploration in Madagascar, the available information is mostly limited to surface exploration, such as geological and structural maps, as well as remote sensing interpretations (Collins, 2006; Roig et al., 2012; Tucker et al., 2014). Geophysical surveys and seismic data have

provided a general understanding of the lithospheric structure of Madagascar (Paul et al., 2017; Wysession et al., 2016), yielding information on the uppermost mantle, and the average thickness of the Madagascar crust, including the average thickness of the sedimentary rocks and crystalline basement (Rindraharisaona et al., 2017; Pratt et al., 2017; Andriampenomanana et al., 2017). The average thickness of sedimentary sequences varies from 2 to 6 km (Rindraharisaona et al., 2017; Pratt et al., 2017; Andriampenomanana et al., 2017). For this reason, the conceptual models were drawn to a maximum depth of 5 km.

### **2.5.1 North region**

#### **2.5.1.1 Ambilobe area**

The Ambilobe area is located in a normal fault zone called Andavakoera, which delineates the contact between sedimentary sequences and basement rocks (Table 2.2). It forms a depression 120 km long and 3 to 5 km wide. It is oriented NE-SW in the direction of the major faults, which have cut the basement and sedimentary cover since the Triassic (Lardeaux et al., 1999). Undifferentiated NW-SE faults and strike-slip faults with dextral or sinistral movements are also observed (Figure 2.2b). The latter are associated with recent E-W rifting that likely triggered the formation of the vast Neogene-Quaternary alkaline volcanic fields in the North and Central regions of Madagascar (Bertil et al., 1998; Melluso et al., 2000). An N-S cross-section has been drawn to represent the conceptual model (Figure 2.2c).

The sedimentary sequence unconformably overlying the Neoproterozoic metamorphic bedrock is part of the Ambilobe Basin. It consists of Permian sandstones and conglomerates of the Sakamena Group, which are covered by Eotriasic shale and Upper Triassic sandstones of the Isalo Groups which also called Isalo I. The latter overlies either Permo-Triassic deposits or Neoproterozoic basement. The sandstones of Isalo I group form an imposing escarpment 400 to 500 m high along a depression dipping 5 to 30° to the northwest. Metre-scale quartz-barite veins and faults, having the same N 050°E to N 150°E strike, intersect the sediment cover as well as the basement. Recent alluvial deposits are found in the depression on top of the Ambilobe basin sequence. The Neoproterozoic basement is predominantly mica schist of the Betsiaka Group and muscovite-amphibole orthogneiss and garnet-amphibolite of the Milanoa Group (Figure

2.2b), which stabilized in the greenschist and amphibolite metamorphic facies (Thomas et al., 2009; Tucker et al., 2014).

Thermal water mainly emerges along the NE-SW direction of the depression through fractures cutting the shale unit, such as the hot springs near the villages of Ambakirano and Betsiaka (Figure 2.2b). These hot springs likely originate in the Permian or Triassic sandstones, believed to be possible host rocks, while the Eotriassic shales are potential cap rocks (Table 2.3). Following the general topography, the fluids are thought to circulate from north to south, as shown on the conceptual model (Figure 2.2c). At the surface, the springs in the villages reach temperatures of 59 and 72°C, respectively. According to chemical geothermometers (Gunnlaugsson et al., 1981), the geothermal reservoir temperature can be 140 to 180°C (Table 2.3). The carbon dioxide concentration of the hot spring water is moderate to high (from 200 to 4000ppm), which can cause calcite scaling and corrosion during geothermal exploitation (Gunnlaugsson et al., 1981).

The average thickness of the crust in the Ambilobe area is 33 km, including an average of 4 km of sedimentary rocks (Pratt et al., 2017; Andriampenomanana et al., 2017), forming a potential thermal blanket that could help induce a geothermal gradient steeper than  $35^{\circ}\text{C km}^{-1}$ , which is considered moderate in this study. Recent magmatism occurred from 14 Ma to 0.83 Ma (Buchwaldt, 2006) and has been described by Estrade (2014). The main volcanic massif in the North region, known as the Amber Massif, is located about 50 km from the Ambilobe area (Figure 2.2a). Thus, the Ambilobe heat source is mainly attributed to the thinning of the crust in an extensional structural setting.

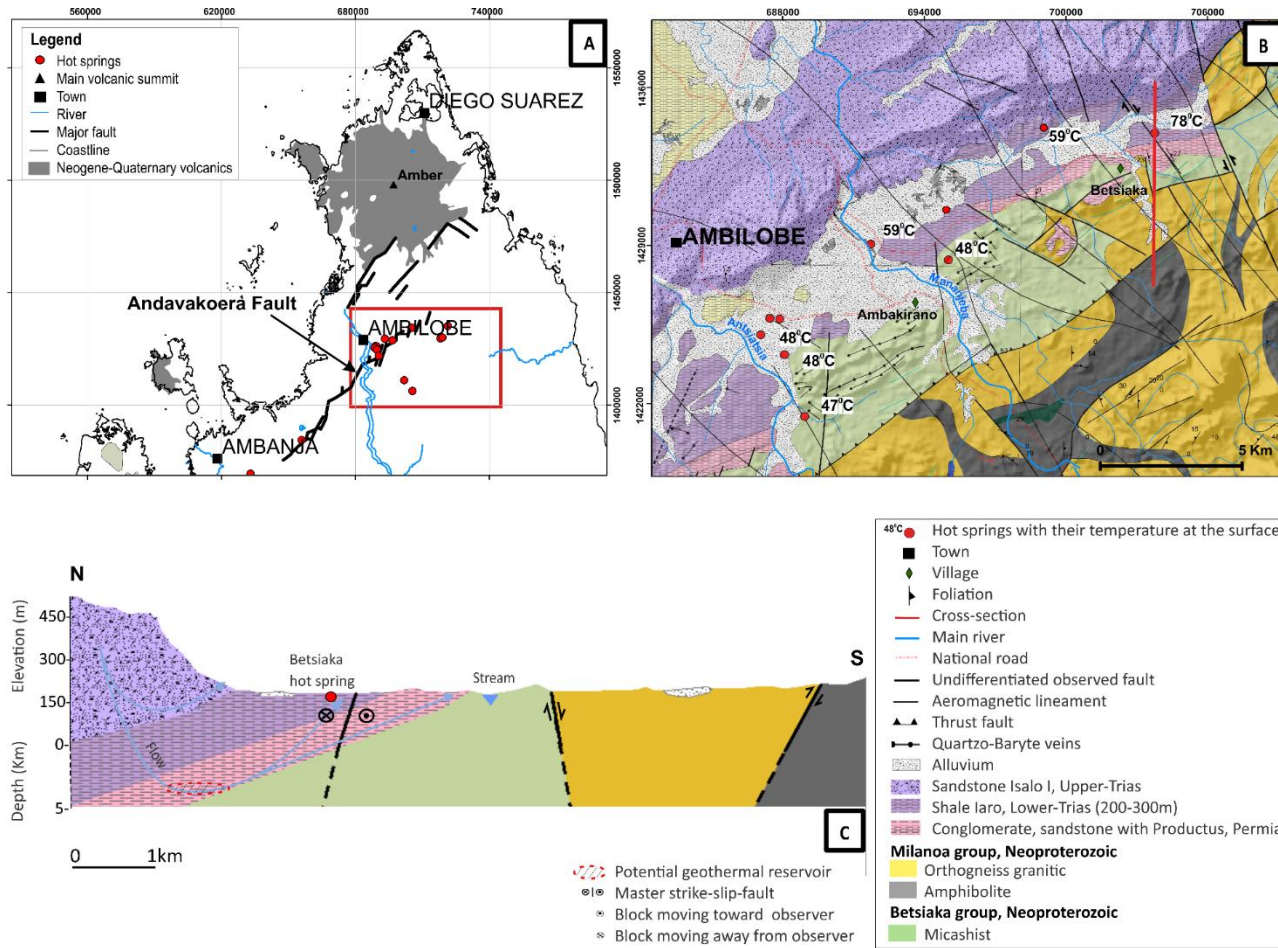


**Figure 2.2** (a) Location of Ambilobe geothermal area, (b) Detailed geology showing the position of hot springs, (modified from Roig et al., 2012), and (c) Conceptual model of Ambilobe geothermal system in the Andavakoera fault zone. The vertical scale of the elevation profile, which was created using ASTER imagery, has been exaggerated compared to the depth scale, which is based on the structure of the crust and uppermost mantle beneath Madagascar (Andriampenomanana et al., 2017)

### **2.5.1.2**

### **Ambanja area**

The Ambanja area is characterized by a 25-km-long graben oriented NW-SE direction with an average width of 4 km (Table 2.2, Figure 2.3b). The timing of the brittle tectonic activity that generated the Sambirano Graben is not exactly known, but most probably formed during the early Tertiary, before the first Miocene volcanic eruptions in this area, as suggested by Rossi (1980), with major reactivation until the Quaternary (Mottet, 1982). The graben formed in Proterozoic basement units, predominantly composed of paragneiss belonging to the Sambirano Group. The depression was filled with detrital and alluvial sediments. Permo-Trias sandstones and shale successions appear only in the northwest. Basalts and basanites are found in the eastern part of the graben, while ignimbrites have been observed mostly in the southern part. The volcanic deposits, between 600 and 700 m thick, include lapilli and tuff overlying ignimbrites. These volcanic deposits originated from the neighbouring stratified volcanic complexes of the Tsaratanana Massif.

Hot springs emerge mostly along the NW-SE striking fractures and faults bounding the graben (Figure 2.3b). Our conceptual model proposes that NW-SE graben faults, with currently unknown depth, can be a potential path for subsurface flow. Fluids circulate mainly from SW to NE and from NE to SW on both sides of the valley. This interpretation is consistent with the topography, where recharge occurs along topographic highs, and water flows toward valleys with a lower altitude (Figure 2.3c). There is no evidence that porous units can form permeable host rocks as in the Ambilobe area. The host rocks are thought to be fractured basement rocks (Table 2.3). The hot springs are located close to the faults and have a temperature of 48 to 72°C. Using chemical geothermometers, Gunnlaugsson et al. (1981) estimated that fluid temperature can reach 140 to 200°C inside the geothermal reservoir, corresponding to a moderate enthalpy and a dominant liquid state. A low concentration of solids and dissolved gases were also observed (Table 2.3).

The period of magmatism giving rise to the alkaline intrusion observe in the northeastern part of the graben (Figure 2.3a) is dated between 27 and 20 Ma , followed by a more recent volcanism period of 17 to 15 Ma for the Tsaratanana Massif (Buchwaldt, 2006) and described by Estrade (2014). It can be assumed that a fossil magma chamber is possibly located beneath the Tsaratanana volcanic massif, which can be related to the origin of the alkaline intrusive complexes as shown in Figures 2.3c. Therefore the recent

magmatism and the decay of radiogenic elements in recently crystallized rock may be providing additional heat to the heat originating from a shallow mantle in the Ambanja area. But, the average crustal thickness and lithosphere depth, 30 km and 50 km, respectively, are the same as in the Ambilobe area (Wysession et al., 2016; Pratt et al., 2017; Andriampenomanana et al., 2017). This shallow Moho depth is believed to be the most important heat source contributing the increase of geothermal gradient, which is expected to be moderate.

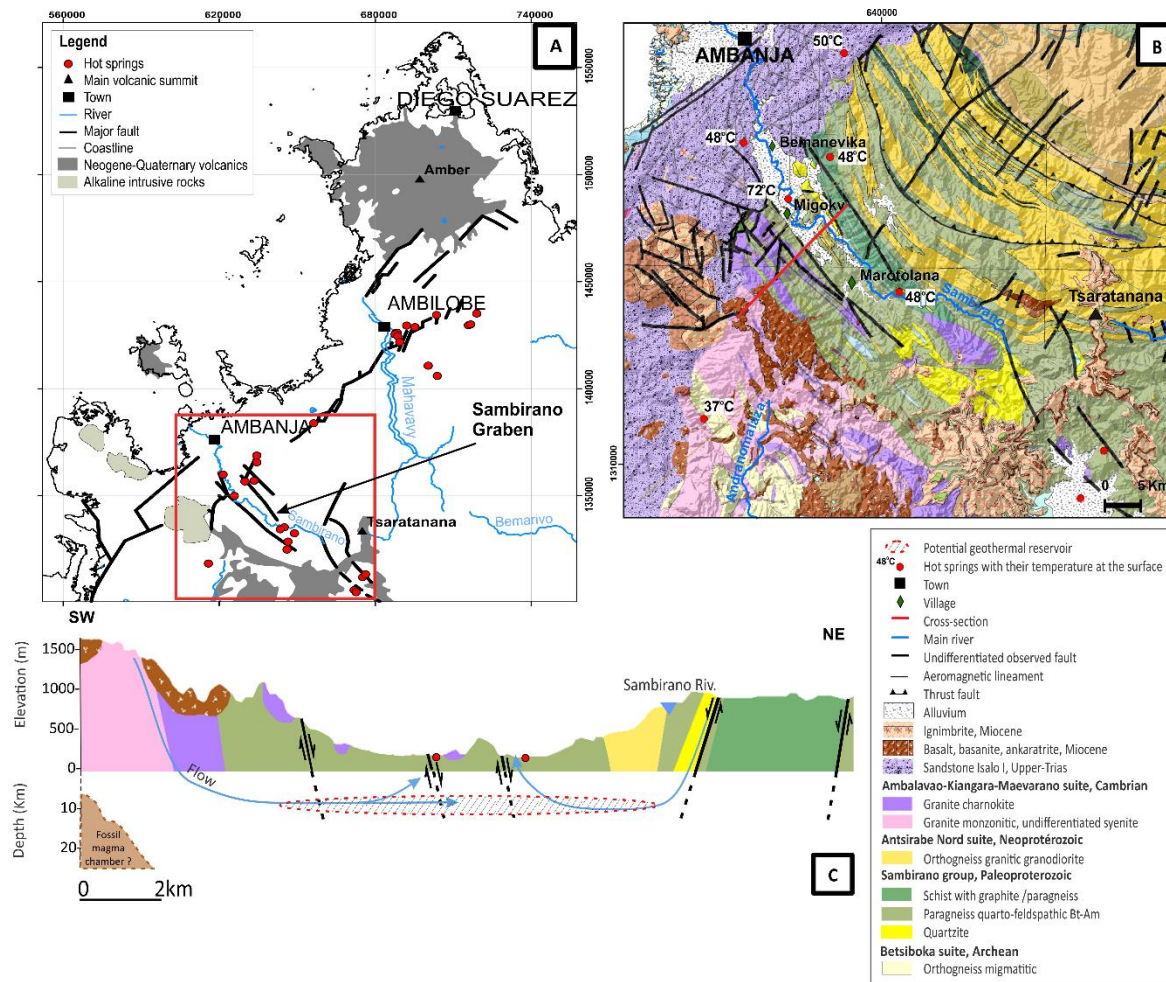


**Figure 2.3** (a) Location of Ambanja geothermal area, (b) Detailed geology showing position of thermal springs, (modified from Roig et al., 2012), and (c) Conceptual model of the Ambanja geothermal system in the Sambirano graben. The vertical scale of the elevation profile, which was created using ASTER imagery, has been exaggerated compared to the depth scale, which is based on the structure of the crust and uppermost mantle beneath Madagascar (Andriampenomanana et al., 2017)

## **2.5.2      Central region**

### **2.5.2.1      Itasy area**

The Itasy area is one of the most seismically active volcanic regions in the central part of Madagascar, with earthquake magnitudes up to 4 (Rakotondrainibe, 1977; Bertil et al., 1998; Ramarolahy, 2016). In this part of the country, Cenozoic volcanic deposits overlying the Precambrian basement form numerous domes (upper-Oligocene to Pleistocene), scoria cones and lava flows of trachytic to basanitic composition (Figure 2.4b). The latter is predominantly composed of migmatitic gneiss belonging to the Antananarivo Domain (Table 2.2 and 2.3). Magnetotelluric and magnetic surveys revealed that the Pleistocene volcanic deposits and lavas are only 50 to 100 m thick (Ratsimbazafy., 1987). Geysers, travertine mounds and aragonite deposits are common landscape features. The conceptual model of the Itasy area is based on geological structures and regional lineaments. Three small strike-slip basins – Trefa, Ifanja and Lake Itasy – were created by complex displacements along NNE strike-slip fault zones (Figures 2.4b and 2.4c). These small basins are interpreted as pull-apart basins (Table 2.2) (Andrianaivo et al., 2010b). Major N-S discontinuities, such as faults, suggest regional E-W extension. Active faulting is responsible for the seismicity in this region (Ramarolahy, 2016).

In such trans-tensional geothermal systems, the hydrothermal flow paths are characterized by basinward-dipping faults, and the fluids are more likely to migrate along the pathways of hanging-wall faults and fracture planes (Reed, 1983; Hochstein, 1988). Hence, for the Itasy area, the upward migration of fluids is facilitated by steeply dipping NNE strike-slip normal faults. This can explain the presence of hot springs in the northwestern part of the volcanic area (Figure 2.4b). Moreover, it is assumed that the NNE-striking faults dip to both the east and west in the Itasy area. The strike-slip faults bounding the pull-apart basin structures dip to the NW and SE, as represented in the cross-section (Figure 2.4c). Although an exact recharge area for the thermal water cannot be pinpointed, it is most likely from the surrounding Itasy Mountain Range.

The deep geothermal reservoir is related to fractured Precambrian basement, which may represent the host rocks because no potential units with primary porosity have been found. The basement rocks are migmatitic orthogneiss and paragneiss (Table 2.3). The average temperature of the geothermal reservoir is estimated by geothermometers to be

around 170 to 240°C (Gunnlaugsson et al., 1981; Sarazin et al., 1986). Hot spring temperatures range between 24 and 57°C. These temperatures are lower than the hot springs in the North region.

The heat source is believed to be a fossil magma system since the volcanic activity lasted from 27 to 3 Ma (Bardintzeff et al., 2010; Rufer et al., 2014). This could be related to a recently crystallized magma chamber originating in the lower part of the lithospheric mantle (Bardintzeff et al., 2010), which situated at 50 km depth beneath the crust. The latter is less than 40 km thick (Wysession et al., 2016; Pratt et al., 2017; Andriampenomanana et al., 2017). As in Ambanja and Ambilobe areas, a moderate geothermal gradient is expected.

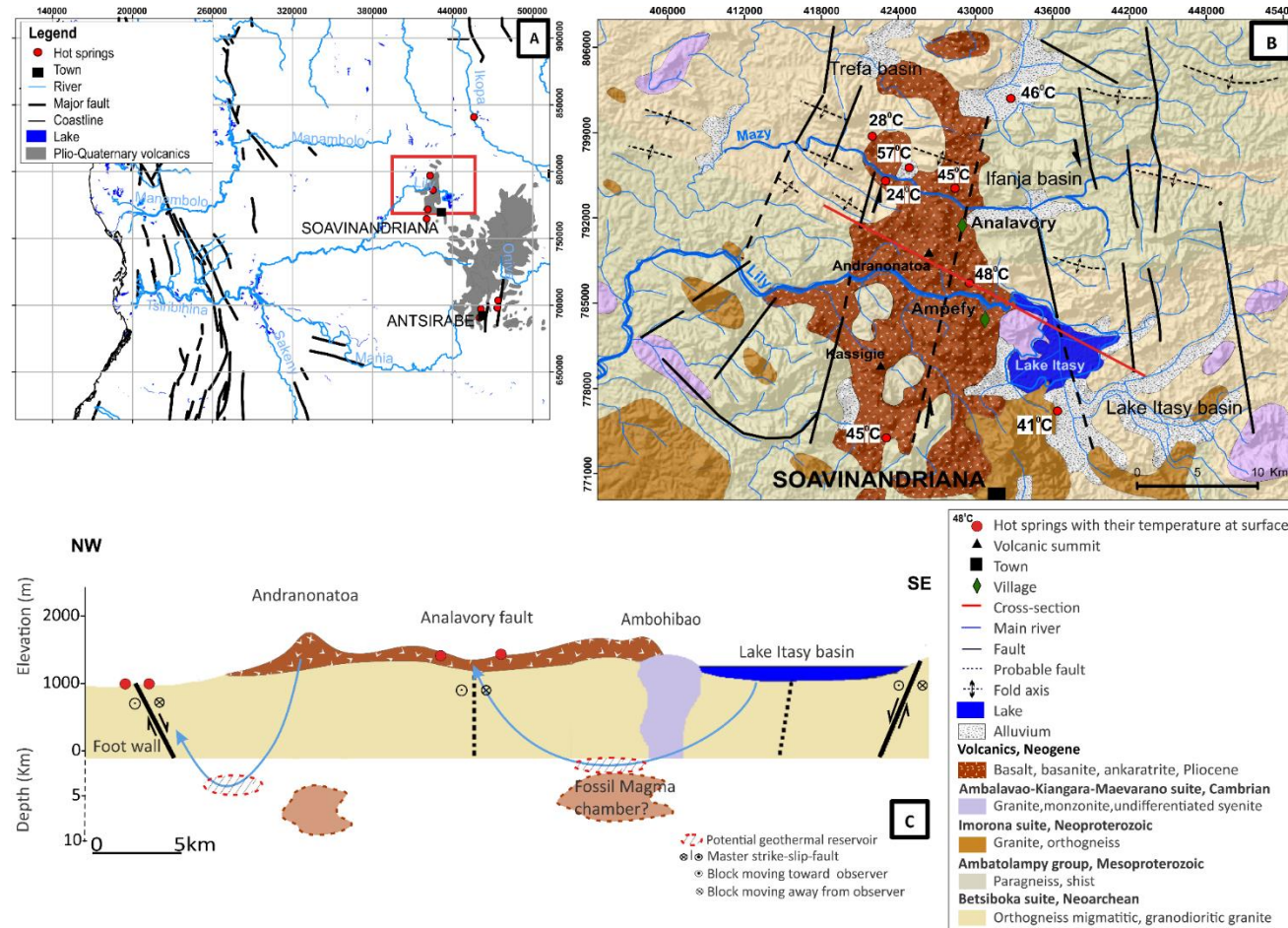


**Figure 2.4** (a) Location of the Itasy geothermal area, (b) Detailed geology showing the position of thermal springs (modified from Andrianaivo et al., 2010b), and (c) Conceptual model of the Itasy pull-apart basin geothermal system, (modified from Andrianaivo et al., 2010a). The vertical scale of the elevation profile, which was created using ASTER imagery, has been exaggerated compared to the depth scale, which is based on the structure of the crust and uppermost mantle beneath Madagascar (Andriampenomanana et al., 2017).

### **2.5.2.2**

### **Antsirabe basin**

The Antsirabe Basin is one of the large Neogene alluvial basins in the highlands occupying a half-graben structure (Figure 2.5; Table 2.2). The extension regime during the Pleistocene created the Manandona and Sahatsio half-grabens (Figure 2.5c), delimited by the large Betampona Escarpment and the Mandray Fault, respectively, both of which are west-dipping normal faults (Figure 2.5b and 2.5c). The Antsirabe Basin is dominated by Upper Oligocene to Pleistocene volcanic rocks and extensive flood basalts and trachytes of unknown thickness (Bardintzeff et al., 2010). Most of those originated from the main crest of the Pliocene volcanic massif of Ankaratra (Rufer, 2009), and were covered by 25 m of cinerites and more than 10 m of Neogene lacustrine sediments (Rasoanimanana et al., 2012). A Precambrian metamorphic basement, which belongs to the Archaean Antananarivo Domain, underlies these formations and consists of orthogneiss migmatite of the Betsiboka suite and granite monzonitic of the Imorona suite.

Water can circulate at depth through fractures in the Precambrian basement, which is assumed to be the host rock (Table 2.3). The weathered basalt forming arenaceous layers is considered to be a permeable formation through which meteoric recharge can occur (Figure 2.5b). The deep circulation of underground water is thought to follow the general topography from E to W (Figure 2.5c). Normal faults and NE-SW fractures would favour rising fluids, which would explain the presence of hot springs emerging along the Sahatsio Valley and the Antsirabe hot springs, which are aligned in a N-S direction. These hot springs temperatures reach 38 to 57°C, and the temperature of the geothermal reservoir is estimated to be around 150 to 160°C, possibly up to 240°C, according to chemical geothermometers calculated by Gunnlaugsson et al., (1981). However, Sarazin et al., (1986) concluded that the geothermal reservoir temperature should not exceed 150°C by using a silica geothermometer to estimate temperature since the water of the Antsirabe hot springs has mixed with superficial groundwater.

In the Antsirabe area, the average crustal thickness and lithosphere depth, 40 and 50 km, respectively, are the same as those found in the Itasy area (Wysession et al., 2016; Pratt et al., 2017; Andriampenomanana et al., 2017). As the volcanism is too old (28 to 3 Ma) to constitute an active heat source, the thermal gradient is expected to be close to or below the moderate range.

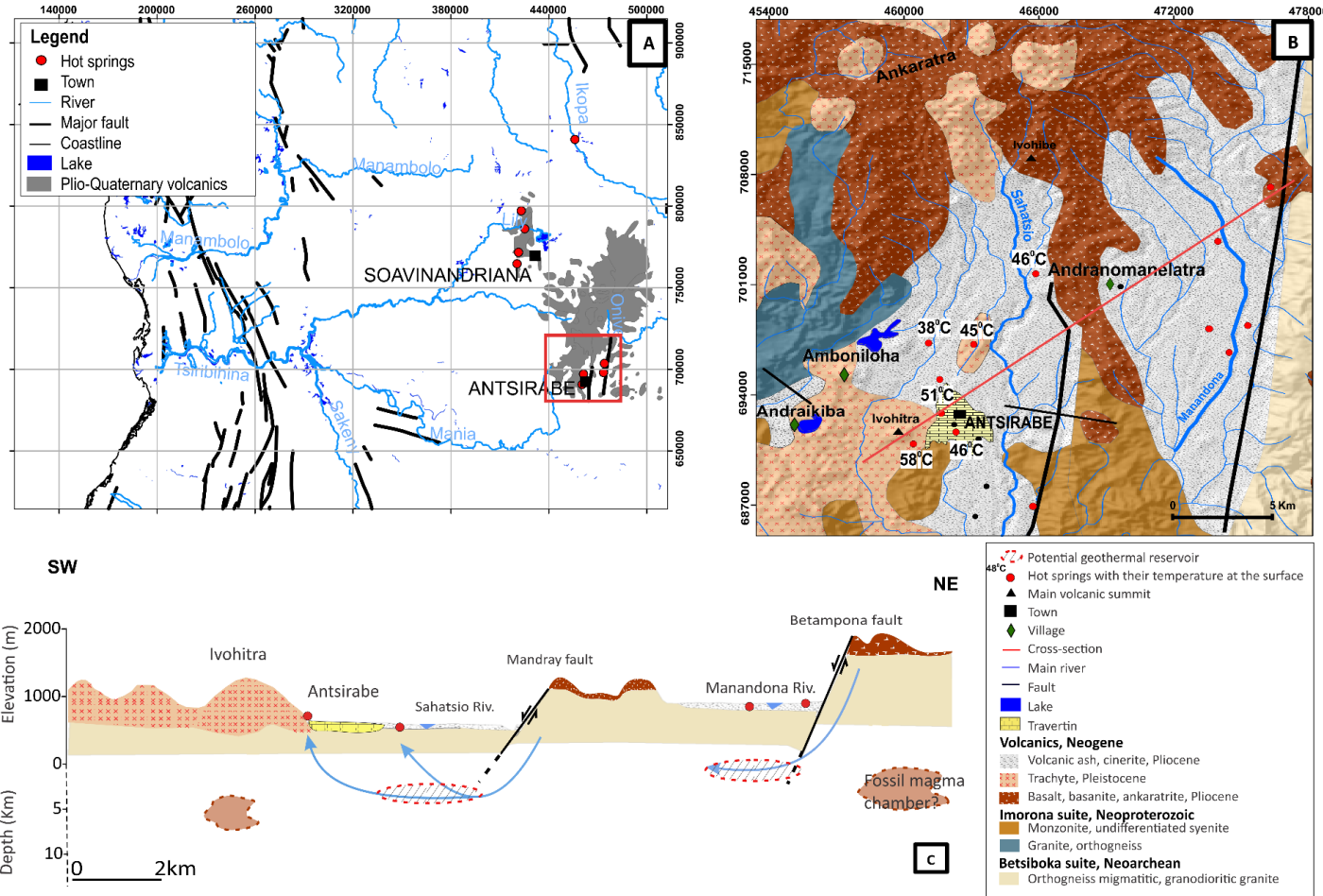


**Figure 2.5** (a) Location of the Antsirabe geothermal area, (b) Detailed geology showing the position of the hot springs, (modified from Rufer 2009), and (c) Conceptual model of the Antsirabe Basin geothermal system, (adapted from Rasoanimanana et al., 2012). The vertical scale of the elevation profile, which was created using ASTER imagery, has been exaggerated compared to the depth scale, which is based on the structure of the crust and uppermost mantle beneath Madagascar (Andriampenomanana et al., 2017).

### **2.5.3 West region**

#### **2.5.3.1 Miandrivazo area**

This area is located in a fault zone marking the contact between the metamorphic basement and the Morondava sedimentary basin (Figure 2.6; Table 2.2). The hot springs are observed from the town of Miandrivazo in the north to the village of Malaimbandy in the south (Figure 2.6a). The Proterozoic basement, which is intersected by Cretaceous doleritic dykes, is dominated by tonalitic-granitic orthogneiss of the Dabolava Suite and amphibolite bearing paragneiss belonging to the Ikalamavony Group (Melluso et al., 2001; Tucker et al., 2014). The Karoo sediments in this area are 2 km thick and consist of conglomerates, sandstones and red clays of the Sakoa Group, and Permian red clay of the Sakamena Group, overlying the basement. Syn-sedimentary normal faults trending N110°E (Piqué et al., 1999a) are also observed from Miandrivazo to Malaimbandy (Figures 2.6a and 2.6b).

The hot springs located near Malaimbandy align in an N-S direction and are observed where doleritic dykes occur (Figure 2.6b and 2.6c). Fractures in the doleritic dykes are assumed to control the ascent of the thermal water, as proposed by Gunnlaugsson et al., (1981). A local E-W groundwater flow driven by topography was assumed for our conceptual model to explain the hot springs near Malaimbandy (Figure 2.6c). Fractured paragneiss and orthogneiss in the basement units are considered potential host rocks since the sedimentary rock cover is relatively thin (Table 2.3). Hot springs in the area reach 30 to 51°C at the surface, and the geothermal reservoir temperature is estimated to be 140 to 170°C (Gunnlaugsson et al., 1981).

This region, where the average crustal thickness is estimated to be 36 km, including 3 km of sedimentary deposits (Andriampenomanana et al., 2017), is an inactive magmatic province since the latest volcanic activity was in the Cretaceous (Melluso et al., 2001). Therefore, the heat source of the area is related to the thin continental crust and the geothermal gradient is moderate.

#### **2.5.3.2 Morondava Basin**

The conceptual model for the Morondava Basin was built by combining surface data with seismic profiles (Du Toit et al., 1997; Piqué et al., 1999a; Geiger et al., 2004), following an

E-W cross-section (Figure 2.6c). The Morondava Basin has experienced two main rifting episodes ending with a passive margin evolution (Table 2.2). The Cretaceous flood basalts and dextral strike-slip faulting affected the sedimentary sequences and were active during the second rifting event, when Madagascar moved southward from Eastern Africa along the Davie Fracture Zone during the Upper-Cretaceous (Razafimbelo, 1987; Rajaomazava, 1992; Piqué et al., 1999a; De Wit, 2003). This deformation resulted in the small graben and horst structures of the Morondava Basin, created by faults trending N20°E or N160°E (Coffin et al., 1988; Piqué et al., 1999a). The ages of the observed continental and marine deposits are Upper Carboniferous to Present. They consist of two main lithostratigraphic units. The first is the Karoo Supergroup sequence (upper-Carboniferous to mid-Jurassic), dominated by continental deposits and subdivided into the Sakoa, Sakamena and Isalo groups, which consist of alternating conglomerates, sandstones, limestones, marls and clays. The second is the Post-Karoo Sequence dated from Upper-Jurassic to Lower Cretaceous, consisting essentially of marine deposits (Razafimbelo, 1987; Geiger et al., 2006; Reeves, 2014). All of the sedimentary units dip to the west and vary from 4 to 6 km thick on average (Coffin et al., 1988; Geiger et al., 2006; Piqué et al., 1999a; Rindraharisaona et al., 2017; Andriampenomanana et al., 2017).

The topography is flat enough that it is unlikely to drive regional-scale groundwater flow. Hot springs on the western side of the basin are likely explained by saltwater intrusions, their higher density compared to freshwater causing a hydraulic gradient that forces water upward along faults (Figure 2.6c). Potential host rocks with primary porosity are the Triassic sandstones and limestones of the Isalo Group (Karoo; Table 2.3). Aquifers in these formations are already exploited for groundwater at depths between 50 and 82 m (Mamifarananahary et al., 2007), demonstrating their permeability. The majority of hot springs emerge at the surface of marl, marl-clay or carbonate formations, as observed to the south of Ankilizato village (Figures 2.6b and 2.6c). Furthermore, a series of NNE-SSW trending faults and fractures that formed during the extension of the basin, which collapsed toward the west, control their distribution (Figure 2.6b).

The surface temperatures of springs range from 39 to 42°C. Geothermometers indicate a reservoir temperature between 120 and 140°C (Table 2.3; Gunnlaugsson et al. (1981), which corresponds to a fluid of low enthalpy. In this area, several oil and gas boreholes have been drilled, and the geothermal gradient has been estimated at

$38^{\circ}\text{C km}^{-1}$  (Rider et al., 2011). Therefore, the maximum depth of fluid circulation could be 3 to 4 km.

The average thickness of the crust is very thin in the Morondava Basin, as the Moho is between 18 and 36 km deep (Rindraharisaona et al., 2017; Andriampenomanana et al., 2017). The thin continental crust is believed to contribute to the higher geothermal gradient.

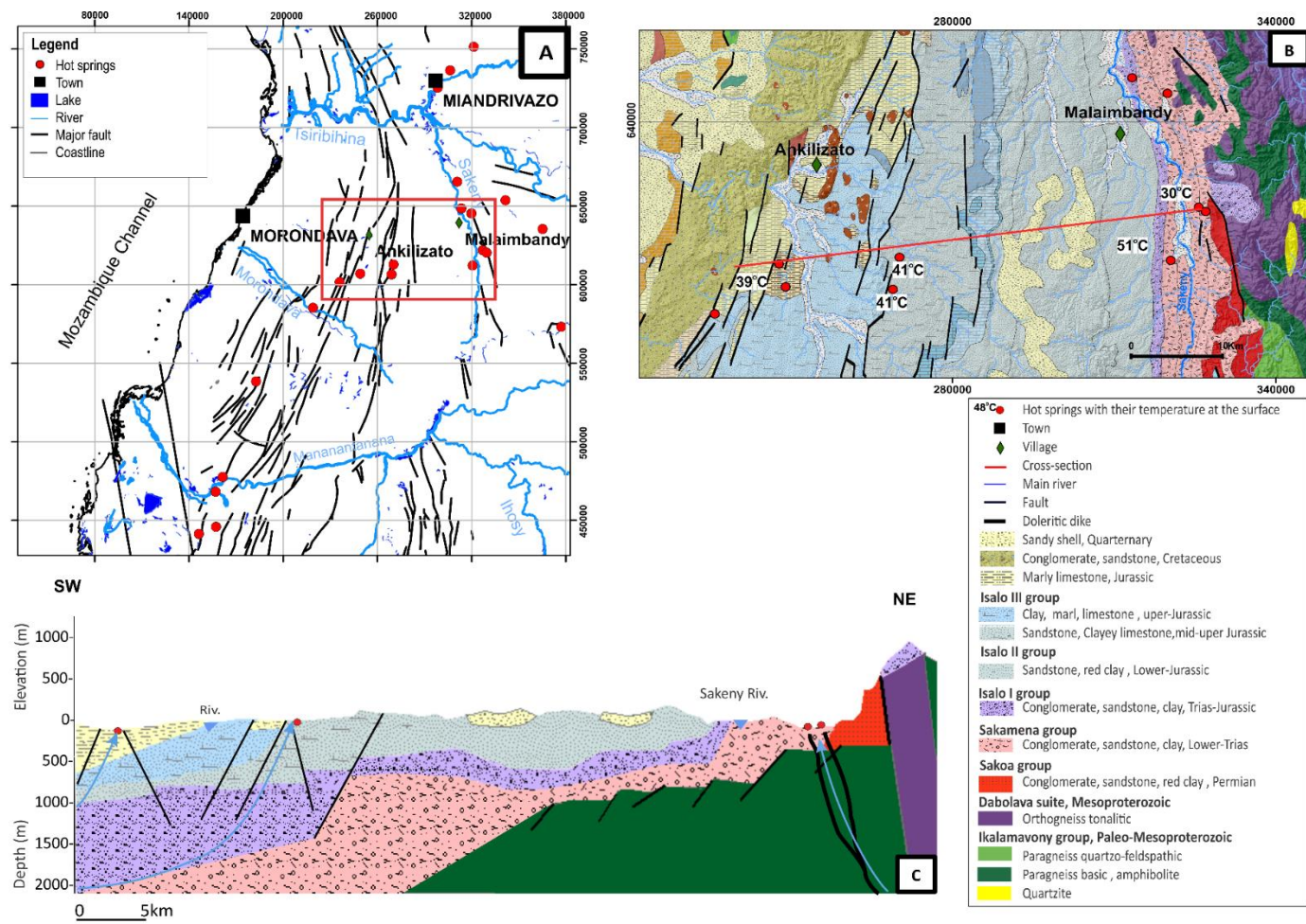


**Figure 2.6** (a) Location of the Miandrivazo and Morondava geothermal areas, (b) Detailed geology showing the position of thermal springs (modified from Roig et al., 2012), and (c) Conceptual model of the Miandrivazo-Morondava geothermal systems. The elevation profile was compiled using ASTER imagery, and the depth scale is based on the seismic profile (Du Toit et al., 1997; Piqué et al., 1999a).

## **2.6 Discussion**

Developing a complete classification of geothermal systems for Madagascar required a thorough characterization of the dominant geologic controls, geothermal play types and heat sources (Table 2.2). The information on these features combining with the geothermal characteristics (Table 2.3) was used to classify the type of system for each geothermal region in this study (Table 2.4). The conceptual models illustrate a general understanding of the groundwater flow and heat transfer mechanisms affecting the geothermal systems, and they highlight, with an acceptable degree of uncertainty, the factors controlling heat sources, formation permeability and fluid migration. Based on this analysis, the classification can be summarized as follows: 1) Geothermal systems in the Morondava area are liquid-dominated, low-temperature systems in a deep sedimentary basin; 2) The Miandrivazo and Ambilobe areas are liquid-dominated, low- to moderate-temperature systems controlled by major boundary faults that delineate the basin-basement contact; 3) The Ambanja, Itasy and Antsirabe areas are liquid-dominated, moderate-temperature systems in a rift setting affecting the basement. Our proposed classification improves the understanding of geothermal systems in Madagascar, which was previously categorized by Andrianaivo (2011) into two types: volcano-tectonic and non-tectonic.

### **2.6.1 Analogue geothermal systems**

The scarcity of data on the geothermal systems of Madagascar is a sign of the country's early stage of geothermal exploration but can be complemented by studying global analogues of geothermal systems at the exploitation stage. Based on geological context, the studied areas in Madagascar share similarities with the northwestern part of the Great Basin in the Basin and Range Province of the USA (Faulds et al., 2010), the Anatolian block of Western Turkey (Yilmazer et al., 2010), and the Main Karoo Basin in South Africa (Campbell et al., 2016a), all of which are considered analogues. In terms of geothermal play and geologic controls, all the analogue systems belong to the extensional domain type. In this context, active faulting and fracturing control the permeability necessary for fluid circulation and heat flow conduits, offering a comparable setting with low- to moderate-enthalpy geothermal energy sources. The analogue geothermal systems differ from each other by their respective plate tectonic, geological and structural settings, and heat sources, but each of their characteristics is comparable to the geothermal areas of Madagascar, as summarized in Table 2.5.

Major geothermal activity occurs in the northwestern part of the Great Basin in the USA, where hydrothermalism is related to transtensional zones and normal faulting, as found in the Walker Lane fault system (Coolbaugh et al., 2005; Faulds et al., 2010). The Ambilobe and Miandrivazo areas in the North and West regions of Madagascar, respectively, share the same characteristics as the Walker Lane geothermal systems, more precisely in the Pyramid Lake fault zone. The latter represents a WNW extensional system, which operates along NW trending lateral strike-slip fault to NNW-striking normal and normal-dextral faults (Faulds et al., 2010). The geothermal system occurs at the intersection between NNW-striking, primarily normal fault and WNW-striking mainly dextral fault (Faulds et al., 2010). The geological formations are dominated by 1 to 2 km of mafic Miocene volcanic rocks intercalated with thin sediments, all overlying a Mesozoic granitic to metamorphic basement (Faulds et al., 2010). The nature of the stratigraphic sequences is the main difference between the Great Basin and the Ambilobe and Miandrivazo areas. The volcanic sedimentary rocks in the Basin and Range Province are considered the host rocks for the thermal fluids (Moeck, 2014), but the fracture and fault setting acts as a major fluid conduit and controls the fluid flow in impermeable formations (Faulds et al., 2010; Wallis et al., 2018). Faulds et al., (2012) also found that the distribution of geothermal reservoirs correlates with areas of higher strain rate. Geothermometry suggests that a deep reservoir at Walker Lane reaches temperatures of 180 to 190°C (Faulds et al., 2010), which compares to the range of expected reservoir temperatures in the Ambilobe and Miandrivazo areas (Gunnlaugsson et al., 1981).

E-W striking normal faults, including major graben-bounding faults, dominate the structural setting in Western Turkey where extensional and transtension zones are active (Faulds et al., 2010; Yilmazer et al., 2010). The Ambanja geothermal area in the Sambirano graben (North region) and the Antsirabe area with half-graben structures (Central region) share similar characteristics with geothermal systems in the Gediz Graben of Western Turkey. The NNE strike-slip faults and pull-apart structures that characterize the Itasy area make the Central region of Madagascar comparable to the geothermal systems of the Marmara region in Turkey where similar NE-SW strike-slip and E-W oblique and normal fault systems have been documented (Simsek, 1997). The main geological formations in Western Turkey are dominated by a Paleozoic basement composed of metamorphic rocks (gneiss, mica schist and marble), overlain by Triassic-Jurassic to Neogene sedimentary rocks (conglomerate-sandstone and clay units ranging from 50 m to 6 km thick), Cenozoic volcanic rocks (Miocene basalt), and finally Quaternary alluvium (Simsek, 1997; Yilmazer et al., 2010). Depending on the dominant lithology in the geothermal areas, the caprock includes clay-rich intervals within the Neogene sedimentary units (Tarcan et

al., 2000), and the reservoir lies in basement rocks and/or partially in Miocene basalts (Faulds et al., 2009). These lithologies are similar to those found in the Ambanja, Itasy and Antsirabe area, but the age of the sedimentary deposits and basement rocks are different. The measured reservoir temperature in the Gediz Graben varies from 85 to 215°C and decreases from east to west (Yilmazer et al., 2010), which compares to 140 to 240°C in the Ambanja, Itasy and Antsirabe areas (Gunnlaugsson et al., 1981).

Geothermal systems in the Morondava Basin in the West region of Madagascar can be compared to those of the Karoo Basin in the Eastern Cape Province of South Africa. The latter is hosted in Permo-Triassic Karoo sedimentary sequences originating from deposits that covered the central part of Gondwana. They are underlain by metamorphic basement rocks of the Namaqua-Natal Belt. Dolerite sills and dykes throughout the Karoo Basin are related to the peak of volcanic activity in South Africa and Lesotho, which was dated at  $183 \pm 1$  Ma (Campbell et al., 2016a). Rock formations in the Morondava Basin are generally expected to have low permeability, similar to the Karoo Basin, except for sandstones representing potential reservoir formations (Campbell et al., 2016a). Conductive heat transfer is expected to be the dominant heat transfer mechanism affecting the temperature in the upper crust.

**Table 2.5 Shared features between Madagascar geothermal areas and global analogues**

Region	North		Central			West	
Area	Ambilobe	Ambanja	Itasy	Antsirabe	Miandrivazo	Morondava	
Age of volcanism	Miocene	Miocene-Pleistocene			Mesozoic		
Heat source	Shallow Moho	Shallow Moho and fossil magma chamber			Shallow Moho		
Lithology	Sedimentary sequences, magmatic to metamorphic basement	Volcanic rocks and deposits, magmatic to metamorphic basement	Neogene deposits, volcanic rocks, magmatic to metamorphic basement	Mesozoic and Permian sedimentary sequences, magmatic to metamorphic basement			
Structural setting or regime	Normal faulting Dextral/sinistral strike-slip faults	Graben	Pull-apart basin	Half-graben	Normal faulting	Horst-graben structure in passive margin basin	
Dominant geologic control	Quaternary faulting	Miocene-Quaternary active faulting			Faults/fractures		
Analogue	Walker Lane, Great Basin, USA	Gediz Graben, Western Turkey			Walker Lane, Great Basin, USA	Main Karoo Basin, South Africa	

### 2.6.2 Heat source and heat transfer mechanism

Cenozoic volcanism in northern Madagascar has two assumed origins following the hypotheses advanced by various authors. Michon (2016) proposed that volcanism was generated by deformation of the lithosphere, as observed on the volcanic Comoros Island in the context of the southern termination of the East African Rift. Other authors propose a more regional lithospheric extension, allowing local asthenospheric upwelling beneath a thin crust caused by crustal extension and collapse (Wysession et al., 2016; Paul et al., 2017; Pratt et al., 2017). The mantle lithosphere is expected to be thin in the volcanic provinces of North and Central Madagascar, as well as in the West Region where Miandrivazo and Morondava geothermal systems are located. Delamination of the lithosphere at its mature stage can even be absent in such extensional zones (Pratt et al., 2017; Wysession et al., 2016), as is the case below the Great Basin in the Western United States (Meissner et al., 1998). The average thickness of the Great Basin crust is between 15 and 56 km, whereas the depth of Moho in Turkey varies between 24 and 48 km, and the

thinnest crustal thickness (20–35 km) is found on the western coast of Anatolia (Tezel et al., 2013). According to Faulds et al., (2009); Faulds et al., (2010), the main factor causing higher heat flow in the Great Basin, as in Western Turkey, is extensional crustal thinning. This is due to the shallow depth of the Moho, although recent intrusions and/or volcanism can coincide with extensional zones.

In the Morondava area of Madagascar (West region), where the Moho depth is the shallowest at 18 km (Andriampenomanana et al., 2017), the heat source is related to crustal thinning. In the Main Karoo Basin, the crust beneath the Mesoproterozoic Namaqua-Natal Metamorphic Belt basement has an average thickness of 40 to 50 km (Delph et al., 2014). However, this basement is rich in heat-producing elements. The uranium concentration is about 10–54 ppm (Andreoli et al., 2006), which can release heat by the decay of radiogenic elements and affect heat flow (Dhansay et al., 2017).

Geothermal plays can be broadly separated into two types related to the heat transfer mechanism, which is either convection or conduction. Applying the existing catalogue of geothermal play types introduced by Moeck (2014); Moeck (2018), the geothermal systems of Madagascar are characterized by fault-controlled extensional domains (Table 2.2) and convection-dominated heat transfer is expected, although conductive heat transfer may occur outside fractured zones.

### 2.6.3 Fluid origin and flow

Most thermal spring water in Madagascar is carbon dioxide-rich, dilute ( $\text{Cl} < 200 \text{ ppm}$ ) and saturated in calcite (Besairie, 1959; Gunnlaugsson et al., 1981; Sarazin et al., 1986; Hambintsoa et al., 2017). The Ambanja, Ambilobe, Itasy and Antsirabe areas, which have the highest estimated reservoir temperatures (140–240°C), belong to the high-carbonate water type, in which carbonate concentration can be up to 500 ppm (Gunnlaugsson et al., 1981). The high bicarbonate, low chloride composition indicates that thermal fluids have mixed with cooler groundwater or meteoric water as it circulates in upwelling zones along faults (Truesdell, 1975). Due to the highly fractured and faulted crustal structures hosting the geothermal systems in Madagascar, there is considerable potential for meteoric water to infiltrate into deeper aquifers and for groundwater to ascend along faults, depending on their dip directions (Reed, 1983; Moreno et al., 2018). This is why faults have been assumed to be flow paths in our conceptual models for all six Madagascar geothermal areas (Figure 2.2 to 2.6). Assuming that the geothermal systems have normal to moderate geothermal gradients between 30 and 38°C  $\text{km}^{-1}$  (Rider et al.,

2011), the fluid sources can be found at depths of 3 to 8 km considering that the expected reservoir temperature is between 120 and 240°C (Gunnlaugsson et al., 1981). Although these estimated temperature ranges have inherent uncertainty because they were produced using chemical thermometers before the advances of Giggenbach's seminal work, the same temperature ranges are obtained when using the Giggenbach diagram based on the chemical composition of the hot springs water as reported in Gunnlaugsson et al. (1981).

The hot springs in the prospective areas of Madagascar are usually located near faults, and the fluid flow appears controlled by tectonic structures. The temperature of the hot springs is likely to decrease at the end of their flow path before reaching the surface, as a result of dilution with cold superficial waters and conduction-convection heat processes (Reed, 1983; Ferguson et al., 2009; Moreno et al., 2018;). The fluids of geothermal systems in Madagascar are thus related to the deep circulation of meteoric water along faults and fractures, similar to the geothermal systems of the Basin and Range Province where there is no active magmatism (Muffler, 1975).

## 2.7 Concluding remarks

Geothermal areas in Madagascar are commonly associated with extensional domains (Arthaud et al., 1990; Piqué et al., 1999b; Andrianaivo et al., 2010a), where major structures such as faults and fractures are the geological controls on fluid flow. Such systems involve heat transfer mechanisms dominated by free convection along the permeable fracture path, whereas heat conduction is likely to occur outside permeable fracture paths. The main source of the heat is crustal thinning, which is locally associated with recently crystallized intrusions, both of which increase the geothermal gradient.

This study categorizes the six main geothermal areas of Madagascar into three distinct classes of geothermal systems: 1) Graben bounder-fault liquid-dominated moderate-temperature (Ambilobe and Miandrivazo areas), 2) fossil magmatic liquid-dominated moderate-temperature (Ambohitra, Itasy and Antsirabe areas), and 3) sedimentary liquid-dominated low-temperature (Morondava area).

Despite the differences in the overall tectonic setting and geological formations, this classification made it possible to compare the geothermal systems of Madagascar to other typical geologic systems in which geothermal reservoirs have already been discovered and developed. The geothermal systems of the Great Basin (USA), the Anatolian Block (Western Turkey) and the Main Karoo Basin (South Africa) shared similarities with those in Madagascar. This finding has

potentially important implications for developing Madagascar's geothermal systems, where geothermal energy sources are associated with secondary porosity features such as fractures.

Conceptual models were constructed for each geothermal area of Madagascar where the geothermal play type provides fundamental knowledge to guide future exploration activities. Such models can be updated when new data become available and constitute a foundation upon which further knowledge can be built. The acquisition of borehole temperature data is the next step to better define heat flow and geothermal energy sources in Madagascar.

Combining the geothermometer estimates of reservoir temperatures from previous studies with our new classification for geothermal systems, it is possible to envision the production of geothermal electricity in the Ambilobe, Ambanja, Itasy, Antsirabe and Miandrivazo areas, and direct-use geothermal energy projects could be possible for aquaculture, agriculture and cooling in the Morondava area.

### **3 DEUXIÈME ARTICLE: ASSESSMENT OF PETROPHYSICAL ROCK PROPERTIES IN NORTH MADAGASCAR: IMPLICATIONS FOR GEOTHERMAL RESOURCE EXPLORATION**

---

Évaluation des propriétés pétrophysiques des roches dans le nord de Madagascar: implications pour l'exploration des ressources géothermiques

**Auteurs :**

<sup>1</sup>M. Rajaobelison, <sup>1</sup>J. Raymond, <sup>1</sup>M. Malo and <sup>2</sup>C. Dezayes <sup>3</sup>S. Larmagnat

<sup>1</sup> Institut national de la recherche scientifique, 490 de la Couronne, Québec, QC G1K 9A9, Canada

<sup>2</sup> Bureau de recherches géologiques et minières, 3 Avenue Claude Guillemin, 45100 Orléans, France

<sup>3</sup>Geological Survey of Canada

490, rue de la Couronne, Québec (Québec) G1K 9A9 Canada

**Titre de la revue ou de l'ouvrage :**

Natural Resources Research

19 Juin 2021

<https://doi.org/10.1007/s11053-021-09875-9>

**Contribution des auteurs :**

MR a travaillé sur la collecte des données et a rédigé le manuscrit. JR et MM ont dirigé le projet, en fournissant le soutien logistique ; CD a fourni des commentaires et des documents utiles pour l'amélioration du manuscrit. SL a fourni des commentaires sur l'amélioration de la méthodologie ; JR, MM, CD, SL, rédaction - révision et édition. Tous les auteurs ont relu le manuscrit et ont apporté leurs commentaires et leurs idées.

**Lien entre l'article ou les articles précédents et le suivant :**

Le premier chapitre présente un catalogue des systèmes géothermiques de chaque région d'intérêt à Madagascar. Le catalogue est une manière d'organiser les données pour mettre en évidence l'importance des contextes géologiques, de la température du sous-sol et des facteurs dominants qui contrôlent la circulation du fluide et/ou la source de chaleur dans les systèmes géothermiques. Un modèle conceptuel pour chaque système géothermique de chaque région d'intérêt a été défini et illustre ces éléments importants. Parmi les régions d'intérêt catégorisés dans le catalogue, les systèmes géothermiques de la zone d'Ambilobe et d'Ambohibao au Nord de Madagascar, caractérisés respectivement par un contexte de faille bordière de graben et par la présence d'une chambre magmatique fossile et ayant une ressource à température modérée ont été étudiés dans le second chapitre. Le but est de mieux comprendre et de réduire les incertitudes concernant certains éléments importants des systèmes géothermiques identifiés pour leur modèle conceptuel respectif, notamment les propriétés thermohydrauliques des formations dominantes des deux zones ainsi que le mécanisme de transfert de chaleur qui est associé.

### **3.1 Introduction**

Madagascar is currently facing an energy supply problem. The infrastructure is underdeveloped and the per-capita consumption is low. Most of the population uses traditional biomass such as firewood and charcoal as their primary energy source, thereby accelerating deforestation, water resource degradation, biodiversity and soil loss. Imported petroleum fuels dominate the local energy industry. In 2016, only 24 % of the population had access to electricity, generated by hydropower and thermal plants (Panos et al., 2016; Ritchie, 2019). Madagascar's energy transition policy aims to increase the household electricity coverage and reduce the country's dependence on fossil energy by developing alternative and renewable sources. The development of geothermal energy is proposed as a local, environmentally friendly and renewable option, suitable for direct-use purposes and future electricity generation, even though the cost of drilling can sometimes be a barrier to its implementation.

Several reconnaissance surveys and detailed studies of hot springs and geothermal areas have been carried out in Madagascar since 1960. Some of these early studies included measurements of surface temperature, water and gas flow, water and gas analyses of hot springs, and reservoir temperature estimates using chemical geothermometers (Besairie, 1959; Gunnlaugsson et al., 1981; Hambinintsoa et al., 2017). The geothermal areas of the North, Central and Western regions of Madagascar, which are commonly associated with extensional domains, have been classified into three distinct play type systems: 1) liquid-dominated moderate-temperature graben border faults, 2) liquid-dominated moderate-temperature fossil magmatic systems, and 3) low-temperature sedimentary sequences. In all three types of geothermal systems, major structures such as faults and fractures play an important role in the fluid flow path (Rajaobelison et al., 2020).

To identify potential reservoirs and develop a geothermal system, it is essential to evaluate or anticipate the heat transfer mechanisms prevailing at depth. Indeed, understanding heat transfer mechanisms can help explain the temperature distribution at depth (e.g., Langevin et al., 2020; Lei et al., 2020). Moreover, the choice and viability of energy extraction methods depend on such mechanisms for both shallow and deep systems. The dominant heat transfer mechanism operating in a geothermal system can be 1) conduction in petrothermal systems, 2) forced convection in transitional systems where external means are used to force the fluid over an area, such as fluid rising along fractures and faults subjected to a regional hydraulic gradient, or 3) natural (or free) convection in hydrothermal systems where heat moves through fluid motion caused by natural means such as the buoyancy effect (Sass et al., 2012; Moeck, 2014).

At the early geothermal exploration stage, when deep borehole data are lacking, the characterization of heat transfer mechanisms can be inferred by assessing the thermal and hydraulic properties of the main lithologic units cropping out in the study area or at outcrop analogues of the target area (e.g., Sass et al., 2012; Götz et al., 2015; Campbell et al., 2016a; Weydt et al., 2018; Miranda et al., 2020). Further studies have evaluated changes in thermohydraulic properties affected by hydrothermal alteration at depth (Mielke et al., 2015; Mielke et al., 2016). Rock permeability, the main parameter controlling fluid heat and mass transfer (Zharikov et al., 2005), is particularly important to evaluate. Thermal properties are also essential when describing diffusive heat transfer mechanisms. Such hydraulic and thermal properties can be assessed by laboratory methods, examples of which are presented in Filomena et al. (2014). Sass et al. (2012), who introduced the concept of thermofacies, demonstrated that permeability and thermal conductivity are dependent on lithofacies, which can be used to distinguish petrothermal and hydrothermal systems. The corresponding heat transfer mechanisms are conduction and convection. According to the classification of Moeck (2014), conduction-dominated plays can be described by their porosity to permeability ratios to distinguish enhanced geothermal systems (EGS) associated with petrothermal or hydrothermal resources from non-conventional or conventional hydrothermal resources. Data acquisition is thus essential before proceeding to subsurface studies and can help justify the drilling of boreholes to better define resources and envision possible exploitation scenarios.

This study focused on the Ambilobe and Ambanja areas in North Madagascar (Figure 3.1) to better characterize their geothermal systems, both related to extensional regime and classified as moderate-temperature resources (Rajaobelison et al., 2020). These geothermal energy sources could be exploited for direct-use purposes and electricity generation. We present the first evaluation of the petrophysical properties for the main lithologic units in both areas. Thermostratigraphic rock units were classified according to the thermofacies concept (Sass et al., 2012) put forward to identify the prevailing heat transfer mechanisms. Such information was previously unavailable for Madagascar, which now faces critical energy challenges and is in need of such fundamental knowledge if it is to improve its geothermal exploration status.

The objective of this work was to describe the relevant hydraulic and thermal rock properties that affect potential geothermal resources to identify potential targets for further geothermal exploration.

## **3.2 Geologic settings**

### **3.2.1 Ambilobe**

The Ambilobe area is located in the Andavakoera normal fault zone, which delineates the contact between sedimentary sequences and basement rocks. It forms a depression 120 km long by 3 to 5 km wide (Figure 3.1b). At the surface, hot springs reach temperatures of 59 to 72°C. According to chemical geothermometers (Gunnlaugsson et al., 1981), the reservoir temperature ranges from 140 to 180°C. The Ambilobe area is classified as a liquid-dominated, moderate-temperature, graben border fault geothermal system (Rajaobelison et al., 2020).

The basement rocks belong to the Bemarivo domain (Thomas et al., 2009; Tucker et al., 2014), predominantly micashist and amphibolite units from the Betsiaka Group. The latter is a metasedimentary rock stabilized in greenschist and amphibolite facies. In other areas, the Bemarivo domain is composed of granodioritic orthogneiss, derived from intrusive igneous rocks of the Antsirabe North Suite, and amphibolites, representing volcano-sedimentary rocks of the Daraina-Milanoa Group (Thomas et al., 2009; Tucker et al., 2012). Full descriptive details of these groups, including lithologic variations, petrography and mineralogy, can be found in the British Geological Survey research report (BGS-USGS-GLW 2008).

Sedimentary sequences belonging to the Karoo Supergroup (Figure 3.2) are part of Ambilobe Basin (Besairie, 1952). The base of the sequences begins with Permian sandstone and conglomerate of the Sakamena Group, unconformably overlying Proterozoic metamorphic bedrock. This is followed by Eotriassic shale between 200 to 300 m thick, overlain by Upper Triassic sandstone (Isalo I) of the Isalo Group. The Isalo I sandstone dips 5 to 30° to the west and forms an escarpment 400 to 500 m high that dominates the topography. Recent alluvial deposits derived from the weathering of sandstone and metamorphic basement rocks fill the depression. Examples of the typical field appearance of the various geological formations in the study area are shown in Figure 3.3.

The orientations of the main fault and fracture systems are dominantly NNW-SSE, NE-SW and N-S, as shown by the rose diagram in Figure 3.1b.

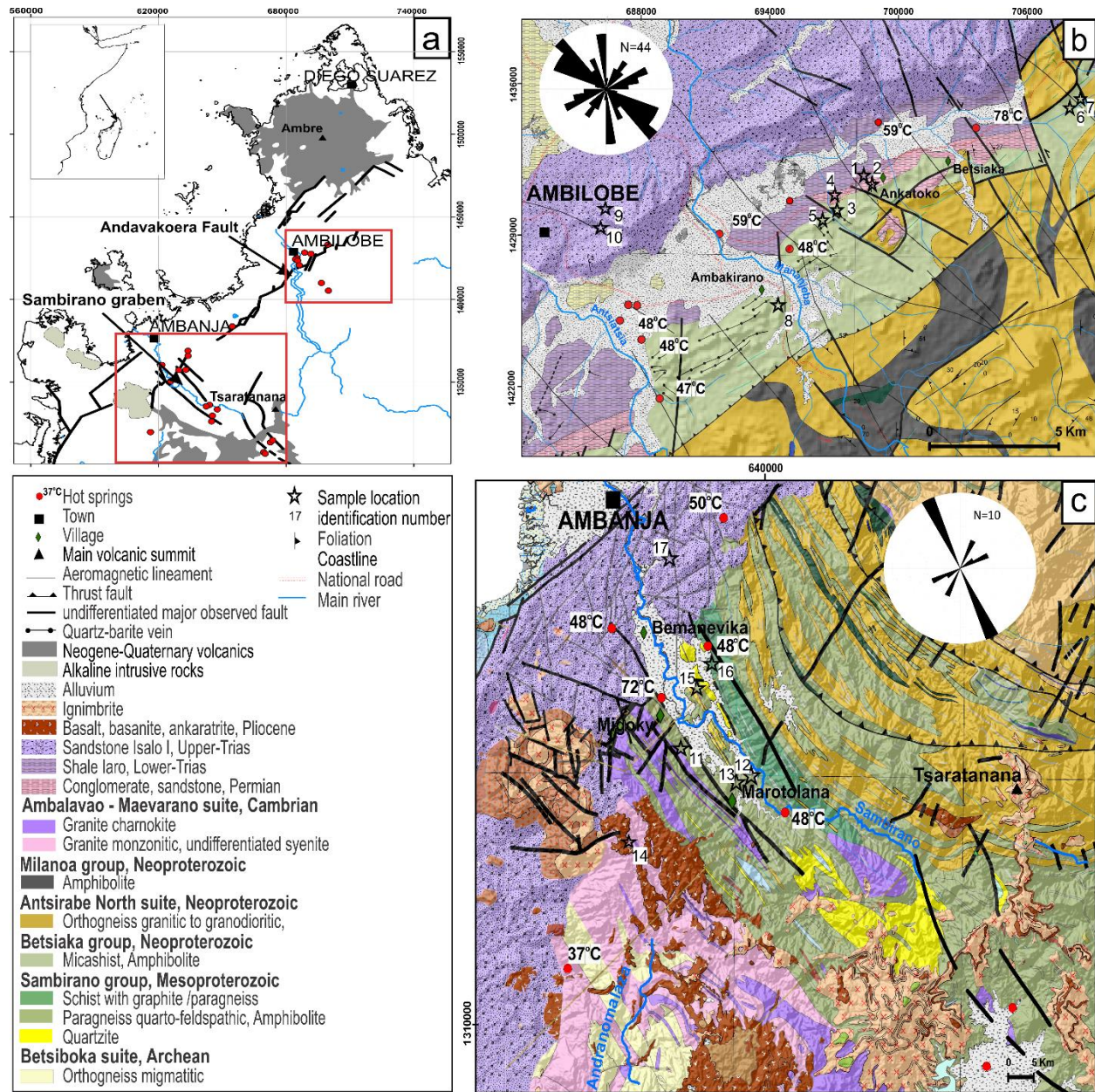


**Figure 3.1** (a) Location of the Ambilobe and Ambanja geothermal areas in North Madagascar, and (b and c) Geological maps of the study areas, (modified from Roig et al., 2012), showing temperature data (

Gunnlaugsson et al., 1981) and the numbered locations of collected rock samples. Rose diagrams illustrate the principal trend of faults and fractures using field data collected in 2018.

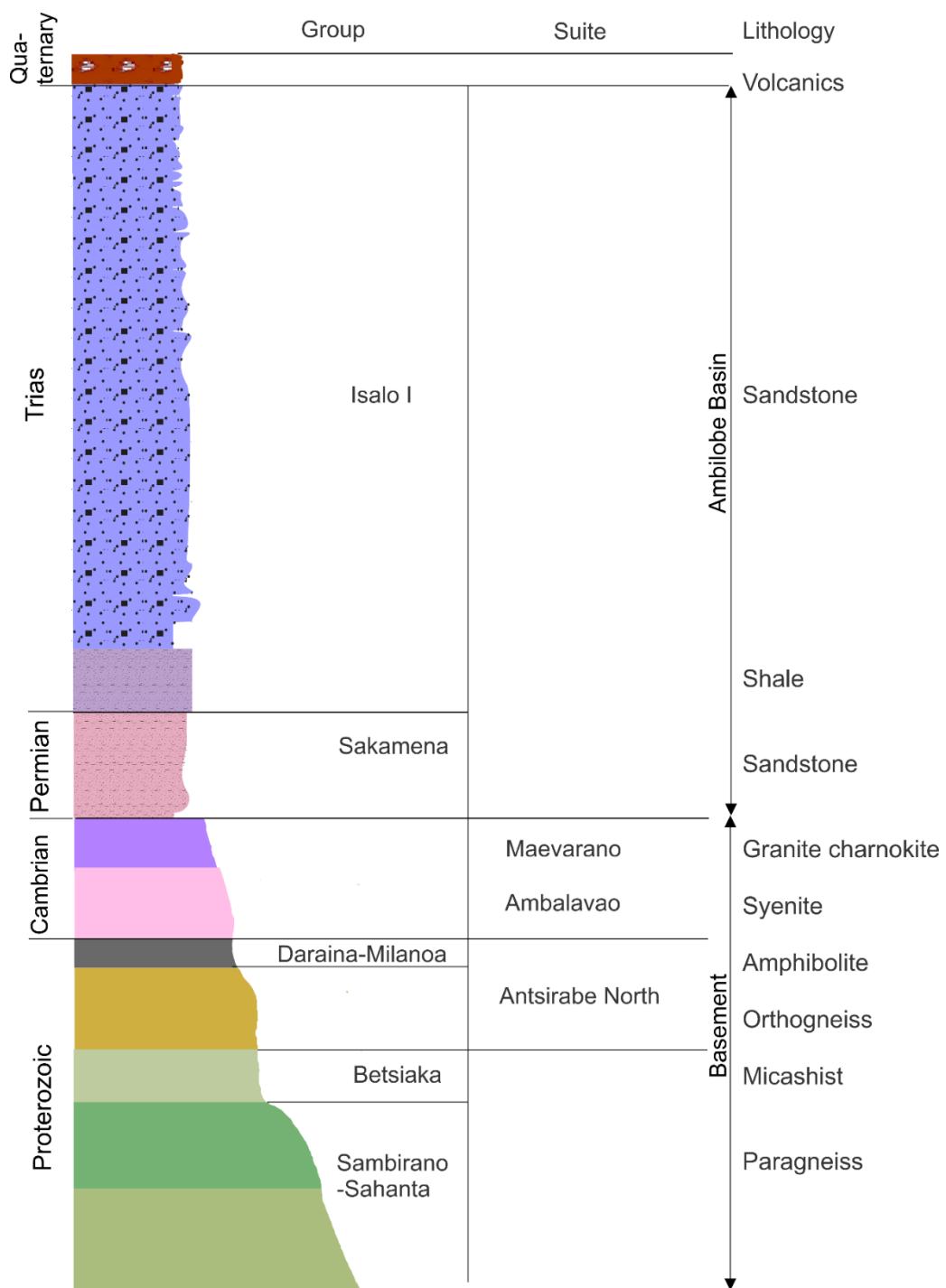


**Figure 3.2** Synthesized stratigraphic column of the Ambilobe and Ambanja geothermal areas (adapted from Besairie, 1946). Same legend as Figure 3.1.

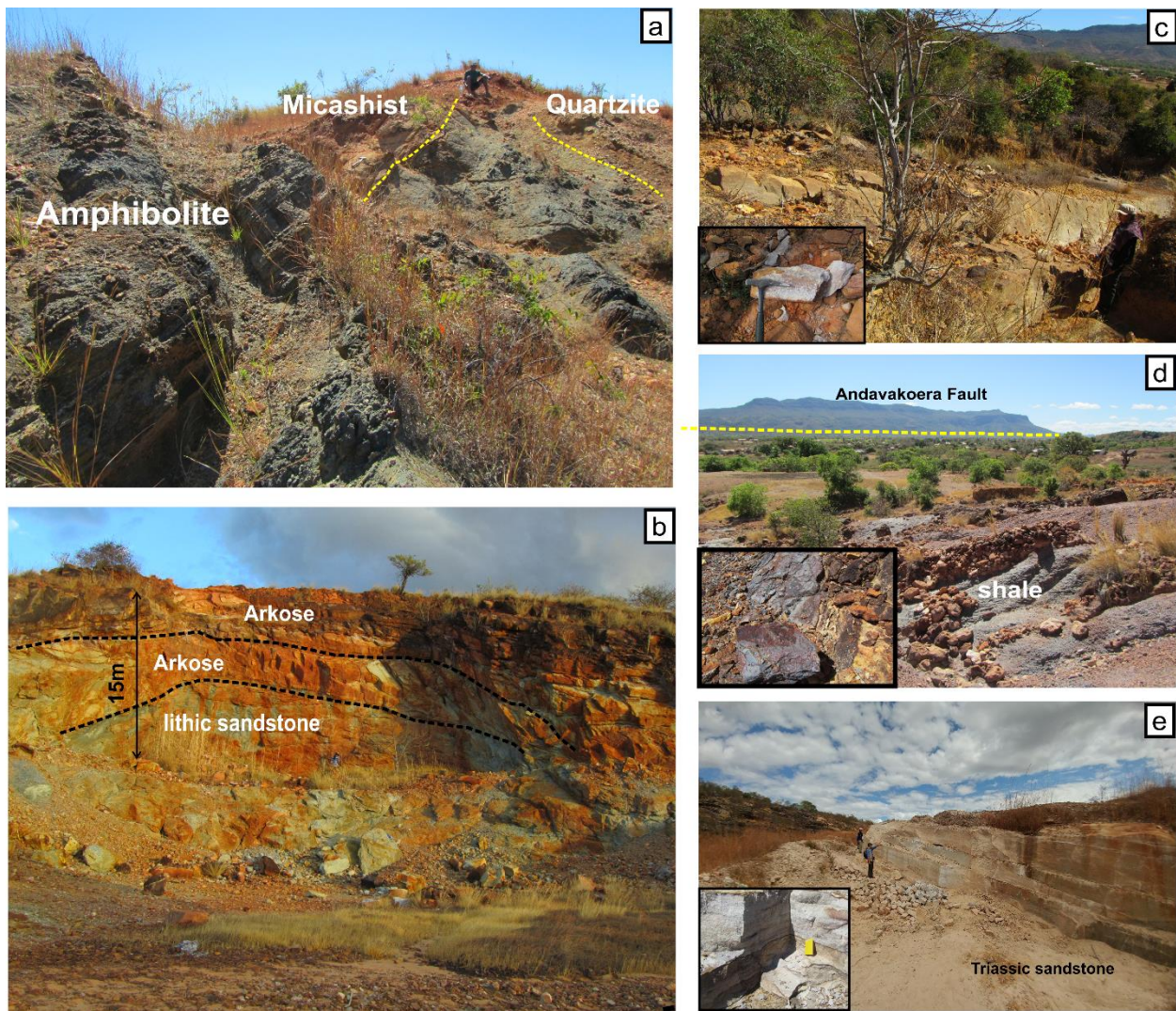


**Figure 3.3** Photographs of outcrop exposures in the Ambilobe area (numbers in parentheses refer to the sample locations in Figure 3.1): (a, 6) weathered basement rocks from Betsiaka Group; (b, 1) Greenish-grey to brown Permian sandstones in an abandoned quarry near the village of Ankatoko; (c, 2) typical Permian sandstone formation from the Sakamena Group, with close-up of one of the dark reddish purple layers; (d, 5) Eotriassic shale showing fissile texture, with close-up of the weathered surface and sealed fracture network; and (e, 9 and 10) Triassic sandstones in an artisanal active quarry, with close-up of laminations.

### 3.2.2 Ambanja

The Ambanja area is characterized by a 25 km-long graben oriented NW-SE with an average width of 4-8 km (Figure 3.1c). The hot springs are located close to the border faults of the graben and have a temperature range of 48 to 72 °C. Using chemical geothermometers, Gunnlaugsson et al. (1981) estimated that fluid temperature can reach 140 to 200 °C inside the geothermal reservoir, corresponding to a moderate enthalpy and a dominant liquid state. The Ambanja area

is classified as a liquid-dominated, moderate-temperature, fossil magmatic system due to its location where the Moho is shallow and where fossil magma chambers are believed to be the heat source (Rajaobelison et al., 2020).

The Proterozoic basement consists of high-grade (upper amphibolite to granulite facies) metasedimentary gneiss of the Sambirano-Sahanta Group rocks belonging to the Bemarivo domain (Thomas et al., 2009; Tucker et al., 2012). The Sambirano-Sahanta group is predominantly paragneiss (Figure 3.4), amphibolite and quartzite, intruded by Cambrian undifferentiated syenite of the Maevarano Suite (Thomas et al., 2009; Tucker et al., 2014). Triassic sandstone deposits of Isalo Group appear only in the northwest. Quaternary volcanic rocks are represented mainly by basalt, although volcanic deposits such as lapilli tuff and volcanic breccias, up to 600 and 700 m thick have been observed in the southern part of the graben. These pyroclastic deposits originated from the stratified Pleistocene and Eocene volcanic complexes of the neighbouring Tsaratanana and Ambondrona areas (Rossi, 1980; Estrade et al., 2014). The graben was filled with detrital and alluvial sediments.

The main faults and fractures are dominantly NNW-SSE, as shown in the rose diagram of field measurements on the geological map in Figure 3.1c.



**Figure 3.4** Photographs of outcrop exposures in the Ambanja area (numbers in parentheses refer to the sample locations in Figure 3.1): (a, 13) and (b, 11–12) paragneiss from Proterozoic basement rocks with a close-up of the gneissic texture; (c) cliff section of laterite-capped brown to rusty red, weathered Triassic sandstone in contact with the weathered basement; and (d, 11) Triassic sandstone cut by a fracture (black dotted line), with close-up of freshly broken sandstone where a portable permeameter was used to take permeability measurements.

### 3.3 Materials and laboratory analysis

#### 3.3.1 Sample preparation and measurement workflow

A total of 54 samples were collected from 17 outcrop locations (Figure 3.1; Table 3.1). The sampled rocks included Quaternary volcanics, Permian and Triassic sediments and Proterozoic metamorphic basement, representing the dominant geological units in the study areas.

**Table 3.1 Summary of geological material sampled and used in the present study, indicating age and geological unit. Outcrop locations correspond to Figure 3.1**

Rock type	Sedimentary				Metamorphic and igneous basement					Extrusive
Lithology	Sandstone	Shale	Breccia	Quartz-barite veins	Paragneiss	Mica schist	Amphibolite	Orthogneiss	Syenite	Basalt
Age	Permian-Triassic	Eotriassic	Post-Triassic	Post-Triassic	Paleo-proterozoic	Neo-proterozoic	Neo-proterozoic	Neo-proterozoic	Cambrian	Pliocene
Geological unit	Isalo and Sakamena groups	Isalo I			Sambirano-Sahanta Group	Betsiaka Group	Sambirano-Sahanta Group	Betsiaka Group	Betsiaka Group	Maevarano Suite
Outcrop location	2, 4, 9, 10, 17	1	2	5	11–13, 16	3, 5	6, 11	7, 8, 15	14	14
Number of samples (n)	19	5	2	3	14	2	7	3	2	2

Geological units are taken from (Besairie, 1952; Thomas et al., 2009; Tucker et al., 2014).

Petrographic analyses were conducted on thin sections using an optical microscope (Nikon Eclipse L200) to identify minerals, define grain size and roundness, and describe the texture and special features of the rocks such as millimetric fractures, joints, seams and sedimentary structures. Images of entire thin sections were also taken using a slide scanner (PowerSlide 5000) at an optical resolution of 5000 dpi. These images were analyzed using free JMicronVision 1.2.7 software (Roduit, 2007) to quantified mineral contents using the object extraction setting and point counting with 400 points per photograph of an entire thin section, and the recursive grid setting (Higgins, 2017; Navelot et al., 2018).

Sandstone samples were described using a combination of the Pettijohn and Folk classifications and plotted on a QFL diagram (quartz–feldspar–lithic fragments; Folk, 1954; Pettijohn et al., 1972). Basement rocks were plotted on QFM (quartz–feldspar–mafic minerals) and QP (quartz–plagioclase) diagrams (Debon et al., 1988) to determine the general composition of the metamorphic rocks and compare them to other rock samples from the study area collected by Thomas et al. (2009).

Measurements of thermophysical rock properties were performed at the Open Geothermal Laboratory at INRS (Raymond et al., 2017). Sedimentary and basement rocks were dried prior to analysis for at least 12 hours in a conventional oven at 115 °C, which is recommended before using the thermohydraulic devices (Coretest Systems Inc., 2017), except for the shale samples which were dried at 60 °C to avoid inducing microcracks and the formation of dehydroxylate clay

minerals (American Petroleum Institute, 1998; Campbell et al., 2016a; Gasparini et al., 2013; Li, 2019). The steps to determine the thermohydraulic properties are summarized in Figure 3.5.

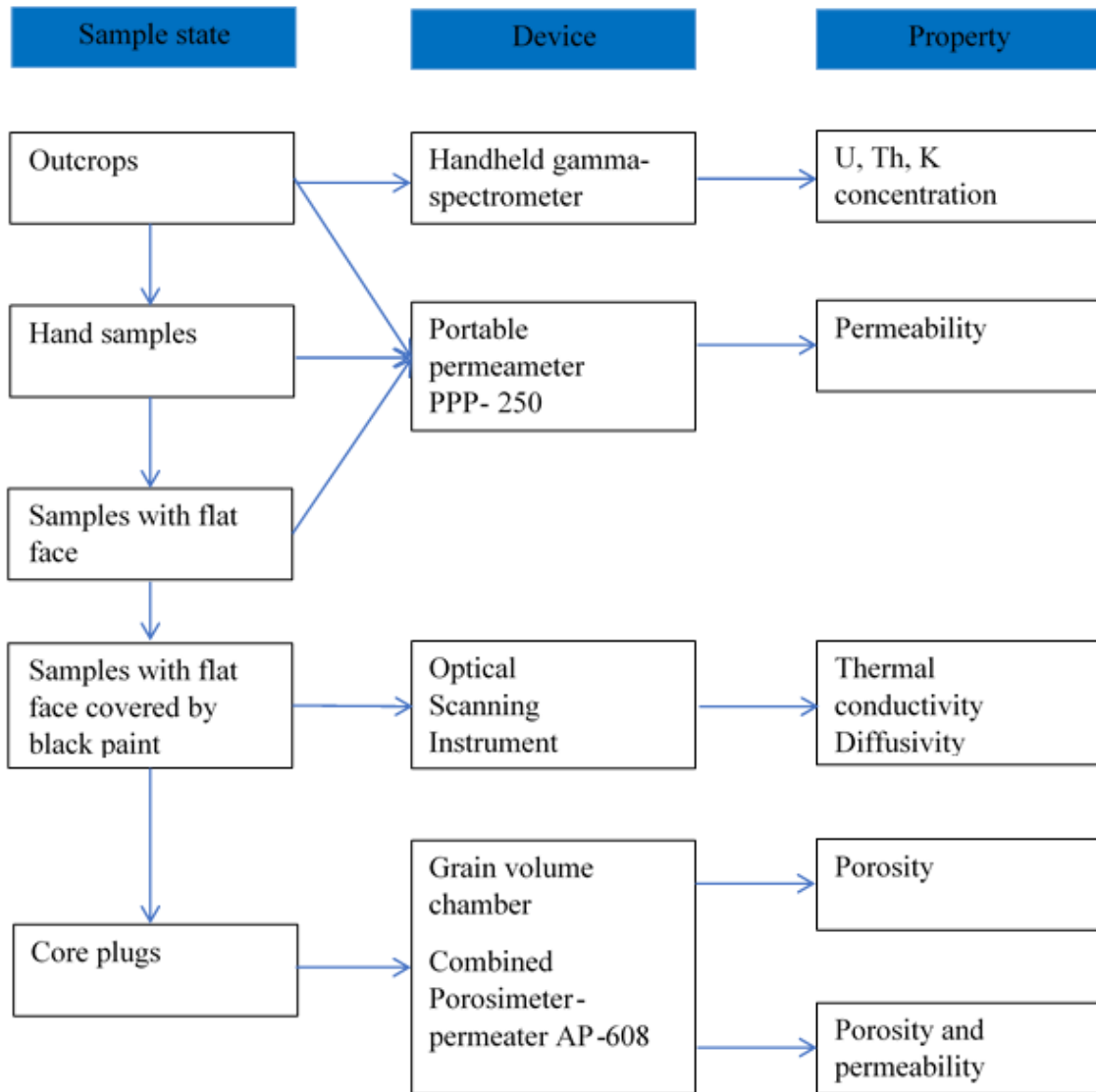


**Figure 3.5      Summary of steps to assess hydraulic and thermal properties in outcrop exposures and rock samples.**

### **3.3.2 Hydraulic properties**

#### **3.3.2.1 Gas permeability**

The portable PPP-250 probe permeameter from Core Laboratories was used to measure air permeability directly at outcrops (Figure 3.4d; ~10 % of measurements) and on hand samples in the laboratory (~90 % of measurements). The transient pressure decay method is used with this device, injecting compressed air with the initial pressure set to 0.24 MPa (35 psi) in the rock. The probe tip with a neoprene seal is pressed against a flat rock surface, and when the gas diffuses into the rock, the device measures the rate of pressure decay: a faster decay rate indicates higher permeability. The range of permeability evaluated with this instrument is  $9.9 \times 10^{-19} \text{ m}^2$  to  $4.9 \times 10^{-12} \text{ m}^2$  (0.001 mD to 5 D; Core Lab Instruments, 2016). Measurements were made parallel and perpendicular to bedding, laminations and foliation planes. The Klinkenberg correction (Tanikawa et al., 2009; Al-Jabri et al., 2015) cannot be applied when using this instrument, potentially leading to overestimations of liquid permeability. Therefore, caution should be applied when using air permeability values. The quality of the seal and surface roughness also play critical roles in the quality of permeability values (Filomena et al., 2014). However, other studies have successfully used the PPP-250 to measure outcrop permeability (McKinley et al., 2007; Beatty, 2010; Haffen et al., 2013). Moreover, the work of (Farquharson et al., 2015) yielded a good agreement between permeability estimates from the hand-held permeameter and well-constrained laboratory measurements.

#### **3.3.2.2 Porosity**

An automated AP-608 permeameter-porosimeter from Core Test Systems (Raymond et al., 2017) was coupled with a grain volume chamber to evaluate porosity on core plug samples. Porosity calculations were based on grain volume measurements using the following equation:

$$\emptyset = \frac{V_{bl} - V_{gr}}{V_{bl}} \times 100 \quad (3.1)$$

where  $\emptyset$  ( % ) is the porosity,  $V_{bl}$  ( $\text{m}^3$ ) the bulk volume and  $V_{gr}$  ( $\text{m}^3$ ) the grain volume.

Grain volume measurements were performed using nitrogen gas expansion based on Boyle's Law, where the pressure exerted by a given mass of an ideal gas is inversely proportional to the volume it occupies (American Petroleum Institute, 1998). A cylindrical core plug, with a diameter of 38.1 mm and length of 25.4 to 101.6 mm, was prepared from each outcrop sample. The grain

volume or matrix in the rock is determined from the initial pressure of the gas chamber and the core chamber pressure at equilibrium, assuming a constant temperature and number of gas moles. Porosity was estimated at a 13.8 bar with a measurement range of 0.001 to 0.4 (Raymond et al., 2017).

### **3.3.2.3 Permeability and porosity under pressurized conditions**

Transient permeability and porosity measurements were performed on the same core plugs used for the porosity tests. The measurements were taken with a combined AP-608 gas permeameter-porosimeter from Coretest Systems, using nitrogen for the gas source. Permeability analysis under confined pressure relies on the transient pressure decay method (American Petroleum Institute, 1998). The pressure is monitored as the gas flows through the rock sample to infer permeability using Darcy's law. The Klinkenberg correction is taking account by the instrument due to the gas slippage effect when calculating the permeability to liquid (Tanikawa et al., 2009). The device determines also the turbulence correction factor, automatically applying the Forchheimer correction (American Petroleum Institute, 1998; Coretest Systems Inc., 2017). However, it is almost negligible in low-permeability samples. Porosity was determined according to the method described above, except that confining pressure was varied. Permeability and porosity analyses were conducted under confining pressures ranging from 3.4 to 68.6 MPa (500–9950 psi) with a pressure differential of 3.4 MPa, although this adjusted from one sample to another, depending on the response of the sample to the applied confining pressure range. The device stops calculating the permeability when the value falls below the detection limit, thereby defining the reservoir's representative minimum and maximum pressures. For each pressure, an equilibrium timeout of one minute is sufficient for core samples with medium and high permeabilities and at least two minutes for low permeability. The instrument can evaluate porosities between 0.001 and 0.40 and permeabilities between  $10^{-19}$  and  $10^{-11}$  m<sup>2</sup> (0.001 mD to 10 D).

### **3.3.3 Thermal properties**

Transient thermal conductivity (TC) and diffusivity (TD) were determined with the optical scanning method using an infrared scanner developed by LGM Lippmann (Popov et al., 1999; Popov et al., 2016). Hand samples, ranging from 40 to 500 mm long, were sawed and their flat surfaces painted with black enamel to ensure proper infrared absorption. The prepared samples were placed between reference materials and analyzed along a scan line using a moving optical head

equipped with an infrared heat source and temperature sensors. The standard references are two quartz and titanium alloy couples with known TC and TD values of  $0.70\text{--}1.35 \text{ W m}^{-1} \text{ K}^{-1}$ ,  $0.40\text{--}0.83 \times 10^{-6} \text{ m}^2 \text{ s}^{-1}$ , and  $6.52\text{--}13.3 \text{ W m}^{-1} \text{ K}^{-1}$  and  $2.74\text{--}3.58 \times 10^{-6} \text{ m}^2 \text{ s}^{-1}$ , respectively. Both reference materials are recommended for measuring the thermal properties of natural materials like rocks (Popov et al., 2016). Temperature sensors positioned before and after the heat source measure undisturbed (cold) and disturbed (hot) temperatures, from which thermal conductivity  $\lambda$  ( $\text{W m}^{-1} \text{ K}^{-1}$ ) and diffusivity  $\alpha$  ( $\text{m}^2 \text{ s}^{-1}$ ) can be calculated by comparing the results to those of the reference samples placed before and after the rock sample. Local measurements along each scan line reveal heterogeneities caused by variations in mineralogical composition, porosity, fracture density, intergrain contacts, cementation, and pore and fracture aspect ratios. The calculated thermal heterogeneity coefficient,  $F$ , is defined as the maximum difference in conductivity along the scanning line divided by the average value (Popov et al., 2016) and was determined for every scan line on every sample. Using the combined TC-TD mode at a scanning speed of  $5 \text{ mm s}^{-1}$ , measurements were taken parallel and perpendicular to bedding, laminations or rock foliation planes in order to highlight the anisotropies caused by those structures. The range is  $0.2$  to  $25 \text{ W m}^{-1} \text{ K}^{-1}$  for TC and  $0.6 \times 10^{-6}$  to  $3.0 \times 10^{-6} \text{ m}^2 \text{ s}^{-1}$  for TD, with accuracies of  $3$  and  $5 \%$ , respectively (Popov et al., 2016). The volumetric heat capacity,  $\rho c$  ( $\text{MJ K}^{-1} \text{ m}^{-3}$ ), was deduced from the TC and TD measurements according to the equation:

$$\rho c = \frac{\lambda}{\alpha} \quad (3. 2)$$

where  $\rho$  ( $\text{kg m}^{-3}$ ) is the density calculated from the bulk volume of sample  $V_{bl}$  divided by its weight, and  $c$  ( $\text{J K}^{-1} \text{ kg}^{-1}$ ) is the specific heat capacity. The  $\rho$  and  $V_{bl}$  parameters were obtained when performing porosity measurements.

### 3.3.4 Heat-producing elements and radiogenic heat production

The concentrations of heat-producing elements, such as radioisotopes  $^{238}\text{U}$ ,  $^{232}\text{Th}$  and  $^{40}\text{K}$ , were evaluated in the field using an RS-230 BGO hand-held gamma-ray spectrometer on outcrops. The instrument uses a  $103 \text{ cm}^3$  Bismuth Germanium Oxide (BGO) crystal detector, which has better efficiency than a similarly sized NaI-crystal. The detector is connected to 1024-channel spectra and set up with an energy range of 30 to 3000 keV (e.g., Döse et al., 2014; Cao et al., 2018). The standard deviation is  $< 7 \%$  (Löfberg, 2013). Radiogenic heat production ( $A$ ;  $10^{-6} \text{ W m}^{-3}$ ) was calculated using the empirical relationship of Rybach (1988):

$$A = 10^{-5} \rho(9.51c_U + 2.56c_{Th} + 3.50c_K) \quad (3. 3).$$

where  $c_U$  (ppm),  $c_{Th}$  (ppm) and  $c_K$  (%) are the concentrations of the respective radiogenic elements.

## 3.4 Results

### 3.4.1 Lithology and petrography

#### 3.4.1.1 Sedimentary rocks

The Permian and Triassic sandstone formations are grey to greenish-grey or brown on fresh surfaces, and light grey or dark brown to rusty red when weathered. Numerous small quartz veins fill fractures in the sandstones. Cross-bedding is present, and laminations range in thickness from a few millimetres to 1 cm. Permian sandstone locally contains fossilized plant debris or organic matter, but Triassic sandstone is devoid of both. Based on thin section petrography, sandstones are medium-grained and moderately to well sorted, with rounded to subrounded quartz displaying characteristic undulose extinction. Feldspar grains display signs of weathering, and the sedimentary matrix also contains muscovite and biotite (Figures 3.6a–d). On average, the rocks contain 18 to 58 % quartz, 28 to 58 % feldspar and 3 to 16 % lithic fragments in a clay-sized matrix, classifying them as arkose to lithic arkose (Figure 3.6h).

The Lower Triassic (Eotriassic) shale has massive or fissile texture with dark grey to yellowish colour when weathered. Two distinct lithologies were observed: 1) dark grey shale with fossiliferous nodules (fish and ammonites) and numerous small quartz veins bounded by rusty selvages; and 2) massive clay shale devoid of fossils. In thin sections, the shale contains angular to subangular quartz grains (15 to 20 % on average) in a clay-sized matrix (Figure 3.6e–f).

Local brecciation caused by faulting is observed in the Permian sandstones. The collected breccia samples comprise centimetric angular clasts in siliceous cement, cut by millimetric quartz veins (Figure 3.6g).

Quartz-barite ‘veins’ are metric to hectometric in length and confined to weathered lateritic basement or sedimentary rocks. The collected samples display massive textures. The quartz-barite occurrences present as veinlets, lenses or white to translucent anhedral crystals with minor pyrite and galena inclusions.

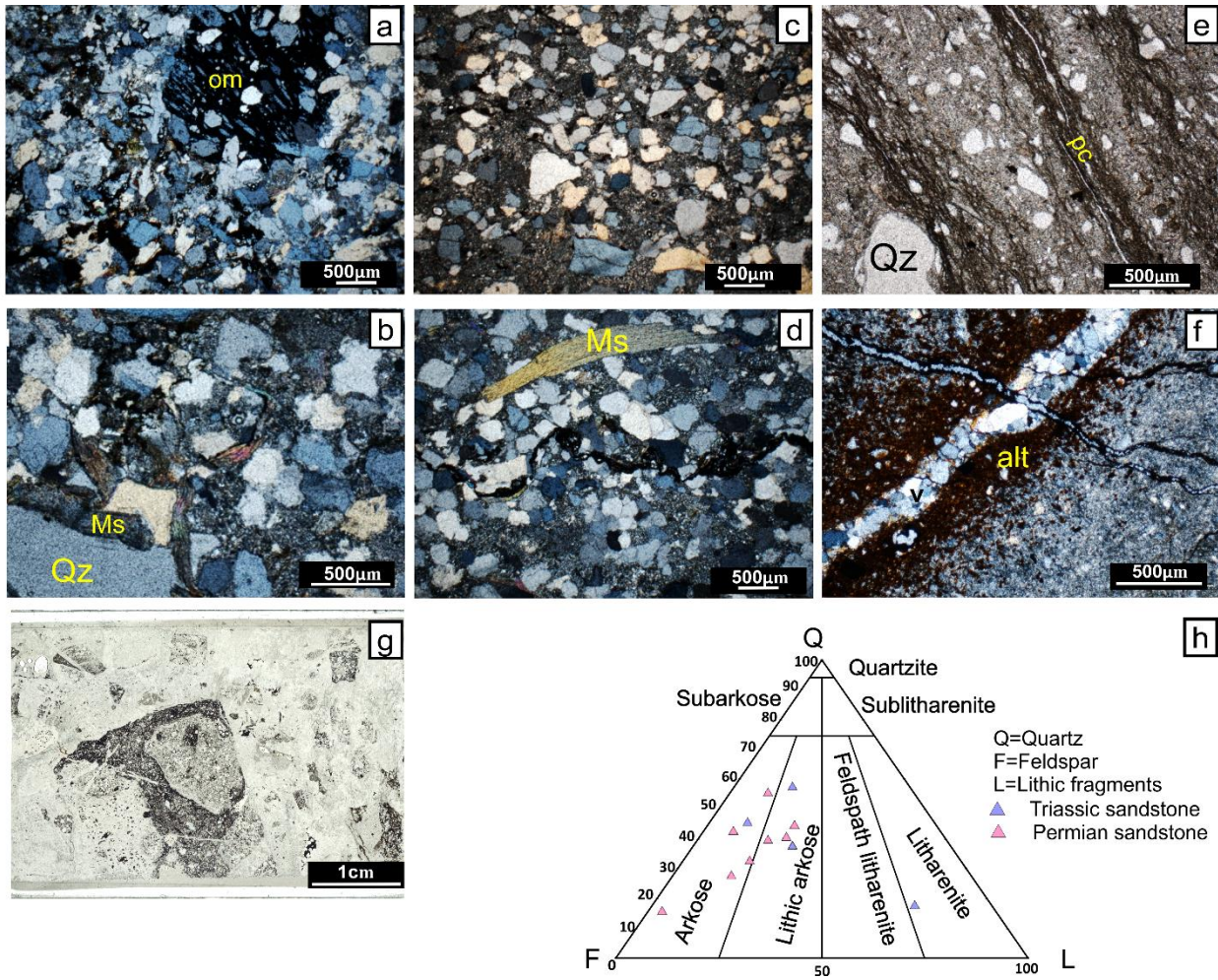


**Figure 3.6** Thin section photomicrographs (plane-polarized light) of sandstone and shale from the Ambilobe and Ambanja areas of North Madagascar (numbers in parentheses refer to sample locations in Figure 3.1): (a, 1 and b, 4) Permian sandstone with medium-grained, well-sorted, angular to subrounded quartz (Qz) and feldspar grains, muscovite (Ms) and organic matter (om); (c, 9 and d, 17) medium-grained Triassic sandstone with moderately to well-sorted, angular to subrounded quartz and feldspar grains with prevalent intergranular microfissures; (e, 1) Fossil-free Eotriassic shale showing compaction cleavage (pc); (f, 1) Eotriassic shale with micrometric veins of quartz and alteration; (g, 2) Scanned image of entire thin section of breccia; and (h) Classification of the sandstone samples using a ternary QFL diagram.

### 3.4.1.2 Basement rocks

The paragneiss samples are medium- to coarse-grained, containing on average 33 % quartz, 44 % feldspar and 23 % mafic minerals (Figure 3.7a). One of the samples is garnet-rich (Figure 3.7b). The granitic orthogneiss is leucocratic, strongly foliated and medium-grained, containing on average 36 % quartz, 49 % feldspar and 16 % mafic minerals that include garnet (Figure 3.7c). Based on the mineralogical proportions, it is as quartzofeldspathic gneiss with granodioritic to

granitic composition, similar to the gneiss described in Thomas et al. (2009). Amphibolite samples have an average content of 2 % quartz, 25 % feldspar and 70 % mafic minerals that include hornblende (Figure 3.7d). The mica schist samples are medium-grained with a lepidoblastic texture and partially weathered feldspar and mica minerals based on the presence of clay in the matrix. The analyzed samples contain on average 25 % quartz, 24 % feldspar and 51 % mica (Figure 3.7e). The syenite is leucocratic, coarse-grained and contains 85 % feldspar and 15 % mafic minerals, including aegirine (Figure 3.7f). The basalt samples display porphyritic texture with augite phenocrysts floating in a fine-grained crystallized (microlites) groundmass (Figure 3.7g).

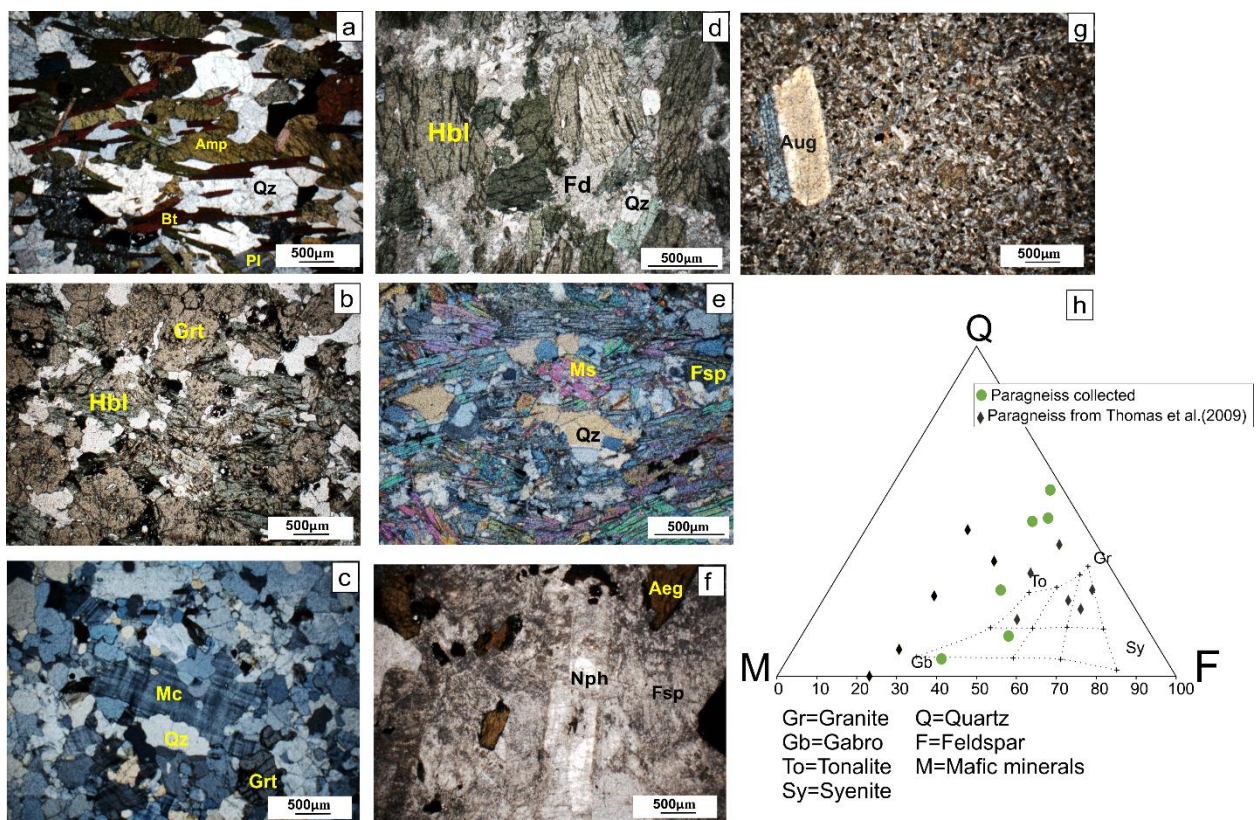


**Figure 3.7** Thin section photomicrographs (plane-polarized light) of basement rocks from the Ambilobe and Ambanja areas in North Madagascar (numbers in parentheses refer to sample locations in Figure 3.1): (a, 11) Biotite paragneiss with lepidoblastic texture; (b, 11) paragneiss with garnet-rich granoblastic texture; (c, 3) orthogneiss; (d, 6) amphibolite; (e, 7) mica schist; (f, 14) syenite; (g, 14) porphyritic basalt; and (h) ternary QFM diagram combined with QP diagram showing the major mineral contents of the paragneiss samples from the Ambilobe and Ambanja areas and their main compositional range. The plotted paragneiss samples are from

Thomas et al. (2009). Qz=quartz, Ms=muscovite, Bt=biotite, Pl=plagioclase, Mc=microcline, Fsp=feldspar, Amp=amphibole, Hbl=hornblende, Nph=nepheline, Aug= augite, Aeg=aegirine.

### 3.4.2 Hydraulic properties

Measured with the grain volume method, the mean porosity of sedimentary rocks in both areas ranges from 0.007 to 0.10 (Table 3.2), with the highest average (maximum mean) obtained for Permian sandstone. Measured with the portable permeameter, the mean permeability of sedimentary rocks is between  $3.0 \times 10^{-16}$  and  $1.0 \times 10^{-14} \text{ m}^2$  (0.3–10.1 mD), with Permian sandstone again having the highest average. For basement rocks, the porosity mean ranges from < 0.001 to 0.11, with the highest average for mica schist. The mean permeability for basement rocks varies between  $< 1.0 \times 10^{-19} \text{ m}^2$  and  $1.0 \times 10^{-14} \text{ m}^2$  (0.001–10.1 mD), with the highest average obtained for orthogneiss. The porosity and permeability means for the syenite intrusion are below the detection limit (dl) of the instruments.

**Table 3.2**      **Hydraulic properties of rocks from the Ambilobe and Ambanja areas.**

Rock type	Sedimentary					Metamorphic and igneous basement				Extrusive	
Rock lithology	Permian Sandstone	Triassic Sandstone	Eotriassic Shale	Breccia	Quartz-barite vein	Para gneiss	Mica schist	Amphibolite	Ortho-gneiss	Syenite	Basalt
∅ vol (fractional)											
Arithmetic Mean	0.10	0.07	0.08	0.07	0.01	0.02	0.11	0.06	0.05	<dl	0.01
Min–Max	0.03–0.44	0.0–0.13	0.0–0.09	–	0.0–0.01	0.01–0.04	–	0.05–0.09	0.02–0.07	–	0.01
Standard deviation	0.08	0.03	0.01	–	–	0.01	–	0.23	0.03	–	0.15
Number of samples (n)	10	5	2	1	1	11	1	5	2	1	2
Total number of measurements (N)	23	9	4	2	2	12	2	4	2	2	4
Parallel											
k (m <sup>2</sup> )	$1.0 \times 10^{-14}$	$1.0 \times 10^{-14}$	$1.1 \times 10^{-14}$	–	–	$3.2 \times 10^{-15}$	$7.6 \times 10^{-15}$	$8.9 \times 10^{-16}$	$1.0 \times 10^{-14}$	<dl	$3.0 \times 10^{-16}$
k (mD)											
Geometric Mean	10.6	10.4	11.3	–	–	3.2	7.7	0.9	10.7	<dl	0.3
Min–Max	40.2–5.6	28.5–2.4	22.1–4.2	–	–	8.7–0.5	14.9–3.8	1.6–0.3	12.0–9.6	–	–
Standard deviation	8.5	7.3	6.1	–	–	3.2	5.2	0.4	8.5	–	7.3

∅ – porosity, k – permeability obtained from portable permeameter (PPP-250), dl – detection limit = 0.001 for porosity and 0.001 mD, or  $10^{-19}$  m<sup>2</sup>, for permeability

**Table 3.2** Hydraulic properties of rocks from the Ambilobe and Ambanja areas. (suite)

Rock type	Sedimentary					Metamorphic and igneous basement				Extrusive	
Rock lithology	Permian Sandstone	Triassic Sandstone	Eotriassic Shale	Breccia	Quartz-barite vein	Paragneiss	Mica schist	Amphibolite	Orthogneiss	Syenite	Basalt
<b>Perpendicular</b>											
k (m <sup>2</sup> )	9.2 × 10 <sup>-15</sup>	7.6 × 10 <sup>-15</sup>	7.7 × 10 <sup>-15</sup>	—	—	2.7 × 10 <sup>-15</sup>	7.5 × 10 <sup>-15</sup>	1.1 × 10 <sup>-15</sup>	8.7 × 10 <sup>-15</sup>	—	3.0 × 10 <sup>-16</sup>
k (mD)											
Geometric Mean	9.3	7.7	7.6	—	—	2.7	7.6	1.1	8.8	—	0.3
Min–Max	14.6–6.5	20.9–1.4	13.8–4.0	—	—	8.6–0.5	20.8–4.2	1.7–0.7	8.8	—	0.3
Standard deviation	2.6	5.6	4.1	—	—	—	3.7	9.4	0.7	—	—
k (m <sup>2</sup> )	1.0 × 10 <sup>-14</sup>	9.3 × 10 <sup>-15</sup>	9.8 × 10 <sup>-15</sup>	1.0 × 10 <sup>-14</sup>	3.0 × 10 <sup>-16</sup>	3.1 × 10 <sup>-16</sup>	7.5 × 10 <sup>-16</sup>	8.9 × 10 <sup>-16</sup>	1.0 × 10 <sup>-14</sup>	<dl	4.9 × 10 <sup>-16</sup>
k (mD)											
Geometric Mean	10.1	9.4	9.9	10.3	0.3	3.1	7.6	0.9	10.1	<dl	0.5
Min–Max	22.1–5.6	28.5–1.4	22.1–4.0	18.1–8.1	1.3–0.7	8.7–0.5	20.8–3.8	1.7–0.3	12.0–8.8	—	0.6–0.3
Standard deviation	7.1	6.0	6.29	3.74	0.3	3.3	6.0	0.5	1.7	—	0.1
Number of samples (n)	10	9	5	2	3	14	2	2	3	1	2
Total number of measurements (N)	81	73	39	18	12	72	18	18	9	3	6

Ø – porosity, k – permeability obtained from portable permeameter (PPP-250), dl – detection limit = 0.001 for porosity and 0.001 mD, or 10<sup>-19</sup> m<sup>2</sup>, for permeability.

The results reveal that permeability values obtained with the hand-held PPP-250 permeameter can be up to three orders of magnitude higher than those measured with the AP-608 permeameter-porosimeter at the lowest pressure of 3.4 MPa (Figure 3.8).

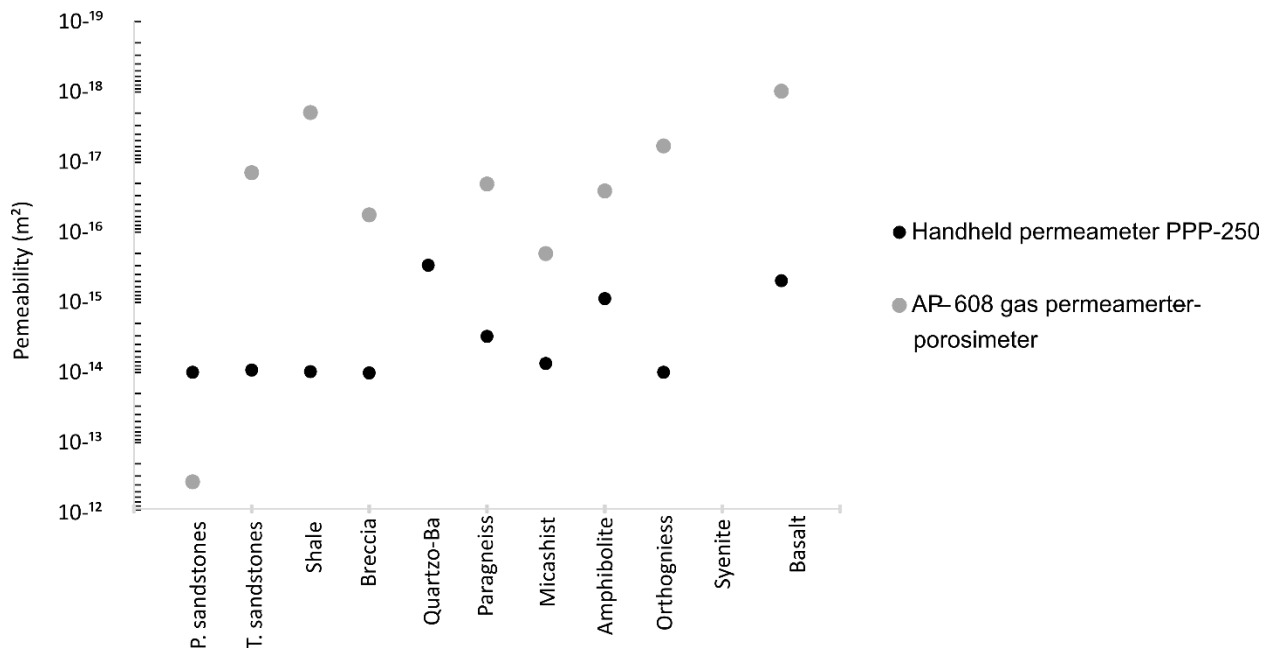


**Figure 3.8 Comparison of permeability values obtained with a hand-held permeameter and a gas permeameter-porosimeter. P stands for Permian and T for Triassic**

The porosity and permeability values obtained with the AP-608 gas permeameter-porosimeter under varying pressure conditions are presented in Figures 3.9a and 3.9b. The results reveal that both porosity and permeability decrease as a function of confining pressure. When applying the lithostatic pressure formula, the confining pressure range of 3.4 to 48.3 MPa (500–7000 psi) corresponds to depths of 130 to 1500 m, assuming that the average rock density is  $2700 \text{ kg.m}^{-3}$ . The permeability of all samples, ranging from  $10^{-15}$  to  $10^{-18} \text{ m}^2$  (10.1–0.01 mD) decreased by one order of magnitude or less over this pressure range; specifically, the porosity of Permian sandstone and mica schist decreased from 0.08 to 0.06, breccia from 0.08 to 0.075, and Triassic sandstone, with the highest porosity, from 0.12 to 0.10. The porosity of the most porous amphibolite sample decreased from 0.06 to 0.05. The lowest porosity values belong to paragneiss, orthogneiss and basalt, all less than 0.03, some falling below the detection limit of the device (<0.001).

A cross-plot of permeability versus porosity using the results from all lithologies indicates that permeability generally decreases with decreasing porosity (Figure 3.10). No clear trend could be

determined for breccia or basalt due to the limited number of samples. Lithotypes form distinct clusters, the ranges of which increase with the heterogeneity.

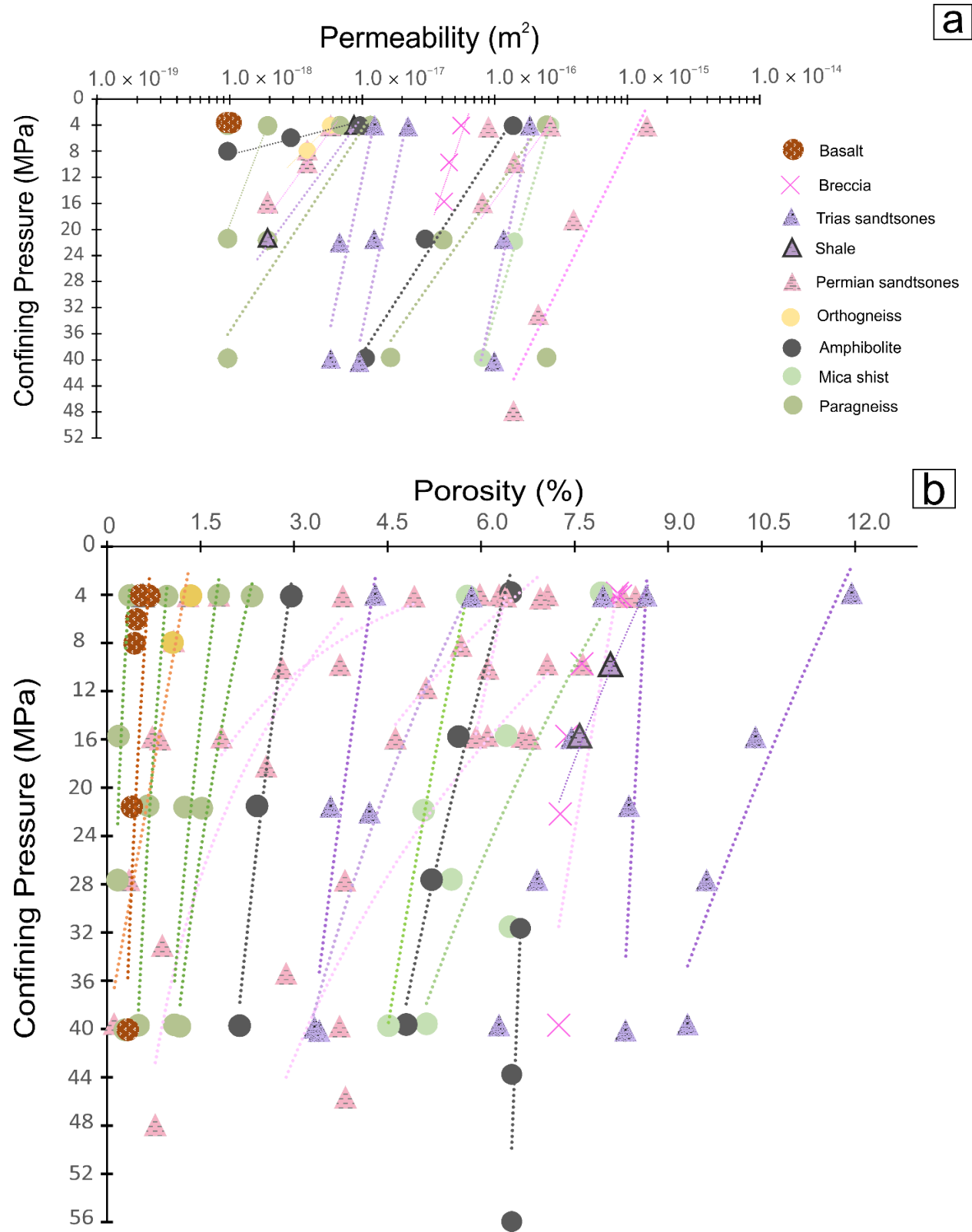


**Figure 3.9** a) Permeability and b) porosity versus confining pressure for analyzed rock samples from the Ambilobe and Ambanja areas. A logarithmic regression curve is shown for each sample.

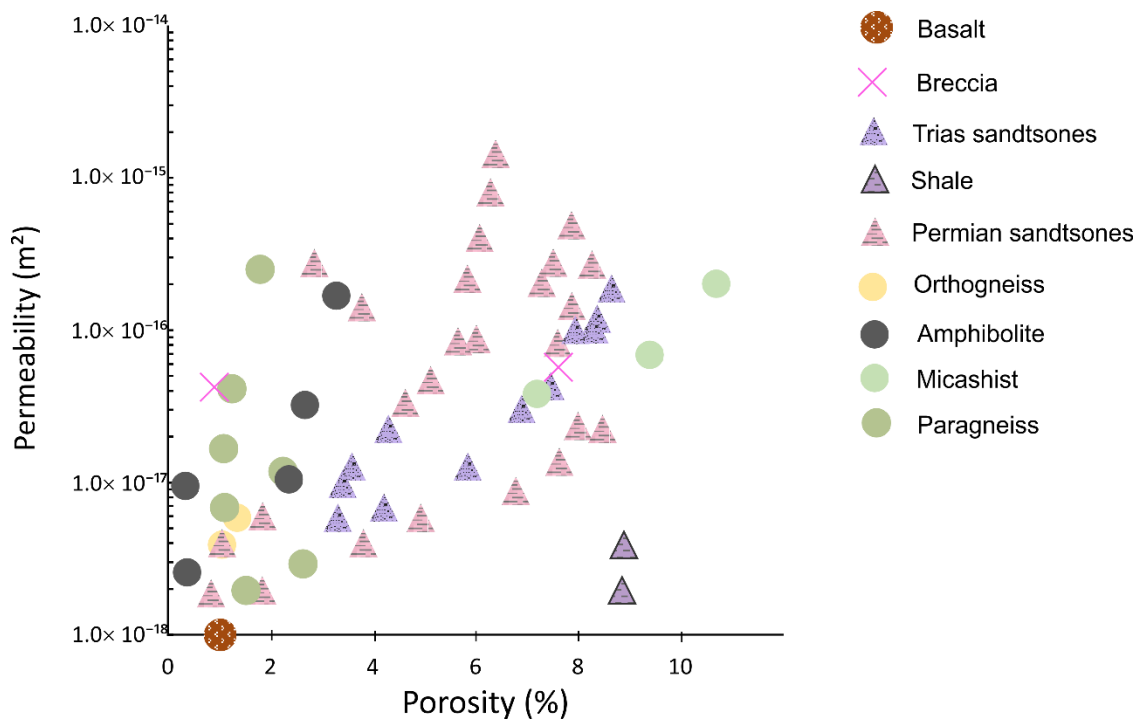


**Figure 3.10** Cross-plot of permeability versus porosity for all studied lithotypes.

### 3.4.3 Thermal properties

The thermal properties of samples from both areas are presented in Figure 3.11 and the measurement statistics are summarized in Table 3.3. Thermal conductivity for the sedimentary samples varies between  $3.6$  and  $4.9\text{ W m}^{-1}\text{ K}^{-1}$  in both areas, whereas basement rocks range from  $2.5$  to  $3.4\text{ W m}^{-1}\text{ K}^{-1}$ . Mica schist and syenite have the same mean value of  $2.6\text{ W m}^{-1}\text{ K}^{-1}$ , and basalts have the lowest mean of  $2.4\text{ W m}^{-1}\text{ K}^{-1}$ . The mean thermal diffusivity of all rocks varies from  $1.0$  to  $2.4 \times 10^{-6}\text{ m}^2\text{ s}^{-1}$  and the heat capacity ranges between  $2.1$  and  $2.6\text{ MJ m}^{-3}\text{ K}^{-1}$ , with the highest value for shale. The mean thermal heterogeneity coefficient ( $F$ ) is  $0.1$  to  $0.4$  (Table 3.3).

**Table 3.3 Thermal property statistics of rocks from the Ambilobe and Ambanja areas.**

Rock type	Sedimentary				Metamorphic and igneous basement				Extrusive	
Rock lithology	Permian-Triassic Sandstone	Eotriassic Shale	Breccia	Quartz-barite vein	Para-gneiss	Mica schist	Amphibolite	Ortho-gneiss	Syenite	Basalt
$\lambda$ (Wm <sup>-1</sup> K <sup>-1</sup> )										
Arithmetic mean	3.6	2.5	3.3	4.9	2.7	2.6	2.5	3.4	2.6	2.4
Min-Max	2.7–6.3	1.3–4.1	2.7–4.0	3.9–5.7	1.7–0.0	1.8–3.5	1.6–4.3	2.6–0.6	1.9–3.4	2.2–2.6
G (%)	4.9	8.0	10.8	4.9	10.6	6.5	6.6	7.1	3.4	3.5
Mean F	0.2	0.2	0.4	0.2	0.3	0.3	0.3	0.3	0.1	0.2
$\alpha$ (10 <sup>-6</sup> m <sup>2</sup> s <sup>-1</sup> )										
Mean	1.6	1.2	1.6	2.4	1.4	1.1	1.1	1.5	1.1	1.0
Min-Max	1.0–3.3	0.4–2.5	1.2–2.4	1.9–3.1	0.6–0.8	0.9–1.5	0.6–3.6	1.0–0.5	0.8–1.7	0.9–1.1
$\rho c$ (MJ m <sup>-3</sup> K <sup>-1</sup> )										
Mean	2.3	2.6	2.0	2.1	2.2	2.2	2.4	2.2	2.3	2.4
Min-Max	2.6–2.3	1.5–3.1	1.7–2.0	2.2–2.1	1.7–0.2	1.9–2.2	1.6–2.4	2.1–0.2	2.1–2.3	2.5–2.4
Total number of measurements (N)	1661	490	254	472	1515	139	577	186	77	270
Number of samples (n)	18	5	2	3	14	2	4	3	1	2

$\lambda$  Thermal conductivity,  $\alpha$  Thermal diffusivity,  $\rho c$  Volumetric heat capacity, F= thermal heterogeneity coefficient, G= standard deviation divided by mean (Popov et al., 2016).

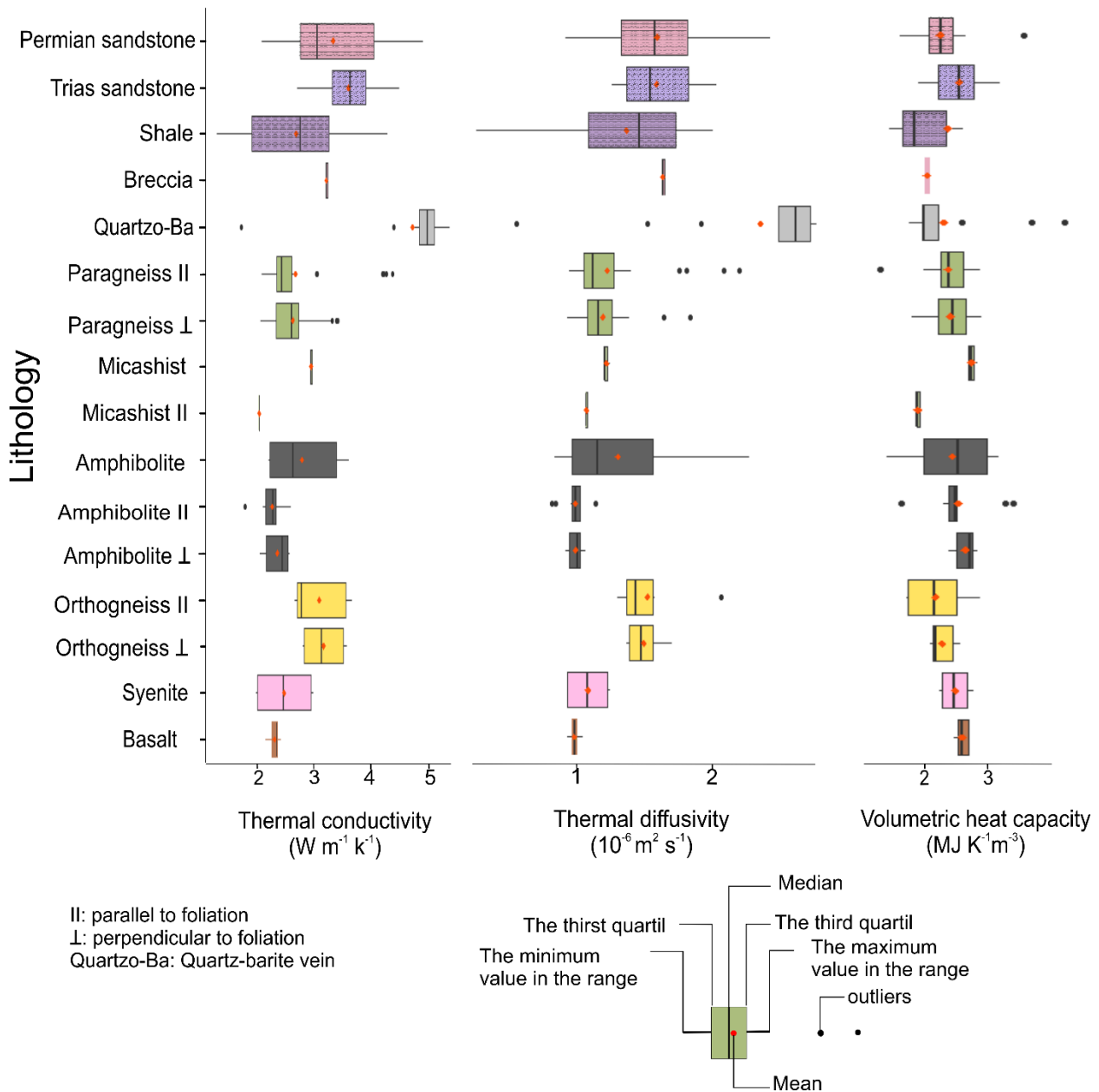


**Figure 3.11 Whisker plots of thermal properties classified by geological unit for basement and sedimentary rocks from the Ambilobe and Ambanja areas.**

The porosity and thermal relationships evaluated under dry conditions, as shown in Figure 3.12, reveal that low-porosity sandstones have the highest thermal conductivity.

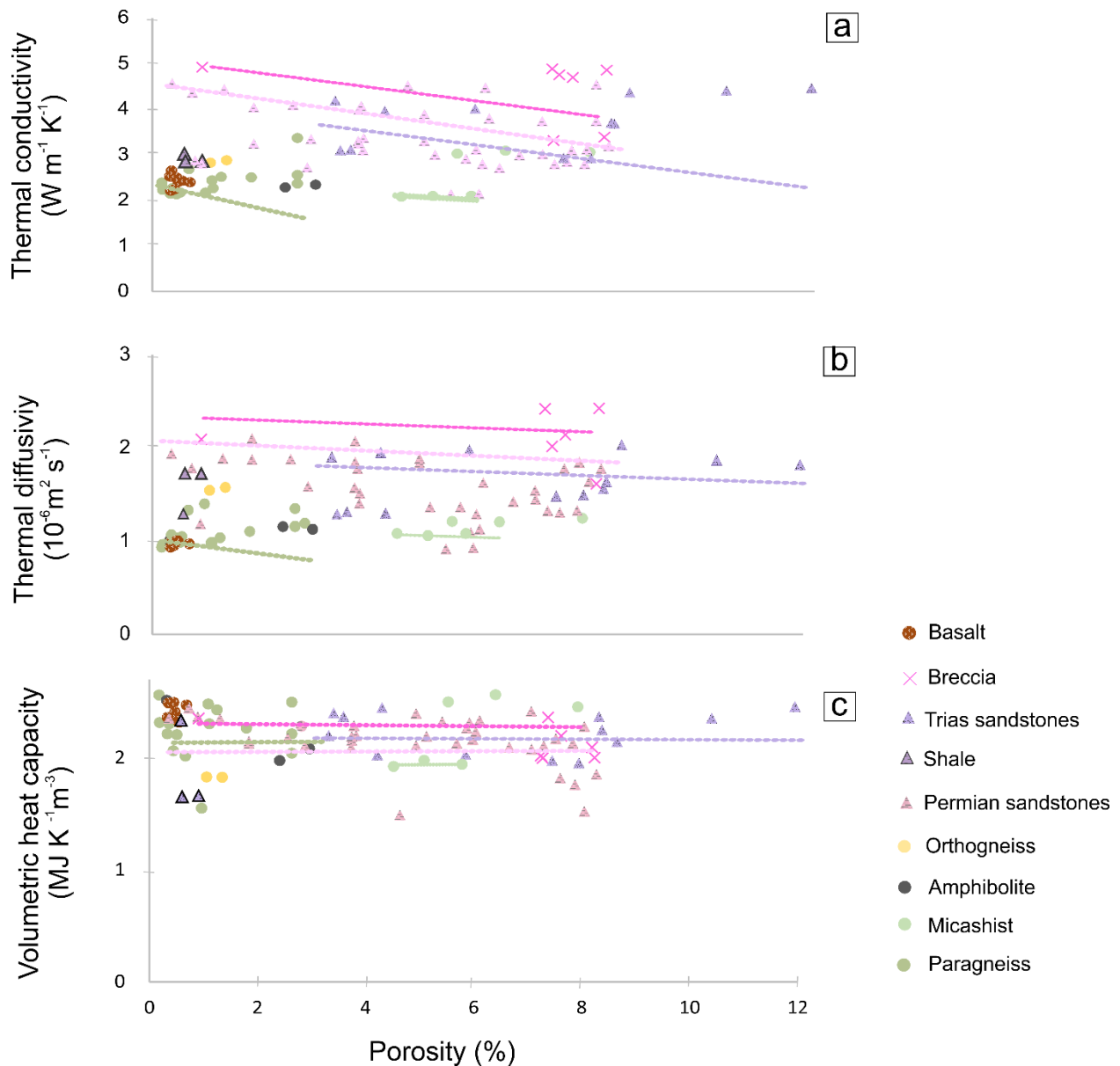


**Figure 3.12** Thermal properties as a function of porosity. The lines correspond to the trend of a) thermal conductivity calculated for dry samples using the Maxwell equation (Heap et al., 2020), b) effective diffusivity and c) Volumetric heat capacity.

#### 3.4.4 Heat-producing elements and radiogenic heat production

Field radiometric and mass spectrometry methods were used to determine the U, Th and K contents of the main lithologies in the Ambilobe and Ambanja areas and to calculate internal heat generation (Eq. 3.3; Table 3.4). The lithologies with the highest concentrations of radiogenic elements, also reflecting the highest thorium concentrations, are basalt ( $14.05 \mu\text{g kg}^{-1}$ ), followed by Triassic sandstone ( $10.85 \mu\text{g kg}^{-1}$ ) and syenite ( $8.5 \mu\text{g kg}^{-1}$ ). This is reflected in the calculated

internal heat generation, with basalt having a range of  $1.44\text{--}2.38 \times 10^{-6} \text{ W m}^{-3}$ , followed by syenite (mean of  $1.35 \times 10^{-6} \text{ W m}^{-3}$ ) and sedimentary rocks (mean of  $1.25 \times 10^{-6} \text{ W m}^{-3}$ ).

**Table 3.3 Heat-producing elements, rock densities and radiogenic heat production of the main geological units in the Ambilobe and Ambanja areas.**

	U (mg kg <sup>-1</sup> )	Th (mg kg <sup>-1</sup> )	K (%)	ρ (kg m <sup>-3</sup> )	A ( $\times 10^{-6} \text{ W m}^{-3}$ )
Permian Sandstone (n = 7)				n = 7	
Arithmetic					
mean	1.88	7.26	2.17	2490	1.14
Triassic Sandstone (n = 2)				n = 2	
Arithmetic					
mean	2.20	10.85	0.70	2447	1.25
Shale (n = 4)				n = 3	
Arithmetic					
mean	1.50	3.78	1.15	2385	0.72
Quartz-barite vein (n = 4)				n = 1	
Arithmetic					
mean	2.90	5.40	1.10	2636	1.20
Paragneiss + orthogneiss (n = 8)				n = 8	
Arithmetic					
mean	0.26	3.10	1.09	2678	0.38
Mica schist (n = 2)				n = 2	
Arithmetic					
mean	0.90	3.50	2.00	2439	0.58
Amphibolite (n = 2)				n = 2	
Arithmetic					
mean	0.55	4.55	2.30	2883	0.72
Syenite (n=1)					
Arithmetic					
mean	2.00	8.53	2.60	2700	1.35
Basalt (n = 2)				n = 2	
Arithmetic					
mean	2.5	14.05	1.8	2890	1.90

n – number of samples U: Uranium, Th: Thorium, K: Potassium, ρ:density, A: radiogenic heat generation

### 3.5 Discussion

#### 3.5.1 Implications of mineral content on petrophysical properties and heat production

The mineral content of the rock matrix and the porosity have an impact on thermal conductivity, which can be further influenced by alteration process that occur under reservoir conditions implying the fluid characteristics effects. Considering that the temperature range of the Ambilobe and Ambanja reservoirs is 140–200 °C, hydrothermal alteration, such as argillic, is expected to occur with increasing depth and temperature. Clays from the kaolin group appear at temperatures under 200 °C (Simmons et al., 2000). Clay minerals replace primary plagioclase and mafic

silicates like pyroxene, amphibole, and biotite (Pirajno, 2009). Rocks such as amphibolite and mica schist, the dominant lithologies in the Ambilobe area, contain the latter (pyroxene, amphibole and biotite) (Figure 3.7a, 3.7c and 3.7d) and are thus more susceptible to argillic alteration than granodioritic to granitic quartzofeldspathic gneiss, the dominant lithology in the Ambanja area. Therefore, the basement rocks of Ambilobe are expected to have higher porosities than those of Ambanja. The precipitation of secondary mineral phases (e.g., clay, hydrothermal quartz and feldspar) in primary pore spaces can reduce porosity. Advancing alteration causes the dissolution and recrystallization of primary minerals, such as the replacement of large, dense plagioclase phenocrysts by microcrystalline clays to increase the porosity. The low-porosity medium-grained Permian and Triassic sandstones in Ambilobe and Ambanja are considered examples of this as clay, hydrothermal quartz and feldspar microcrystalline clays were observed (Figure 3.6a–d).

When analyzing the mineral content of rocks, quartz is regarded as having a significant influence on thermal conductivity since this mineral has a high thermal conductivity:  $6.5\text{--}11.3 \text{ W m}^{-1}\text{K}^{-1}$ , parallel to the crystal's optical c-axis (Clauser et al., 1995). The quartz-barite veins have the highest thermal conductivity values, followed by the Permian and Triassic sandstones and the orthogneiss, which is consistent with their higher quartz content (Table 3.3; Figure 3.6).

The highest internal heat generation is found in the basalt, the syenite intrusion and the Triassic feldspar-rich sandstone, explained by their high thorium concentrations (Table 3.4). The high thorium value in the sandstone is believed to originate from the erosion of alkaline rocks (Wedepohl, 1978). Most worldwide geothermal data linked to heat generation indicate a clear concentration of long-lived radioisotopes in upper crust layers composed of felsic and intermediate magmatic rocks (Huenges et al., 2011; Eppelbaum et al., 2014). Also, heat production increases as a function of increasing felsic and alkali contents in the rocks (Hasterok et al., 2017), similar to what was observed for intrusive syenite and basalt rocks in North Madagascar. Our results show that relative heat production is higher in sandstone compared to paragneiss, which aligns with work that confirms important heat production in acidic rock compositions ( $1.80 \mu\text{W m}^{-3}$ ) compared to basic rocks ( $0.67 \mu\text{W m}^{-3}$ ) (e.g., Rybach, 1978; Eppelbaum et al., 2014 and citations therein).

### 3.5.2 Hydraulic properties

To date, the porosity and matrix permeability of Madagascar rocks have been mainly investigated by petroleum companies, but the data remain unpublished and inaccessible. The matrix permeability measured for all rock types in both the Ambilobe and Ambanja areas is relatively low

when compared to the permeability required for an effective geothermal reservoir. Impermeable formations are considered to have a permeability of  $< 10^{-15} \text{ m}^2$ , whereas permeable formations can have a permeability exceeding  $10^{-12} \text{ m}^2$  (e.g., Sass et al., 2012). Values in between, such as those of North Madagascar, are therefore considered low. Although permeabilities estimated with hand-held and gas permeameters can differ (Figure 3.8), their averages remain in the lower permeability range.

However, it should be noted that this study evaluated matrix permeability only, which is an important limitation that does not consider the effect of fractures. In situ well tests would be necessary to assess formation permeability related to fractures but drilled wells are not available at the moment. Therefore, at this stage of study, the measured permeability likely underestimates the formation permeability or represents the lower bound of permeability in each formation. Indeed, despite the uncertainty related to fracture aperture, density, length and orientation, which typically vary with depth, the findings from laboratory experiments available in the literature show that the matrix permeability can increase up to six orders of magnitude when low permeability sandstones are fractured (Kushnir et al., 2018). The work of (Heap et al., 2016) further highlights the fact that laboratory measurements on intact rocks with low permeability can significantly underestimate the equivalent permeability of fractured volcanic rocks. The equivalent permeability of fractured sandstones was shown to increase to  $10^{-9} \text{ m}^2$  while that of shale and basalt increased to  $10^{-12} \text{ m}^2$ . Hence, fractures are critical features affecting the formation permeability in low-porosity rocks.

The hydraulic properties of rock samples from the Ambanja and Ambilobe areas were compared with the porosity and permeability ranges of known geothermal systems worldwide, which were determined from laboratory and in situ methods (Table 3.5). Some of those geothermal systems are being studied for geothermal energy development while others are currently in operation. In general, the data reported for sedimentary rocks from near-surface to relatively shallow depths in the Rhine Graben (Germany), the North German Basin (central and west Europe) and the Karoo Basin (South Africa) are comparable to those obtained in the Ambilobe and Ambanja geothermal areas, despite the fact that the depth of sample collection and laboratory methods are different. On average, the range of hydraulic properties for Permian sandstone in the Rhine Graben (Haffen et al., 2013; Heap et al., 2017) and the North German Basin (Zimmermann et al., 2008; Zimmermann et al., 2010; Haffen et al., 2013) is close to those for the outcropping Permian sandstones in the Ambilobe area, whereas the permeability and porosity of Permian sandstone in the Karoo Basin (Campbell et al., 2016a; Campbell et al., 2016b) is lower. The hydraulic

properties of Triassic sandstones from the Rhine Graben (Haffen et al., 2013; Heap et al., 2017) is comparable to Triassic sandstone outcrops in the Ambilobe and the Ambanja areas. In contrast, the range of hydraulic properties for Triassic sandstone in the North German Basin and the Pannonian Basin (Hungary) are higher (Sass et al., 2012; Moeck, 2014). The Eotriassic shales from Ambilobe have higher porosity than shales from the British Columbia Basin (Canada; Garet et al., 2015). Proterozoic paragneiss outcrop samples from Kuujjuaq (Canada; Miranda et al., 2020) and gneiss from the Mid-German Crystalline High (Germany; Bär et al., 2020; Weinert et al., 2020) have a similar porosity and permeability range compared to the paragneiss averages of Ambilobe and Ambanja. However, the porosity and permeability published for gneissic outcrops on the Kola Peninsula (Russia) and gneiss from the KTB (Kontinentales Tiefbohrprogramm der Bundesrepublik) superdeep boreholes in Germany (Zharikov et al., 2005) are lower. The granitic basement rocks in the Rhine Graben (Hettkamp et al., 1999; Guillou-Frottier et al., 2013) and the Paleozoic granite Tetipanapa forming the Los Humeros and Acoculco geothermal fields in Mexico (Bär et al., 2020; Weydt et al., 2021) have the same values as igneous outcrops in the Ambanja graben.

The results of this study are limited by the relatively small number of samples and are not considered representative of the entire range of hydraulic properties in the Ambilobe and Ambanja areas due to the heterogeneity of each lithology. The low matrix porosity and permeability of both areas do not preclude the presence of reservoir formations, but secondary porosity features, such as fractures, are needed for permeability to be significant. Hot springs located along faults (Figure 3.1) and the extensional tectonic setting suggest that permeability is linked to major fracture zones that potentially transect the crust. Using field observations of surface rock exposures, it is currently difficult to anticipate fracture behaviour at depth. The data in the literature (Table 3.5) from worldwide geothermal systems, especially those currently under operation, further suggest that viable geothermal resources can be found in rocks with low primary porosity if a high density of structural features, especially fractures, enhances permeability.

**Table 3. 4 Average porosity and permeability obtained from measurements on core plugs: examples from around the world compared to rock units in the Ambilobe and Ambanja geothermal areas. The mean permeability for the present study corresponds to the average of values obtained from the portable permeameter and combined gas porosimeter-permeameter**

Rock type	Geological system	Method	Depth range (km)	$\varphi$ (Fractional)	$k$ ( $m^2$ )	Reference
Upper Triassic Isalo Group/ medium-grained sandstone	Ambilobe (Andavakoera) fault zone and Ambanja graben	Grain volume porosimeter	Outcrop	Mean 0.07 0–0.13	Mean $10^{-14}$	Present study
		Transient gas permeability		Mean 0.05 0.01–0.08	$10^{-14}$ – $4.10^{-14}$ Mean $3.10^{-17}$ $3.10^{-17}$ – $2.1^{-16}$	
Upper Triassic Stuttgart Formation/weakly cemented fluvial sandstone	North German Basin (central and west Europe)	Bulk volume porosity	0.6–0.7	Mean 0.26 0.05–0.35	Mean $10^3$ $2.10^{-17}$ – $5.10^{-12}$	Moeck (2014) and references therein
		Transient gas permeability				
Upper Triassic, Mecsek Mountains/sandstone	Pannonian Basin (Hungary)	Transient gas permeability	Outcrops	–	$5.10^{-14}$ – $10^{-13}$	Sass et al. (2012)
		Bulk volume porosity				
		Transient gas permeability				
Triassic Buntsandstein Formation/sandstone	Rhine Graben (Germany)	Helium pycnometry	1–1.35	Mean 0.21 0.01–0.20	Mean $10^{-14}$ $6.10^{-16}$ – $10^{-13}$	Haffen et al. (2013)
		Steady-state gas permeability				
		~ 0.03–0.2				

$\varphi$  – porosity,  $k$  – permeability, KTB – Kontinentales Tiefbohrprogramm der Bundesrepublik

**Table 3.5 Average porosity and permeability obtained from measurements on core plugs: examples from around the world compared to rock units in the Ambilobe and Ambanja geothermal areas. The mean permeability for the present study corresponds to the average of values obtained from the portable permeameter and combined gas porosimeter-permeameter (suite)**

Rock type	Geological system	Method	Depth range (km)	$\phi$ (Fractional)	k (m <sup>2</sup> )	Reference
Permian Ripon Formation/sandstone	Karoo Basin (South Africa)	Bulk volume porosity Transient gas permeability	Outcrop 0.9–2.4	Mean 0.01 0.0–0.4 Mean 0.01 0.04–0.02	Mean 10 <sup>-15</sup> 10 <sup>-17</sup> –10 <sup>-16</sup> Mean 10 <sup>-18</sup> 10 <sup>-18</sup> –10 <sup>-18</sup>	
Permian Ripon Formation/sandstone						Campbell et al. (2016a);
Permian Ripon Formation /medium-grained sandstone			Outcrop	Mean 0.05 0.00–0.04	Mean 5.10 <sup>-17</sup> 7.10 <sup>-18</sup> –10 <sup>-16</sup>	Campbell et al. (2016b)
Permian Ripon Formation /medium-grained sandstone			0.9–2.4	Mean 0.02	< 10 <sup>-18</sup>	
Lower Permian Rotliegend Formation/fluvial sandstone	North German Basin (central and west Europe)	Transient gas permeability	Outcrop	–	8.10 <sup>-14</sup> –9.10 <sup>-13</sup>	Sass et al. (2012)
Lower Permian Rotliegend Formation/sandstone		In situ flowmeter with nitrogen gas	4.0–4.2	Mean 0.1 0.08–0.12	Mean 1–10 <sup>-15</sup> 10 <sup>-17</sup> –10 <sup>-13</sup>	Huenges et al. (2002); Zimmermann et al. (2010); Zimmermann et al. (2008)
Permian Buntsandstein Formation/sandstone	Rhine Graben (Germany)	Bulk volume porosity Transient gas permeability	1.35–1.4	Mean 0.08 0.03–0.13	Mean 2.10 <sup>-15</sup> 5.10 <sup>-16</sup> –10 <sup>-14</sup>	Haffen et al. (2013)

$\phi$  – porosity, k – permeability, KTB – Kontinentales Tiefbohrprogramm der Bundesrepublik

**Table 3.5 Average porosity and permeability obtained from measurements on core plugs: examples from around the world compared to rock units in the Ambilobe and Ambanja geothermal areas. The mean permeability for the present study corresponds to the average of values obtained from the portable permeameter and combined gas porosimeter-permeameter (suite)**

Rock type	Geological system	Method	Depth range (km)	$\phi$ (Fractional)	k (m <sup>2</sup> )	Reference
Eotriassic Isalo I /shale	Ambilobe (Andavakoera) fault zone	Grain volume porosimeter	Outcrop	Mean 0.08 0.08–0.09	Mean 10 <sup>-14</sup> 10 <sup>-15</sup> –4.10 <sup>-14</sup>	Present study
		Transient gas permeability		Mean 0.007 0.006–0.009	Mean 2.10 <sup>-18</sup> 10 <sup>-18</sup> –4.10 <sup>-14</sup>	
Triassic Doig Formation/shale	Dawson Creek (Canada)	Mercury immersion coupled with helium pycnometry	Outcrop	Mean 0.03	–	Garet et al. (2015)
Triassic Nicola Group/shale	Mt. Morrisey (Canada)	Gas pressure permeameter and mini-permeameter	Outcrop	Mean 0.009	–	Sass et al. (2012)
Proterozoic Bemarivo Formation/amphibolite gneiss	Ambilobe (Andavakoera) fault zone and Ambanja graben	Grain volume porosimeter Transient gas permeability	Outcrop	Mean 0.02 0.01–0.04 0.001–0.03	2.10 <sup>-15</sup> –9.10 <sup>-15</sup> 0–10 <sup>-16</sup>	Present study
Paleoproterozoic Southeastern Churchill Province/paragneiss	Kuujuaq (Canada)	Bulk volume porosity Transient gas permeability	Outcrop	Mean 0.06	<10 <sup>-18</sup>	Miranda et al. (2020)
Late Ordovician–Early Devonian/gneiss	Mid-German Crystalline High (Germany)	Bulk volume porosity	Quarries, outcrops, wells	Mean 0.01 0.0001–0.010	–	Bär et al. (2020); Weinert et al. (2020)
Archean Kola Series/amphibolite gneiss	Kola superdeep boreholes (Russia)	In situ pressure-temperature steady state argon gas permeability and porosity	Outcrop	0.05–0.001	10 <sup>-18</sup> –8.10 <sup>-18</sup>	Zharikov et al. (2005)
Paleoproterozoic/meta gabbro, amphibolite	KTB superdeep boreholes (Germany)		3.6–3.8	0.01–0.02	10 <sup>-17</sup> –2.10 <sup>-17</sup>	

$\phi$  – porosity, k – permeability, KTB – Kontinentales Tiefbohrprogramm der Bundesrepublik

**Table 3.5 Average porosity and permeability obtained from measurements on core plugs: examples from around the world compared to rock units in the Ambilobe and Ambanja geothermal areas. The mean permeability for the present study corresponds to the average of values obtained from the portable permeameter and combined gas porosimeter-permeameter (suite)**

Rock type	Geological system	Method	Depth range (km)	$\varphi$ (Fractional)	k (m <sup>2</sup> )	Reference
Bemarivo Formation/igneous rock	Ambanja graben	Grain volume porosimeter Transient gas permeability	Outcrop	<0.001–0.01	$<10^{-18}$ – $3.10^{-16}$ $0$ – $10^{-18}$	Present study
Crystalline rock, granitic rock	Rhine Graben shoulder	Stationary flow tests and/or pressure pulse argon gas permeability and porosity	1.4–3.7 3.7–5	0.09 0.01	$10^{-17}$ – $10^{-19}$ $10^{-17}$	Guillou-Frottier et al. (2013); Hettkamp et al. (1999)
Granitic rock	Carmmenellis (England)		0–2	–	$10^{-15}$ – $7.10^{-15}$	Björbsson et al. (1990); Pine (1983)
Paleozoic Tetipanapa/granite	Los Humeros (Mexico)	Bulk volume porosity	outcrops	Mean 0.01 0.004–0.01	$1.24.10^{-18}$ $8.29.10^{-18}$	Bär et al. (2020); Weydt et al. (2021)

$\varphi$  – porosity, k – permeability, KTB – Kontinentales Tiefbohrprogramm der Bundesrepublik

### **3.5.3 Thermal properties**

Sandstones with high quartz content are expected to be better heat conductors compared to quartz-poor paragneiss and can be qualified as insulating rocks. The thermal conductivity of the metamorphic basement rocks and sedimentary rocks in the Ambilobe and Ambanja areas can be qualified as moderately heterogenous. According to Albert et al. (2017), high thermal inhomogeneity is defined by  $F > 0.35$  and low thermal heterogeneity by  $F < 0.1$ . The mean thermal heterogeneity coefficients presented in Table 3 lie between these values. Foliated rocks, like paragneiss, mica schist and amphibolite, show significant anisotropy in thermal conductivity. When foliations in the rock units are more or less subvertical, the thermal conductivity perpendicular to foliation must be considered when modelling or evaluating terrestrial heat flow that is expected to be dominantly vertical (Deming, 1994). In terms of volumetric heat capacity, the shale and amphibolite formations have the best heat storing potential although there is some variability among units.

The thermal conductivity, thermal diffusivity and volumetric heat capacity of rocks with similar matrix mineralogy decreases as the porosity increases (Figure 3.12). For example, the thermal conductivity of both the mica schist and Triassic sandstone decreases with increasing porosity but at different rates. Some results deviate from the observed trend because the thermal properties measured by the infrared scanner along the scan lines do not necessarily correlate with the average matrix porosity of the entire sample. Moreover, the porosity range of the Madagascar rocks is quite narrow. Therefore, it is difficult to apply the Maxwell equation to predict changes in thermal properties, as was done by Heap et al. (2020) whose analytical porosity results exceeded 0.1 and for which an appropriate correlation could be established.

### **3.5.4 Heat Production**

Assuming that the U, Th, and K contents of samples from the study areas are representative of the different crustal layers in Madagascar, the mean heat production for the Ambilobe and Ambanja sedimentary rocks is comparable to that produced in the Earth's sedimentary crustal layers, which is  $1.39 \times 10^{-6} \text{ W m}^{-3}$  (Eppelbaum et al., 2014 and references therein), or from 0.95 to  $1.21 \times 10^{-6} \text{ W m}^{-3}$  in Phanerozoic rocks (Jaupart et al., 2016). However, the heat production in the metamorphic basement rocks in this study tend to be lower than that reported by Jaupart et al. (2016) for Proterozoic basement rocks, which is  $0.73$  to  $0.90 \times 10^{-6} \text{ W m}^{-3}$ . The radiogenic element contents of the main formations in the study areas are generally not high enough to

produce significant amounts of heat except for basalt and syenite (Table 3.4). Basalt is found near the surface but is not thick enough to be a significant heat source, while syenite intrusions, if found at depth with a similar chemical composition, could be ( $1.35 \times 10^{-6}$  W m<sup>-3</sup>).

### 3.5.5 Heat transfer mechanism

The thermofacies concept proposed by Sass and Götz (2012) is based on a permeability-thermal conductivity diagram, which this work improved by identifying conductive versus insulating rocks using boundaries corresponding to less than 2.5 W m<sup>-1</sup> K<sup>-1</sup> and greater than 3.5 W m<sup>-1</sup> K<sup>-1</sup>, respectively (Figure 3.13). This approach identified the insulating potential of the mica schist and paragneiss, where a higher geothermal gradient is normally anticipated in rocks of such relatively low thermal conductivity. Moreover, Sass and Götz (2012) suggested that the transitional state of conductive to conductive-convective heat transfer can occur within low permeability rocks (>10<sup>-15</sup> m<sup>2</sup>; Figure 3.13). Applying the thermofacies concept, the dominant heat transfer mechanism expected for the rock matrix in the Ambilobe and Ambanja areas is heat conduction, which is similar to what is expected for sandstone of the Karoo Basin (Campbell et al., 2016a; Campbell et al., 2016b). The ratio of porosity versus permeability for the Ambanja and Ambilobe rocks is further evidence in favour of conductive heat transfer in the rock matrix (Figure 3.14). In fact, Permian and Triassic sandstone are characterized by a proportional ratio of porosity to permeability, and this ratio is obviously affected by depth (Figure 3.14)

Advective heat transfer is expected where permeability is >10<sup>-15</sup> m<sup>2</sup>. For example, the sandstones from the North Germany Basin, the Pannonian Basin and the Rhine Graben present characteristics of forced and free convective heat transfer (Sass et al., 2012; Haffen et al., 2013). The latter are qualified as transitional systems in which matrix permeability is higher than that observed in the Ambilobe and Ambanja areas. However, permeability can be higher when secondary features are present, such as fractures, although these are challenging to consider when assessing permeability using hand samples in the laboratory. In the field, fractures, joints and veins were frequently observed, especially in the Triassic and Permian sandstones. Despite the measurement of low matrix permeability and porosity in the Ambilobe and Ambanja areas, the occurrence of thermal springs along major faults or in a graben structure (Figure 3.1) confirms that advective heat transfer can take place within fractured rocks. Therefore, the Ambilobe and Ambanja geothermal systems can be qualified as petrothermal systems where forced convective heat transfer can occur along faults, preferentially crustal faults reaching significant depths (>10 km; Ferguson et al., 2009; Moreno et al., 2018). Forced and free convection is common in

the extensional play type (López et al., 1995; Simms et al., 2004; Moeck et al., 2015; Moeck et al., 2019), which is the case of Madagascar. However, free convective heat transfer is unlikely because volcanism in North Madagascar is dormant (> 50,000 years old.) and convection giving rise to hot springs must be triggered by external forces, such as regional groundwater flow. The elevation difference between mountain summits and valleys is about 0.4 to 1.2 km in the Ambilobe and Ambanja areas, over a horizontal distance of 8 to 20 km, which can be sufficient to create a strong hydraulic gradient between groundwater recharge to discharge zones. Faults experiencing a strong hydraulic gradient can provide a path for water to rise to the surface, locally leaving conductive heat transfer as the dominant regime in the two study areas.

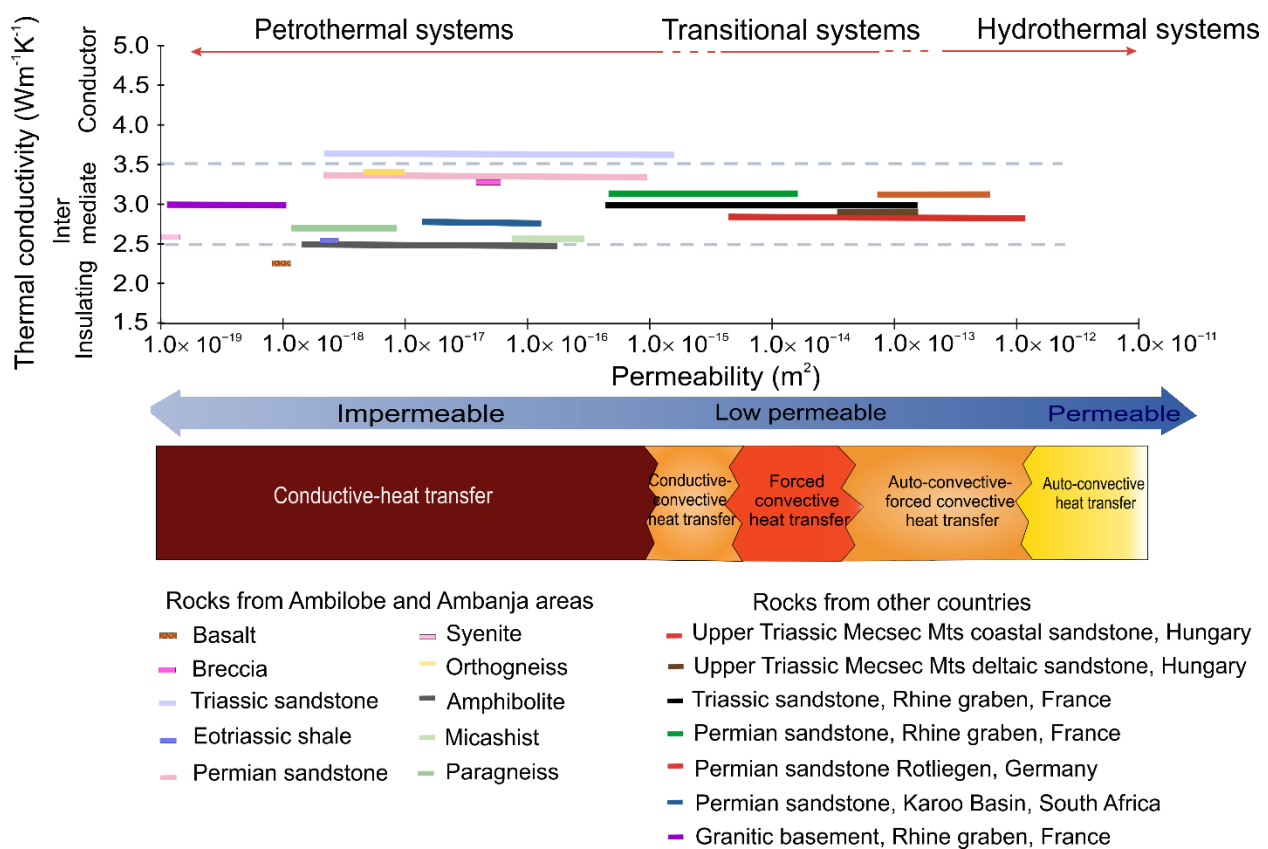


**Figure 3.13** Expected heat transfer mechanism according to the thermofacies concept of Sass et al. (2012). Data from other geothermal systems are also presented: Hungary Basin (Sass et al., 2012), Rhine Graben (Haffen et al., 2013; Hettkamp et al., 1999), and Karoo Basin (Campbell et al., 2016a; Campbell et al., 2016b)

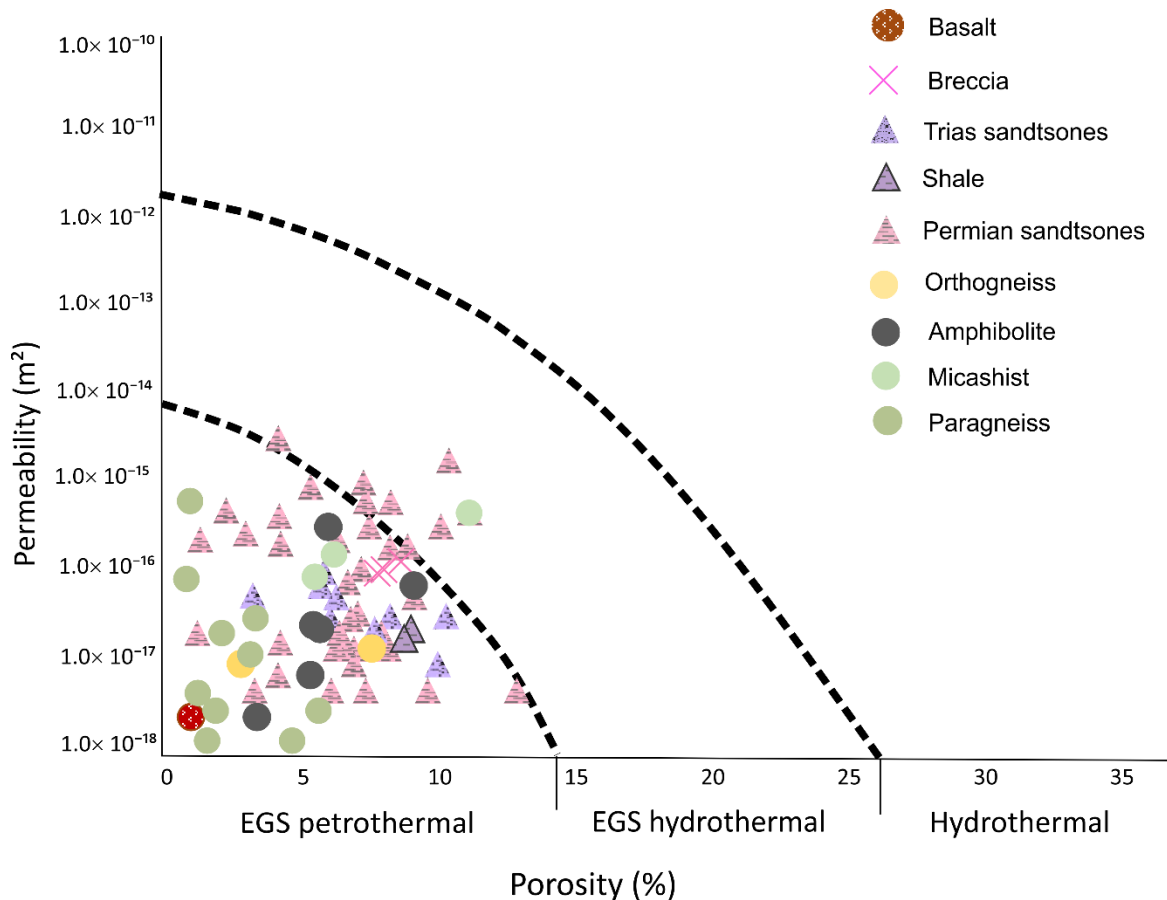


**Figure 3.14** Porosity versus permeability data from this study linked to potential geothermal development, based on the diagram developed by (Moeck, 2014; Moeck et al., 2019). EGS= enhanced geothermal system.

### 3.5.6 Implications for geothermal exploration

Unfractured rock formations with high porosity and permeability that are known to host conventional geothermal reservoirs (Manning et al., 1999) are unlikely to be found in the Ambilobe and Ambanja areas. Enhanced geothermal systems, where rock permeability can be increased by stimulation to produce fluids at higher flow rates (Tester et al., 2006; Huenges et al., 2011; Kusumawardani et al., 2019), could potentially be developed (Figure 3.14). Geothermal exploration targets should focus on crustal faults associated with extensional domains, such as the Ambilobe fault zone and the Ambanja graben. Tectonic reworking of sedimentary and basement rocks can significantly improve permeability in fault zones (Petford, 2003). In turn, the faults can control the migration pathway to fluids giving rise to hot springs or warm temperature at shallow depths (e.g., Faulds et al., 2015). The main heat source is associated with a shallow Moho in both areas and a recently crystallized volcanic system in Ambanja (Rajaobelison et al., 2020). In addition, heat transfer mechanisms can be affected by the insulating potential of mica

schist and paragneiss and the heat generation potential of syenite, which are only found in the Ambanja area (Figure 3.1). This is correlated with the results of chemical geothermometers, which suggest a slightly higher reservoir temperature for Ambanja (140–200 °C) compared to Ambilobe (140–180 °C), based on previous studies in Madagascar (Gunnlaugsson et al., 1981; Rajaobelison et al., 2020).

### 3.6 Conclusions

This first evaluation of thermal and hydraulic properties of the rock units in North Madagascar provided an initial and qualitative evaluation of heat transfer mechanisms affecting the geothermal resources in the Ambilobe and Ambanja areas. The study indicates that conductive heat transfer in rocks of low permeability is expected for such petrothermal systems in extensional domains, where field evidences such as hot springs suggest that forced convection locally occurs along fault zones. The absence of insulating and heat-generating rocks in the Ambilobe area could affect its geothermal gradient and thus its resource potential. Development would rely on EGS, and deep fault zones in extensional settings should be the main exploration targets.

The petrophysical properties assessed in this study provide fundamental knowledge that can be used to better understand the geothermal systems of North Madagascar with an improved thermostratigraphic scale highlighting the insulating potential of rocks, which is important for petrothermal systems. Thermohydraulic properties can be used as a next step to quantitatively evaluate heat transfer mechanisms using numerical modelling in order to guide future geothermal exploration in the Ambilobe and Ambanja areas. Numerical simulation of heat transfer in these geothermal areas using measured rock properties should be conducted at the regional scale to quantify subsurface temperatures. Further structural geological work to characterize fault zones and evaluate stress directions, as well as geophysical surveys (e.g., magnetotelluric) will help image deep structures and will be required when moving Ambilobe and Ambanja to the next geothermal exploration stage. Deep temperature logs and well data are critical to advancing geothermal exploration in Madagascar and represent the next step in estimating the heat flow and geological gradient in this region of Madagascar. Thus, the present study helps justify further geothermal exploration with potential drilling to develop renewable resources in North Madagascar.

## **4 TROISIÈME ARTICLE: UNDERSTANDING HEAT TRANSFER ALONG EXTENSIONAL FAULTS: THE CASE OF AMBILOBE AND AMBANJA GEOTHERMAL SYSTEMS IN MADAGASCAR**

---

Comprendre le transfert de chaleur le long des failles d'extension : cas des systèmes géothermiques d'Ambanja et Ambilobe, Madagascar

**Auteurs :**

<sup>1</sup>M. Rajaobelison, <sup>1</sup>J. Raymond, <sup>1</sup>M. Malo and <sup>2</sup>C. Dezayes <sup>3</sup>S. Larmagnat

<sup>1</sup> Institut national de la recherche scientifique, 490 de la Couronne, Québec, QC G1K 9A9, Canada

<sup>2</sup> Bureau de recherches géologiques et minières, 3 Avenue Claude Guillemin, 45100 Orléans, France

<sup>3</sup>Geological Survey of Canada

490, rue de la Couronne, Québec (Québec) G1K 9A9 Canada

**Titre de la revue ou de l'ouvrage :**

Geothermics

Soumis

**Contribution des auteurs :**

MR : Collecte des données, enquête, conceptualisation, méthodologie, rédaction - préparation de la version originale. JR et MM : Supervision, ressources, direction du projet. JR, CD et MR : Validation. JR, MM, CD et SL : Rédaction - Révision et édition. Tous les auteurs ont revu le manuscrit, ont lu et approuvé la version publiée du manuscrit.

**Lien entre l'article ou les articles précédents et le suivant :**

Le chapitre précédent présente les données sur les propriétés thermohydrauliques des formations qui dominent les deux zones d'intérêt, soit Ambilobe et Ambanja dans le Nord de Madagascar. Ces propriétés ont permis d'identifier la conduction comme le mécanisme de transfert de chaleur dominant à l'extérieur des grandes zones de failles. Ces propriétés sont utilisées dans le présent chapitre dans lequel des modèles numériques sont développés pour mieux comprendre le transfert de chaleur par convection forcée le long des failles responsables de la remontée des fluides afin d'expliquer la présence des sources chaudes dans ces zones.

## 4.1 Introduction

Economic activity in the northern region of Madagascar relies on export products such as vanilla, cocoa and coffee that are grown and transformed locally. Madagascar is in fact one of the largest vanilla exporters in the world (UNComtrade, 2018). The energy used to transform these products heavily relies on fossil fuels and wood. Off-grid communities, mainly in remote areas, use traditional biomass such as firewood and charcoal as their main source of energy and are thus leading to deforestation and water resources degradation, along with biodiversity and soil loss, as in many communities of Madagascar. Renewable sources such as geothermal energy are expected to play a larger role in future energy production.

Ambilobe and Ambanja, two areas located in North Madagascar, have been characterized for their geothermal potential and classified as a graben border-fault liquid-dominated moderate-temperature system and a fossil magmatic liquid-dominated moderate-temperature system, respectively (Rajaobelison et al., 2020). Within this classification scheme referring to the extensional type, faults and lithological-diagenetic characteristics affecting porosity are thought to control formation permeability. Reported by Rajaobelison et al., (2021), the average matrix permeability of rocks without fractures in these two areas was evaluated to vary between  $10^{-13}$  and  $10^{-18} \text{ m}^2$ , which is low, while the average porosity is ~5.7 %, which can be classified as low or poor (5–10 %) according to Levorsen et al., (1967). However, this matrix permeability has to be considered as the lower bound of the formation permeability that can likely be increased by fractures in such an extensional tectonic setting. The occurrence of thermal springs along major faults or in a graben structure in Ambilobe and Ambanja confirms that advective heat transfer can take place within fractured rocks (Rajaobelison et al., 2021). The equilibrium formation temperature at depth calculated by means of geothermometers (Gunnlaugsson et al., 1981) is estimated to range from 140 to 200 °C, a temperature high enough to be used for scalding vanilla bean (~60°C) and for greenhouse heating (> 40 °C, Lindal, 1973), as well as for electricity generation (> 80 °C, Grasby et al., 2011; Tomarov et al., 2017). Fluid may also generate electricity from geothermal energy source lower than 120 °C by using an optimized Organic Rankine Cycle (e.g., Liu et al., 2017; Tillmanns et al., 2017; Shi et al., 2019; Chagnon-Lessard et al., 2020).

The depth at which geothermal sources can be found, the geothermal gradient and the Earth heat flux density is currently unknown in North Madagascar as no geothermal exploration borehole has been drilled so far. Previous works allowed to classify geothermal play types and evaluate rock thermo-hydraulic properties from surface outcrops to better understand heat transfer mechanisms at depth (Rajaobelison et al., 2020, 2021). Crustal-scale faults have been identified as potential targets for geothermal exploration, but further work was needed to better understand the role of faults on subsurface heat transfer mechanisms controlling the depth and extent of geothermal sources. The influence of faults must be taken into account when exploring geothermal energy sources, especially large-scale faults that have been identified from surface geological mapping and are indicated on geological maps of Madagascar elaborated by Roig et al., (2012) and Tucker et al., (2014). Numerical modeling was therefore used to simulate groundwater flow and heat transfer according to various fault scenarios affecting such geothermal energy source associated with petrothermal systems found in this extensional domain of Madagascar.

Numerical modeling has been previously used to simulate the distribution of temperature at depth to better understand faulted geothermal reservoirs (Corbel et al., 2012; Hao et al., 2012; Holzbrecher et al., 2010; Bakhsh et al., 2016). If faults behave as conduits and increase permeability (Ferrill et al., 2004), they can be a target for geothermal exploration, but if they behave as barriers and decrease the permeability (Gibson, 1998), they can cause compartmentalization of reservoirs, which can generate difficulties for access and exploitation of the geothermal resources (Loveless et al., 2014). Prediction and modeling of coupled fluid flow and heat transfer processes in naturally and fractured rock systems represent a critical component for energy recovery analysis (Hao et al., 2012). In addition, numerical modeling of hydrothermal systems has often been conducted to explain hot spring occurrences and explore their controlling factors (Forster et al., 1989; López et al., 1995; McKenna et al., 2004; Bense et al., 2008; Guillou-Frottier et al., 2013; Magri et al., 2016; Volpi et al., 2017; Taillefer et al., 2018). Recent works of Szijártó et al., (2019); Szijártó et al., (2021) investigated with numerical modeling the conditions that can induce and favor forced convection. The work of Moreno et al., (2018) additionally highlighted that fault dip or angle with respect to the regional groundwater flow orientation driven by topography can affect the rise of groundwater and consequently hot spring occurrence and temperature.

The objective of this study was to understand the role of faults on forced convective heat transfer giving rise to hot springs in North Madagascar, providing fundamental knowledge to improve geothermal exploration concepts. Our working hypothesis is that fault dip at depth, which is currently unknown, can affect the rise of hot fluids. We therefore developed numerical groundwater flow and heat transfer models aiming to reproduce hot springs temperature near the surface since this is the only information available in the area to validate simulations. Favorable fault characteristics benefiting to geothermal energy sources were identified to help further geothermal exploration.

## 4.2 Geological setting

### 4.2.1 Tectonic framework and fault system

The Bemarivo domain is one of the six geodynamic domains making Shield rocks in the North of Madagascar where are located the two geothermal areas of interest: Ambilobe and Ambanja. This domain has been interpreted as an assemblage of two juvenile arc terranes (Figure 4.1). The age of the northern and southern terranes, which form the Neoproterozoic Bemarivo domain, is between c. 750 and 720 Ma (Thomas et al., 2009; Tucker et al., 2014). A major ductile structure called Antsaba shear zone (ASZ) with east–west trending, separates both terranes. The shear zone is about 15 km wide at its widest location to the west (Thomas et al., 2009). According to Armistead et al., (2019) this shear zone correspond to subduction zone along which the amalgamation of the northern and southern terranes occurred. Nevertheless, the Bemarivo domain is considered one domain, opposite to the suggestion of Thomas et al., (2009) and Armistead et al., (2019); based on lithostratigraphy and ages reported by Tucker et al., (2014). The Bemarivo domain is a terrane of Cryogenian igneous rocks, with a cryptic Paleoproterozoic basement, that was accreted to the Greater Dharwar Craton in latest Ediacaran to earliest Cambrian time (0.53–0.51 Ga; Tucker et al., 2014).

Mesozoic and younger movements along the Antsaba shear zone produced a variety of brittle faults and dykes related to the break-up of Gondwana and rifting in the Mozambique Channel. In fact, the extensional phases from Triassic to Jurassic (Karoo rift), gave rise to the NNE-SSW and NNW-SSE faults and the faults with general strike of N140-N160 have been transformed as wrench faults with dextral movement during Jurassic-upper Cretaceous times, coherent with the development of the Davie Ridge (Lardeaux et al., 1999). Numerous NE-SW and NW-SE faults are consistent with the identified faults and

the regional Plio-Quaternary direction of extension, i.e. N65°E to N85°E observed in the volcanic region of Montagne d'Ambre, in the extreme north of Madagascar (Chorowicz et al., 1997).

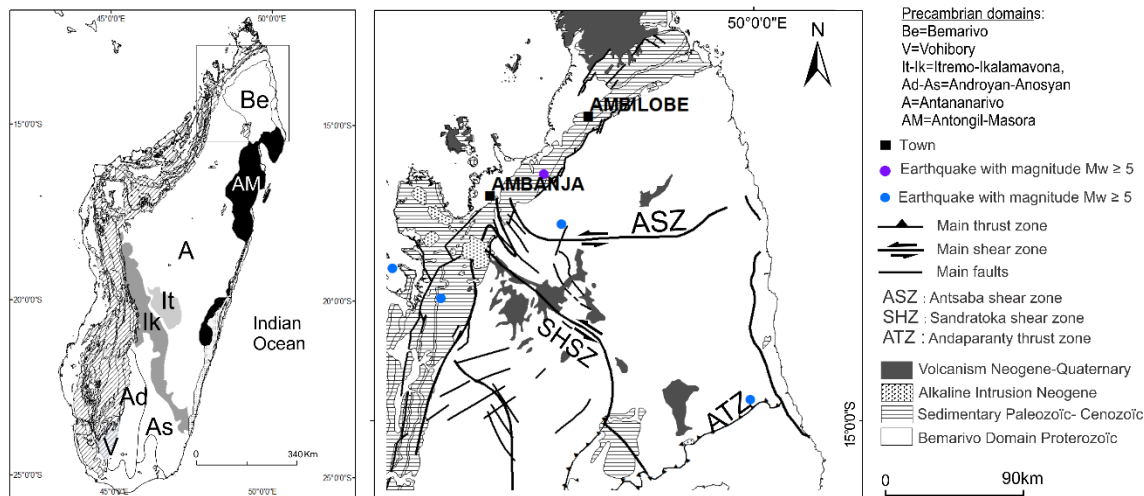


**Figure 4.1** Simplified geological map with close-up to tectonic framework of Bemarivo domain in northern Madagascar (modified from Thomas et al., 2009; Armistead et al., 2019) and where the areas of interest: Ambilobe and Ambanja are located. The geological map in the right side shows the main six geodynamic Precambrian domains that form the Madagascar Shield (modified from De Waele et al., 2011; Tucker et al., 2014).

Ambilobe area is located in a normal fault zone called Andavakoera, a major NE-SW fault delineating the contact between sedimentary sequences and basement rocks of the northern Bemarivo domain. Numerous undifferentiated NW–SE faults and NW–SE strike-slip faults with dextral or sinistral movements are also observed. Among the strike-slip faults are the faults near the Betsiaka hot spring as well as the Ranomafana and Ankatakata undifferentiated normal faults (Figure 4.2b). The main faults and fractures system are dominated by the NNW–SSE; NE–SW and N–S direction, as it is shown on the rose diagram (Figure 4.2b).

Ambanja area is located in the graben structure formed in Proterozoic basement units of the southern terrane of Bemarivo domain. The graben orientation is NW–SE and its average width is 4 km. The main faults and fractures are dominated by the NNW– SSE direction as shown in the rose diagram of measured fracture orientation in the field and by faults on the geological map (Figure 4.2b).

#### **4.2.2 Favorable structural patterns**

According to the comprehensive inventory of the structural setting of known geothermal systems in the extensional to transtensional terrane of the Great Basin region in the western USA, Faulds et al., (2015) identified the favorable dominant pattern of faulting that host geothermal activity, especially in a region where the bulk of the geothermal resources are likely blind or hidden. Applying the same principles to Ambilobe and Ambanja areas, the identified favorable fault structures are 1) major normal fault segments, i.e. near displacement maxima of Andavakoera NE-SW fault and the fault-borders of Ambanja graben structure with NW-SE direction (Figure 4.2b and 4.2c), and 2), fault intersections between two normal faults or between normal faults and transverse oblique-slip faults (Figure 4.2b).

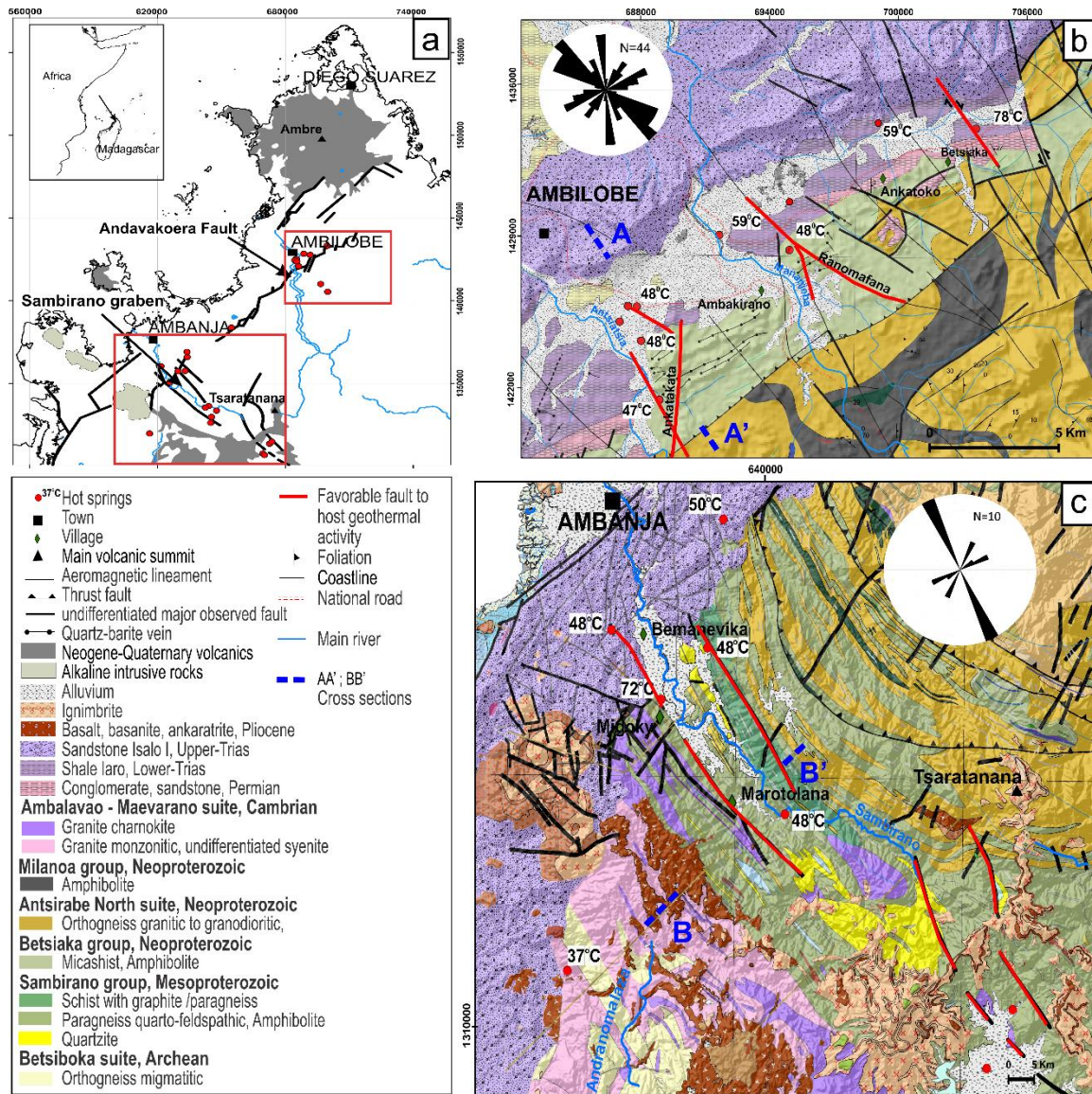


**Figure 4.2** (a) Location of Ambilobe and Ambanja geothermal areas with (b) and (c) being detailed geology (modified from Roig et al., 2012). The rose diagrams illustrate the major direction of faults and fractures that was established from field data collected in 2018.

At the surface, hot springs reach a temperature varying from 50 to  $72^{\circ}\text{C}$  in both areas (Besairie, 1959; Gunnlaugsson et al., 1981). The high concentration of Mg of hot springs and plotting the results on immature water, as shown by the ternary Na-K-Mg diagram of Giggenbach (1988) in Figure 4.3, indicate dilution of the geothermal fluid along its way to the surface. The geothermal fluid is thus mixed with meteoric and shallow groundwater.

According to chemical geothermometers (Gunnlaugsson et al., 1981) and using the Giggenbach diagram (Figure 4.3), the reservoir temperature in the areas of Ambilobe and Ambanja is expected at 140 and 200 °C, respectively.

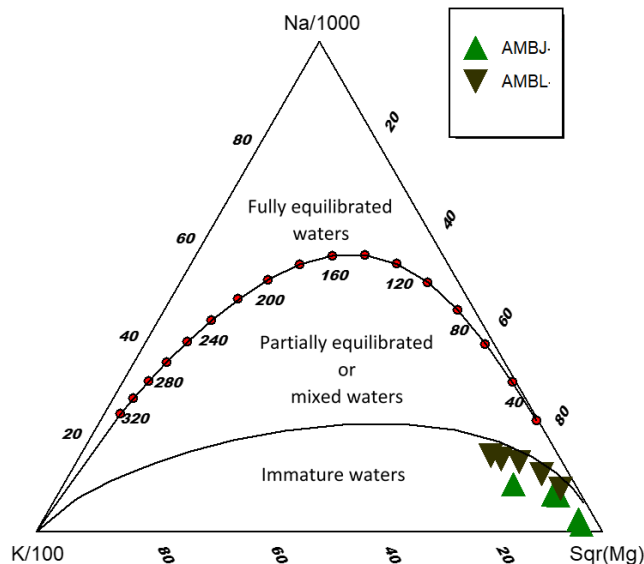


**Figure 4.3** Chemical composition of water on a ternary Na-K-Mg diagram (Giggenbach, 1988) for hot springs of Ambilobe (AMBL) and Ambanja (AMBJ). The concentration of Na, K, Mg was reported by Gunnlaugsson et al., (1981).

#### 4.2.3 Lithosphere structure and geological formation

In the Bemarivo domain, Moho is placed at 33 km depth (Andriampenomanana et al., 2017). The upper crust has a thickness up to 20.5 km and is assumed mainly composed of paragneiss and sedimentary rocks which have an average thickness of 4 km. The lower crust is assumed to be made of mafic rocks with an average thickness of 12.5 km.

The geological formations of the Ambilobe and Ambanja areas and their thermo-hydraulic properties are described in the previous works of Rajaobelison et al., (2020, 2021). Permo-triassic sedimentary rocks of Ambilobe Basin overlying the Proterozoic basement of Bemarivo domain are the main formations in Ambilobe area. Proterozoic basement rocks of the Bemarivo domain are the only geological formations in Ambanja area (Figure 4.2).

## **4.3 Numerical model developpement**

### **4.3.1 Conceptual models**

Models geometry illustrated in Figure 4.4 account for the topography through NNW-SSE (AA') and NE-SW (BB') cross sections (Figure 4.2), which represent, respectively, the Andavakoera normal fault zone delineating the contact between sedimentary sequences and the basement rocks in Ambilobe and the graben structure in Ambanja. The dominant sedimentary and basement units are considered in the models. The geological cross sections were drawn perpendicular through the main undifferentiated observed faults near hot springs occurrences. The faults represented in the models are the post-Triassic Ankatakata normal oblique-slip faults striking N010° and N120° respectively, in the Ambilobe area, while they are the major border-faults for Ambanja graben. These faults are reported in the geological map of Madagascar by Roig et al., (2012).

Different modeling scenarios were defined to investigate the influence of fault dip with respect to the groundwater flow and heat transfer processes (Table 4.2). The dips are comprised between 60 and 85° for the two models since dips from 60 to 90° was shown to cause variations on the pressure and temperature of subsurface fluids (Cherubini et al., 2013). These modeling scenarios were based on the geological maps of Ambanja and Ambilobe, although there is still a lot of uncertainties about fault dip and down-dip continuity at depth, which justifies the use of various scenarios. The models simulate the potential temperature distribution for the two geothermal areas of Ambilobe and Ambanja according to the influence of fault dip.

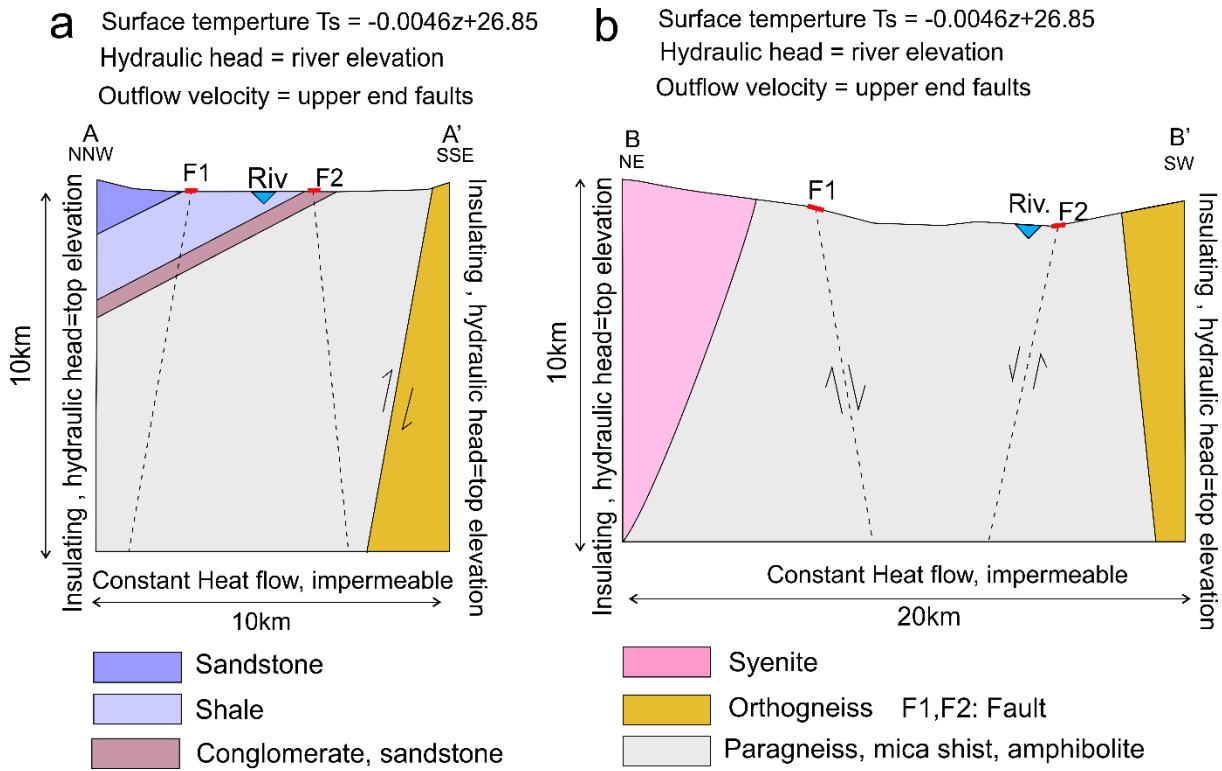


**Figure 4.4** Geometry and boundary conditions of the 2D numerical model based on the geological cross-section (AA') and (BB') in Figure 4.2 representing a) Ambilobe in the Andavakoera normal fault zone with basement–sediments contact, and b) Ambanja graben. Riv stands for River.

**Table 4.1** Fault scenarios

Area	Faults	Dip	Scenario
Ambilobe	F1; F2	No fault	0
		70° NW; 85° SE	1
		60° NW; 60° SE	2
		80° SE; 75° SE	3
		80° NW; 85° NW	4
Ambanja	F1; F2	No fault	0
		80° SW; 80° NE	1
		75° NE; 80° NE	2
		75° NW; 80° NW	3

### 4.3.2 Physical mechanisms simulated

The subsurface module of COMSOL Multiphysics, allowing to couple groundwater flow simulated with Darcy's law and heat transfer in porous media, was used with a finite element scheme to develop the models. This allowed simulating forced convective heat transfer which occurs along major faults where the host rock is considered as an equivalent porous medium. Steady-state flow and heat transfer were solved using the parameters summarised in Table 4.2. Sedimentary rocks as well as granitic and

paragneiss basement were considered as low permeable 2D units with the use of the equivalent porous medium, where fluids can circulate. Faults are discrete 1D linear elements superposed to the 2D porous medium, where flow and heat transfer is solved simultaneously. Coupling between heat transfer and fluid motion occurs through the velocity field.

#### **4.4 Geometry and unit properties**

- Ambilobe

The model has a width of 10 km and a depth of 10 km (Figure 4.4a). The sedimentary rock units dip 20-30 degrees to the NE. There are 5 lithological domains with different material properties shown in Table 4.2. The reverse fault F marks the contact between the micashist and orthogneiss formations and F1, F2 are the mains faults represented in the models.

- Ambanja

The model has a rectangular geometry having a width of 20 km and a depth of 10 km (Figure 4.4b). It is divided into 3 lithological domains with different material properties (Table 4.2) where the border faults of the graben are represented by F1 and F2 with their respective properties presented in Table 4.2.

**Table 4.2 Model input parameters**

Parameter	Value								Unit	Reference
Area	Ambilobe									
Formation	Sediments									
Geological Units	Permian Sandstone	Eo Triassic shale	Triassic sandstone	Mica Shist Amphibolite	Ortho-gneiss	Syenite	Para-gneiss			
Mean $\phi$	0.07	0.08	0.07	0.11	0.05	0.001	0.02	Fractional		
Mean $k$	1.4 $\times 10^{-13}$	1.0 $\times 10^{-17}$	$\times 10^{-16}$	1.0 $\times 10^{-15}$	1.0 $\times 10^{-16}$	1.0 $\times 10^{-18}$	1.0 $\times 10^{-15}$	$m^2$	Rajaobelison et al., (2021)	
Mean $\lambda$	3.6	2.5	3.5	2.6	3.4	2.6	2.7	$W m^{-1} K^{-1}$		
Mean $\rho$	2542	2382	2628	2735	2678	2700	2678	$Kg.m^{-3}$		
Mean $c$	904	875	919	879	846	875	830	$J Kg^{-1} K^{-1}$		
Mean A	1.14	0.72	1.25	0.58	0.38	1.35	0.38	$10^{-6} W m^{-3}$		
Thickness Model		4		6		10		km		
Depth of crust			33					km		
Upper Crust (UC)			20.5					km	Andriampenomanana et al., (2017)	
Lower Crust (LC)			12.5					km		
Mean A (UC)			1.5					$10^{-6} W m^{-3}$	Horton et al., (2016)	
Mean A (LC)			0.72							
A Total Crust			1.2					$10^{-6} W m^{-3}$		
Faults Properties			F1; F2							
Aperture		Min		Mean		Max				
D <sub>f</sub>		$250 \times 10^{-6}$		$1.1 \times 10^{-3}$		$2 \times 10^{-3}$		m		
Permeability		$10^{-14}$		$10^{-10}$		$10^{-7}$		$m^2$		
K <sub>f</sub>										

$\lambda$  = thermal conductivity,  $\rho$  = density,  $c$  = heat capacity, A= Radiogenic heat production

#### **4.4.1 Thermohydraulic properties**

Thermohydraulic properties of model units were based on average properties measured in the laboratory for each geological formation reported by Rajaobelison et al., (2021) and now summarized in Table 4.2. The porosity  $\phi$  and permeability  $k$  ( $m^2$ ) were evaluated with transient measurements using the combined AP-608 gas permeameter–porosimeter from Core Test Systems with nitrogen as the gas source. The average bulk density  $\rho$  ( $Kg\ m^{-3}$ ) was obtained when performing porosity assessment. The optical scanning method was used with an infrared scanner developed by LGM Lippmann to determine transient thermal conductivity  $\lambda$  ( $Wm^{-1}\ K^{-1}$ ) and diffusivity  $\alpha$  ( $m^2\ s^{-1}$ ). The heat capacity,  $c$  ( $J\ Kg^{-1}\ K^{-1}$ ), was deduced from the thermal conductivity and thermal diffusivity assessment (Popov et al., 1999, 2016).

#### **4.4.2 Internal heat generation**

The internal radiogenic heat generation ( $A$ ;  $10^{-6}\ W\ m^{-3}$ ) for each rocks presented in Table 4.2 was estimated from the concentration on the radiogenic elements U, Th and K reported by Rajaobelison et al., (2021).

#### **4.4.3 Faults properties**

In this study, the faults aperture and permeability were assumed to range from  $250\ \mu m$  to  $0.2\ cm$  and  $10^{-14} - 10^{-7}\ m^2$ , respectively (Table 4.2). These ranges are based on the literature, reporting values obtained from various in-situ hydraulic tests performed at geothermal sites ( e.g., Jeong et al., 2001; Holzbecher et al., 2011) and from numerical simulation studies of groundwater flow in discrete fracture models taken as examples (e.g., Bisdom et al., 2016; Guillou-Frottier et al., 2013). The minimum fault aperture range correspond to that observed under a normal stress of  $20\ MPa$  in a laboratory experiment and which validated the cubic law for laminar flow of fluids through open fractures (Witherspoon et al., 1980).

### **4.5 Meshing**

The mesh is gradually refined from bottom to top and also close to the faults to avoid convergence problem and where more accuracy is required at location where flow and

temperature contrasts can be important (Figure 4.5). A non-structured mesh with triangular elements was used and the mesh statistics are summarised in the Table 4.3.

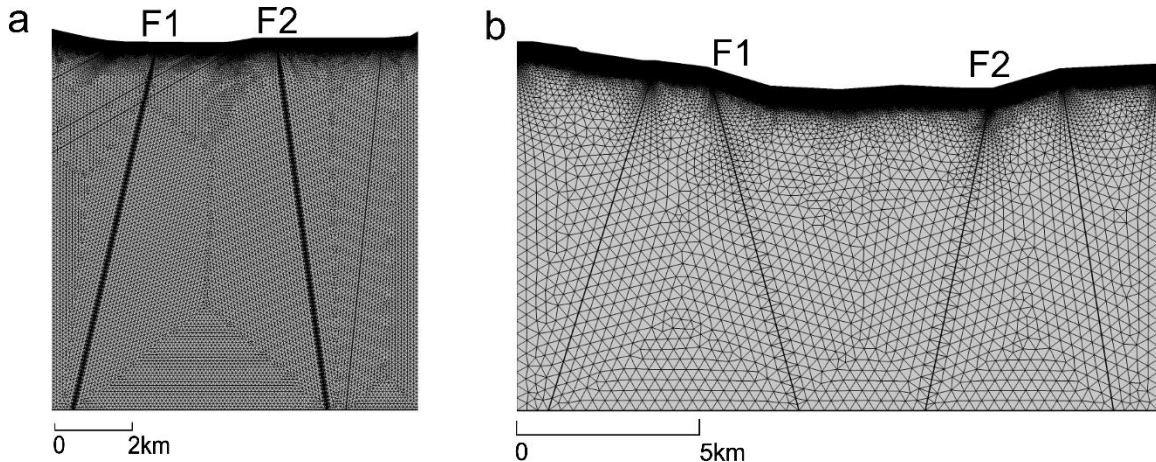


**Figure 4.5** Finite element mesh of the 2D numerical models for a) Ambilobe in the Andavakoera normal fault zone with basement–sediments contact, and b) the graben of Ambanja.

**Table 4.3** Mesh statistics of Ambilobe and Ambanja 2D models

	Ambilobe	Ambanja	Unit
Number of element	101 672	274 403	
Maximum element size	104	404	m
Minimum element size	0.208	0.404	m
Nodes	49 506	137 998	

To verify that the temperature solution is independent of the element size, a mesh convergence study was undertaken such as a chosen cutline are sampled uniformly from the models at different mesh size. Then we compute the parameter  $\sigma$  defined by:

$$\sigma = \sqrt{\frac{1}{N} \sum_{i=1}^N (\Delta T_i)^2} \quad (4.1)$$

where  $N$  is the sample number,  $\Delta T_i$  is the temperature variation at a depth  $x_i = (i-1)D/N-1$  along the chosen cutline when we vary the mesh size of the model. Here  $D$  is the depth of the model. It is showed that a stable solutions can obtained above  $10^4$  elements with a difference of about  $1^\circ\text{C}$  or less (Figure 4.6).

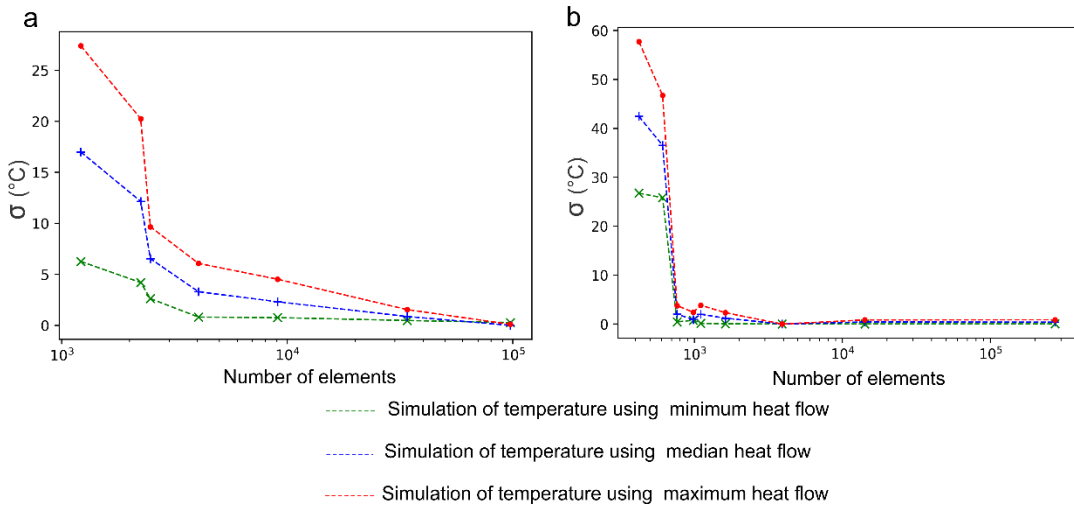


**Figure 4.6** A mesh convergence study a) for Ambilobe and b) for Ambanja models.

## 4.6 Boundary conditions

### 4.6.1 Groundwater flow

Topography-driven groundwater flow affecting forced convection was reproduced by imposing lateral flow boundary conditions (Smith et al., 1983; Woodbury et al., 1985; López et al., 1995; Tóth, 2009). The lateral boundaries of the model are assigned a constant hydraulic head equal to the topographic elevation (Figure 4.4). The segment representing the river in the model valleys are also assigned to a constant hydraulic head value equal to its nodal elevation. An outflow boundary was assigned at the upper end of the faults to allowing fluids to exit the faults at surface. The base of the models was assumed impermeable.

### 4.6.2 Heat transfer

A constant temperature was specified at the surface of the models and assumed to be a linear function of the altitude. The relationship between the temperature at the surface ( $T_s$ ) and the altitude ( $z$ ) is:

$$T_s = -0.0046z + 26.85 \quad (4.2)$$

where  $-0.0046$  and  $26.85$  °C are constants that were determined from average annual temperatures at available meteorological stations in different locations of Madagascar.

The location of the stations are Antsiranana, Mahajanga, Antananarivo and Tolagnaro (Table 4.4; Stalenberg et al., 2018).

**Table 4.4 Data from selected meteorological stations in Madagascar**

Station	Antsiranana	Mahajanga	Antananarivo	Tolagnaro
Altitude (m)	105	27	1268	22
Average annual temperature (°C)	24.7	27	19.5	24

The lower boundary of the models, which is located at 10 km, was assigned a second type condition of constant heat flow (Table 4.5), defined according to the Curie point depth (CPD; Tanaka et al., 1999) and the internal heat generation in the crust. Heat flow at the CPD ( $Q_{CPD}$ , mWm<sup>-2</sup>) was initially calculated considering the surface ( $T_0 = 20$  °C) and Curie temperature ( $T_{CPD} = 580$  °C) with:

$$Q_{cpd} = \lambda \frac{T_{CPD} - T_0}{Z_{CPD}} - A \frac{Z_{CPD}}{2} \quad (4.3)$$

where  $A$  (10<sup>-6</sup> W m<sup>-3</sup>) is the average heat generation due to radioactive decay of elements in the crust, which is the weighted average of the lower and upper crust heat generation. The internal heat generation in the upper crust and lower crust were estimated to  $1.5 \times 10^{-6}$  W m<sup>-3</sup> and  $0.72 \times 10^{-6}$  W m<sup>-3</sup> (Table 4.2 ; Horton et al., 2016).  $\lambda$  (W m<sup>-1</sup> K<sup>-1</sup>) is the average thermal conductivity of the crust and  $Z_{CPD}$  (m) is the CPD. The range of CPD was estimated at 10 to 33 km corresponding to the average Moho depth in the North Madagascar, using the centroid method of Tanaka et al. (1999) and according to the available world map of the CPD (Li et al., 2017).

Then the heat flux at 10km ( $Q_{10}$ , mWm<sup>-2</sup>) was calculated with:

$$Q_{10} = Q_{cpd} + A_{LC} H_{LC} + A_{UC} (H_{UC} - H_{model}) \quad (4.4)$$

where  $H_{LC}$  and  $H_{UC}$  are the thickness of the lower crust and the upper crust, respectively, and  $H_{model}$  is the thickness of the model,  $A_{LC}$  and  $A_{UC}$  are the heat generation of the lower crust and the upper crust, respectively (Table 4.2).

**Table 4.5 Parameters for heat transfer boundary condition**

Parameters	Value			Unit
Surface temperature	$T_s = -0.0046z + 26.85$			°C
Heat flow at base ( $Q_{10}$ )	Min 50	Mean 99	Max 148	mWm <sup>-2</sup>

Adiabatic heat transfer conditions were applied to the lateral boundaries.

## 4.7 Parameters sensitivity

The sensitivity of the model variable parameters was evaluated using the parametric sweep function implemented in COMSOL Multiphysics. The values assigned to the varied parameters were the minimum, mean and maximum identified for each variables where there is uncertainty. These variables are heat flow at the base as well as aperture and permeability of faults (Table 4.2). The combination of these three parameters with the different scenarios of fault dips (Table 4.1) allowed to carry out ninety-six simulations for Ambilobe 2D model and eighty-one simulations for the 2D graben model of Ambanja.

## 4.8 Results

### 4.8.1 2D subsurface temperature distribution

The different scenarios shown in Figures 4.7 and 4.9 are for base conditions using the value of heat flow ranging from the minimum, median and maximum with the average fault properties (Tables 4.1 and 4.2). The results reveal that a high temperature is found when heat flow is maximum. It is also shown that the faults allow the fluids, as well as the heat, to ascend compared with the scenario '0' without faults. Temperature profiles as a function of depth along fault lines (Figures 4.8 and 4.10) show which simulations best reproduce the temperature of the hot springs near the surface. The depth at which the reservoir temperature occurs can also be found with simulation results, assuming the chemical geothermometer provide a reliable estimate of the reservoir temperature. The most realistic scenarios are when hot spring temperature is found near the surface and the reservoir temperature is found at a reasonable depth, approximately under 2 km. The most representative simulation cases for Ambilobe are found in scenario 1, with the maximum value of heat flow and the fluids rising along fault F2, in scenario 2 when heat flow is maximum and then fluids are rising along fault F1 and finally in scenarios 3 and 4 when the heat flow value is median or maximum and fluids rise along faults F2 (Figures 4.7 and 4.8).

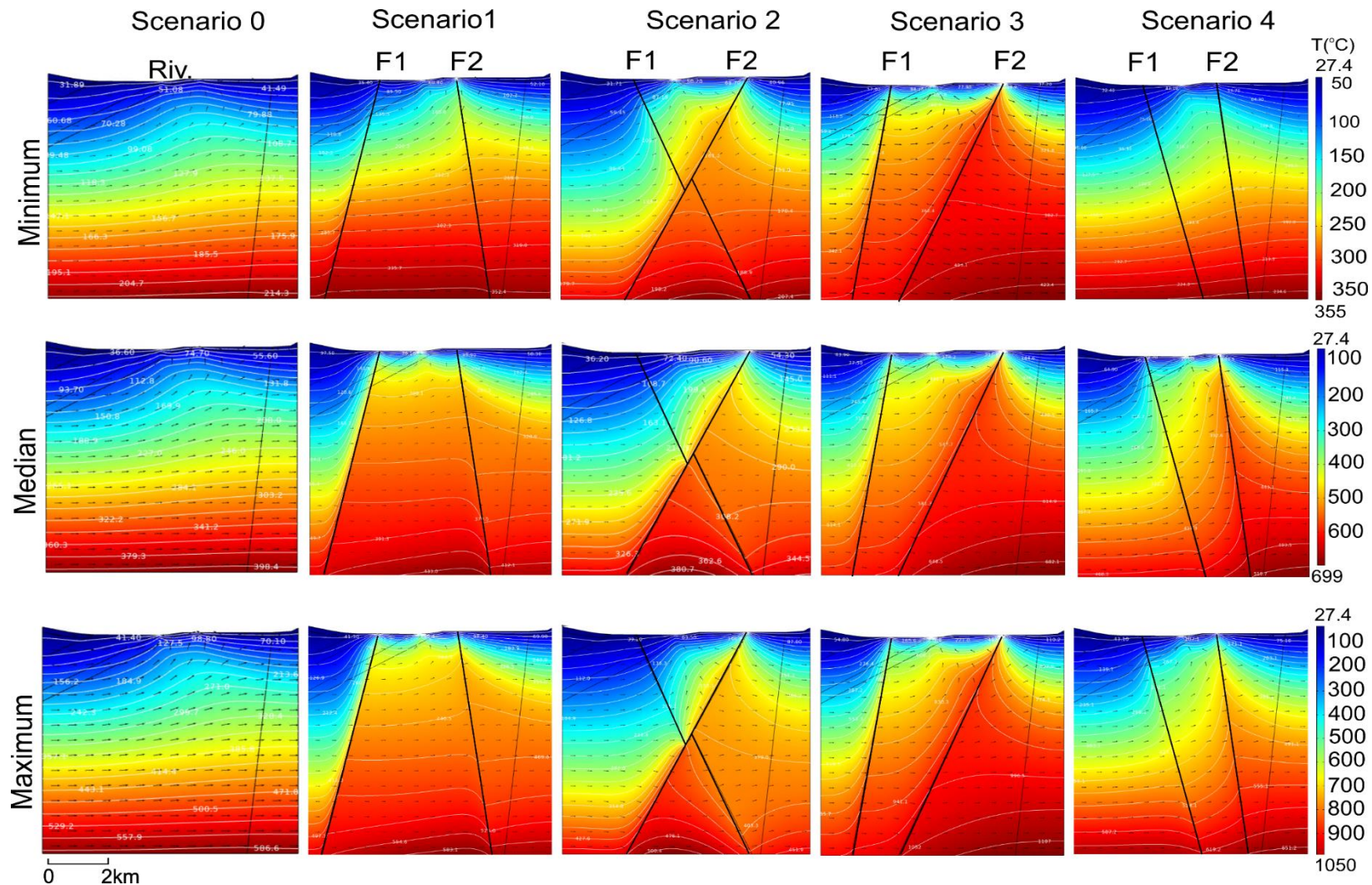


**Figure 4.7** Simulated temperature distribution for Ambilobe 2D model considering the variation of the fault dip and the variation of the heat flux at the 10 km depth. The black arrows show the velocity field and flow direction, the white lines are isotherms

The most representatives cases for the graben of Ambanja are found in scenario1 with median and maximum values of heat flow with fluids rising along fault F2 (Figures 4.9 and 4.10).

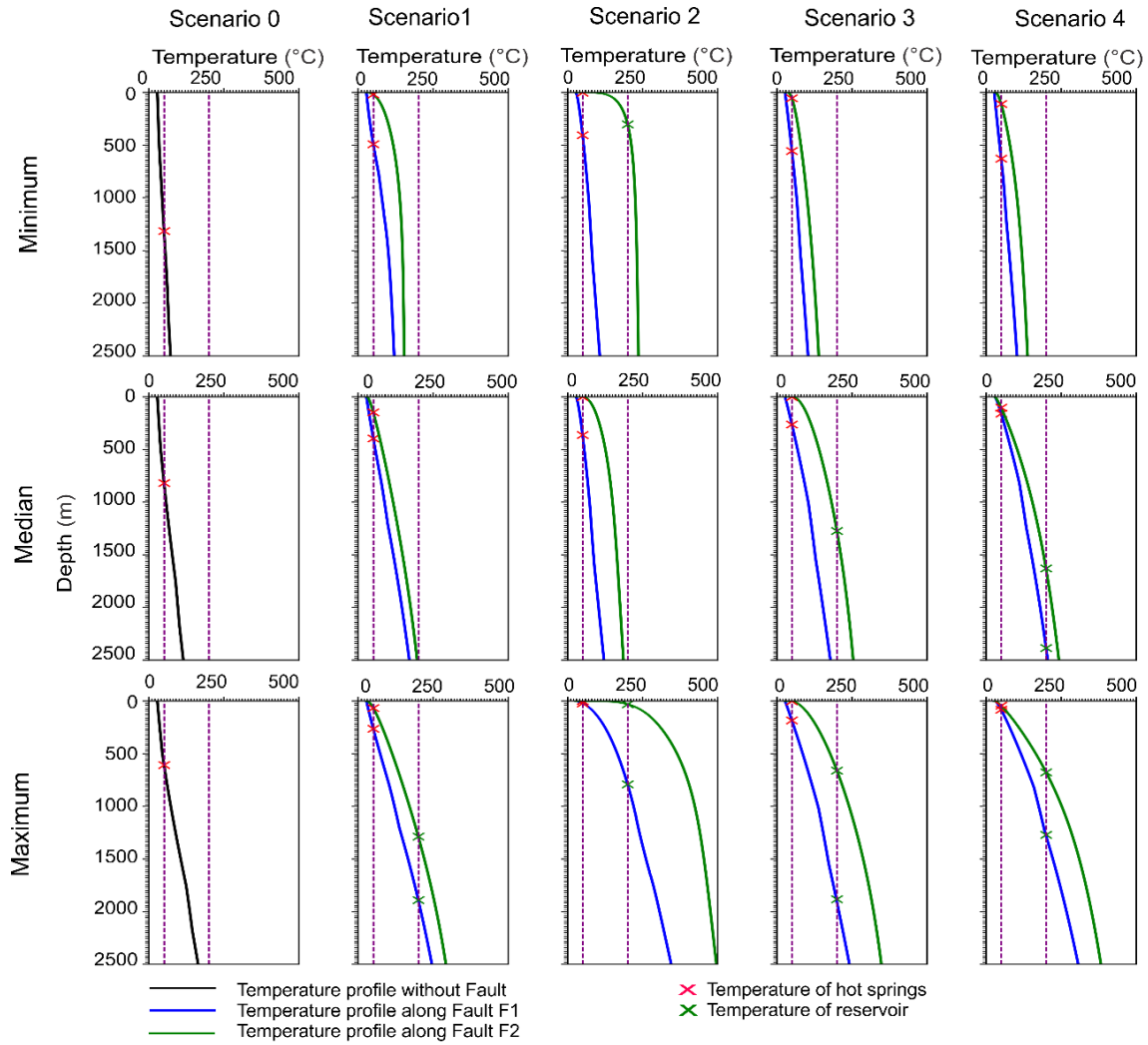


**Figure 4.8 Temperature profiles as a function of depth along the fault lines for the Ambilobe 2D model.**  
The temperature profiles in scenario 0 are obtained from an average cutline drawn in the model without faults.

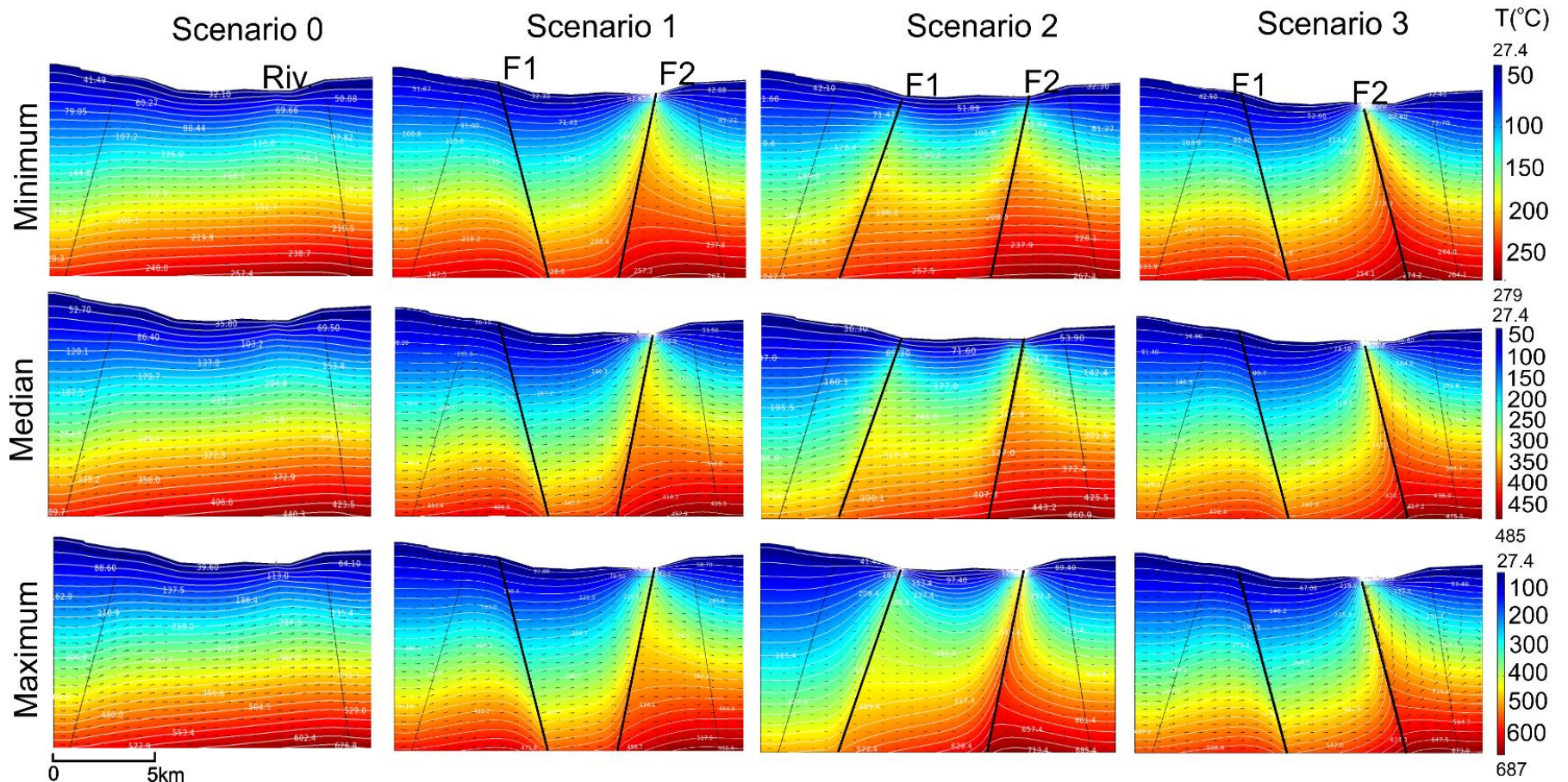


**Figure 4.9** Simulated temperature distribution for Ambanja 2D model considering the variation of the fault dip and the variation of the heat flux at the 10 km depth. The black arrows show the velocity field and flow direction, the white lines are isotherms.

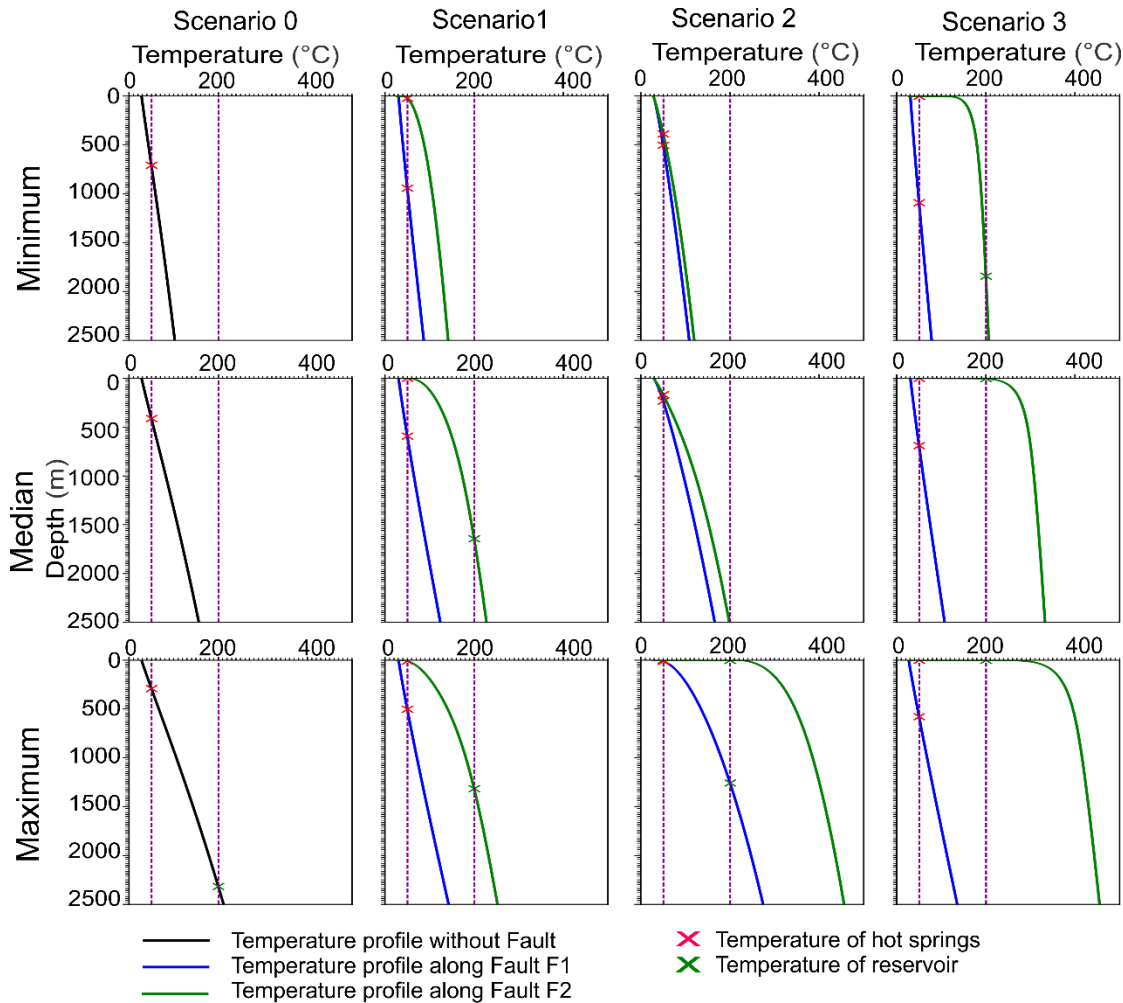
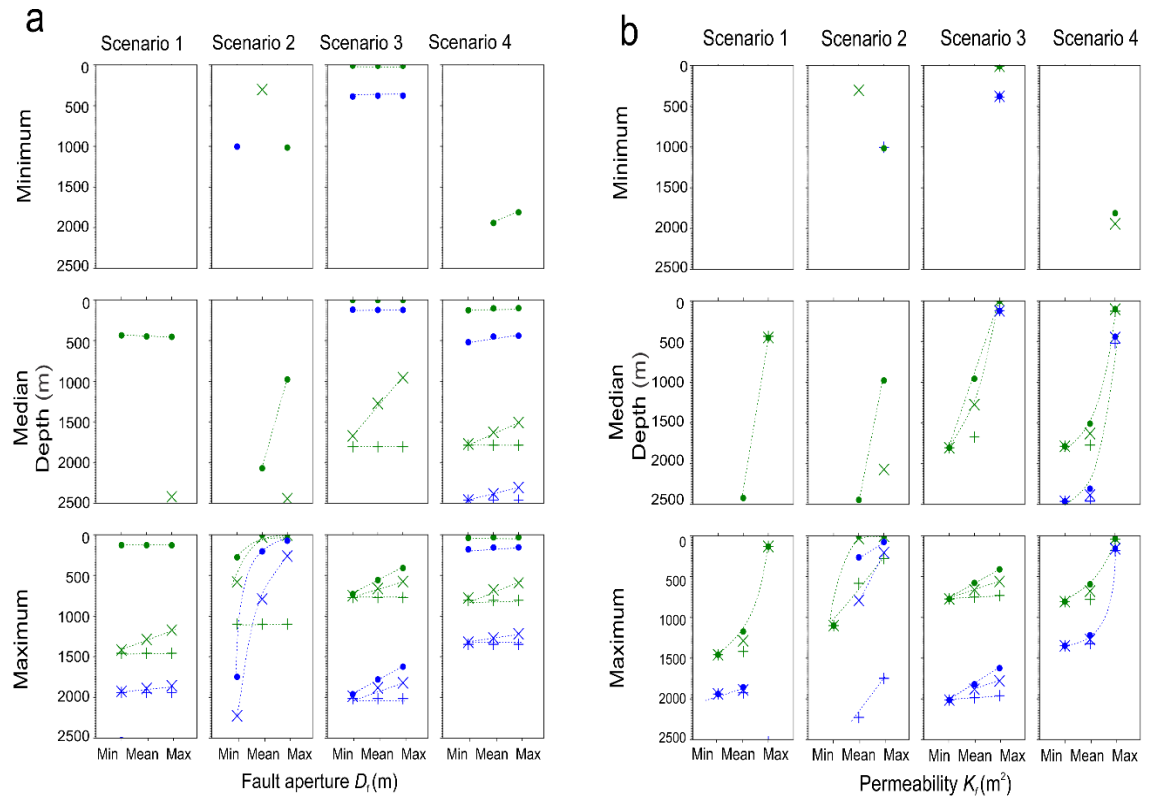


**Figure 4.10 Temperature profiles as a function of depth along the fault lines for the Ambanja 2D model.**  
The temperature profiles in scenario 0 are obtained from an average cutline drawn in the model without faults.

#### 4.8.2 Parameters sensitivity

For each scenario, the variation of depth at which the reservoir temperature can be reached when varying the fault aperture and permeability was investigated (Figures 4.11 and 4.12).



Temperature of reservoir along F1 : +  $K_f$ =Min;  $\times$ ,  $K_f$ =Mean;  $\bullet$ ,  $K_f$ =Max  
 Temperature of reservoir along F2 : +  $K_f$ =Min;  $\times$ ,  $K_f$ =Mean;  $\bullet$ ,  $K_f$ =Max

Temperature of reservoir along F1 : +  $D_f$ =Min;  $\times$ ,  $D_f$ =Mean;  $\bullet$ ,  $D_f$ =Max  
 Temperature of reservoir along F2 : +  $D_f$ =Min;  $\times$ ,  $D_f$ =Mean;  $\bullet$ ,  $D_f$ =Max

**Figure 4.11 Depth variation of reservoir temperature along the fault lines for the Ambilobe 2D model according to different scenarios of fault dips a) as a function of heat flow and fault aperture, and b) as a function of heat flow and fault permeability. The dotted line indicates the trend of depth variation.**

The results reveal that the depth of reservoir temperature decreases with increase of heat flow, fault aperture and fault permeability. For example, in scenario 1 (Figure 4.11a) with the minimum value of fault aperture ( $D_f$ ) and maximum value of fault permeability ( $K_f$ ), the depth of reservoir temperature decreases from >2500 to 200 m along fault F2 when the heat flow increases from the minimum to the maximum. For the same scenario 1, with the maximum value of heat flow and mean value of fault permeability, the depth of reservoir temperature decreases from 1400 to 1100 m along the fault F2 by increasing the value of fault aperture. In scenario 3 (Figure 4.11b), with the minimum fault permeability and maximum fault aperture, the depth of reservoir temperature decreases from >2500 to 750 m along fault F2 according to heat flow. For the same scenario 3, with the maximum value of heat flow and mean value of fault permeability, the depth at which the temperature of reservoir is reached, decreases from 800 to 400 m along the fault F2 by increasing the fault aperture. The pessimistic cases in the scenarios 1 and 2 are when there

is no point on the plots for the minimum heat flow because the reservoir temperature is always situated at depth >2500 m despite the increases of fault aperture and permeability.

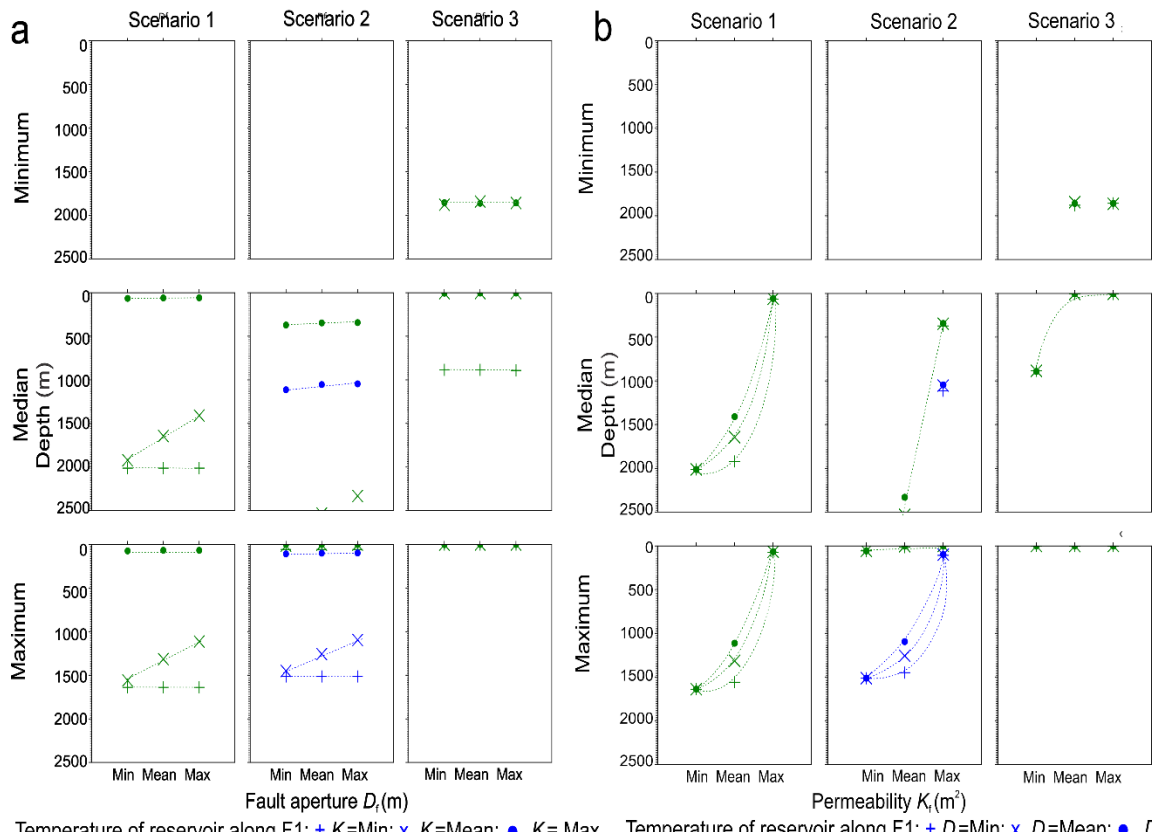


**Figure 4.12** Depth variation of reservoir temperature along the fault lines for the Ambanja 2D model according to different scenarios of fault dips a) as a function of heat flow and fault aperture, and b) as a function of heat flow and fault permeability. The dotted line indicates the trend of depth variation.

The parameter sensitivity trend described for Ambilobe, according to different fault dip scenarios, is the same for Ambanja model (Figure 4.12). The pessimistic cases correspond to the scenarios 1 and 2 with the minimum value of heat flow since the reservoir temperature is found at depth >2500 m despite the increases of fault aperture and permeability.

## 4.9 Discussion

### 4.9.1 Implications of groundwater flow boundary conditions

The hydraulic head applied to the lateral boundaries of the model allows to reproduce a topography-driven groundwater flow from NNE to SSE in Ambilobe and from NW to SE in Ambanja model. Surface recharge is neglected since the goal is to evaluate the impact of faults

intercepting the regional flow path. At the river segment, the flow vectors are directed toward the surface and the river constitutes a discharge zone (Figures 4.7 and 4.9). The magnitude of ascending flow vectors increases when faults intercept ascending flow vectors. The impact of regional flow path was previously highlighted by Taillefer et al., (2018), who suggested that topography (i.e., an elevated water table) is the key factor controlling fluid pathways and the hot spring distribution in the Têt hydrothermal system, Eastern Pyrénées, France. Similar conclusions can be made for Ambilobe and Ambanja where the topography-driven groundwater flow impacts forced convective heat transfer along the faults. The flow lines within the models show that the fluids originating from higher elevation reach an important depth where it can be heated and then directed toward the surface through permeable faults (Figures 4.7 and 4.9). This also confirms that hydraulic heads and hydrological budgets control the regional groundwater flow systems in an extensional domain geothermal play as mentioned by Moeck, (2014).

#### **4.9.2 Implications of faults on groundwater flow and heat transfer**

Faults play a fundamental role in the movement of fluids and distribution of pore pressure, and therefore exert considerable influence over the temperature distribution. This is well illustrated when comparing scenario 0 without faults to other scenarios with faults (Figures 4.7 and 4.9). The fault serves as a conduit for the upflow of fluids. Temperature along faults can be up to 150 °C higher than on both adjacent areas (Figure 4.7 and 4.9). Heat transfer becomes conductive in the surrounding host rock where bulk permeability is lower than the high-permeability zones because fluids are drained towards the fault where convection occurs. Faults create permeability heterogeneities in the crust, which are known to affect fluid flow and convective heat transfer and hence impacting hot spring location (Faulds et al., 2010; Faulds et al., 2015), especially at their intersections (Person et al., 2012; Belgrano et al., 2016). This is consistent with the numerical modeling of deep fluid flow associated to the crustal-scale normal faults in the South-central Canadian Cordillera (Ferguson et al., 2009), where the contrast permeability between the host rock and faults, acting as conduits for preferential fluid flow, have the greatest influence on the development of thermal systems. However, the presence of a fault does not necessarily imply hot springs unless the fault meets the favorable conditions which allow the fluids with the heat to ascend and reach the surface (e.g., López et al., 1995; Thiébaud, 2008).

Simulation scenario 3 made for Ambilobe 2D model clearly illustrates favorable conditions where the simulated surface temperature increases along both F1 and F2 faults (Figure 7; Table 1), when the fault dip is < 90° and facing fluid flow, in favor of fluid ascension. On the other hand, if

the dip of a fault is opposite to the fluid flow ( $> 90^\circ$  facing fluid flow), like fault F1 in scenario 1 and 3 for Ambanja graben (Figure 9; Table 1), the hydraulic gradient between both end of the fault is lower and the simulated temperature near the surface is less important. Similar results were found by Moreno et al., (2018) who simulated the impact of faults on fluid circulation from the basement underlying the Nevado del Ruiz volcanic complex in Colombia where hot springs manifestations are observed. However, the Ambilobe 2D model, in scenario 1 along F2 and scenario 2 along F1 showed that fluids can rise to surface even along a fault with a dip that is toward the fluid flow when it is close to a river acting as a discharge zone (Figure 4.7 and 4.8). It is the same case in scenario 4. This suggests that both the fault dip and its distance from a discharge zone where the hydraulic head can be low are important characteristics in favor of fluid ascension.

Additionally, convective heat transfer along faults implies dilution of ascending fluids mixing with groundwater of shallower origin. The half of the ascending fluids will come in the upper 75 % of the fault length (Ferguson et al., 2009). This can explain the significant mixing of geothermal fluids with shallower groundwater which is confirmed by the Giggenbah diagram in Figure 4.3 and the resulting cooling that occurred along the fault from the reservoir depth to the surface since boiling hot springs do not occur in the Ambilobe and Ambanja geothermal fields.

#### 4.9.3 Parameters sensitivity

The influence of the heat flow at the base of the model, fault aperture and fault permeability was evaluated because of uncertainty associated to those model inputs. Varying any of these parameters results in significant differences in the pressure, velocity, and temperature field enhancing fluid pathway along the fault.

The basal heat flow used in our models provides a first estimation of heat flow range for the geothermal region in North Madagascar, which is comparable to the known heat flow of the proposed analogue geothermal systems for Ambilobe and Ambanja (Rajaobelison et al., 2020). In zones of extension and continental rifts, regional heat flow estimates are significantly high, generally from 75 to 125  $\text{mW m}^{-2}$ , as mentioned by Jaupart et al. (2015). The range of heat flow for the Great Basin (USA) is from 50 to  $\sim 120 \text{ mW m}^{-2}$ , averaging roughly to  $90 \text{ mW m}^{-2}$  (Blackwell et al., 2004). In Western Turkey, particularly in the Gediz graben, the heat flow varies from  $\sim 50$  to  $140 \text{ mW m}^{-2}$ , with values exceeding  $\sim 100 \text{ mW m}^{-2}$  (Yilmazer et al., 2010). In the present study, the value of heat flow at the base impact the temperature distribution at depth and thus influence the geothermal gradient along permeable faults (Figure 4.8, 4.9 and 4.11, 4.12). Moreover a higher basal heat flow amplifies the convective regime when the fault permeability also increase

(López et al., 1995). In turn, the depth at which the reservoir temperature is reached decrease. However, the thermal spring distribution does not appear to be a function of heat flow. A high heat flow can be associated with higher temperature near fault surface but hot spring temperature can be found near fault surface in any of the favorable fault scenarios regardless of heat flow (Figures 4.2).

Fault aperture has an impact on the heat transfer along the fault, which is amplified for cases with a high fault permeability  $k_f > 10^{-14} \text{ m}^2$  allowing fluid ascension like shown in the scenarios 1 and 2 for Ambilobe 2D model of Figure 11a. Indeed, a small fault aperture  $D_f > 250 \mu\text{m}$  combined with a moderate to high fault permeability ( $10^{-10}-10^{-7} \text{ m}^2$ ) allows the hot fluid to be found at shallow depth,  $< 2 \text{ km}$  to the surface. Increasing fault permeability allows to transit from petrothermal to transitional systems and this parameter is therefore identified as a critical factor in numerical models. By varying the fault permeability in the model, the transmissivity to flow along faults becomes significant when fault permeability is higher than  $10^{-14} \text{ m}^2$ , attracting the hot upwelling fluids at depth (Figure 4.11b and 4.12b). There is also an optimum combination of country rock (host rock) and fault permeabilities needed, to obtain subsurface temperature distributions consistent with observed thermal springs (Forster et al., 1989). This means the permeability difference between the country rock and the fault allow to increase or decrease the spring temperature (Forster et al., 1989; López et al., 1995; Ferguson et al., 2009). In the present study, 4 to 7 orders of magnitude permeability difference between the country rock and the fault contributes to depress the thermal field. This decrease is due to downward flux of recharge water while high-temperature discharge associated with upward flow occurs along the fault plane. In fact, the pressure that forces the water to the surface is mainly supplied by the difference in elevation between the recharge and discharge areas.

However, it is well known that fractures and faults can seal and re-open with time, through multiple tectonic constraints (e.g., Ingebritsen et al., 2010). The current seismicity with a magnitude  $M_w > 5$  in the study areas (Bertil et al., 1998) suggest that faults may maintain an efficient permeability over the time.

#### 4.9.4 Model limitation

As a first step, a simplified model is necessary to understand the flow and heat transfer mechanisms influencing the temperature distribution in the geothermal system where crustal scale faults can control the fluid migration pathway. The fault permeability and the host rock are assumed constant with depth, although it can decrease with the increase of the confining pressure

(Rajaobelison et al., 2021). With this assumption, forced convection vs conduction is obviously favored. Indeed, permeability probably decreases with depth, in the basement because of contrasting mechanical properties of minerals contents of the rocks such as mica and feldspar and in the fault due to sealing by the mineral precipitation (Stober et al., 2015).

The structural information available in the study area is an important limitation to the models. The simplification of the flow model is a result of inherent uncertainties that can lead to inaccurate results. Therefore, more structural data including dip angle and fracture density measured during field investigations would help to better constrain the fault dip, aperture and permeability in the numerical model. Moreover, statistical features summarized from field data are needed for the stochastic processes in discrete fracture models (e.g., Ivanova et al., 2012). It is currently difficult to anticipate fracture behaviour at depth but geophysical surveys (e.g., gravity and magnetotelluric surveys) would further help image deep structures to build more accurate 2D models and even eventually develop 3D models around faults. However, the fluid flow and heat transfer models including discrete fractures presented in this study, consider the hypothesized fault geometry to analyze the physical processes along each fault, which is an advantages over other modeling approaches such as fracture continuum model.

Even though these aspects limited our modeling approach, the present modelling work successfully reproduces hot springs temperature observed at surface, with consistent reservoir temperatures at reasonable the depths.

#### **4.9.5 Geothermal exploration**

In this study, favorable fault characteristics triggering fluid ascension and beneficial to geothermal energy sources are identified and can be target to further geothermal exploration. Namely, the targets are normal faults with dip < 90° oriented toward the regional fluid flow path following the topography. The faults must have permeability higher than the host rock corresponding to the critical range of permeability for which forced convection occurs, combined to a minimum aperture of 250 µm.

The results of simulation additionally revealed that an average drilling depth of 1 to 2 km along favorable faults is estimated to reach the temperature interval 150–200 °C (Figures 4.8 and 4.10). This can have an impact on geothermal project cost since drilling cost increases nonlinearly with depth (e.g., Augustine et al., 2006 ).

## 4.10 Conclusions

This study reports unprecedented 2D numerical models simulating groundwater flow and heat transfer according to a realistic topography and fault hypothesis to better understand heat transfer mechanisms involved with the geothermal systems of the Ambilobe normal fault zone and Ambanja graben in northern Madagascar. Numerical simulation allows defining the large-scale temperature field in such extensional-type geothermal systems. Simulated temperature distribution appear to be characteristics of conductive heat transfer in low permeability rock matrix and forced convective heat transfer along faults facilitating fluid ascension under favorable conditions.

The present results supports previous interpretations of conceptual models in northern Madagascar, where conduction is the dominant heat transfer mechanism in low permeability rock matrix, except along faults that can experience a strong hydraulic gradient and provide a path for water to rise with forced convective heat transfer as the dominant mechanism (Rajaobelison et al., 2020, 2021).

Numerical models used in this study can be considered as a predictive tool to help define geothermal exploration strategies in such normal fault zone and graben geological contexts. Further hydrogeological assessment based on stable isotopes analyses on springs and groundwaters analysis can help to improve and support the simulated fluid circulation concept by defining infiltration altitude, and enabling the fluids origin to be determined. Deep borehole data such as temperature logs will also be required for the next step to realistically constrain the temperature prediction and advance geothermal exploration that appears favorable in North Madagascar.



## **5 DISCUSSION GÉNÉRALE ET CONCLUSIONS**

---

Compte tenu des travaux décrits dans cette thèse ayant mené au développement de connaissances, à la description et à la compréhension du contexte géologique de Madagascar, il apparaît que le pays dispose d'un potentiel en ressources géothermiques. Ces dernières sont réparties dans des zones particulières de son socle précambrien aussi bien volcanique que tectono-métamorphique et dans ses bassins sédimentaires. L'étape de développement de la phase initiale d'exploration qui contribue à la délimitation de la ressource géothermique s'inscrit ainsi dans la suite logique de l'évaluation du potentiel des socles précambriens fracturés d'où l'intérêt de ce projet doctoral qui a permis de caractériser et d'évaluer cette ressource dans la région Nord de Madagascar.

Moyennant des méthodes et techniques, à la fois fiables et novatrices, mais aussi abordables, ce projet a permis de qualifier ce potentiel en ressource géothermique afin d'envisager son exploitation future. Les outils méthodologiques utilisés ont apporté des solutions d'exploration pour caractériser et identifier des contextes géologiques structuraux ayant un potentiel géothermique similaire à celui de champs géothermique analogues. Toutefois, les techniques de mesure et d'évaluation utilisées dans ce projet et couramment utilisées pour la caractérisation des réservoirs sédimentaires ont dû être adaptées pour être appliquées dans un contexte de socle précambrien faillé, ce qui constitue une avancée scientifique face à l'exploration des ressources géothermiques profondes.

### **5.1 Les principaux résultats de la thèse et ses contributions**

La classification des sources d'énergie géothermique a récemment été améliorée pour inclure le concept de *geothermal play type* par analogie au thème pétrolier (Moeck, 2014). L'étude complétée pour l'île de Madagascar a considéré ces nouveaux concepts de classification des ressources pour améliorer la compréhension des facteurs contrôlant les sources d'énergie géothermique du pays. Présenté dans le chapitre 2, le résultat qui répond aux deux premiers sous-objectifs de cette thèse, est un premier catalogue des systèmes géothermiques de Madagascar. Les systèmes géothermiques de six zones potentielles ont été classifiés en trois catégories considérant les contextes géologique et tectonique combinés à la température du réservoir géothermique potentiel (Tableau 2.4). Les trois classes sont caractérisées par : 1- un contexte de grande faille bordière de graben dont la phase du fluide du réservoir est à dominance liquide avec une température modérée (zones d'Ambilobe et de Miandrivazo), 2- la présence

d'une chambre magmatique fossile dont la phase du fluide du réservoir est à dominance liquide avec une température modérée (zones d'Ambohibao, d'Itasy et d'Antsirabe), et 3- un contexte sédimentaire dont la phase du fluide du réservoir est à dominance liquide avec une basse température (bassin de Morondava). Les ressources géothermiques de Madagascar sont généralement associées à des domaines d'extension définis comme étant le principal *geothermal play type* ce qui caractérise et regroupe les systèmes géothermiques des six zones potentielles. Chaque modèle conceptuel du système géothermique développé pour chaque zone d'exploration est présenté par des coupes 2D interprétées sur lesquelles sont schématisées les caractéristiques physiques du système, y compris les structures géologiques, l'écoulement des fluides, les formations perméables et imperméables, et la source de chaleur (Figures 2.2 à 2.6). Ce catalogue a permis de comparer les systèmes géothermiques de Madagascar à d'autres systèmes géothermiques jugés analogues et ailleurs dans le monde pour lesquels les ressources géothermiques ont déjà été découvertes et/ou développées.

Bien que Madagascar soit à un stade moins avancé de l'exploration, les concepts sur l'exploration géothermique peuvent être améliorés en évaluant les propriétés pétrophysiques des roches échantillonnées sur des affleurements et utilisées comme analogues des formations géologiques profondes. L'analyse de ces propriétés apporte des informations qui contribuent à mieux évaluer la ressource géothermique et les stratégies d'exploration de la région. Dans le chapitre 3 qui répond au 3<sup>e</sup>, 4<sup>e</sup> et 5<sup>e</sup> sous-objectifs de la thèse, notre étude a fourni des connaissances fondamentales sur les propriétés thermohydrauliques des roches afin d'aider à identifier les mécanismes de transfert de chaleur associés aux ressources géothermiques dans les contextes tectoniques d'extension des régions d'Ambilobe et d'Ambohibao au nord de Madagascar. Les résultats montrent des valeurs de porosité faibles comprises entre 0.007 à 0.10 pour les formations sédimentaires et <0.001 à 0.11 pour celles du socle (Tableau 3.2). La perméabilité de la matrice des formations sédimentaires et du socle varie de moins de  $1.0 \times 10^{-19}$  à  $1.1 \times 10^{-14} \text{ m}^2$  (<0,001 à 11 mD), tandis que la conductivité thermique moyenne est de  $\sim 3.8 \text{ W m}^{-1} \text{ K}^{-1}$  et  $\sim 2.7 \text{ W m}^{-1} \text{ K}^{-1}$ , respectivement. La porosité et la perméabilité diminuent sous l'effet de la pression qui augmente en profondeur. Les valeurs de perméabilité inférées ne représentent que la limite inférieure de la plage de perméabilité possible. En effet, la perméabilité peut être plus élevée lorsque des fractures sont présentes, ce qui est difficile à considérer lors d'analyses effectuées avec des échantillons de petite taille en laboratoire. Les relations entre la porosité et la conductivité thermique évaluées en conditions sèches, révèlent que les grès à faible porosité ont la conductivité thermique la plus élevée. Selon l'orientation des mesures, les roches ne présentent qu'une faible anisotropie c'est-à-dire d'un ordre de grandeur ou moins dans la

perméabilité et la conductivité thermique (Tableau 3.2 et Figures 3.11). Les unités thermostratigraphiques définies selon le concept de thermofaciès (Figure 3.13) montrent que les systèmes géothermiques sont qualifiés de systèmes pétrothermaux à transitoires dans lesquels le transfert de chaleur par conduction domine pour les roches à faible perméabilité. Toutefois, les failles et les roches fracturées qui y sont associées pourraient former des conduits perméables qui favorisent la convection forcée entraînée par l'écoulement régional des eaux souterraines, ce qui est mis en évidence par les sources thermales inventoriées.

Sur la base des résultats de cette précédente analyse, le chapitre 4 traitant le 6<sup>e</sup> sous-objectif de la thèse, présente le rôle des failles dans le processus de transfert de chaleur par convection forcée donnant lieu à des sources chaudes. Plus spécifiquement, les simulations ont permis de déterminer quelles conditions de failles favorisent la remontée de fluides géothermiques dans la zone de failles normales d'Ambilobe et la structure de graben d'Ambaranja. Des modèles bidimensionnels d'écoulement de fluide couplé au transfert de chaleur ont été développés à partir des sections transversales orientées perpendiculairement aux failles et à la topographie régionale des deux zones. Les données structurales de surface ont permis de définir des scénarios de failles plausibles et de simuler l'ascension des fluides chauds en essayant de reproduire la température des sources thermales entre 50 à 70 °C (Figures 4.8 et 4.10). Les simulations numériques révèlent que les failles plongeant dans la direction opposée à l'écoulement des eaux souterraines induit par la topographie se sont avérées favorables pour reproduire la température des sources chaudes lorsque la perméabilité de la faille est  $>10^{-14} \text{ m}^2$ . Par ailleurs, les failles situées dans une zone de décharge hydraulique, soit près d'une rivière étaient les plus favorables à l'ascension des fluides, quel que soit leur pendage. Un flux thermique imposé à la base du modèle entre 90 et 148  $\text{mW m}^{-2}$  à 10 km a permis d'atteindre une température de réservoir de 150 à 200 °C à 2 km de profondeur ou moins, le long des failles favorables.

## **5.2 Implications pour l'exploration géothermique dans les zones géothermiques d'Ambilobe et d'Ambaranja**

### **5.2.1 Ambilobe**

Dans le secteur d'Ambilobe, les grès du Permien sont la formation la plus poreuse (0.10) et la plus perméable ( $1.0 \cdot 10^{-14} \text{ m}^2$ ) du secteur, bien que les micashistes aient parfois une porosité appréciable (0.11) et que l'orthogneiss puisse aussi être perméable, soit au plus  $1.0 \cdot 10^{-14} \text{ m}^2$  (Tableau 3.2). Le potentiel isolant du micaschiste et de l'amphibolite ainsi que des shales qui ont la meilleure capacité pour stocker de la chaleur ( $\sim 2.6 \text{ MJ m}^{-3} \text{ K}^{-1}$ ) pourrait affecter leur gradient

géothermique et donc leur ressource puisqu'un gradient plus élevé est anticipé dans des roches ayant une conductivité thermique relativement faible ( $< 2$  à  $2.5 \text{ W m}^{-1} \text{ K}^{-1}$ ). La production de chaleur interne la plus élevée se trouve le grès feldspathique du Trias, due à leurs concentrations élevées en thorium.

### 5.2.2 Ambanja

Pour Ambanja, les amphibolites sont à la fois les plus poreuses et les plus perméables 0.06 et  $8.9 \cdot 10^{-16} \text{ m}^2$  des formations analysées (Tableau 3.2). L'amphibolite est à la fois isolante  $\sim 2.5 \text{ W m}^{-1} \text{ K}^{-1}$  et possède le meilleur potentiel de stockage de chaleur en termes de capacité thermique volumétrique. La production de chaleur interne la plus élevée se trouve dans le basalte. Toutefois, les coulées de basalte se trouvant près de la surface ne sont pas assez épaisses pour être une source de chaleur significative. Les intrusions de syénite dans la zone d'Ambanja, si elles se trouvent en profondeur avec une composition chimique similaire que celle des basaltes, pourraient être une source de chaleur et contribuer à l'augmentation du gradient géothermique.

La perméabilité et la porosité de la matrice mesurées pour tous les types de roches échantillonnées dans les zones d'Ambilobe et d'Ambanja sont relativement faibles par rapport à celles requises pour un réservoir géothermique conventionnel. Par contre la présence de structures géologiques, telles que des failles et des fractures, diaclases, filons ou contacts sédimentaires, pourraient augmenter de façon significative la perméabilité. Sur le terrain, des fractures, des joints et des veines ont été fréquemment observés, en particulier dans les grès du Trias et du Permien à Ambilobe et dans les paragneiss à Ambanja. Étant donné que la plage de température des réservoirs d'Ambilobe et d'Ambanja est comprise entre 140 et 200 °C, on s'attend à ce qu'une altération hydrothermale, telle que l'argile, se produise lorsque la profondeur et la température augmentent. Les roches telles que l'amphibolite et le micaschiste, les lithologies dominantes dans la région d'Ambilobe, contiennent des minéraux tels que le pyroxène, l'amphibole et la biotite (Figures 3.7b à 3.7e). Elles sont donc plus sensibles à l'altération argileuse que les gneiss quartzofeldspathiques et granodioritiques à granitiques, la lithologie dominante dans la région d'Ambanja. Par conséquent, les roches du socle fracturé d'Ambilobe pourraient avoir une perméabilité plus élevée que celles d'Ambanja.

Dans les deux zones étudiées, les failles crustales qui sont responsables de la remontée des fluides et des sources chaudes par convection forcée devraient donc être ciblées pour une exploration géothermique plus poussée. Il s'agit de failles normales caractérisées par un pendage entre 60 et 85°, idéalement orientées dans la direction opposée de l'écoulement des fluides

régionaux qui suivent la topographie. Les modèles développés démontrent que les failles doivent avoir une perméabilité supérieure à celle de la roche hôte correspondant à la gamme critique de perméabilité pour laquelle la convection forcée se produit, combinée à une ouverture minimale de 250 µm.

### **5.3 Étapes futures pour un développement géothermique de la région du Nord de Madagascar**

L'établissement d'un catalogue des ressources géothermiques des régions d'intérêt de Madagascar peut servir de guide pour anticiper les stratégies et méthodes d'exploration les plus appropriées en fonction du contexte géologique et en se basant sur les expériences des régions présentant un contexte géologique similaire et des systèmes géothermiques déjà développés.

Dépendamment du stade de développement de l'activité géothermique, le manque de données disponibles, mais aussi leur qualité implique des incertitudes sur la conception des systèmes géothermiques. Dans un programme d'exploration géothermique typique, chaque étape de l'exploration correspond à des activités de terrain impliquant le développement de modèles conceptuels représentant la meilleure compréhension actuelle du système géothermique (Sertac et al., 2015). À la fin de chaque phase, une décision est alors prise pour mener des activités d'exploration supplémentaires, de forer le premier puits d'exploration ou de quitter le champ.

Pour Ambilobe et Ambanja, les phases ultérieures de l'exploration doivent se poursuivre pour affiner et vérifier les éléments d'hypothèses des modèles conceptuels qui sont : l'épaisseur, la distribution ainsi que les structures en profondeur des formations géologiques ; les caractéristiques des failles en profondeur, la présence d'aquifère et les modèles de mélange dans la circulation des fluides par l'analyse des données géochimiques d'eau souterraine, et les modèles d'isothermes.

Ainsi, les stratégies et méthodes proposées pour les travaux d'exploration futurs pour les zones d'intérêt, Ambilobe et Ambanja, sont les suivants (Figure 5.1):

- Sondages géophysiques pour imager les structures profondes ;
- Forage d'exploration carotté pour interceper les failles profondes ;
- Mesure de température dans les forages, réalisation de diagrphies pour inférer la conductivité thermique, la porosité et le calcul du flux de chaleur terrestre ;
- Amélioration des modèles numériques basés sur les données géophysiques et de forages et définition de cibles pour les forages de production ;

- Forage de production d'un plus gros diamètre et essais Lugeon pour évaluer la perméabilité de façon in situ dans les zones de failles.

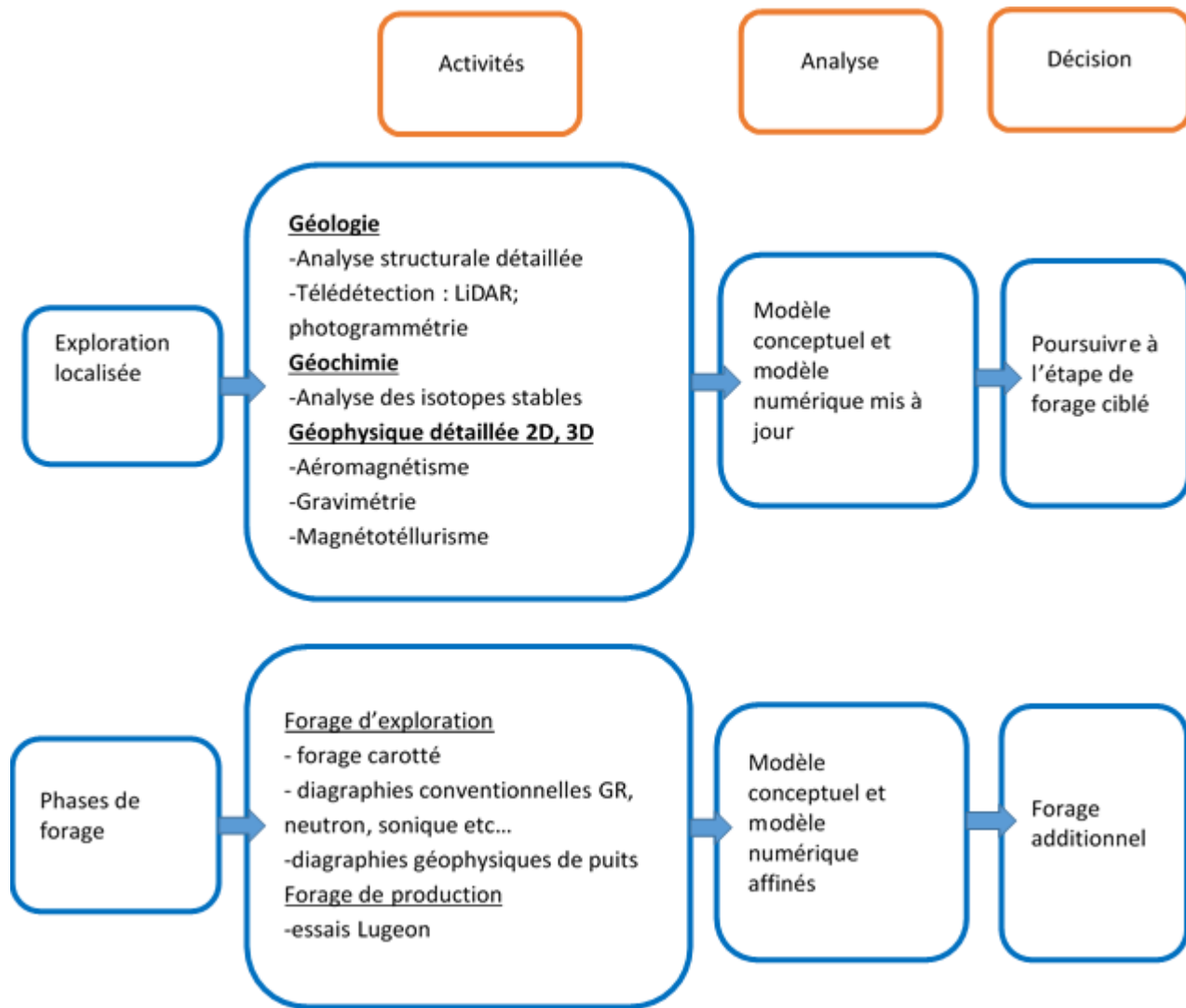


Figure 5.1 Programme d'exploration géothermique pour les zones d'intérêt : Ambilobe et Ambanja. Les différentes phases comportent les activités à poursuivre, les analyses et les options de décision qui sont basées sur les stratégies pour l'exploration dans les régions à contexte extensif proposées par Hervey et al., (2014); Sertac et al., (2015).

### 5.3.1 Sondages géophysiques pour imager les structures profondes

L'analyse d'images LiDAR et aéromagnétiques ainsi que des sondages magnétotelluriques permettraient de mieux délimiter la distribution des formations géologiques et de leur structures en profondeur ou de détecter des formations intrusives génératrices de chaleur (Grebbey et al., 2011 ; Carrea et al., 2016), mais également de caractériser la structure des failles en profondeur.

Les cartes gravimétriques de Bouguer peuvent améliorer l'interprétation en profondeur des failles majeures en contrignant leur géométrie (Cashman et al., 2009; Represas et al., 2013). Cependant aucune technique d'exploration ne fournit à elle seule la clé d'un modèle conceptuel réussi et affiné et aucun modèle conceptuel ne peut être confirmé si ce n'est que par des données de forages et des essais en puits.

### **5.3.2 Forage d'exploration carotté pour intercepter les failles profondes**

Le forage constitue un échantillonnage continu et inaltéré à travers les failles. Il va permettre de délimiter les variations à l'échelle du micromètre au décimètre de la lithologie et de la structure des roches de faille en identifiant les principales gouges, les zones bréchiques et mylonitiques ainsi que la série des cataclasites. La caractérisation des structures internes des principales failles et zones de faille est une étape importante pour comprendre les attributs physiques bruts des failles géologiques, notamment leurs propriétés mécaniques, sismiques et hydrauliques. De nombreuses études ont abordé ce sujet, et la vision de la structure des zones de faille associées aux principales failles à l'échelle de la croûte terrestre s'est considérablement développée ces dernières années (par ex: Wibberley et al., 2003 ; Boullier, 2011; Holdsworth et al., 2011; Toy et al., 2015).

Une des principales questions géologiques abordées par les projets de forage des zones de faille utile pour les projets d'exploration géothermique est la suivante : Quelles sont les propriétés physiques (vélocités sismiques, résistivité électrique, densité, porosité, perméabilité) des matériaux des zones de faille par rapport aux roches hôtes, et comment varient-elles dans le temps et l'espace ?

### **5.3.3 Mesure de température dans les forages, réalisation de diagraphies et évaluation de la distribution spatiale des propriétés hydrauliques**

L'estimation du gradient géothermique moyen et du flux de chaleur moyen pour la région du Nord de Madagascar à partir de l'estimation de la profondeur du point de Curie considéré dans cette thèse doit être vérifiée et évalué au niveau des zones d'intérêt, soit Ambilobe et Ambanja, par des mesures de températures dans les forages ou à l'aide des données corrigées sur la température du fond de forage (par ex: Deming et al., 1988; Majorowicz et al., 2020) pour inférer la conductivité thermique, la porosité et calculer le flux de chaleur terrestre.

Bien que les méthodes de laboratoire fournissent un ordre de grandeur pour la porosité et la perméabilité ainsi qu'une évaluation fiable de la conductivité thermique, des méthodes ont été

développées pour évaluer ces propriétés *in situ* en considérant les effets de la profondeur, des fractures et des hétérogénéités associés. Des diagraphies conventionnelles telles que les rayons gamma, neutrons et sonique permettront d'évaluer indirectement la porosité totale et secondaire des formations (Harvey et al., 2005; Zhou et al., 2018). Il s'agit notamment de quantifier la porosité de fissures dans les roches et l'impact prépondérant des fractures sur la perméabilité des roches qui n'ont pas été quantifiés dans cette étude.

Tandis que, les diagraphies géophysiques de puits sont une autre méthodologie couramment utilisée pour inférer la conductivité thermique qui tient compte des conditions *in situ* sur des roches non seulement sèches mais saturées (par ex: Hartmann et al., 2005; Fuchs et al., 2013; Nasr et al., 2018), et évaluer la concentration de radioéléments (par ex: Caldwell et al., 1963; Hertzog et al., 1979).

La distribution de la porosité, de la perméabilité et de la température doit être évaluée. La cartographie géostatistique des propriétés à l'échelle des zones d'intérêt, pourra ensuite être réalisée avec des données d'analyse de carottes à grande échelle (c'est-à-dire à l'échelle du puits) à l'aide de l'algorithme de krigage ordinaire, en utilisant l'extension "Geostatistical Analyst" du logiciel ArcGIS® 9.3 (par ex: Weides et al., 2013).

#### **5.3.4 Amélioration des modèles numériques basés sur les données géophysiques et de forages et définition de cibles pour les forages de production**

La simulation bidimensionnelle d'écoulement de fluide couplé au transfert de chaleur s'est basée sur la coupe géologique simplifiée ainsi que sur les données des propriétés thermohydrauliques mesurées en laboratoire. L'incertitude sur les données de pendage des failles et leur extension en profondeur doit être réduite. Les données de forage et de puits d'exploration des campagnes géophysiques seront nécessaires pour obtenir un modèle géologique de sous-surface plus représentatif (par ex: Akar et al., 2011). Une approche de modélisation en 3D serait l'objectif ultime pour progresser vers la définition de modèles de réservoir. La modélisation en 3D permet d'interpoler la géométrie des structures géologiques et constitue un moyen efficace de comprendre ses caractéristiques. Notamment sur les valeurs et le sens du pendage des failles, leur densité et celles des fractures qui demandent des données structurales supplémentaires mesurées sur le terrain. Les futurs travaux de terrain plus détaillés tels que les levés des indicateurs cinématiques, couplés à des méthodes photogrammétries (par ex: Lianheng et al., 2020) et de télédétection pourront être envisagés. Cela contribuera à mieux contraindre l'inclinaison des failles dans les modèles numériques ainsi que, de leur ouverture.

### **5.3.5 Forage de production d'un plus gros diamètre et essais packer pour évaluer la perméabilité de façon in situ dans les zones de failles**

Une fois que les failles et les zones de faille auront été ciblées, des forages de production d'un plus gros diamètre (~12 cm) pourront être réalisés. Étant données la faible perméabilité des formations et l'absence de données sur les propriétés hydrauliques des failles ainsi que leur variation en profondeur, des essais Lugeon sont à effectuer pour inférer de façon in situ la perméabilité hydraulique des zones de failles (Almen et al., 1986; Jacky, 1998; Mejías et al., 2009 ; Beauheim et al., 2014;). Ces auteurs décrivent les essais hydrauliques dans les sédiments de faible perméabilité utilisant la méthode essais Lugeon aussi bien que dans les roches cristallines ou des formations à faible et moyenne perméabilité, en considérant les effets des fractures et des hétérogénéités associés. Ces tests hydrauliques sont réalisés entre deux obturateurs afin d'obtenir un ordre de grandeur de la perméabilité du milieu (par ex: Almen et al., 1986; Stephen Hickman et al., 1998; Luthi, 2005; Stober et al., 2015).

## **5.4 Évaluation préliminaire économique**

Si la consommation annuelle en électricité à Madagascar demeure stable dans les 10 prochaines années, soit celle estimée en 2016 de 1.6 milliard de kWh (The World Factbook, 2021), elle serait largement couverte par une production d'énergie géothermique comparable à celle de la Turquie. En effet, le potentiel technique total de production d'électricité géothermique de la Turquie pour des systèmes hydrothermaux peut être estimé à 4500 MW (36 milliards de kWh/an), produits avec des puits d'une profondeur allant jusqu'à 3 km avec un tarif de subventionnement de 10.5 USD/kWh et une garantie d'achat de 10 ans (Mertoglu et al., 2019 ; Wietze et al., 2021).

Avec cette même capacité de production, on peut envisager pour Madagascar également une réduction de l'énergie de la biomasse. La consommation annuelle en bois s'élevait, en 2015, à plus de 12.3 millions de tonnes soit près de 30 millions de kWh (Ministère de l'énergie et des hydrocarbures, 2015).

L'une des méthodes couramment utilisées pour évaluer la rentabilité économique d'une centrale géothermique est le *Levelized Cost of Energy* (LCOE), signifiant « coût actualisé de l'énergie ». Le LCOE définit le coût unitaire de l'énergie sur l'ensemble du cycle du projet, nécessaire pour récupérer l'investissement en capital. Il inclut les coûts de maintenance et d'exploitation de la centrale électrique pendant sa durée de vie (NEA/IEA, 2020). Les principaux facteurs de l'analyse du LCOE sont les suivants (NEA/IEA, 2020): 1- le coût d'investissement, 2- le taux moyen de production d'électricité, 3- la durée de vie, 4- le taux d'actualisation, et 5- la disponibilité de

l'installation. Le coût d'investissement de la centrale géothermique est le principal facteur qui affecte sa viabilité économique. En terme de LCOE, la technologie de production d'énergie géothermique est compétitive par rapport aux autres technologies de production d'énergie renouvelable car en Afrique, le LCOE estimé en 2016 pour la biomasse est de 0.19 USD/kWh et varie entre 0.05-0.015 USD/kWh pour le combustible fossile contre 0.15 USD/kWh pour la géothermie. Le LCOE de la technologie géothermique en Amérique du Sud soit (<0.05 USD/kWh) est inférieur à celui de toutes les autres énergies renouvelables (IRENA, 2017; Soltani et al., 2021). Considérant ce coût, l'énergie géothermique a une période d'amortissement de 6 ans ce qui est plus long que pour l'éolien, le photovoltaïque, l'hydroélectricité (grande) et le charbon (Valgardur, 2002 ; Soltani et al., 2021).

## **5.5 Évaluation de l'empreinte carbone pour l'application de l'énergie géothermique comparée à celle de la biomasse**

Les facteurs d'émission de gaz à effet de serre GES associés aux sources d'énergie conventionnelles et renouvelables peuvent être exprimés en émissions équivalentes de CO<sub>2</sub>.soit en grammes d'équivalent carbone par kWh. Sur la base de son cycle de vie, l'énergie géothermique pour la production d'électricité émet en moyenne 38 grammes d'équivalent CO<sub>2</sub> par kWh d'électricité produite contre 230 grammes pour la biomasse ce qui la place au 6e rang parmi tous les types de combustibles (IPCC, 2014). Avec l'énergie géothermique, le taux de réductions des émissions de carbone à Madagascar sera conséquent comparé au taux de CO<sub>2</sub> émis par la biomasse et par le combustible fossile.

L'association de l'énergie géothermique avec d'autre source d'énergie forment des centrales géothermiques hybrides. L'hybridation est également un moyen de réduire les émissions atmosphériques et l'utilisation des sols. Elle permet aussi de réduire les coûts d'exploitation et d'investissement nécessaires et, par conséquent, de raccourcir la période d'amortissement des installations ainsi que la gestion opérationnelle des charges de pointe (Alaica et al., 2017; Soltani et al., 2021). Dans la littérature, l'énergie géothermique est le plus souvent combinée à l'énergie solaire, pour générer de l'énergie supplémentaire ou pour réduire l'énergie consommée à l'exemple de la centrale hybride de Stillwater du Névada aux USA (par ex : DiMarzio et al., 2015) ou encore dans le sud-ouest de la Turquie (Bonyadi et al., 2018). La combinaison de sources géothermiques exploitée en parallèle avec l'énergie solaire peut réduire l'émission de GES par exemple en Australie. Et qu'en considérant uniquement les sources géothermiques, le LCOE a été calculé à 225 USD/MWh, mais il a été abaissé à 165 USD/MWh avec un coût de l'électricité réduit de 20 % (Zhou et al., 2013). La mise en œuvre des systèmes EGS-biomasse aux USA

réduit les émissions de CO<sub>2</sub> de 13 à 15 % (Lukawski, et al., 2013). Les centrales géothermiques hybrides pourraient aussi être bénéfiques pour Madagascar dans sa transition énergétique.



## 6 BIBLIOGRAPHIE

---

- Alaica A, & Dworkin, SB (2017). Characterizing the effect of an off-peak ground pre-cool control strategy on hybrid ground source heat pump systems. *Energy Build* 137: 46-59.
- Akar S, Atalay O, Kuyumcu ÖÇ, Solaroglu UZ, Çolpan B & Arzuman S (2011) 3D Subsurface Modeling of Gümüşköy Geothermal Area, Aydın, Turkey. *Geothermal Resources Council Transactions* 35:669-676.
- Al-Jabri RA, Al-Maamari RS & Wilson OB (2015) Klinkenberg-corrected gas permeability correlation for Shuaiba carbonate formation. *Journal of Petroleum Science and Engineering* 131:172-176.
- Albert K, Schulze M, Franz C, Koenigsdorff R & Zosseder K (2017) Thermal conductivity estimation model considering the effect of water saturation explaining the heterogeneity of rock thermal conductivity. *Geothermics* 66:1-12.
- Almen, Andersson, Carlsson, Hansson & Larsson (1986) *Hydraulic testing in crystalline rock. A comparative study of single-hole test methods*. Technical Report Uppsala, Sweden, 183 p.
- American Petroleum Institute (1998) *Recommended practices for core analysis in Recommended Practice 40* (API Publishing Services Washington), p 236.
- Andreoli MA, Hart RJ, Ashwal LD & Coetzee H (2006) Correlations between U, Th content and metamorphic grade in the western Namaqualand Belt, South Africa, with implications for radioactive heating of the crust. *Journal of Petrology* 47(6):1095-1118.
- Andriampenomanana F, Nyblade AA, Wysession ME, Durrheim RJ, Tilmann F, Julià J, Pratt MJ, Rambolamanana G, Aleqabi G & Shore PJ (2017) The structure of the crust and uppermost mantle beneath Madagascar. *Geophysical Journal International* 210 (3):1525-1544.
- Andrianaivo L (2011) Caractéristiques générales des systèmes et des régions géothermiques de Madagascar. *Madamines* 2:11-21.
- Andrianaivo L & Ramasiarinoro V (2010a) Structural Model of the Itasy Geothermal Prospect in Central Madagascar: Preliminary Review. World Geothermal Congress (Bali, 25-29 April), p 9.
- Andrianaivo L & Ramasiarinoro VJ (2010b) Relation between Regional Lineament Systems and Geological Structures: Implications for Understanding Structural Controls of Geothermal System in the Volcanic Area of Itasy, Central Madagascar. World Geothermal Congress (Bali, 25-29 April), p 9.
- Armistead SE, Collins AS, Merdith AS, Payne JL, Cox GM, Foden JD, Razakamanana T & De Waele B (2019) Evolving Marginal Terranes During Neoproterozoic Supercontinent Reorganization: Constraints From the Bemarivo Domain in Northern Madagascar. *Tectonics* 38(6):2019-2035.
- Armstead HC, H. (1973) *Geothermal energy: review of research and development*. UNESCO, Paris. 186 p.
- Arthaud F, Grillot J-C & Raunet M (1990) La tectonique cassante à Madagascar: son incidence sur la géomorphologie et sur les écoulements. *Canadian Journal of Earth Sciences* 27(10):1394-1407.

- Augustine C, Tester JW, Anderson B, Petty S & Livesay B (2006 ) A comparison of geothermal with oil and gas well drilling costs. 31st Workshop on Geothermal Reservoir Engineering. (Stanford University, 30 February), p 15.
- Axelsson G (2013) Conceptual models of geothermal systems–introduction. Short Course V on Conceptual Modelling of Geothermal Systems in El Salvador. (Santa Tecla, February 24 - March 2), p 12.
- Axelsson G (2008) Production capacity of geothermal systems. Workshop for Decision Makers on the Direct Heating Use of Geothermal Resources in Asia. (Tianjin, 11-18 May), p 14.
- Bakhsh KJ, Nakagawa M, Arshad M & Dunnington L (2016) Modeling thermal breakthrough in sedimentary geothermal system, using COMSOL multiphysics. 41st Workshop on Geothermal Reservoir Engineering, Stanford, California. (Stanford University, 22-24 February), p 12.
- Bär K, Reinsch T & Bott J (2020) The PetroPhysical Property Database (P3) – a global compilation of lab-measured rock properties. *Earth System Science Data* 12(4):2485-2515.
- Bardintzeff JM, Liegeois JP, Bonin B, Bellon H & Rasamimanana G (2010) Madagascar volcanic provinces linked to the Gondwana break-up: Geochemical and isotopic evidences for contrasting mantle sources. *Gondwana Research* 18(2-3):295-314.
- Beatty CV (2010) *Characterization of small scale heterogeneity for prediction of acid fracture performance*. Maître ès sciences (M.Sc.) (Texas A & M University, College Station, Texas). 90 p.
- Beauheim RL, Roberts RM & Avis JD (2014) Hydraulic testing of low-permeability Silurian and Ordovician strata, Michigan Basin, southwestern Ontario. *Journal of Hydrology* 509:163-178.
- Belgrano TM, Herwegh M & Berger A (2016) Inherited structural controls on fault geometry, architecture and hydrothermal activity: an example from Grimsel Pass, Switzerland. *Swiss Journal of Geosciences* 109(3):345-364.
- Bense VF, Person MA, Chaudhary K, You Y, Cremer N & Simon S (2008) Thermal anomalies indicate preferential flow along faults in unconsolidated sedimentary aquifers. *Geophysical Research Letters* 35(24).
- Bertil D & Regnoult MJ (1998) Seismotectonics of Madagascar. *Tectonophysics* 294(1):57-74.
- Besairie H (1959) *Contribution à l'étude des sources minérales et des eaux souterraines de Madagascar*. Travaux du Bureau Géologique 92, Service Géologique Antananarivo.
- Besairie H (1952) Les formations du Karoo à Madagascar. *Symposium sur les séries de Gondwana*, Teichert C (Ed.) International Geological Congress, Algiers. p 181-186.
- Besairie H (1946) *La géologie de Madagascar en 1946*. Annales géologiques du service des mines 12, Sgf, Paris 15e, 32 p.
- Bisdom K, Bertotti G & Nick HM (2016) The impact of in-situ stress and outcrop-based fracture geometry on hydraulic aperture and upscaled permeability in fractured reservoirs. *Tectonophysics* 690:63.
- Björbsson G & Bodvarsson G (1990) A survey of geothermal reservoir properties. *Geothermics* 19(1):17-27.
- Blackwell DD & Richards M (2004) The 2004 geothermal map of North America explanation of resources and applications. *Geothermal Resources Council Transactions* 28:317-320.

- Bonyadi N, Johnson E, & Baker D, (2018). Technoeconomic and exergy analysis of a solar geothermal hybrid electric power plant using a novel combined cycle. *Energy Convers Management* 156: 542-554.
- Boullier A-M (2011) Fault-zone geology: lessons from drilling through the Nojima and Chelungpu faults. Geological Society, London, *Special Publications* 359(1):17-37.
- Buchwaldt, R. (2006). *The geology of the neoproterozoic and cenozoic rocks of north Madagascar*. PhD thesis, University of Washington, USA, p.357.
- Caldwell RL, Baldwin WF, Bargainer JD, Berry JE, Salaita GN & Sloan RW (1963) Gamma-ray spectroscopy in well logging. *Geophysics* 28(4):617-632.
- Campbell SA, Lenhardt N, Dippenaar MA & Götz AE (2016a) Geothermal energy from the Main Karoo Basin (South Africa): an outcrop analogue study of Permian sandstone reservoir formations. *Energy Procedia* 97:186-193.
- Campbell SA, Mielke P & Götz AE (2016b) Geothermal energy from the Main Karoo Basin? New insights from borehole KWV-1 (Eastern Cape, South Africa). *Geothermal Energy* 4(1):9.
- Cao Q, Shan Y, Feng B, Zhang E, Lu H & Yang Y (2018) Application examples and effects of RS-230 spectrometer in uranium exploration. *Wutan Huatan Jisuan Jishu* 40:118-125.
- Carrea D, Abellan A, Humair F, Matasci B, Derron M-H & Jaboyedoff M (2016) Correction of terrestrial LiDAR intensity channel using Oren–Nayar reflectance model: An application to lithological differentiation. *ISPRS Journal of Photogrammetry and Remote Sensing* 113:17-29.
- Cashman PH, Trexler JH, Muntean TW, Faulds JE, Louie JN, Oppliger GL, Oldow J & Cashman P (2009) Neogene tectonic evolution of the Sierra Nevada–Basin and Range transition zone at the latitude of Carson City, Nevada. Late Cenozoic Structure and Evolution of the Great Basin–Sierra Nevada Transition: *Geological Society of America Special Paper* 447:171-188.
- Chagnon-Lessard N, Mathieu-Potvin F & Gosselin L (2020) Optimal design of geothermal power plants: A comparison of single-pressure and dual-pressure organic Rankine cycles. *Geothermics* 86:101787.
- Cherubini Y, Cacace M, Blöcher G & Scheck-Wenderoth M (2013) Impact of single inclined faults on the fluid flow and heat transport: results from 3-D finite element simulations. *Environmental Earth Sciences* 70(8):3603-3618.
- Chorowicz J, Bardintzeff JM, Rasamimanana G, Chotin P, Thouin C & Rudant JP (1997) An approach using SAR ERS images to relate extension fractures to volcanic vents: examples from Iceland and Madagascar. *Tectonophysics* 271(3):263-283.
- Chorowicz J (1990) Dynamics of the different basin-types in the East African rift. *Journal of African Earth Sciences (and the Middle East)* 10(1):271-282.
- Chovelon P (1984) *Géothermie haute enthalpie. Ressources et intervenants par pays*. Rapport du Bureau de recherches géologiques et minières B.R.G.M. 84SGN 178 SPG, Paris 1-123 p.
- Clauser C & Huenges E (1995) Thermal conductivity of rocks and minerals. *Rock Physics and Phase Relations*, Ahrens TJ (Ed.) AGU Reference Shelf 3. p 105-126.
- Coffin MF & D. RP (1988) Evolution of the Conjugate East African-Madagascan Margins and The Western Somali Basin. *Geological Society of America Special papers* 226:78.

- Collins AS (2006) Madagascar and the amalgamation of Central Gondwana. *Gondwana Research* 9(1):3-16.
- Coolbaugh MF, Arehart GB, Faulds JE & Garside LJ (2005) Geothermal systems in the Great Basin, western United States: Modern analogues to the roles of magmatism, structure, and regional tectonics in the formation of gold deposits. *Geological Society of Nevada Symposium 2005: Window to the World*, Rhoden HN, Steininger RC & Vikre PG (Eds.) Geological Society of Nevada, Reno. p 1063–1081.
- Corbel S, Schilling O, Horowitz FG, Reid LB, Sheldon HA, Timms NE & Wilkes P (2012) Identification and Geothermal Influence of Faults in the Perth Metropolitan Area, Australia. 37th Workshop on Geothermal Reservoir Engineering. (Stanford University, 30 January–1 February), p 8.
- Core Lab Instruments (2016) *PPP-250 Portable probe permeameter operations manual*. Tulsa, United States), p 6.
- Coretest Systems Inc. (2017) *AP-608 Automated Permeameter-Porosimeter operator's manual*. Morgan Hill, United States), p 7-4.
- Cucciniello C, Melluso L, Anton P, Jourdan F, Morra V, Roberto & Grifa C (2017) From olivine nephelinite, basanite and basalt to peralkaline trachyphonolite and comendite in the Ankaratra volcanic complex, Madagascar: 40Ar/39Ar ages, phase compositions and bulk-rock geochemical and isotopic evolution. *Lithos* 274-275:363-382.
- Cucciniello C, Tucker R, Jourdan F, Melluso L & Morra V (2016) The age and petrogenesis of alkaline magmatism in the Ampasindava Peninsula and Nosy Be archipelago, northern Madagascar. *Mineralogy and Petrology* 110(2-3):309-331.
- De Waele B, Thomas RJ, Macey PH, Horstwood MSA, Tucker RD, Pitfield PEJ, Schofield DI, Goodenough km, Bauer W, Key RM, Potter CJ, Armstrong RA, Miller JA, Randriamananjara T, Ralison V, Rafahatelo JM, Rabarimanana M & Bejoma M (2011) Provenance and tectonic significance of the Palaeoproterozoic metasedimentary successions of central and northern Madagascar. *Precambrian Research* 189(1):18-42.
- De Wit MJ (2003) Madagascar: heads it's a continent, tails it's an island. *Annual Review of Earth and Planetary Sciences* 31(1):213-248.
- Debon F & Le Fort P (1988) A cationic classification of common plutonic rocks and their magmatic associations : principles, method, applications. *Bulletin de Minéralogie* 111:493-510.
- Delph JR & Porter RC (2014) Crustal structure beneath southern Africa: insight into how tectonic events affect the Mohorovičić discontinuity. *Geophysical Journal International* 200(1):254-264.
- Deming D (1994) Estimation of the thermal conductivity anisotropy of rock with application to the determination of terrestrial heat flow. *Journal of Geophysical Research: Solid Earth* 99(B11):22087-22091.
- Deming D & Chapman DS (1988) Heat Flow in the Utah-Wyoming Thrust Belt From Analysis of Bottom-Hole Temperature Data Measured in Oil and Gas Wells. *Journal of Geophysical Research: Solid Earth* 93(B11):13657-13672.
- Dhansay T, Musekiwa C, Ntholi T, Chevallier L, Cole D & de Wit MJ (2017) South Africa's geothermal energy hotspots inferred from subsurface temperature and geology. *South African Journal of Science* 113:1-7.

- Dickson MH & Fanelli M (2003) *Geothermal Energy: Utilization and Technology*. UNESCO, New York. 205 p.
- DiMarzio G, Angelini L, Price W, Chin C, & Harris S, (2015) The Stillwater Triple Hybrid Power Plant: Integrating Geothermal, Solar Photovoltaic and Solar Thermal Power Generation. In World Geothermal Congress. (Melbourne, 19-25 April), p 5
- Döse M, Silfwerbrand J, Jelinek C & Trägardh J (2014) Evaluation of the I-index by use of portable hand-held spectrometer and laboratory methods in a rock assessment of Swedish concrete by use of different crushed aggregates. *Mineralproduksjon* 5:A35-A52.
- Du Toit SR & Kidston AG (1997) *The hydrocarbon potential of the East Africa continental margin*. Alconsult International, Canadian International Development Agency, Calgary. 132 p.
- Eppelbaum L, Kutasov i & Pilchin A (2014) *Index Eppelbaum et al Applied Geothermics*. Springer Heidelberg New York Dordrecht London. 757 p.
- Erdlac RJ, Jr. (2011) A Geologic Systems-Based Classification For Geothermal Energy. AAPG/SPE/SEG Hedberg Conference. (Napa, 14-18 March), p 4.
- Erdlac RJ, Jr., Gross P & McDonald E (2008) A Proposed New Geothermal Power Classification System. *Geothermal Resources Council Transactions* 32:379-384.
- Estrade G (2014) *Le complexe cénozoïque alcalin d'Ambohimirahavavy à Madagascar: origine, évolution et minéralisations en métaux rares*. Philosophiae Doctor (Ph.D.) (Université Toulouse III Paul Sabatier, Toulouse). 320 p.
- Estrade G, Béziat D, Salvi S, Tiepolo M, Paquette J-L & Rakotovao S (2014) Unusual evolution of silica-under- and -oversaturated alkaline rocks in the Cenozoic Ambohimirahavavy Complex (Madagascar): Mineralogical and geochemical evidence. *Lithos* 206-207(Supplement C):361-383.
- Falcone G, Antics M, Bayrante L, Conti P, Grant M, Hogarth R, Juliussen E, Mijnlieff H, Nador A, Ussher G & Young K (2016) *Specifications for the application of the United Nations Framework Classification for Fossil Energy and Mineral Reserves and Resources 2009 (UNFC 2009) to Geothermal Energy Resources*. Economic Commission for Europe (ECE) 28 p.
- Farquharson J, Heap MJ, Varley NR, Baud P & Reuschlé T (2015) Permeability and porosity relationships of edifice-forming andesites: A combined field and laboratory study. *Journal of Volcanology and Geothermal Research* 297:52-68.
- Faulds JE & Hinz NH (2015) Favorable tectonic and structural settings of geothermal systems in the Great Basin region, western USA: Proxies for discovering blind geothermal systems. World Geothermal Congress. (Melbourne, 19-25 April), p 6.
- Faulds, J. E., Hinz, N., Kreemer, C., & Coolbaugh, M. (2012). Regional patterns of geothermal activity in the Great Basin Region, Western USA: correlation with strain rates. *Geothermal Resources Council Transactions*, 36, 897-902.
- Faulds J, Coolbaugh M, Bouchot V, Moeck I & Oguz K (2010) Characterizing structural controls of geothermal reservoirs in the Great Basin, USA, and Western Turkey: Developing successful exploration strategies in extended terranes. World Geothermal Congress. (Bali, 25-30 April), p 1.
- Faulds JE, Bouchot V, Moeck IS & Oguz K (2009) Structural controls of geothermal systems in western Turkey: A preliminary report. *Geothermal Resources CouncilTransactions* 33:375-381.

- Ferguson G, Grasby SE & Hindle SR (2009) What do aqueous geothermometers really tell us? *Geofluids* 9(1):39-48.
- Ferrill DA, Sims DW, Waiting DJ, Morris AP, Franklin NM & Schultz AL (2004) Structural framework of the Edwards Aquifer recharge zone in south-central Texas. *GSA Bulletin* 116(3-4):407-418.
- Filomena C, Hornung J & Stollhofen H (2014) Assessing accuracy of gas-driven permeability measurements: a comparative study of diverse Hassler-cell and probe permeameter devices. *Solid Earth* 5(1):1-11.
- Folk RL (1954) The distinction between grain size and mineral composition in sedimentary-rock nomenclature. *The Journal of Geology* 62:344-359.
- Forster C & Smith L (1989) The influence of groundwater flow on thermal regimes in mountainous terrain: A model study. *Journal of Geophysical Research: Solid Earth* 94(B7):9439-9451.
- Fuchs S & Förster A (2013) Well-log based prediction of thermal conductivity of sedimentary successions: a case study from the North German Basin. *Geophysical Journal International* 196(1):291-311.
- Gallup DL (2009) Production engineering in geothermal technology: a review. *Geothermics* 38(3):326-334.
- Garet RL, Chalmers R & Bustin M (2015) Porosity and pore size distribution of deeply-buried fine-grained rocks: Influence of diagenetic and metamorphic processes on shale reservoir quality and exploration. *Journal of Unconventional Oil and Gas Resources* 12:134-142.
- Gasparini E, Tarantino SC, Ghigna P, Riccardi MP, Cedillo-González EI, Siligardi C & Zema M (2013) Thermal dehydroxylation of kaolinite under isothermal conditions. *Applied Clay Science* 80-81:417-425.
- Geiger M & Schweigert G (2006) Toarcian–Kimmeridgian depositional cycles of the southwestern Morondava Basin along the rifted continental margin of Madagascar. *Facies* 52(1):85.
- Geiger M, Clark DN & Mette W (2004) Reappraisal of the timing of the breakup of Gondwana based on sedimentological and seismic evidence from the Morondava Basin, Madagascar. *Journal of African Earth Sciences* 38(4):363-381.
- Genter A, Evans K, Cuenot N, Fritsch D & Sanjuan B (2010) Contribution of the exploration of deep crystalline fractured reservoir of Soultz to the knowledge of enhanced geothermal systems (EGS). *Comptes Rendus Geoscience* 342(7):502-516.
- Gibson RG (1998) Physical character and fluid-flow properties of sandstone-derived fault zones. *Geological Society, London, Special Publications* 127(1):83-97.
- Giese J, Berger A, Schreurs G & Gnos E (2011) The timing of the tectono-metamorphic evolution at the Neoproterozoic–Phanerozoic boundary in central southern Madagascar. *Precambrian Research* 185(3):131-148.
- Giggenbach W, F. (1988) Geothermal solute equilibria. Derivation of Na-K-Mg-Ca geoindicators. *Geochimica et Cosmochimica Acta* 52(12):2749-2765.
- Götz AE, Sass I & Török Á (2015) Geothermal energy from the Pannonian Basins System: An outcrop analogue study of exploration target horizons in Hungary. EGU General Assembly Conference. (Vienna, 12-17 April), p 21.

- Grasby SE, Allen DM, Bell S, Chen Z, Ferguson G, Jessop A, Kelman M, Majorowicz M, Ko J, Moore M, Raymond J & Therrien R (2011) *Geothermal energy resource potential of Canada*. Natural Resources Canada. 332 p.
- Grebby S, Naden J, Cunningham D & Tansey K (2011) Integrating airborne multispectral imagery and airborne LiDAR data for enhanced lithological mapping in vegetated terrain. *Remote Sensing of Environment* 115(1):214-226.
- Guillou-Frottier L, Carré C, Bourgine B, Bouchot V & Genter A (2013) Structure of hydrothermal convection in the Upper Rhine Graben as inferred from corrected temperature data and basin-scale numerical models. *Journal of Volcanology and Geothermal Research* 256:29-49.
- Gunnlaugsson E, Arnorsson S & Matthiasson M (1981) *Madagascar-Reconnaissance survey for geothermal resources*. Report, Projet MAG/77/104, Contract 141/79,VIRKIR, p.101.(Unpublished).
- Haffen S, Geraud Y, Diraison M & Dezayes C (2013) Determination of fluid-flow zones in a geothermal sandstone reservoir using thermal conductivity and temperature logs. *Geothermics* 46:32-41.
- Hambinintsoa RAH, Ranaivoarisoa A & Blessent D (2017) Hydrogeochemical Characterization of Thermomineral Waters in the Central Highlands of Madagascar. UNESCO IGCP636. (Santiago de Chile, 20-24 November), p 4.
- Hao Y, Fu P, Johnson SM & Carrigan CR (2012) Numerical studies of coupled flow and heat transfer processes in hydraulically fractured geothermal reservoirs. *Geothermal Resources Council Transactions* 36:453–458.
- Hartmann A, Rath V & Clauser C (2005) Thermal conductivity from core and well log data. *International Journal of Rock Mechanics and Mining Sciences* 42(7):1042-1055.
- Harvey PK & Brewer TS (2005) On the neutron absorption properties of basic and ultrabasic rocks: the significance of minor and trace elements. *Geological Society, London, Special Publications* 240(1):207-217.
- Hasterok D & Webb J (2017) On the radiogenic heat production of igneous rocks. *Geoscience Frontiers* 8(5):919-940.
- Heap MJ, Kushnir ARL, Vasseur J, Wadsworth FB, Harlé P, Baud P, Kennedy BM, Troll VR & Deegan FM (2020) The thermal properties of porous andesite. *Journal of Volcanology and Geothermal Research* 398:106901.
- Heap MJ, Kushnir ARL, Gilg HA, Wadsworth FB, Reuschlé T & Baud P (2017) Microstructural and petrophysical properties of the Permo-Triassic sandstones (Buntsandstein) from the Soultz-sous-Forêts geothermal site (France). *Geothermal Energy* 5(1):26.
- Heap MJ & Kennedy BM (2016) Exploring the scale-dependent permeability of fractured andesite. *Earth and Planetary Science Letters* 447:139-150.
- Hertzog R & Plasek R (1979) Neutron-excited gamma-ray spectrometry for well logging. *IEEE Transactions on Nuclear Science* 26(1):1558-1567.
- Hervey C, Beardsmore G, Moeck I, Ruter H & Bauer S (2014) *Best practices guide for geothermal exploration*. IGA Service GmbH, Bochum University of Applied Science, Bochum, Germany. 186 p.
- Hettkamp T, Hettkamp G, Fuhrmann F & Rummel (1999) Hydraulic properties in the Rhine Graben basement material. *Bulletin d'Hydrogéologie* 17:143-150.

- Higgins MD (2017) Quantitative investigation of felsic rock textures using cathodoluminescence images and other techniques. *Lithos* 277:259-268.
- Hinz N, Coolbaugh M, Shevenell L, Stelling P, Melosh G & Cumming W (2016) Favorable structural-tectonic settings and characteristics of globally productive arcs. 41st Workshop on Geothermal Reservoir Engineering. (Stanford University, 22-24 February ), p 8
- Hochstein MP (1990) *Classification and assessment of geothermal resources. Small geothermal resources: A guide to development and utilization*, Dickson Mary H. & Fanelli M. (Eds.) UNITAR, New York. p 31-57.
- Hochstein MP, Zhongke Y & Ehara S (1990) The fuzhou geothermal system (People's Republic of China): Modelling study of a low temperature fracture-zone system. *Geothermics* 19(1):43-60.
- Hochstein MP (1988) Assessment and modelling of geothermal reservoirs (small utilization schemes). *Geothermics* 17(1):15-49.
- Holdsworth RE, van Diggelen EWE, Spiers CJ, de Bresser JHP, Walker RJ & Bowen L (2011) Fault rocks from the SAFOD core samples: Implications for weakening at shallow depths along the San Andreas Fault, California. *Journal of Structural Geology* 33(2):132-144.
- Holzbecher E, Oberdorfer P, Maier F, Jin Y & Sauter M (2011) Simulation of Deep Geothermal Heat Production 2011 COMSOL Conference. (Stuttgart, 26-28 October), p 6.
- Holzbrecher E, Wong L & Litz M-S (2010) Modelling flow through fractures in porous media. COMSOL Conference. (Paris, 17-19 Novembre), p 19.
- Horton F, Hacker B, Kylander-Clark A, Holder R & Jöns N (2016) Focused radiogenic heating of middle crust caused ultrahigh temperatures in southern Madagascar. *Tectonics* 35(2):293-314.
- Huenges E & Ledru P (Eds) (2011) *Geothermal energy systems: exploration, development, and utilization*. John Wiley & Sons. 487 p.
- Huenges E, Hurter S, Saadat A, Köhler S & Trautwein U (2002) The in-situ geothermal laboratory Groß Schönebeck: learning to use low permeability aquifers for geothermal power. 27th Stanford Geothermal Workshop. (Stanford University, 28-30 January ), p 4.
- Ingebritsen SE & Manning CE (2010) Permeability of the continental crust: dynamic variations inferred from seismicity and metamorphism. *Geofluids* 10(1-2):193-205.
- Intergovernmental Panel on Climate Change (IPCC) (2014) *Energy Systems. In: Climate Change 2014: Mitigation of Climate Change. Contribution of Working Group III to the Fifth Assessment*. Report of the Intergovernmental Panel on Climate Change. Cambridge University Press, p 88.
- International renewable energy agency (IRENA) (2018) *Renewable power generation costs in 2017*. Report Abu Dhabi, p 160.
- Ivanova VM, Sousa R, Murrihy B, & Einstein H (2014) Mathematical algorithm development and parametric studies with the GEOFRAC three-dimensional stochastic model of natural rock fracture systems. *Computers & Geosciences* 67:100-109.
- Jacky M (1998) Rôle de la fracturation dans la détermination de la conductivité hydraulique des calcaires - Apport des méthodes directes et indirectes Role of the fracturing for the determination of limestones hydraulic conductivity Contribution of direct and undirect methods for investigation. *Bulletin de la Societe Geologique de France* 169:765-773.

- Jaupart C, Mareschal J-C & Iarotsky L (2016) Radiogenic heat production in the continental crust. *Lithos* 262:398-427.
- Jaupart C, Labrosse S, Lucaleau F & Mareschal JC (2015) *Temperatures, Heat and Energy in the Mantle of the Earth*. Treatise on Geophysics, Schubert G (Ed.) Elsevier, Amsterdam, 2nd Ed Vol 7. p 223-270.
- Jeong W-C, Cho Y-S & Song J-W (2001) A numerical study of fluid flow and solute transport in a variable-aperture fracture using geostatistical method. *KSCE Journal of Civil Engineering* 5(4):357-369.
- Kushnir ARL, Heap MJ & Baud P (2018) Assessing the role of fractures on the permeability of the Permo-Triassic sandstones at the Soultz-sous-Forêts (France) geothermal site. *Geothermics* 74:181-189.
- Kusky TM, Toraman E & Raharimahefa T (2007) The Great Rift Valley of Madagascar: an extension of the Africa–Somali diffusive plate boundary? *Gondwana Research* 11(4):577-579.
- Kusumawardani R, Utami AGSF, Moningka MF & Prabowo TR (2019) Study of hydraulic fracturing stimulation to improve geothermal wells productivity. IOP Conference Series: *Earth and Environmental Science* 254:012023.
- Langevin H, Fraser T & Raymond J. (2020) *Assessment of thermo-hydraulic properties of rock samples near Takhini Hot Springs, Yukon*. Yukon Exploration and Geology 2019, Macfarlane KE (Ed.) Geological Survey, Yukon, p 57–73.
- Lardeaux JM, Martelat JE, Nicollet C, Pili E, Rakotondrazafy R & Cardon H (1999) Metamorphism and Tectonics in Southern Madagascar: An Overview. *Gondwana Research* 2(3):355-362.
- Ledru P & Guillou Frottier L (2010) *Reservoir Definition. Geothermal Energy Systems*, Huenges E (Ed.) Wiley-VCH Verlag GmbH & Co. KGaA, Weinheim p 1-36.
- Lee KC (2001) Classification of geothermal resources by exergy. *Geothermics* 30(4):431-442.
- Lei J, Pan B, Guo Y, Fan Y, Xu Y & Zou N (2020) The temperature distribution model and its application to reservoir depth prediction in fault-karst carbonate reservoirs. *Arabian Journal of Geosciences* 13(14):676.
- Levorsen AI & Berry FA (1967) *Geology of petroleum*. WH Freeman San Francisco. 724 p.
- Li CF, Lu Y & Wang J (2017) *A global reference model of Curie-point depths based on EMAG2*. Scientific Report 7:45129.
- Li Z (2019) *Physical properties of a thermally cracked andesite and fluid-injection induced rupture at laboratory scale*. Philosophiae Doctor (Ph.D.) (Université Paris sciences et lettres, Paris). 194 p.
- Lianheng Z, Dongliang H, Jingyu C, Xiang W, Wei L, Zhiheng Z, Dejian L & Shi Z (2020) A practical photogrammetric workflow in the field for the construction of a 3D rock joint surface database. *Engineering Geology* 279:105878.
- Lindal B (1973) Industrial and other applications of geothermal energy. *Geothermal energy* :135-148.
- Liu X, Wei M, Yang L & Wang X (2017) Thermo-economic analysis and optimization selection of ORC system configurations for low temperature binary-cycle geothermal plant. *Applied Thermal Engineering* 125:153-164.

- Löfberg L ( 2013) *Comparing two field gamma spectrometers: RS 230 and GR 320*. Internal report, Radiation Detection Systems Ab.
- López DL & Smith L (1995) Fluid flow in fault zones: analysis of the interplay of convective circulation and topographically driven groundwater flow. *Water resources research* 31(6):1489-1503.
- Loveless S, Pluymaekers M, Lagrou D, Eva, Doornenbal H & Laenen B (2014) Mapping the Geothermal Potential of Fault Zones in the Belgium-Netherlands Border Region. *Energy Procedia* 59:351-358.
- Luthi SM (2005) Fractured reservoir analysis using modern geophysical well techniques: application to basement reservoirs in Vietnam. *Geological Society, London, Special Publications* 240(1):95-106.
- Lukawski M, Vilaetis K, Gkogka L, Beckers K, Anderson B, & Tester J ( 2013) A proposed hybrid geothermal-natural gas-biomass energy system for cornell university. Technical and economic assessment of retrofitting a low-temperature geothermal district heating system and heat cascading solutions. 38th Workshop on geothermal reservoir engineering. (Stanford university, 11-13 February), p 10.
- Magri F, Möller S, Inbar N, Möller P, Raggad M, Rödiger T, Rosenthal E & Siebert C (2016) 2D and 3D coexisting modes of thermal convection in fractured hydrothermal systems - Implications for transboundary flow in the Lower Yarmouk Gorge. *Marine and Petroleum Geology* 78:750-758.
- Majorowicz JA & Grasby SE (2020) Heat transition for major communities supported by geothermal energy development of the Alberta Basin, Canada. *Geothermics* 88:101883.
- Mamifarananahary E, Rajaobelison J, Ramaroson V & Rahobisoa J (2007) Groundwater recharge process in the Morondava sedimentary Basin, Southwestern Madagascar. 3rd HEP MAD'07 international conference. (Antananarivo, 10 – 15 September), p 10-15.
- Manning C & Ingebritsen S (1999) Permeability of the continental crust: Implications of geothermal data and metamorphic systems. *Reviews of Geophysics* 37(1):127-150.
- Martelat J-E, Lardeaux J-M, Nicollet C & Rakotondrazafy R (2000) Strain pattern and late Precambrian deformation history in southern Madagascar. *Precambrian Research* 102(1):1-20.
- McCoy-West AJ, Milicich S, Robinson T, Bignall G & Harvey CC (2011) Geothermal resources in the Pacific Islands: The potential of power generation to benefit indigenous communities. 36th Workshop on Geothermal Reservoir Engineering. (Stanford University, January 31 - 2 February ), p 7.
- McKenna J, R. & Blackwell D, D. (2004) Numerical modeling of transient Basin and Range extensional geothermal systems. *Geothermics* 33(4):457-476.
- McKinley JM & Warke PA (2007) Controls on permeability: implications for stone weathering. *Geological Society, London, Special Publications* 271(1):225-236.
- Meissner R & Mooney W (1998) Weakness of the lower continental crust: A condition for delamination, uplift, and escape. *Tectonophysics* 296:47-60.
- Mejías M, Renard P & Glenz D (2009) Hydraulic testing of low-permeability formations: A case study in the granite of Cadalso de los Vidrios, Spain. *Engineering Geology* 107(3):88-97.
- Mertoglu O, Simsek S, Basarir N, & Paksoy H,( 2019) Geothermal Energy Use, Country Update for Turkey. European Geothermal Congress. (Den Haag, 11-14 June), p 10.

- Melluso L, Tucker RD, Cucciniello C, A.P, Morra V, Zanetti A & Rakotoson RL (2018) The magmatic evolution and genesis of the Quaternary basanite-trachyphonolite suite of Itasy (Madagascar) as inferred by geochemistry, Sr-Nd-Pb isotopes and trace element distribution in coexisting phases. *Lithos* 310-311:50-64.
- Melluso L, Morra V, Brotzu P & Mahoney J (2001) The Cretaceous Igneous Province of Madagascar: Geochemistry and Petrogenesis of Lavas and Dykes from the Central-Western Sector. *Journal of Petrology* 42:1249–1278.
- Melluso L & Morra V (2000) Petrogenesis of Late Cenozoic mafic alkaline rocks of the Nosy Be archipelago (northern Madagascar): relationships with the Comorean magmatism. *Journal of Volcanology and Geothermal Research* 96(1):129-142.
- Michon L (2016) *The volcanism of the Comoros archipelago integrated at a regional scale. Active Volcanoes of the Southwest Indian Ocean:Piton de la Fournaise and Karthala*, Bachèlery P, Lénat J-F, Di Muro A & Michon L (Éds.) Springer-Verlag, Heidelberg. p 333-344.
- Mielke P, Weinert S, Bignall G & Sass I (2016) Thermo-physical rock properties of greywacke basement rock and intrusive lavas from the Taupo Volcanic Zone, New Zealand. *Journal of Volcanology and Geothermal Research* 324:179-189.
- Mielke P, Nehler M, Bignall G & Sass I (2015) Thermo-physical rock properties and the impact of advancing hydrothermal alteration — A case study from the Tauhara geothermal field, New Zealand. *Journal of Volcanology and Geothermal Research* 301:14-28.
- Ministère de l'énergie et des hydrocarbures (2015) *Lettre de Politique de l'énergie de Madagascar 2015-2030*.Madagascar, <http://www.ore.mg/Publication/Rapports/LettreDePolitique.pdf>.
- Miranda MM, Giordano N, Raymond J, Pereira AJSC & Dezayes C (2020) Thermophysical properties of surficial rocks: a tool to characterize geothermal resources of remote northern regions. *Geothermal Energy* 8(1):4.
- Moeck IS, Dussel M, Weber J, Schintgen T & Wolfgramm M (2019) Geothermal play typing in Germany, case study Molasse Basin: a modern concept to categorise geothermal resources related to crustal permeability. *Netherlands Journal of Geosciences* 98:e14.
- Moeck IS (2018) Geothermal plays, geological analogs, resources assessment, exploration chance, risk evaluation. 12th Asian Geothermal Symposium. (Daejeon, 10-12 November), p 7.
- Moeck IS, Beardsmore Graeme & C. HC (2015) Cataloging Worldwide Developed Geothermal Systems by Geothermal Play Type. World Geothermal Congress. (Melbourne, 19-25 April), p 9.
- Moeck I & Beardsmore G (2014) A new ‘geothermal play type’catalog: Streamlining exploration decision making. 39th Workshop on Geothermal Reservoir Engineering. (Stanford University, 24-26 February), p 8.
- Moeck IS (2014) Catalog of geothermal play types based on geologic controls. *Renewable and Sustainable Energy Reviews* 37:867-882.
- Moreno D, Lopez-Sanchez J, Blessent D & Raymond J (2018) Fault characterization and heat-transfer modeling to the Northwest of Nevado del Ruiz Volcano. *Journal of South American Earth Sciences* 88:50-63.
- Mottet G (1982) Tectonique et volcanisme dans le massif du Tsaratanana-Ankaizina (Nord de Madagascar). Bulletin de l'Association de Géographes Français 59<sup>e</sup> année, pp. 109-112.

- Mougenot D, Recq M, Virlogeux P & Lepvrier C (1986) Seaward extension of the East African rift. *Nature* 321(6070):599-603.
- Muffler PJ (1979) *Assessment of geothermal resources of the United States, 1978*. Survey circular 790,170 p.
- Muffler PJ & Cataldi R (1978) Methods for regional assessment of geothermal resources. *Geothermics* 7(2):53-89.
- Muffler PJ (1975) Tectonic and hydrologic control of the nature and distribution of geothermal resources. 2nd U.N. Symposium on the Development and Use of Geothermal Resource. (San Francisco, 20-29 May), p 10.
- Nasr M, Raymond J, Malo M & Gloaguen E (2018) Geothermal potential of the St. Lawrence Lowlands sedimentary basin from well log analysis. *Geothermics* 75:68-80.
- Navelot V, Géraud Y, Favier A, Diraison M, Corsini M, Lardeaux J-M, Verati C, Mercier de Lépinay J, Legendre L & Beauchamps G (2018) Petrophysical properties of volcanic rocks and impacts of hydrothermal alteration in the Guadeloupe Archipelago (West Indies). *Journal of Volcanology and Geothermal Research* 360:1-21.
- Nicholson K (1993) *Geothermal fluids*. Springer Verlag, Berlin. 264 p.
- Nuclear Energy Agency (NEA) & International Energy Agency (IEA) (2020) *Projected Costs of Generating Electricity 2020*. Paris: OECD Publishing, p 13.
- Nyakabwa-Atwoki RK (2020) The Role of Donor Funds in Reducing Risks and Attracting Foreign Investments for Africa's Geothermal Resource Development. 45th Workshop on Geothermal Reservoir Engineering. (Stanford University, February 10-12), p 11.
- Omenda P (2018) Geothermal Outlook in East Africa: Perspectives for Geothermal Development. Regional Workshop on Geothermal Financing and Risk Mitigation in Africa. (Nairobi, 31 January – 2 February), p 11.
- Panos E, Densing M & Volkart K (2016) Access to electricity in the World Energy Council's global energy scenarios: An outlook for developing regions until 2030. *Energy Strategy Reviews* 9:28-49.
- Paul JD & Eakin C (2017) Mantle upwelling beneath Madagascar: evidence from receiver function analysis and shear wave splitting. *Journal of Seismology* 21(4): 825-836.
- Person M, Hofstra A, Sweetkind D, Stone W, Cohen D, Gable CW & Banerjee A (2012) Analytical and numerical models of hydrothermal fluid flow at fault intersections. *Geofluids* 12(4):312-326.
- Petford N (2003) Controls on primary porosity and permeability development in igneous rocks. *Geological Society, London, Special Publications* 214(1):93-107.
- Pettijohn FJ, Potter PE & Siever R (1972) *Sand and Sandstone*. Springer-Verlag, New York, 1. 631 p.
- Phethean J, Kalnins LM, van Hunen J, Biffi PG, Davies RJ & McCaffrey KJW (2016) Madagascar's escape from Africa: A high-resolution plate reconstruction for the Western Somali Basin and implications for supercontinent dispersal. *Geochemistry Geophysics Geosystems* 17(12):5036-5055.
- Pine R (1983) Pressure transient analysis for large scale hydraulic injections in the Carnmenellis Granite, England. 9th Workshop Geothermal Reservoir Engeineering. (Standford University, 13-15 December ), p 12.

- Piqué A, Laville E, Bignot G, Rabarimanana M & Thouin C (1999a) The initiation and development of the Morondava Basin [Madagascar] from the Late Carboniferous to the Middle Jurassic: sedimentary, palaeontological and structural data. *Journal of African Earth Sciences* 28(4):931-948.
- Piqué A, Laville E, Chotin P, Chorowicz J, Rakotondraompiana S & Thouin C (1999b) L'extension à Madagascar du Néogène à l'Actuel: arguments structuraux et géophysiques. *Journal of African Earth Sciences* 28(4):975-983.
- Pirajno F (2009) *Hydrothermal Processes and Mineral Systems*. Springer, Dordrecht. XLI, 1250 p.
- Popov YA, Beardsmore G, Clauser C & Roy S (2016) ISRM suggested methods for determining thermal properties of rocks from laboratory tests at atmospheric pressure. *Rock Mechanics and Rock Engineering* 49(10):4179-4207.
- Popov Y, F. C. Pribnow D, H. Sass J, Williams C & Burkhardt H (1999) Characterization of rock thermal conductivity by high-resolution optical scanning. *Geothermics* 28(2), 253-276.
- Pratt MJ, Wysession ME, Aleqabi G, Wiens DA, Nyblade AA, Shore P, Rambolamanana G, Andriampenomanana F, Rakotondraibe T & Tucker RD (2017) Shear velocity structure of the crust and upper mantle of Madagascar derived from surface wave tomography. *Earth and Planetary Science Letters* 458:405-417.
- Rajaobelison M, Raymond J, Malo M, Dezayes C & Larmagnat S (2021) Assessment of Petrophysical Rock Properties in North Madagascar: Implications for Geothermal Resource Exploration. *Natural Resources Research* 30(5):3261-3287.
- Rajaobelison M, Raymond J, Malo M & Dezayes C (2020) Classification of geothermal systems in Madagascar. *Geothermal Energy* 8(1):22.
- Rajaomazava (1992) *Étude de la subsidence du bassin sédimentaire de Morondava (Madagascar) dans le cadre de l'évolution géodynamique de la marge est-africaine*. Philosophiae Doctor (Ph.D.) (Université des Sciences et Techniques du Languedoc, Montpellier). 195 p
- Rakotondrainibe (1977) *Contribution à l'étude de la séismicité à Madagascar*. Philosophiae Doctor (Ph.D.) (Université d'Antananarivo, Antananarivo). 145 p.
- Ramarolahy RA (2016) *Etude du mécanisme au foyer de la zone volcanique d'Itasy: Sismologie*. Editions universitaires européennes EU. 104 p.
- Rasamimanana G, Bardintzeff J-M, Rasendrasoa J, Bellon H, Thouin C, Gioan P & Piqué A (1998a) Les épisodes magmatiques du Sud-Ouest de Madagascar (bassin de Morondava), marqueurs des phénomènes de rifting crétacé et néogène. *Comptes Rendus de l'Académie des Sciences - Series IIA - Earth and Planetary Science* 326:685-691.
- Rasamimanana G, Bardintzeff JM, Thouin C, Rasamimanana G, Rasendrasoa J, Bellon H, Pique A & Gioan P (1998b) Rifting-related magmatic episodes of South-Western Malagasy (Morondava basin). *Comptes Rendus de l'Academie des Sciences Serie 2, Sciences de la Terre et des Planetes* (10t326):685-691.
- Rasamimanana G (1996) *Caractérisation géochimiques et géochronologiques de trois épisodes magmatiques (Crétacé, Miocène terminal et Quaternaire) à Madagascar, associés aux phénomènes de rifting*. Philosophiae Doctor (Ph.D.) (Université Paris-Sud, Orsay). 234 p.
- Rasoanimanana RR, Gérard Nicoud G, Mietton M & Paillet A (2012) Réinterprétation des formations superficielles pléistocènes du bassin d'Antsirabe (Hautes Terres Centrales de Madagascar). *Quaternaire* 23(4):339-353.

- Ratsimbazafy JB, (1987) *Éléments structuraux acquis par géophysique (méthodes magnétique et magnétotellurique) dans la région volcanique de l'itasy (centre de Madagascar)* Philosophiae Doctor (Ph.D.) (Observatoire d'Antananarivo, Antananarivo). 192 p. [http://biblio.univ-antananarivo.mg/pdfs/ratsimbazafyJeanBA\\_PC\\_DOC3\\_87.pdf](http://biblio.univ-antananarivo.mg/pdfs/ratsimbazafyJeanBA_PC_DOC3_87.pdf)
- Raymond J, Comeau F, Malo M, Blessent D & Lopez-Sanchez I (2017) The Geothermal Open Laboratory: A Free Space to Measure Thermal and Hydraulic Properties of Geological Materials. UNESCO IGCP636. (Santiago de Chile, 20-24 November), p 4.
- Razafimbelo E (1987) *Le bassin de morondava (Madagascar): synthèse géologique et structurale*. Philosophiae Doctor (Ph.D.) (Université Louis Pasteur, Strasbourg). 219 p.
- Reed MJ (1983) *Assessment of low-temperature geothermal resources of the United States-1982*. Survey Circular 892, USGS, 73 p.
- Reeves C (2014) The position of Madagascar within Gondwana and its movements during Gondwana dispersal. *Journal of African Earth Sciences* 94:45-57.
- Represas P, Monteiro Santos FA, Ribeiro J, Ribeiro JA, Almeida EP, Gonçalves R, Moreira M & Mendes-Victor LA (2013) Interpretation of gravity data to delineate structural features connected to low-temperature geothermal resources at Northeastern Portugal. *Journal of Applied Geophysics* 92:30-38.
- Rezaie M & Aghajani H (2013) A new combinational terminology for geothermal systems. *International Journal of Geosciences* 4(1):43-48.
- Rider M & Kennedy M (2011) *The Geological Interpretation of Well Logs*. Rider-French, Scotland, 3rd. 432 p.
- Rindraharisaona EJ, Tilmann F, Yuan X, Rumpker G, Giese J, Rambolamanana G & Barruol G (2017) Crustal structure of southern Madagascar from receiver functions and ambient noise correlation: Implications for crustal evolution. *Journal of Geophysical Research Solid Earth* 122(2):1179-1197.
- Rindraharisaona EJ, Guidarelli M, Aoudia A & Rambolamanana G (2013) Earth structure and instrumental seismicity of Madagascar: Implications on the seismotectonics. *Tectonophysics* 594(Supplement C):165-181.
- Ritchie H (2019) Access to Energy. OurWorldInData.org, <https://ourworldindata.org/energy-access> (Consulté le 12 décembre 2020)
- Roberts GG, Paul JD, White N & Winterbourne J (2012) Temporal and spatial evolution of dynamic support from river profiles: a framework for Madagascar. *Geochemistry, Geophysics, Geosystems* 13(4):1-23.
- Roduit N (2007) JMicrоВision : un logiciel d'analyse d'images pétrographiques polyvalent. Philosophiae Doctor (Ph.D.) (Université de Genève). 129 p.
- Roig JY, Tucker RD, Delor C, Peters SG & Théveniaut H (2012) Carte géologique de la République de Madagascar à 1/1000000. Ministère des Mines, PGRM, Antananarivo, République Madagascar.
- Rossi G (1980) Quelques aspects d'une haute montagne tropicale : le massif du Tsaratanana (Madagascar). *Revue de géographie alpine* 68:153-172.
- Rufer D, Preusser F, Gnos E, Schreurs G & Berger A (2014) Late Quaternary volcanic history of the Vakinankaratra volcanic field (central Madagascar): insights from luminescence dating of phreatic eruptions. *Bulletin of Volcanology* 76:65.

- Rufer D (2009) *Characterization and age determination of Quaternary volcanism in the southern Ankaratra region (central Madagascar) through novel approaches in luminescence dating*. Philosophiae Doctor (Ph.D.) (University of Bern, Bern). 150 p.
- Rufer D, Guido S, Alfons B, Edwin G & Igor V (2006) Cenozoic alkaline volcanism in central Madagascar in the context of intracontinental rifting. 4th Swiss Geoscience Meeting Abstract. (Bern, 24-25 November).
- Rybacz L (1988) *Handbook of Terrestrial Heat-Flow Density Determination*. Springer, Dordrecht. 478 p.
- Rybacz L (1978) The relationship between seismic velocity and radioactive heat production in crustal rocks: An exponential law. *Pure and applied geophysics* 117(1):75-82.
- Sanyal SK (2005) Classification of geothermal systems—a possible scheme. 30th Workshop on Geothermal Reservoir Engineering. (Stanford University, January 31-February 2), p 8.
- Sarazin G, Michard G & Pastor L (1986) Geochemical study of the geothermal field of Antsirabe (Madagascar). *Geochemical Journal* 20(1):41-50.
- Sass I & Götz AE (2012) Geothermal reservoir characterization: a thermofacies concept. *Terra Nova* 24(2):142-147.
- Schintgen TV, Wuttke MW, Agemar T & Moeck IS (2019) Refinement of the geothermal play type concept by comparison of two foreland basins. European Geothermal Congress. (Den Haag, 11-14 June), p 7.
- Sertac A & Young KR (2015) Assessment of New Approaches in Geothermal Exploration Decision Making. 40th Workshop on Geothermal Reservoir Engineering. (Stanford, 26-28 January), p 12
- Shi W & Pan L (2019) Optimization Study on Fluids for the Gravity-Driven Organic Power Cycle. *Energies* 12(4):732.
- Simmons SF & Browne PRL (2000) Hydrothermal Minerals and Precious Metals in the Broadlands-Ohaaki Geothermal System: Implications for Understanding Low-Sulfidation Epithermal Environments. *Economic Geology* 95(5):971-999.
- Simms MA & Garven G (2004) Thermal convection in faulted extensional sedimentary basins: theoretical results from finite-element modeling. *Geofluids* 4(2):109-130.
- Simsek S (1997) Geothermal potential in northwestern Turkey. *Active Tectonics of Northwestern Anatolia: The Marmara Poly-Project : a Multidisciplinary Approach by Space-geodesy, Geology, Hydrogeology, Geothermics and Seismology*, Schindler C & Martin P (Éds) Vdfhochschulverlag AG under ETH, Zurich. p 111-124.
- Smith L & Chapman D (1983) On the thermal effects of groundwater flow: 1. Regional scale systems. *Journal of Geophysical Research* 88:593-608.
- Soltani M, Farshad K, Mohammad S, Behnam R, Mohammad J, Kobra G, et al. (2021) Environmental, economic, and social impacts of geothermal energy systems. *Renewable and Sustainable Energy Reviews*, 140:1-25.
- Stenberg E, Hutchinson MF & Foley WJ (2018) Using historical normals to improve modern monthly climate normal surfaces for Madagascar. *International Journal of Climatology* 38(15):5746-5765.

- Stephen Hickman MZ & Benoit R (1998) Tectonic controls on reservoir permeability in the Dixie valley, Nevada, geothermal field. 23d Workshop on Geothermal Reservoir Engineering. (Stanford, 26-28 January ), p 8.
- Stober I & Bucher K (2015) Hydraulic conductivity of fractured upper crust: insights from hydraulic tests in boreholes and fluid-rock interaction in crystalline basement rocks. *Geofluids* 15(1-2):161-178.
- Szijártó M, Galsa A, Tóth Á & Mádl-Szönyi J (2021) Numerical analysis of the potential for mixed thermal convection in the Buda Thermal Karst, Hungary. *Journal of Hydrology: Regional Studies* 34:100783.
- Szijártó M, Galsa A, Tóth Á & Mádl-Szönyi J (2019) Numerical investigation of the combined effect of forced and free thermal convection in synthetic groundwater basins. *Journal of Hydrology* 572:364-379.
- Taillefer A, Guillou-Frottier L, Soliva R, Magri F, Lopez S, Courrioux G, Millot R, Ladouce B & Le Goff E (2018) Topographic and Faults Control of Hydrothermal Circulation Along Dormant Faults in an Orogen. *Geochemistry, Geophysics, Geosystems* 19(12):4972-4995.
- Tanaka A, Okubo Y & Matsubayashi O (1999) Curie point depth based on spectrum analysis of the magnetic anomaly data in East and Southeast Asia. *Tectonophysics* 306(3):461-470.
- Tanikawa W & Shimamoto T (2009) Comparison of Klinkenberg-corrected gas permeability and water permeability in sedimentary rocks. *International Journal of Rock Mechanics and Mining Sciences* 46(2):229-238.
- Tarcan G, Filiz S & Gemici U (2000) Geology and geochemistry of the Salihli geothermal fields, Turkey. World Geothermal Congress. (Kyushu Tohoku, May 28-June 10), p 6.
- Tester JW, Anderson BJ, Batchelor AS, Blackwell DD, DiPippo R, Drake E, Garnish J, Livesay B, Moore MC & Nichols K (2006) *The future of geothermal energy: Impact of enhanced geothermal systems (EGS) on the United States in the 21st century*. Technical Report INL/EXT-06-11746, Massachusetts Institute of Technology, 372 p.
- Tezel T, Shibutani T & Kaypak B (2013) Crustal thickness of Turkey determined by receiver function. *Journal of Asian Earth Sciences* 75:36-45.
- The World Factbook (2021), <https://www.cia.gov/the-world-factbook/references/country-data-codes/> (Consulté le 14 mars 2021)
- Thiébaud E (2008) *Fonctionnement d'un système hydrothermal associé à un contact tectonique alpin (La Léchère, Savoie)*. Philosophiae Doctor (Ph.D.) (Université de Savoie, Chambéry). 307 p.
- Thomas B, Waele B, Schofield DI, Goodenough K, Horstwood M, Tucker R, Bauer W, Annells R, Howard K, Walsh G, Rabarimanana M, Rafahatelo JM, Ralison AV & Randriamananjara T (2009) Geological evolution of the Neoproterozoic Bemarivo Belt, northern Madagascar. *Precambrian Research* 172:279-300.
- Tillmanns D, Gertig C, Schilling J, Gibelhaus A, Bau U, Lanzerath F & Bardow A (2017) Integrated design of ORC process and working fluid using PC-SAFT and Modelica. *Energy Procedia* 129:97-104.
- Tomarov G & Shipkov A (2017) Modern geothermal power: Binary cycle geothermal power plants. *Thermal Engineering* 64(4):243-250.
- Tóth J (2009) *Gravitational systems of groundwater flow – Theory, evaluation, utilization*. Cambridge University Press, Cambridge, UK. 294 p.

- Toy VG, Boulton CJ, Sutherland R, Townend J, Norris RJ, Little TA, Prior DJ, Mariani E, Faulkner D, Menzies CD, Scott H & Carpenter BM (2015) Fault rock lithologies and architecture of the central Alpine fault, New Zealand, revealed by DFDP-1 drilling. *Lithosphere* 7(2):155-173.
- Truesdell AH (1975) Summary of Section III: Geochemical Techniques in Exploration. Second United Nations Symposium on the Development and Use of Geothermal Resources. (San Francisco, 20-29 May), p iii-xxviii.
- Tucker R, Roig JY, Moine B, Delor C & Peters SG (2014) A geological synthesis of the Precambrian shield in Madagascar. *Journal of African Earth Sciences* 94:9-30.
- Tucker R, Peters S, Roig J, Théveniaut H & Delor C (2012) Notice explicative des cartes géologique et métallogéniques de la République de Madagascar à 1/1,000,000).
- Tsekhmistrenko M, Sigloch K, Hosseini K, & Barruol G (2021) A tree of Indo-African mantle plumes imaged by seismic tomography. *Nature Geoscience* 14(8):612-619.
- UNComtrade (2018) International Trade Statistics Database. <https://comtrade.un.org/> (Consulté le 8 mars 2021).
- Valgardur S (2002) Investment cost for geothermal power plants. *Geothermics* 31(2): 263-272.
- Varet J (2012) La géothermie pour la production d'électricité. <http://www.encyclopediae-dd.org/encyclopedia/terre/la-geothermie-pour-la-production-d.html> (Consulté le 08 juin 2021)
- Volpi G, Magri F, Frattini P, Crosta GB & Riva F (2017) Groundwater-driven temperature changes at thermal springs in response to recent glaciation: Bormio hydrothermal system, Central Italian Alps. *Hydrogeology Journal* 25(7):1967-1984.
- Voninirina A & Andriambelosoa S (2014) *Étude sur l'énergie à Madagascar*. Rapport, Sonapar, 46 p.
- Wallis IC, Rowland JV & Dempsey D (2018) The Relationship between Geothermal Fluid Flow and Geologic Context: A Global Review. *Geothermal Resources Council Transactions* 42:19.
- Wedepohl KH (1978) *Handbook of Geochemistry*. Springer-Verlag Berlin Heidelberg, 1. 947 p
- Weides S, Moeck I, Majorowicz J, Palombi D & Grobe M (2013) Geothermal exploration of Paleozoic formations in Central Alberta. *Canadian Journal of Earth Sciences* 50(5):519-534.
- Weinert S, Bär K & Sass I (2020) Database of Petrophysical Properties of the Mid-German Crystalline High. *Earth System Science Data Discuss.* 2020:1-34.
- Weydt LM, Ramírez-Guzmán ÁA, Pola A, Lepillier B, Kummerow J, Mandrone G, Comina C, Deb P, Norini G, Gonzalez-Partida E, Avellán DR, Macías JL, Bär K & Sass I (2021) Petrophysical and mechanical rock property database of the Los Humeros and Acoculco geothermal fields (Mexico). *Earth System Science Data* 13(2):571-598.
- Weydt LM, Bär K, Colombero C, Comina C, Deb P, Lepillier B, Mandrone G, Milsch H, Rochelle CA, Vagnon F & Sass I (2018) Outcrop analogue study to determine reservoir properties of the Los Humeros and Acoculco geothermal fields, Mexico. *Advances in Geosciences* 45:281-287.
- White DE (1973a) *Characteristics of geothermal resources*. *Geothermal Energy*, Stanford University Press, Stanford :69-94.

- White DE (1973b) Characteristics of geothermal resources. *Eos Transactions American Geophysical Union* 54(4):69-94.
- Wibberley CAJ & Shimamoto T (2003) Internal structure and permeability of major strike-slip fault zones: the Median Tectonic Line in Mie Prefecture, Southwest Japan. *Journal of Structural Geology* 25(1):59-78.
- Wietze L, Brauchler R, Richter B, Thorbjörnsson D, Tulinius H, & Axelsson G (2021). Towards More Geothermal Power in Turkey. World Geothermal Congress 2020+1. (Reykjavik, April - October), p 5.
- Williams CF, Reed MJ & Anderson AF (2011) Updating the classification of geothermal resources. 36th Workshop on Geothermal Reservoir Engineering. (Stanford University, 31 January - 2 February), p 7.
- Windley BF, Razafiniparany A, Razakamanana T & Ackerman D (1994) Tectonic framework of the Precambrian of Madagascar and its Gondwana connections: a review and reappraisal. *Geologische Rundschau* 83(3):642-659.
- Witherspoon PA, Wang JSY, Iwai K & Gale JE (1980) Validity of Cubic Law for fluid flow in a deformable rock fracture. *Water Resources Research* 16(6):1016-1024.
- Woodbury AD & Smith L (1985) On the thermal effects of three-dimensional groundwater flow. *Journal of Geophysical Research: Solid Earth* 90(B1):759-767.
- World Bank (2017) Energy Sector Management Assistance Program. World Bank Group, ESMAP.Washington,D.C,<http://documents.worldbank.org/curated/en/171191523257054613/Energy-sector-management-assistance-program-annual-report-2017> (Consulté le 21 mars 2021).
- Wysession M, Pratt M, Andriampenomanana Ny Ony F, Tsiriandrimanana R, Nyblade A, Aleqabi G, Shore P, Tucker R, Wiens D & Rambolamanana G (2016) The Lithospheric Structure of Madagascar. AGU Fall Meeting Abstracts. (San Francisco, 12-16 December).
- Yilmazer S, Pasvanoğlu S & Vural S (2010) The relation of geothermal resources with young tectonics in the Gediz graben (West Anatolia, Turkey) and their hydrogeochemical analyses. World Geothermal Congress. (Bali, 25-29 April), p 10.
- Zharikov AV, Malkovsky VI, Shmonov VM & Vitovtova VM (2005) Permeability of rock samples from the Kola and KTB superdeep boreholes at high P-T parameters as related to the problem of underground disposal of radioactive waste. *Petrophysical properties of crystalline rocks*, Harvey PK, Brewer TS, A. PP & A. PV (Éds) Geological Society, Special Publications, London Vol 240. p 153-164.
- Zhou C, Doroodchi E, & Moghtaderi B (2013) An in-depth assessment of hybrid solar–geothermal power generation. *Energy Convers Management* 74: 88-101.
- Zhou T, Rose D, Millot P, Grover R, Beekman S, Amin MFM, Zamzuri MDB, Ralphie B & Zakwan Z (2018) A Comprehensive Neutron Porosity From a Pulsed Neutron Logging Tool. SPWLA 59th Annual Logging Symposium Abstract. (London, 4- 6 June).
- Zimmermann G, Moeck I & Blöcher G (2010) Cyclic waterfrac stimulation to develop an enhanced geothermal system (EGS)—conceptual design and experimental results. *Geothermics* 39(1):59-69.
- Zimmermann G, Reinicke A, Brandt W, Blöcher G, Milsch H, Holl H, Moeck I, Schulte T, Saadat A & Huenges E (2008) Results of Stimulation Treatments at the Geothermal Research

Wells in Groß Schönebeck, Germany. 33rd Workshop on Geothermal Reservoir Engineering. (Stanford University, 28-30 January), p 5.



## **7 ANNEXE**

---

En supplément de l'analyse pétrophysique présentée dans le 3<sup>e</sup> chapitre de la thèse, les données originales concernant les propriétés thermiques et hydrauliques ont été archivées sur la plateforme Dataverse. Il s'agit des données de densité, porosité, perméabilité, conductivité thermique et diffusivité thermique mesurées au Laboratoire ouvert de géothermie.

Au total, 59 échantillons de roc, dont 29 sédimentaires, 4 magmatiques et 26 métamorphiques, ont été récoltés sur 17 affleurements, soit 10 affleurements à Ambilobe et 7 à Ambanja.

La base de données comprend 3 fichiers :

1. les résultats d'analyse de la conductivité et de diffusivité au scanner infra-rouge TSC ;
2. les résultats d'analyse de la porosité, de la densité et du volume de grain à l'aide d'une chambre de volume de grain à pression de 13.8 bar ainsi que la porosité et perméabilité évaluée au porosimètre-perméamètre combiné sous différentes valeurs de pression ;
3. les résultats d'analyse de la perméabilité évaluée sur le terrain et en laboratoire à l'aide du perméamètre portatif PPP-250 en condition atmosphérique ;

Les fichiers inclus les informations concernant l'identifiant de l'échantillon, le numéro de mesure (ID number ex : TCS0001), le numéro de l'échantillon (# sample), la date de la collecte de donnée, le lieu d'échantillonnage, dimension des échantillons mais aussi des informations stratigraphiques et pétrographiques.

Nom des fichiers:

1. LOG\_Database\_TCS\_Madagascar
2. LOG\_Database\_AP608\_Madagascar
3. LOG\_Database\_PPP250\_Madagascar
4. Readme\_data\_Madagascar\_laboratory\_analysis

Les données sont accessibles via l'adresse URL:

<https://dataverse.scholarsportal.info/privateurl.xhtml?token=1dea8c86-ac0d-4a25-b349-a761edc43ba7>